INFORMATION TO USERS

This manuscript has been reproduced from the microfilm master. UMI films the text directly from the original or copy submitted. Thus, some thesis and dissertation copies are in typewriter face, while others may be from any type of computer printer.

The quality of this reproduction is dependent upon the quality of the copy submitted. Broken or indistinct print, colored or poor quality illustrations and photographs, print bleedthrough, substandard margins, and improper alignment can adversely affect reproduction.

In the unlikely event that the author did not send UMI a complete manuscript and there are missing pages, these will be noted. Also, if unauthorized copyright material had to be removed, a note will indicate the deletion.

Oversize materials (e.g., maps, drawings, charts) are reproduced by sectioning the original, beginning at the upper left-hand corner and continuing from left to right in equal sections with small overlaps. Each original is also photographed in one exposure and is included in reduced form at the back of the book.

Photographs included in the original manuscript have been reproduced xerographically in this copy. Higher quality 6" x 9" black and white photographic prints are available for any photographs or illustrations appearing in this copy for an additional charge. Contact UMI directly to order.

UMI

A Bell & Howell Information Company
300 North Zeeb Road, Ann Arbor MI 48106-1346 USA
313/761-4700 800/521-0600

78-8684

HO, Ping-Pei, 1949-

REORIENTATIONAL RELAXATION KINETICS OF POLYATOMIC MOLECULES IN DIFFERENT STATES OF CONDENSED MEDIA: INVESTIGATED BY PICOSECOND LASER PULSE INDUCED KERR EFFECT.

City University of New York,
Ph.D., 1978
Physics, solid state

REORIENTATIONAL RELAXATION KINETICS OF POLYATOMIC MOLECULES IN DIFFERENT STATES OF CONDENSED MEDIA : INVESTIGATED BY PICOSECOND LASER PULSE INDUCED KERR EFFECT

by

Ping-Pei Ho

A disseration submitted to the Graduate Faculty in Physics in partial fullfillment of the requirement for the degree of Doctor of Philosophy, The City University of New York

1978

This manuscript has been read and accepted for the Graduate Faculty in Physics in satisfication of the disseration requirement for the degree of Doctor of Philosophy

1/18/78
date

Robert R Alfano
Professor Robert R. Alfano
Chairman of Examining Committee

1/18/78
date

Myriam P. Sarachik
Professor Myriam P. Sarachik
Executive Officer

Professor Joel Gersten (City Coolege,CUNY)
Professor Robert Callender (City College,CUNY
Professor Fred Cadieu (Queens College,CUNY)
Professor Thomas Keyes (Yale University)

Supervisory Committee

The City University of New York

ABSTRACT

Knowledge of the rotational motion of molecules is of fundamental importance for the understanding of the physics of molecular interactions in the condensed states of matter. A variety of experimental techniques are available which use the frequency domain to probe the kinetics of the molecular rotational motion. Although investigations based on these techniques have proven to be indispensable to the present understanding of molecular rotational motions, the final chapter in this field is still to be written, and more experimental research is needed.

My research has concentrated on the direct time measurement of molecular reorientational relaxation kinetics associated with the optical Kerr effect induced by picosecond laser pulses in the condensed state of matter. Such states encompass neat liquids, mixed binary liquids, supercooled liquids, and plastic crystals.

The reorientational relaxation time in neat liquids at moderate viscosity and above the melting temperature has been found to be linearly proportional to the measured viscosity. This has been shown in the following materials : nitrobenzene, m-nitrotoluene, and salol.

In the supercooled liquid state of salol, where the temperature is far below the melting temperature, the reorientational relaxation time deviates from the variation of the viscosity. This can be accounted for by the progressive restriction of molecular rotational motion. The internal

frictional force which contributes to the measured viscosity is determined by the translational mode of the molecules. The temperature dependence of the measured viscosity does not have the same characteristics as the molecular reorientational relaxation. There will be two different activation energies from these two different measurements.

We have also studied the molecular reorientational relaxation of molecules in the solid state. In succinonitrile, there are two different crystal structures - cubic and monoclinic. Within the temperature region of the plastic crystal phase (cubic structure), the molecular reorientational motion is due to the gauche-trans isomerization.

In the mixed binary liquids of two components : B and C, the viscosity and the coupled molecular reorientational relaxation times are affected by three types of forces : the interactions between molecules of B-B, C-C, and B-C. The coupled two-component relaxation theory which has been described by Mori, ~~Keyes~~, Kivelson, and Tsay has been successfully fitted to the experimental measured double exponential decay times. At different concentrations of the mixture, the coupled relaxation times are displayed from the uncoupled relaxation times of B and C species molecules, and are dependent on the interspecies pair correlation factor. The magnitude of these two relaxation processes in the optical Kerr effect are shown to be dependent on the size of the nonlinear index of refraction of the original neat liquids, the relaxation times of neat liquids, the pair correlation

factor, and the interspecies pair correlation factor.

The molecular reorientational mechanism in condensed materials may be understood in terms of the combination of the following two processes : the transition of molecule from one equilibrium position by overcoming the activation energy of its environment through collisions and diffusional motion; also, there must be empty site available into which the molecule can jump.

We have also characterized those parameters which affect the transmitted signal in the optical Kerr effect and have measured the nonlinear index of refraction of twenty-nine different liquids. By assuming the shape of the pulses in time and space, we can precisely determine the prompt response curve of the optical Kerr gate $\{\tau_0$(molecular reorientational relaxation time) $\ll \tau_l$(pulse duration)$\}$ and numerically deconvolute all other relaxation times from the decay curves of the signal transmitted through the Kerr cell. Using different cell lengths (up to two centimeters), dispersion effects have shown to be negligible. Since there is no absorption in these liquids, the signal transmitted through the Kerr gate is found to be inversely proportional to the wavelength of the probe pulse. The signal transmitted through the Kerr gate of mixed binary liquids is linearly dependent on the relaxation time of the solution and the concentrations of the Kerr-active solute molecules. The signal transmitted through the Kerr gate at various temperature is inversely proportional to the temperature and is also dependent on the relaxation time of the liquid and the pair correlation factor of the molecule.

For the optical Kerr effect of salol in the supercooled liquid state, we have found that Kerr intensity posesses two distinct decay components. The slowly decaying component is associated with the molecular reorientational motion, while the fast component is assumed to arise from electronic cloud distortion and molecular librations. The latter can not be resolved with picosecond laser pulse for the temperature regions studied. This component follows the laser pulse shapes.

ACKNOWLEDGMENTS

I wish to thank Professor Robert R. Alfano of The City College of New York for his untiring encouragement and continued counsel during this research. I would also thank Dr. Paul Wang of Polytechnic Institute of New York and Professor Jeffrey Steiner of The City College of New York for their assistance in taking the x-ray diffraction pictures of the succinonitrile crystals. Furthermore, I would like to thank the financial support from The National Science Foundation (grant number : GH 41812, DMR 73-02392-A01, and ENG 7680212) and The City University Of New York Faculty Research Award Program to the Picosecond Laser And Spectroscopy Laboratory Of The City College.

Finally, my thanks to Mr. Frank Pellegrino and Mr. Daniel Morris for their assistance in proofreading this manuscript.

Dedicated to my parents and my wife Shean-Lan

TABLE OF CONTENTS

LIST OF TABLES

LIST OF PUBLICATIONS

"Fluorescent Kinetics of Chlorophyll in Photosystems I and II Enriched Fractions of Spinach", Biochemica et Biophysics Acta, 387, 159 (1975), (with W. Yu, R.R. Alfano, and M. Seibert).

"Relaxation of the Optical Kerr Effect of Anisotropic Molecules in Mixed Liquids", Chem. Phys. Lett., 37, 91 (1976), (with W. Yu and R.R. Alfano).

"Triplet Exciton Caging in Two Dimensions", J. Chem.Phys., 64, 5104 (1976), (with S. Arnold, R.R. Alfano, M. Pope, W. Yu, R. Selsby, J. Tharrats, and C.E. Swenberg).

"Nonlinear Optical Effects in Antiferromagnetic $KNiF_3$", Opt. Comm., 19, 261 (1976), (with R.R. Alfano, P.A. Fleury, and H.J. Guggenheim).

"Temperature Dependence of the Rotational Relaxation Times of Anisotropic Molecules in Neat and Mixed Binary Liquids", Chem. Phys. Lett., 50, 74 (1977), (with R.R. Alfano).

"Relaxation Kinetics of Salol in the Supercooled Liquid State Investigated with the Optical Kerr Effect", J.Chem. Phys., 67, 1004 (1977), (with R.R. Alfano).

"Relaxation Kinetics of the Plastic Crystal - Succinonitrile", Phys. Rev. A, (to be published; with R.R. Alfano).

"Coupled Molecular Reorientational Relaxalation Kinetics in Mixed Binary Liquids", J. Chem. Phys., (to be published, with R.R. Alfano).

"Optical Kerr Gate in Liquids", (submitted to be published; with R.R. Alfano).

CHAPTER 1

INTRODUCTION

Knowledge of the rotational motion of molecules is important for a fuller understanding of the physics of molecular motion in liquids and solids. The history of scientific progress in the study of molecular motions in condensed media is indeed vast[1,2]. Newton was the first to formulate an hypothesis for the force required to obtain motion in a viscous fluid; " That the resistance which arises from the lack of slipperiness of the parts of the liquid, other things being equal, is proportional to the velocity with which the point of the liquid are separated from one another[1]." In 1809, Brownian motion was observed, when a small particle suspended in some viscous media underwent a continuously stepped motion. These investigations have proven indispensable to the present understanding of the molecular interactions in the condensed state of matter.

The general concepts and major features of the theory which explains this phenomena originated with the works of van der Waals[3]. The main idea being that for a dense fluid repulsive forces dominate the liquid structure. This means that the shape of the molecule determines the intermolecular correlational attractive force. Dipole-dipole interactions, and other slowly varying interactions play a major role in the structure[3]. Their effects on the thermodynamics properties of a fluid is essentially that of a mean-field potential.

The volume of a liquid is determined by the attractive

internal motion is molecular libration, which occurs when a molecule is free to oscillate in a potential well arising from the local fluctuations of surrounding molecules.

In 1929, the theory of the rotational relaxation time of molecules in liquid was proposed by Debye[4]. He applied a diffusion theory and a macroscopie measurable parameter η (viscosity), which corresponds to the internal frictional force between molecules, to interpret the single particle's rotational relaxation time in liquids. Onsager[9] introduced a reaction field to modify the Lorentz field used in Debye's theory. There are also theories[10] based on the statistical mechanics and Langevin's equation in solving the many particle problem of the molecular interactions that occur in liquids. Recently, a computer simulation method based on the hard core force of molecular interactions was used to study the molecular dynamics.[11] Both a high speed and large storage computer have been used to solve the equation of motion and to do numerical statistical mechanics for a limited number of molecules.

Experimentally, a variety of techniques[6] have been used to probe the dynamics of rotational motion of molecules in the condensed state. Dielectric relaxation[12], microwave absorption[13], infrared[14] and Raman[15] spectroscopy, nuclear[16] and spin[17] relaxation, x-ray[18] and neutron[19] scattering, depolarization of fluorescence[20], depolarized Rayleigh wing scattering[21], and optical Kerr effect[22-25], have all been employed to study the molecular rotational kinetics. Except for the last method, all used the frequency domain to extract information on the rotational kinetics of molecules in the condensed state.

Let us summarize these different methods. The dielectric relaxation[12] experiment employs a electric field (wavelength of about a few centemeters) to investigate the inter- and intra- molecular motion in liquids by measuring the dielectric constants (or permittivity) and losses in terms of the dielectric relaxation time. The microwave absorption experiment[13] uses a monochromatic microwave source (maser in the frequency range of 1 to 100 GHz($0.3cm^{-1}$ to 33 cm^{-1})) to study the absorption and emission by the quasi-quantized rotational energy of free molecules. This absorption spectrum gives information on the shape of the molecule (from the calculation of moment of inertia). Information is also obtained on the molecular structure, internal rotations, energy transfer, and relaxation processes, etc.. Infrared absorption[14] and laser Raman[15] scattering spectroscopy are used to study the rotational isomers of molecules and non-radiative energy transfer processes. In nuclear spin relaxation[16] experiments, a nuclei is used as a probe to study the structure and bonding properties of molecules. This spectrum can be characterized by three types of parameters: chemical shifts, spin-spin coupling constant, and the intensities of the resonance absorption signals. The technique of electron spin resonance spectroscopy[17] is only applied to the study of radicals and radical ions, since it is the spin of the unpaired electron which is used to probe the molecular enviroment. X-ray[18] and neutron[19] scattering use their short wavelengths ($\lambda_{x\text{-ray}} \lesssim 0.1$ A, $\lambda_{neutron} \lesssim 5$ A) to study the atomic and intramolecular structure. By studying the inelastic scattering spectrum, the pair distribution

function can be studied[25]. Depolarization of fluorescence measures the kinetics of the polarization of the fluorescent light. During the fluorescence, the memory of the polarization with respect to the exciting light is lost due to collisions or Brownian of molecules. Depolarized Rayleigh wing scattering[21] measures the linewidth of scattered light from a well defined single mode laser. A linearly polarized single mode laser light is sent into a condensed medium, where the wavelength of the light is much larger than the size of the particle in the medium. The thermal fluctuations cause local fluctuations in density and entropy gives rise to the light scattering from the dense medium. The change in direction of the polarized field arises from the particle's rotation and lack of symmwtry in its structure and shape. The wavelength of the depolarized scattered light is centered at the wavelength of the incident light but its band-width is larger. The broadened linewidth of the depolarized Rayleigh scattering yields information on the reorientational relaxation rate of the molecules.

Recently, picosecond laser techniques[22-25] have been applied to measure directly the time dependence of the Kerr effect associated with the reorientational motion of polyatomic molecules in neat[22,23] and mixed[24,25] liquids.

Each technique[12-22] has its own advantages and disadvantages in studying the molecular rotational motion. Therefore, in order to get a better understanding of molecular rotational motion in the condensed states of matter, more experimental

research is needed. This thesis provides a step in that direction.

In this research thesis, I have used the picosecond optical Kerr technique to directly study the reorientational relaxation kinetics of molecules in different states of condensed matter, such states as neat liquids, mixed binary liquids, supercooled liquids, and plastic crystals. From these studies, information has been obtained on the molecular relaxation process. I have studied the dependence of molecular reorientation motion in liquids on temperature, concentration, viscosity, pair correlation factor, nonlinear index of refraction, and reorientational relaxation time.

This thesis is organized into the following chapters : In chapter 2, a brief historical review of the theory of the molecular reorientational relaxation in condensed media is presented. The theory will cover (1) Langevin's equation of motion for many particles in liquids; (2) the Debye equation for a single particle's rotational relaxation time versus the viscosity; (3) the properties of internal resistive force of molecules - viscosity; (4) temperature dependence of viscosity; (5) the molecular reorientational properties in the supercooled and plastic crystal states; (6) the modified theory of Debye's equation; and (7) Mori's generalized Langevin equation.

In chapter 3, theories of the relaxation mechanisms in mixed liquids are discussed, ranging from the old empirical equations of viscosity in mixed liquids to Hill's effective viscosity theory. The coupled two-component relaxation process deduced from the Mori theory will also be discussed.

In chapter 4, a general theory of the optical Kerr effect is presented from a semi-macroscopic statistical mechanics and nonlinear optics approach. A detailed analysis of all the parameters affecting the transmitted signal in the picosecond induced optical Kerr gate is also given.

In chapter 5, the experimental apparatus and the characteristics of the mode-locked laser pulses are described in detail.

In chapter 6, the results of the experimental program on the direct measurements of the relaxation times with respect to the theory of molecular reorientational relaxation is presented.

A summary of this research is given in chapter 7, and suggestions for future experiments are presented in chapter 8.

References

1. E. Hatshek, "Viscosity of Liquids" (D. Van Nostrand, New York, 1928).
2. F.W. Sears and M.W. Zemansky, "University Physics", (Addison-Wesley Pub. Co. Inc., 1970).
3. H.C. Andersen, Adv. Mol. Relax. Proc., 8, 105, (1975).
4. D.R. Jones, and C.H. Wang, J. Chem. Phys., 66, 1659,(1977).
5. J.W. Wilson, J. Chem. Phys., 7, 377, (1940).
6. W.J. Orville-Thomas, "Internal Rotation in Molecules", (John Wiley and Sons, New York, 1972).
   F. Kohler, "The Liquid State", (Verlag Chemie,Berlin,1972).
7. H. Reiss, Adv. Chem. Phys., 9, 1, (1965).
8. P. Debye, "Polar Molecules", (Dover, New York, 1946).
9. L. Onsager, J. Am. Chem. Soc., 58, 1486, (1934).
10. R. Kubo, J. Phys. Soc. (Japan), 12, 493, (1957).
11. B.J. Berne, J. Chem. Phys., 66, 2821, (1977).
12. C.P. Smyth, "Molecular Relaxation Process", (Academic Press, New York, 1966).
13. W. Gordy and R.L. Cook, "Microwave Molecular Spectra" (Wiley, New York, 1970).
    D.H. Whiffen and H.W. Thompson, Trans. Farad. Soc., 42A 114, (1946).
14. I.H. Hills, "Infrared Spectroscopy and Molecular Structure", (Elsevier, Amsterdam, 1963).
    W.G. Rothschild, J. Chem. Phys., 53, 990, (1970).
15. M.E. Crawford, H.L. Welsh, and J.H. Harrold, Can. J. Phys., 30, 81, (1952).
    W.R.I. Clements nd B.P. Stoicheff,Appl. Phys.Lett.,12,246,(1968).

16. N. Bloembergen, E. Purcell, and R.V. Pound, Phys. Rev., 73, 679, (1948).

V.I.P. Jones and L.A. Ladd, J.Chem.Soc.(B), 1719, (1970).

17. N.S. Angerman and R.B. Jordan, J.Chem.Phys., 54, 837, (1971).

18. R.K. Kruh, Chem. Rev., 62, 319, (1962).

19. L.A. deGraaf, Physica, 40, 497, (1969).

20. F.F. Chen, "Fluorescence: theory, instrumentation and practice, Ed. G. Guilbault", (Dekker, New York, 1967).

21. S.L. Shapiro and H.P. Broida, Phys. Rev., 154, 129, (1967).

E. Zamir, N.D. Gershon, and A. Ben-Reuven,, J. Chem. Phys., 55, 3397, (1971).

D.R. Bauer, G.R. Alms, J.I. Brauman, and R. Pecora, J. Chem. Phys., 61, 2255, (1974).

22. M. Duguay and J. Hansen, Appl. Phys. Lett., 15, 192, (1969).

23. P.P. Ho and R.R. Alfano, J. Chem. Phys., 67, 1004, (1977).

24. P.P. Ho and R.R. Alfano, Chem. Phys. Lett., 50, 74, (1977).

25. P.P. Ho, W. Yu, and R.R. Alfano, Chem. Phys. Lett., 37, 91, (1976).

CHAPTER 2

MOLECULAR ORIENTATIONAL RELAXATION KINETICS IN CONDENSED MEDIA

In this chapter, a general review of the theories associated with the molecular relaxation kinetics will be presented.

Section 2.1 presents the molecular fluctuation in liquids using Langevin's equation. In section 2.2, Debye's theory is outlined for a single particle rotation in a continuum medium. The properties of viscosity in liquids are discussed in section 2.3. This is an important parameter in Debye's equation. In section 2.4, the temperature dependence of the viscosity in liquids is discussed and a comparison is made with the different molecular relaxation kinetics in different states of matter. A brief discussion of the properties of supercooled liquids is given in section 2.5. In section 2.6, three factors are introduced into the Debye theory creating a more realistic model for the explanation of reorientational motion of molecules in liquids. In section 2.7, the molecular rotational motion in solids is described. Mori's theory is outlined in section 2.8, formulating a general transport theory for a many-particle system explicitly giving the solution of the equation of motion for the molecular reorientational motion.

2.1 Molecular Fluctuations in Liquids

In this section, we will discuss how the relaxation process takes place and how the energy is dissipated in liquids.

The statistical fluctuations in liquids at thermal equilibrium are known as Brownian motion. At thermal equilibrium, the molecules in a liquid undergo various types of motion. These motions include the translational motion of the center of mass, the internal motion of the electron around the nucleus relative to its center of mass, the rotational motion of atoms about their molecular axes, and the relative vibrations between nuclei about their equilibrium positions.

To discuss the random motion of a single particle immersed in a liquid at the absolute temperature T, it is assumed that the particle is of mass m, and its center of mass coordinate at time t is designated by $\vec{r}(t)$ with velocity $\vec{v} = d\vec{x}/dt$. The particle changes its position and velocity at every instant through successive collisions. It is almost impossible to describe in detail the interactions of the center of mass coordinate $\vec{r}$ with the many degrees of freedom of its surrounding molecules. These other degrees of freedom can be thought of as forming a heat reservoir at a certain temperature. Their interactions can be lumped into some net force $\vec{F}(t)$ which is effective in detevmining the same dependence of $\vec{r}$. In addition, the particle may also interact with some external field $\vec{f}(t)$, such as the gravitational or electromagnetic field.

To describe the motion of particles in the center of mass coordinate system, we have from Newton's second law of motion :

$$m\, d\vec{v}/dt = \vec{f}(t) + \vec{F}(t) \quad , \qquad (2.1)$$

where $\vec{F}(t)$ is not explicitly known. It depends on the positions of many atoms which are in motion. Thus, $\vec{F}(t)$ is some rapidly varying function of the time and varies in a highly irregular fashion. To formulate the problem in statistical terms, an ensemble (a large number of similarly prepared systems) is considered. Each of these systems consists of a particle and its surrounding medium. For example, the mean value of $\vec{F}(t)$ at time t_i is,

$$\langle \vec{F}(t_i) \rangle = (1/N) \sum_{k=1}^{N} \vec{F}^{(k)}(t_i) \quad , \qquad (2.2)$$

where $\vec{F}^{(k)}(t_i)$ is the net force of the k-th systems contained in the ensemble. The rate at which $\vec{F}(t)$ varies can be characterized by a correlation time τ^*. The time τ^* is quite small, roughly of the order of the mean intermolecular separation divided by the mean molecular velocity. For small molecules, this time is about 10^{-13} seconds. This time measures roughly the mean time between two successive maxima (or minima) of the fluctuating function $\vec{F}(t)$. If the particle is imagined to be stationary, there is no preferred direction in space, and the ensemble average $\vec{F}(t)$ vanishes.

Since $F(t)$ is a rapidly fluctuating function of time, it follows equation 2.1 such that $\vec{v}$ also fluctuates in time. However, superimposed upon these fast fluctuations, $\vec{v}$ may also exhibit a slowly varying time dependence. Thus, we can separate the velocity into two parts ;

$$\vec{v}(t) = \overrightarrow{\vec{v}} + \vec{v}' \quad , \tag{2.3}$$

where $\vec{v}'$ denotes the rapid fluctuatations of $\vec{v}$ ($\vec{v}'$ is less rapid than $\vec{F}(t)$ because $\dot{\vec{v}} \propto \vec{F}/m$, and m is large). The mean value of $\vec{v}'$ vanishes. The slowly varying part $\vec{v}$, though small, is still important. It determines the behavior of the particle motion over long periods of time. Integrating over a time interval τ ($\tau \gg \tau^*$) gives,

$$m\,[\vec{v}(t+\tau) - \vec{v}(t)] = \vec{f}(t)\cdot\tau + \int_t^{t+\tau} \vec{F}(t')\,dt' \quad , \tag{2.4}$$

where $\vec{f}(t)$ is assumed to be constant during the period .

The integration of $\int_t^{t+\tau} \vec{F}(t')\,dt'$ is not small and cannot be neglected over a long period of time. Since $\vec{F}(t)$ is the interaction of a particle with its environment, it always tends to restore the particle back to its equilibrium situation. Suppose, the external force $\vec{f}(t)$ is zero, and the integration of $\vec{F}(t')$ is also zero, then the velocity of the particle $\vec{v}$ is a constant. This is not the case in nature, wher $\vec{F}(t)$ contains a rapidly varying function and also contains a slowly varying part. The slowly varying part of $\vec{F}(t)$ tends to restore the particle to equilibrium. Therefore, we can write

$$\vec{F} = \overrightarrow{\vec{F}} + \vec{F}' \quad , \tag{2.5}$$

where $\vec{F}'$ is the rapidly varying part of $\vec{F}$ whose average value vanished. $\vec{F}$ is a function of $\vec{v}$ such that $\overline{\vec{F}(\vec{v})} = 0$ in equilibrium when $\vec{v} = 0$. This can be written in a general form by :

$$\vec{F} = -\alpha \vec{v} \quad , \tag{2.6}$$

where α is a frictional constant and the minus sign indicates explicitly that the force $\vec{F}$ tend to reduce $\vec{v}$ to zero as time increases. Equation 2.1 together with equations 2.5 and 2.6, and the approximation $\alpha\vec{v} \approx \alpha\vec{v}$, can be expressed by :

$$m\, d\vec{v}/dt = \vec{f}(t) - \alpha \vec{v} + \vec{F}'(t) \quad , \tag{2.7}$$

where the slow component may be written as,

$$m\, d\vec{v}/dt = \vec{f} + \vec{F} = \vec{f} - \alpha\vec{v} \, . \tag{2.8}$$

Equation 2.7 is called the irreversible Langevin equation. It differs from equation 2.1 by explicitly decomposing the force $\vec{F}(t)$ into a slowly varying part ($\alpha\vec{v}$) and a fast fluctuating part ($\vec{F}'(t)$) which is purely random. The mean value always vanishes irrespective of the velocity or position of the particle. Thus equation 2.7 describes the behavior of the particle at all later times once its initial conditions are specified.

Equation 2.7 can be described even more explicitly. Taking the ensemble average of both sides of equation 2.4, we obtain

$$m \langle \vec{v}(t+\tau) - \vec{v}(t) \rangle = \vec{f}(t)\tau + \int_t^{t+\tau} \langle \vec{F}(t') \rangle \, dt' \, . \tag{2.9}$$

If the effect of the particle's motion on the force $\vec{F}$ exerted

on it by the environment is neglected, then we obtain $\langle \vec{F} \rangle = \langle \vec{F} \rangle_{t=0} = 0$. And in equation 2.9, if there is no external force ($\vec{f}(t) = 0$), it reduces to a static condition. The particle will be stationary if it is at rest with respect to the environment at $t = 0$. This is not adequate, if the particle has a velocity $\vec{v}(t)$ at some arbitrary time. In the first approximation, a small system A at this time can be assumed in an equilibrium situation under $\langle \vec{F} \rangle = 0$, and the probability of system A being in such a state is $P(0)$. In the next approximation, $F(t)$ is affected by the motion of the particle, at this situation, as $t' = t + \tau'$, the particle has a velocity $\vec{v}(t+\tau')$. The motion of the particle affects its environment, and if τ' is small, the mean force $\langle \vec{F}(t') \rangle$ depends on the situation at the earlier time t. As the particle velocity changes, the internal equilibrium of the environment is disturbed. After a time of τ^* which is of the order of the time between molecular collisions, the interactions between molecules will have reestablished equilibrium consistent with the new value of the parameter $\vec{v} = \vec{v}(t+\tau')$. In a time interval $\tau' > \tau^*$, the velocity of the particle changes by $\Delta v(\tau')$ and correspondingly, the energy of the whole system changes from E' to $E' + \Delta E'(\tau')$. The probability ratio of finding system A at time t and $t+\tau'$ is:

$$P(t+\tau')/P(t) = e^{\beta \Delta E'}$$

where $\beta = 1/kT$.

The mean value of $\vec{F}$ at $t' = t + \tau'$ is given by,

$$\langle \vec{F}(t) \rangle = \sum_n P_n(t+\tau') \vec{F}_n(t) \approx P_n(0)(1 + \beta \Delta E') \vec{F}_n = \langle (1 + \beta \Delta E') \vec{F} \rangle_o . \tag{2.10}$$

Since $\langle \vec{F} \rangle_o = 0$, the equation 2.10 reduces to

$$\langle \vec{F}(t) \rangle = \beta \langle \vec{F} \Delta E' \rangle_o . \tag{2.11}$$

Equation 2.11, in general, does not vanish.

The energy change for the heat reservoir in the time $t' - t$ is the negative of the work done by the force $\vec{F}$ on the particle. It is given by,

$$\Delta E' = - \int_t^{t'} \vec{v}(t'') \cdot \vec{F}(t'') \, dt''$$

$$\approx - \vec{v}(t) \cdot \int_t^{t'} \vec{F}(t'') \, dt'' . \tag{2.12}$$

By inserting equation 2.12 into equation 2.11, we obtain,

$$\langle \vec{F}(t') \rangle = - \beta \langle \vec{F}(T') \, \vec{v}(t) \cdot \int_t^{t'} \vec{F}(t'') \, dt'' \rangle_o$$

$$= - \beta \vec{v}(t) \cdot \int_t^{t'} \langle \vec{F}(t') \, \vec{F}(t'') \rangle_o \, dt''$$

$$= - \beta \vec{v}(t) \cdot \int_{t-t'}^{0} \langle \vec{F}(t') \, \vec{F}(t'+s) \rangle_o \tag{2.13}$$

From equations 2.9 and 2.13, we have,

$$m \langle \vec{v}(t+\tau) - \vec{v}(t) \rangle = \vec{f}(t) \tau - \beta \vec{v}(t) \cdot \int_t^{t+} dt' \int_{t-t'}^{0} ds \langle \vec{F}(t') \vec{F}(t+s) \rangle \tag{2.14}$$

The last term in equation 2.14 is slowly varying and leads to "dissipation" That is, if $\vec{f}(t) = 0$, the mean velocity $\vec{v}$ goes to zero with increasing time. If $\tau \gg \tau^*$, this dissipation

term can be written by,

$$\int_t^{t+\tau} dt' \int_{t-\tau'}^{0} ds \ \langle \vec{F}(t') \ \vec{F}(t'+s) \rangle_0$$

$$= \int_{-\tau}^{0} ds \int_{t-s}^{t+s} dt' \langle \vec{F}(t'') \ \vec{F}(t'+s) \rangle_0$$

$$= \int_{-\tau}^{0} ds \int_{t-s}^{t+\tau} ds \ \langle \vec{F}(t) \ \vec{F}(t+s) \rangle_0 \quad (\tau+s)$$

$$\xrightarrow{\tau \gg s} \int_{-\infty}^{0} ds \ \langle \vec{F}(t) \ \vec{F}(t+s) \rangle_0 \cdot \tau$$

$$= \tfrac{1}{2} \tau \int_{-\infty}^{\infty} ds \langle \vec{F}(t) \ \vec{F}(t+s) \rangle_0 \ . \qquad (2.15)$$

The calculation in equation 2.15 from the second line to the third line is based on the following : the ensemble average is here taken in the equilibrium situation where the distribution of systems in the ensemble is independent of the absolute value of the time.

By combining equations 2.14 and 2.15 and comparing with equation 2.14, the frictional force constant is defined by

$$\alpha = (1/2kT) \int_{-\infty}^{\infty} \langle \vec{F}(0) \ \vec{F}(s) \rangle_0 \, ds \ , \qquad (2.16)$$

This equation is sometimes called the fluctuation-dissipation theorem.

In this section, I have outlined the irreversible Langevin equation 2.7 and give a simple derivation of the fluctuation-dissipation theorem (equation 2.16). The molecular fluctuations can be solved by these two equations. The time scale of the molecular motion is separated into two different types of motion : fast and slow motions. When the surroundings which interact

with the system come to internal equilibrium very quickly in comparison with the smallest time of interest, the net slow frictional force ($\vec{F} \propto \alpha \vec{v}$) becomes the dynamical description of the system. In equation2.8, if the external field $\vec{f}(t)$ is shut off at a time $t > 0$, the solution is given by :

$$\vec{v}(t) = \vec{v}(0)\ e^{-(\alpha/m)t} , \qquad (2.17)$$

where m/α is the relaxation time of the motion of this system.

2.2 Debye's Theory For The Molecular Orientational Relaxation Process

In 1929, Debye studied the single particle reorientational relaxation time in liquids using a molecular diffusion theory[1]. Over the years, the model has been used to describe a vast amount of data. In this section, we discuss this model following the theory derived by Debye[1].

Debye's model considered a single particle as a sphere immersed in a liquid which behaves as a continuum heat bath. The center of mass of the sphere is located by polar coordinates. When a linearly polarized light beam is sent into a liquid of composed of polar molecules, the distribution function of the molecules changes in time through the interaction of the beam's electric field with the molecular orientation and electronic orbit distortion. The distribution function, f, describes the distribution of the dipole moment of molecules in liquids as a particular angle θ. The angle θ is the angle between the principal axis of the molecule and the direction of the external field (z-axis).

The number of molecules at a given time which have their dipole moments in the direction θ of a solid angle $d\Omega$ is $f \cdot d\Omega$. Due to the external field (which is varying in time) and the nature of the Brownian motion, f is a function of time, too.

For simplicity, Debye made two assumptions for the change of the distribution function $f \cdot d\Omega$ between the initial time 0 and the later observation time δt. First, δt is assumed to be large enough so that all the molecules oriented

in $d\Omega$ at $t = 0$ can shift outside of $d\Omega$ in time δt. Secondly, δt is also assumed to be small enough so that the dipole moment will not shift more than a few degrees during this time interval.

The number of molecules whose moments have entered $d\Omega$ during the interval δt is given by the equation,

$$\delta = \delta t \, (\partial f/\partial t) \, dt = \delta_1 + \delta_2 , \qquad (2.18)$$

where δ_1 denotes the contribution of molecules due to the rotations produced by the external field, and δ_2 denotes the contribution of molecules due to the rotation produced by the Brownian motion.

Let us evaluate δ_2. Suppose a certain probability function P, such that $P \cdot d\Omega$ denotes that the probability function P lies in $d\Omega$ at time $t = 0$, and will have its moment in $d\Omega'$ when $t = \delta t$. Where $d\Omega'$ is a solid angle whose axis makes an angle θ with the axis of the solid angle $d\Omega$ (see figure 1). The total number of molecules whose moments have entered $d\Omega$ due to the Brownian motion in the interval δt is given by,

$$\delta_2 = - f \cdot d\Omega + \int f' \cdot d\Omega' \; P \cdot d\Omega , \qquad (2.19a)$$

where f' is the distribution function corresponding to the angle θ', and the integration is to be carried out over the surface of the sphere of unit radius. The first term in equation 2.19a accounts for all the molecules whose moments rotate out of $d\Omega$ during the interval δt which were there at $t = 0$. The second term of equation 2.18 accounts for all the molecules having moments outside of $d\Omega$ at $t = 0$ which now take up

positions in $d\Omega$ after the δt interval. P is assumed a function of θ alone, and the spatial part of the distribution function f only depends on θ. Since $d\Omega$ is constant with respect to the integration, equation 2.18 can be written by,

$$\delta_2 = d\Omega \left(\int f' P \, d\Omega' - f \right) . \qquad (2.19b)$$

Equation 2.19 can be approximated by taking a Taylor's expansion of f' at angle θ about $d\Omega$,

$$f' = f + (\theta-\theta') \, \partial f/\partial\theta \Big|_{\theta(t=0)} + (\theta-\theta')^2 \tfrac{1}{2} \, \partial^2 f/\partial\theta^2 \Big|_{\theta(t=0)} + \cdots \qquad (2.20)$$

From the second assumption on δt, the probability function P approaches zero very rapidly when θ is large. Therefore, the higher order terms in equation 2.20 can be neglected. Let

$$\theta - \theta' \equiv \xi . \qquad (2.21)$$

we can approximate the equation 2.20 by,

$$\int f' P \, d\Omega' \simeq f \int P \, d\Omega' + \partial f/\partial\theta \int \xi P \, d\Omega' + \tfrac{1}{2} \partial^2 f/\partial\theta^2 \int \xi^2 P \, d\Omega' + \cdots$$

$$= f + \langle\xi\rangle \, \partial f/\partial\theta + \langle\xi^2\rangle \tfrac{1}{2} \, \partial^2 f/\partial\theta^2 . \qquad (2.22)$$

From trigonometry and figure 1, we have

$$\cos\theta' = \cos\theta\cos\Theta + \sin\theta\sin\Theta\cos\phi$$

$$\underset{\Theta\ll 1}{\simeq} \cos\theta + \Theta\sin\theta\cos\phi - \tfrac{1}{2}\Theta^2\cos\theta + \cdots . \qquad (2.23)$$

from equation 2.21 $\theta' = \theta + \xi$ and $\xi \ll 1$, we obtain

$$\cos\theta' = \cos\theta - \xi\sin\theta - \tfrac{1}{2}\xi^2\cos\theta + \cdots , \qquad (2.24)$$

and ξ can be expanded in powers of function of θ by,

$$\xi = A\theta + B\theta^2 + \cdots . \qquad (2.25)$$

where α and β are implicitly function of θ and ϕ. Comparing equations 2.23 and 2.24, we obtain

$$\zeta = - \omega \cos\theta + \tfrac{1}{2} \omega^2 (\cos\theta/\sin\theta) \sin\phi + \cdots \quad . \quad (2.26)$$

such that,

$$\langle \zeta \rangle = \bar{\zeta} = \int P \, d\Omega' = \tfrac{1}{4} \overline{\omega^2} (\cos\theta/\sin\theta) \quad , \quad (2.27)$$

where $$\overline{\omega^2} = \int_0^{\pi} \int_0^{2\pi} \omega^2 \, P \sin^2\theta \, d\theta \, d\phi \, . \quad (2.28)$$

Inserting equations 2.27, 2.28, and 2.22 into equation 2.19, we obtain

$$\delta_2 = d\Omega \, \tfrac{1}{2} \omega^2 \left[(\cos\theta/\sin\theta) \partial f/\partial\theta + (\partial^2 f/\partial\theta^2) \right] \, . \quad (2.29)$$

This equation indicates that there is no influence of the Brownian motion if the distribution function of dipole moment f is independent of θ.

Next, we calculate the contribution of molecules δ_1 which arises from the external field. The torque on a given molecule with a dipole moment $\vec{u}$ in the external field $\vec{F}$ is given by,

$$\vec{M} = \vec{u} \times \vec{F} = -uF \sin\theta \, \hat{m}. \quad (2.30)$$

If the torque M is a constant, then the angular velocity of the rotational motion of the molecule is proportional to the torque ($M = dL/dt$ and $L = Iw$, if M is a constant, we have $d\theta/dt = L/I = Mt/I$). That is, an internal frictional force $\zeta (= I/t)$ resulting from molecular impacts would balance the induced torque. This can be expressed as the following equation,

$$M = \zeta \, d\theta/dt \quad , \quad (2.31)$$

or $$\theta = M/\zeta \, t \quad (2.32)$$

In the time interval δt, the number of molecules whose dipole moments pass through the solid angle at θ are

$$2\pi f M/\zeta \quad \delta t \sin\theta \ , \tag{2.33}$$

and at $\theta + d\theta$ are

$$2\pi f M/\zeta \ \delta t \sin\theta \ + \ \partial/\partial\theta \ (\ 2\pi f(M/\zeta) \delta t \sin\theta) \ d\theta. \tag{2.34}$$

From equations 2.33 and 2.34, δ_1, the net change of the number of molecules within the strip $d\theta$ in the time t is given by :

$$\delta_1 \ = \ - \ \partial/\partial\theta \ (2\pi \ f \ M/\zeta \ \delta t \sin\theta) \ d\theta \ . \tag{2.35}$$

Substituting equations 2.29 and 2.35 into equation 2.18, the molecular diffusion equation is expressed by :

$$\boxed{\partial f/\partial t \ = \ (1/\sin\theta) \quad \partial/\partial\theta \ [\ \sin\theta \ (\theta^2/4\delta t)(\partial f/\partial\theta) \ -(M/\zeta \ )f \ ]} \tag{2.36}$$

In order to solve the equation 2.36, we consider a special solution of the equation 2.36 which expresses the distribution of the dipole moments of molecules. For $\partial f/\partial t = 0$, we use Maxwell-Boltzman equation as a solution of f, we have,

$$f = A \ e^{-E/kT} \ = A \ e^{(uF/kT)\sin\theta} \tag{2.37}$$

This special solution (equation 2.37) and $M = \partial E/\partial\theta$ yields a condition for equation 2.36 as

$$\overline{\theta^2}/4\delta t \ = kT/\zeta \quad . \tag{2.38}$$

This relation can also be derived from the general Langevin equation given in section 2.1 (equation 2.7).

Inserting equation 2.38 into equation 2.37, the final differential equation for the distribution function f as a function of t and θ is obtained

$$\zeta\, \partial f/\partial t = (1/\sin\theta)\ \partial/\partial\theta\ [\sin\theta\ (kT\ \partial f/\partial\theta - M f)]\ . \quad (2.39)$$

This equation will be solved for a static and oscillating applied electric field.

Let us assume that the external static field F is shut off, that is

$$F = \begin{cases} F_o & \text{for } t < 0, \\ 0 & \text{for } t \geq 0. \end{cases}$$

When $t \geq 0$, we have $M = 0$, equation 2.39 reduces to,

$$\partial f/\partial t = (kT/\sin\theta)\ \partial/\partial\theta(\sin\theta\ \partial f/\partial\theta). \quad (2.40)$$

The solution of equation 2.40 for f is obtained by setting for a trial solution

$$f = A\ [1 + uF_o/kT\ R(t)\ \cos\theta]\ , \quad (2.41)$$

where R(t) is an orientational function of time.

Substituting equation 2.41 into equation 2.40, one obtains,

$$\partial R/\partial t = -(2kT/\zeta)\ R\ . \quad (2.42)$$

Defining $\tau_o \equiv \zeta/2kT$, the solution of R from equation 2.42 is

$$R(t) \propto e^{-t/\tau_o}\ , \quad (2.43)$$

The trial solution of equation 2.41 is,

$$f = A\ (1 + uF_o/kT\ \sin\theta\ e^{-t/\tau_o})\ . \quad (2.44)$$

This solution satisfies the boundary conditions at t = 0. It reduces to the approximation of the Maxwell-Boltzmann distribution, and as $t \to \infty$, it gives f = constant. The relaxation time is τ_o. For the sticky boundary condition (discussed in section 2.3), namely, when a sphere of radius a rotates in a continuum of viscosity η , the internal resistive force ζ from the Stokes' equation is

$$\zeta = 8 \pi \eta a^3 \quad . \qquad (2.44)$$

Substituting equation 2.44 into τ_o, the famous Debye equation for single particle rotational relaxation in liquids is obtained

$$\boxed{\tau_o = 4 \pi \eta a^3/kT \quad .} \qquad (2.45)$$

Let's estimate the Debye relaxation time for a typical liquid. For example, water,at room temperature, has viscosity of $\approx$ 1 cp, the radius of the water molecule may be approximated by the equation :

$$a \simeq (\tfrac{1}{4} \pi \, 3 \, M/N)^{1/3} \approx 2 \times 10^{-8} \text{ cm} ,$$

where M is the atomic weight of water, ρ is the density of water, and N is Avogadro's number. From equation 2.45, the relaxation time of water is

$$\tau_o = (3 \times 0.01 \times 10^{-23}) \, (1.38 \times 10^{-16} \times 300)^{-1}$$

$$\approx 2.5 \times 10^{-11} \text{ seconds}$$

$$= 25 \text{ ps.}$$

which is close to the experimental result.

The molecular distribution function of equation 2.39 can be solved for a high frequency external field $F(t) = F_o e^{iwt}$ for all t. The trial solution for equation 2.39 is constructed by :

$$f = A\,(1 + B\,uF_o/kT\;\; e^{iwt}\;\; \cos\theta)\;. \qquad (2.46)$$

The solution is obtained by substituting equation 2.46 into equation 2.39;

$$f = A\,\left[1 + (1 + iw\tau_o)^{-1}\;\; u\,F(t)/kT\,\cos\theta\right]. \qquad (2.47)$$

The angular average of the dipole moment of the molecule is :

$$\bar{m} = \int f\cdot d\Omega\; u\,\cos\theta/\int f\cdot d\Omega \;\; = \;\; u^2/3kT\;\; F_o\, e^{iwt}/(1 + iw\tau_o). \qquad (2.47a)$$

where $\tau_o = 4\pi\eta a^3/kT$ is the Debye relaxation time.

2.3 Viscosity of Liquids

In order to apply the Debye relaxation time, $\tau_o = 4\pi\eta a^3/kT$, to describe the reorientational relaxation kinetic data in liquids, one needs to know the viscosity of the liquids[3-6]. The viscosity is a measurable quantity which represents the internal friction of a fluid or the restriction of a liquid to flow. The frictional force is caused by the collisions between molecules in the microscopic world.

Viscosity often describes the shear force which exists in a fluid. To get a measurement of the shear force during the motion of a fluid, we consider the following experiment. Suppose there are two parallel plane sheets, each of area A, separated by distance h and filled with the liquid (see figure 2.1 below). The liquid is in contact with both surfaces. The upper plate is moving at a speed v_o and the lower is kept stationary. The liquid in contact with the moving surface S moves with the velocity of the surface (sticky boundary), while the liquid in contact to the surface of the lower sheet is at rest. The liquid between the two plates will flow in the same direction with respect to the upper wall and will develop a velocity gradient between the plates. This is shown by different arrow sizes in figure 2.1.

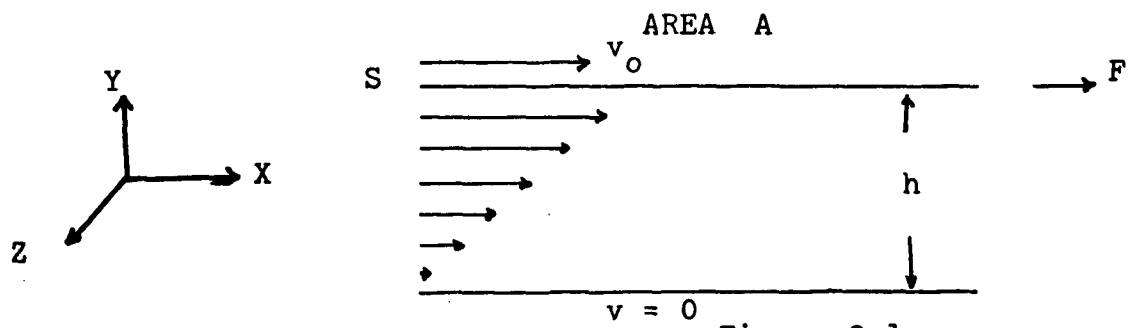

Figure 2.1

In order to maintain the motion, it is necessary that the force F be continuously applied in the positive x direction on the upper plate. This force tends to drag the liquid and the lower plate in the +x-direction. Therefore, an equal force must be exerted in the negative x-direction on the lower plate to hold it steady. Thus there is a shear stress S = F/A exerted on the liquid. In solids, the effect of the stress increases without limit as long as a shear force is applied. The shear force is found to depend on the rate of change of displacement. In figure 2.1, the rate of change of the shearing stress is equal to $v_x(y)/h$, where $v_x(y)/h$ is the velocity of the fluid in the x-direction at position y. The viscosity of the liquid, η , is defined as the ratio of the shearing stress F/A to the ratio of change of the shearing stress :

$$\eta \equiv (F/A)\ (v_x(y)/h)^{-1} \quad . \qquad (2.48)$$

Equation 2.48 is a special case of two flat plates with a uniform velocity increasing along the y direction. In general, the rate of change of displacement can be expressed as the velocity gradient. The viscosity becomes :

$$\eta \equiv (F/A)\ (dv_x(y)/dy)^{-1} \quad . \qquad (2.49)$$

Equation 2.49 can be written in another form as

$$F = \eta A \, dv_x(y)/dy \quad . \qquad (2.50)$$

The unit of viscosity is defined as the poise :
poise = mass/(time x length) = dynes-second/cm^2.

Another way to define the viscosity of liquids is based on the momentum transfer between molecules in collisions[4,7]. This is similar to the motion in a gas. In Andrade's model of viscosity, the molecules in liquids can be regarded as vibrating with a certain frequency ν about their equilibrium positions which vary slowly with time. The transfer of momentum which occurs in a viscous liquid between two layers moving different velocities (see figure 1) is due to collisions of adjacent molecules. This momentum transfer occurs at the extreme of each swing between adjacent molecules. At an infinitesimal time, these two molecules are considered to be one object. This leads to the following definition of viscosity :

$$\eta = (1/3) \; c \, \nu \, m/\sigma \quad , \qquad (2.50)$$

where m is the mass of a molecule, "c" is the probability of collisions, and σ is the average distance between the centres of molecules, σ is defined by

$$\sigma = (N/V)^{-1/3}$$

where N is the number of molecules.

From an hydrodynamic point of view[7,8], viscosity which is a measurement of the rate of change of shear strain between

two layers is proportional to the diffusion constant D. Using the Navier-Stokes equation for a slow steady motion, we have

$$\rho \, d\vec{v}/dt = u \, \nabla^2 \vec{v} - \nabla P \quad , \qquad (2.51)$$

where ρ is the density, $\vec{v}$ is the macroscopic velocity of liquids, ∇P is the pressure, u is the fluidity of the liquid that is the capacity of yielding to the shear stress induced in the layer and $u = 1/\eta$. For a slow steady motion, dv/dt can be omitted. The equation of continuity is another relation that is used to describe the equation of motion.

$$\nabla . \vec{v} = 0 \, . \qquad (2.52)$$

The sticky boundary condition is given by,

$$\vec{v} = \vec{w} \times \vec{r} \quad , \qquad (2.53)$$

where $\vec{w}$ denotes the angular velocity of the spheroid, and $\vec{r}$ is the vector from the center of the spheroid. The liquid in contact with the sphere is moving with the sphere. An example of the sticky boundary condition is a single sphere suspended in an infinitely extended medium. The velocity of the particle is rather small so that nonlocal effects can be neglected. The surface of the liquid layer close to the particle is moving with the surface of the particle. Moreover, there is no slipping between the liquid and the surface of the sphere. Due to the thermally agitated Brownian motion, the sphere's motion is one of randomly flowing against the friction of the environment.

If the pressure $P(\vec{r})$ is assumed to vary slowly, then equation 2. 1 can be written by :

$$\partial(\rho v)/\partial t = u/\rho \; \nabla^2(\rho v) \, . \qquad (2.54)$$

This equation (2.54) can be compared with the self-diffusion equation of molecules in the gaseous state :

$$\partial n/\partial t = D \nabla^2 n \quad , \qquad (2.55)$$

where D is the diffusion constant, and n is the concentration of molecules. The macroscopic density of molecules in liquids $\rho\vec{v}$, is related to D by

$$D = u/\rho \quad . \qquad (2.56)$$

An example which can be used to describe the viscosity in a liquid is a small sphere of radius "a" surrounded by other particles. From Stoke's equation, the resistive force $\vec{F}$ exerted by it when moving with an average velocity $\vec{v}$ with respect to the surrounding particle (the liquid being supposed to remain at rest at large distance) is :

$$\vec{F} = 6\pi a \eta \vec{v} \quad , \qquad (2.57)$$

and

$$\vec{v} = \alpha \vec{F} \quad , \qquad (2.58)$$

where α is the fluidity of the particle under consideration.

From equations 2.57 and 2.58, we obtain

$$\alpha = (6\pi a \eta)^{-1} . \qquad (2.59)$$

Applying the Einstein relation ($a^*=eD/kT$) , we obtain

$$\alpha = D/kT. \qquad (2.60)$$

The rotational friction coefficient (torque/angular velocity) ζ_{rot} of a sphere in a liquid of viscosity η is given by

$$\zeta_{rot} = 8\pi\eta a^3 \quad . \quad \text{(STICKY)} \qquad (2.61)$$

The rotational friction coefficient for spheroids are not much different from those of a sphere of the same volume in the sticky boundary condition. However, in reality, a single particle moving in the dense medium is not described by the sticky model. The surrounding surface might slip. The slipping boundary condition[8] for the Navier-Stokes equation is :

$$\vec{n} \cdot \vec{v} = \vec{n} \cdot (\vec{w} \times \vec{r}) \quad , \quad \text{(on surface)} \qquad (2.62)$$

$$\vec{n} \times (\vec{n} \cdot \vec{s}) = 0. \qquad (2.63)$$

The first condition (equation 2.62) states that no friction enters or leaves the surface, and $\vec{S}$, the stress tensor is given by :

$$\vec{S} = - p.\vec{1} + \eta (\nabla v + v \nabla) \quad . \qquad (2.64)$$

Equation 2.64 states that there is no tangential component of the normal on the surface. Under these conditions, the frictional coefficient for a sphere in uniform translational motion is :

$$\zeta_{trans} = 4 \pi \eta a \quad , \quad \text{(slip)} \qquad (2.65)$$

which is only slightly different from the sticky boundary condition (equation 2.57). While, the rotational friction coefficient of a sphere is

$$\zeta_{rot} \longrightarrow 0 \quad . \quad \text{(slip)} \qquad (2.65a)$$

Therefore, a rotating sphere with slipping boundary condition does not displace any fluid unless it is not a perfect spheroid. While with the sticky boundary condition, a sphere can displace a substantial amount of fluid in either

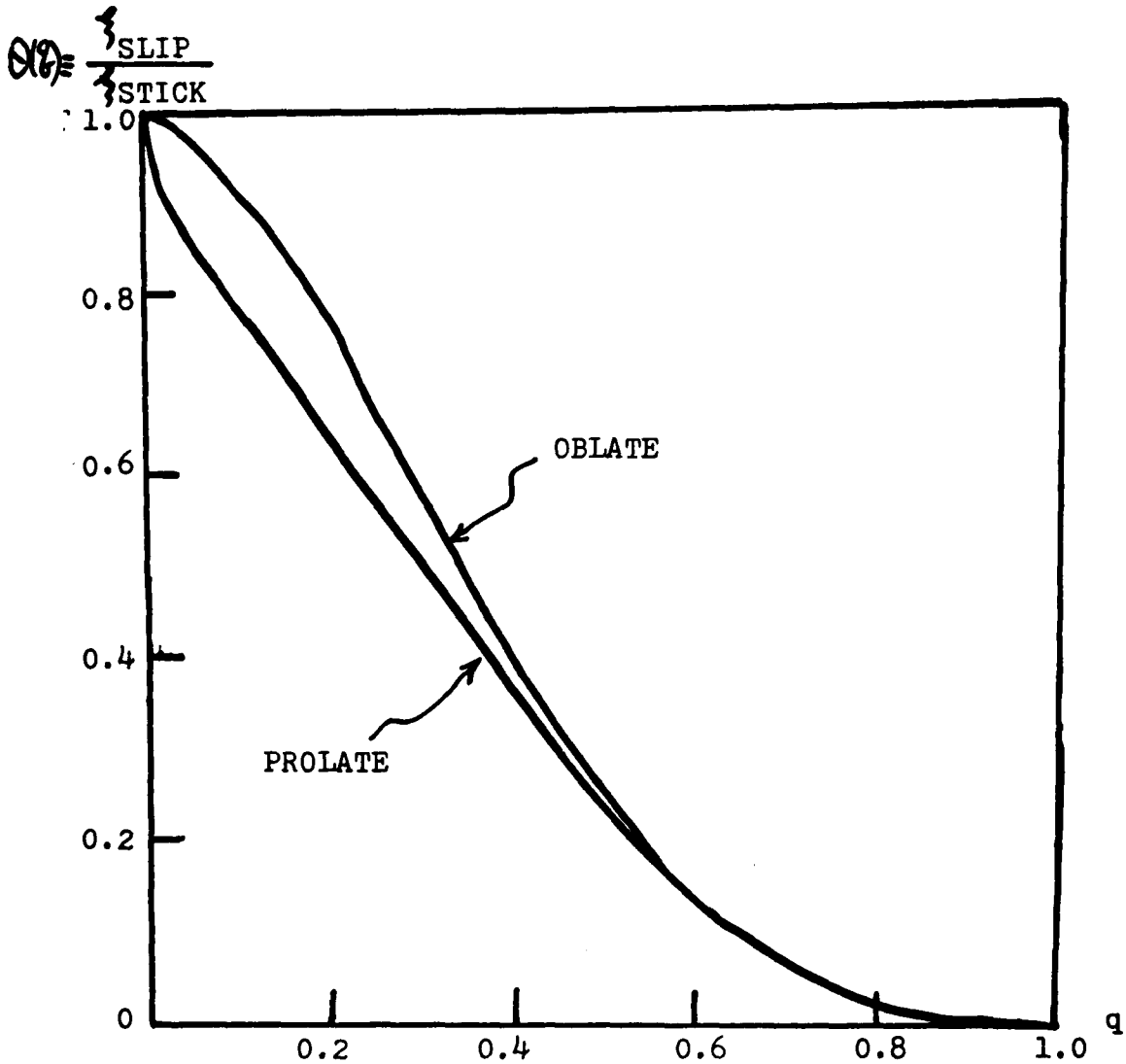

Figure 2.2 The Ratio of the Calculated Rotational Frictional Coefficient $\zeta_{slip}/\zeta_{stick}$ for Prolate Ellipsoids and for Oblate Ellipsoids versus $q \equiv \frac{\text{shorter axis}}{\text{longer axis}}$

L is the length of the tube. At r = R(radius of the capillary), the measured velocity at the center of the capillary is,

$$\eta_{measured} = \Delta P \ R^2/4\eta L \ . \qquad (2.69)$$

The total volume V, collected in t seconds from the viscometer is

$$V = \int_{r=0}^{r=R} v \ t \ 2\pi r \ dr = \pi \Delta P \ R^4/8\eta L \ , \qquad (2.70)$$

which can be rewritten as ,

$$\eta = \pi \Delta P \ R^4 \ t/8VL = K \rho \ t, \qquad (2.71)$$

where K (= $MgR^4/8VL$) is a constant depending on the length and radius of the capillary viscometer, ρ is the density of liquid used in the experiment, and t is the time for a certain amount of liquid to pass through the capillary. For example, the viscosity of distilled water at 20°C is chosen to be 1 cp as a standard. By measuring the time t_w and using $\rho_w = 1 gm/cm^3$, we can obtain the proportional constant K of a certain viscometer. A simple diagram of an Ostwald type viscometer is shown in figure 4 of chapter 5.

The other two kinds of viscometer are used for special experiments. For example, to avoid degrading biological samples under the shear force through a capillary, a Couette viscometer is used. A falling sphere viscometer[10] is used to measure a very viscous medium ($\eta_m \geq 10^8$ cp).

2.4 Temperature Dependence of Viscosity in Liquids

In sections 2.2 and 2.3, we have shown that the viscosity is a necessary macroscopic parameter which is used to describe the molecular reorientational time. In this section, we will concentrate on the temperature dependence of the viscosity in a liquid.. It can be shown that from the Einstein relation (equation 2.60), the diffusional constant is inversely proportional to the viscosity.

The diffusional motion of molecules in the liquid state can be described as a sequence of two steps[7]. First, the molecule transits from its initial equilibrium position into an intermediate state with an increase in potential energy, $\Delta U = E$ (activation energy). Second, the molelucle redistributes from this intermediate state which as a maximum value of its free energy into a new state. In this redistribution process, the activation energy is transferred from the given molecule to its new surroundings so that it cannot immediately get back to its initial position. The time for the molecule to take such a transition path depends on its frictional force, viscosity, as discussed in section 2.2.

The self-diffusion coefficient $D(\propto 1/\eta)$ from the Boltzmann equation is proportional to the expression $\exp(-E/RT)$. The temperature dependence of viscosity in liquids described by Frenkel is :

$$\eta = A \exp(E/RT) \quad , \tag{2.72}$$

where A is a proportional constant, T is the absolute temperature, R is the gas constant, and E is the activation

energy in which molecules must overcome in going from one equilibrium state to another. From Andrade's arguments[11], the viscosity of a liquid described in equation 2.72 decreases as the temperature increases, this is due to the fact that "the temperature agitation interferes with the exchange of momentum at the extremes of libration."[11]

An equation similar to equation 2.72 had been derived by Erying[12]. He assumed that all the vacancies in liquids which have the same volume and the same energy can create holes. He obtained the inverse of the absolute rate of molecular orientation relaxation. This is the well known Arrhenius form for the relaxation time :

$$\tau = B \exp(E_v/kT) , \qquad (2.73)$$

where B is a proportional constant, and E_v is the activation energy.

Besides the activation energy theory, Cohen and Turnbull[13] applied a statistical probability distribution to derive the free volume theory of viscosity. The viscosity of a liquid is,

$$\eta = A \exp(\gamma v_o/v_f) , \qquad (2.75)$$

where A is a proportional constant, v_o is the van der Waal volume of a molecule, and v_f is the free volume which is defined by

$$v_f = \bar{v} - v_o , \qquad (2.76)$$

where $\bar{v}$ is the average volume per molecule allowed in liquids, and γ is a numerical factor needed to correct for the overlap of free volume, with a value between $\frac{1}{2}$ and 1[13]. This equation is based on a hard sphere model of molecules with only repulsive forces. It is assumed that a distribution of hole sizes exists,

and the jump probability is determined only by the chance of finding an adjacent local free volume of sufficient size to jump into. Each molecule is confined to a cage consisting of its neighbors. For diffusional motion of molecules, a fluctuation must appear in the local density which opens up a hole large enough to permit a displacement of the molecule within the cage.

A general theory of viscosity in liquids is given by Macedo and Litovitz[14]. Their model is based on the assumption of quasi-crystalline liquid structure. They combined the Erying[12] and Cohen and Turnbull[13] theory about viscosity of liquids. A molecule is pictured as vibrating about its equilibrium position until the combination of two events occurs : (1) The molecule attains sufficient energy to overcome the attractive forces holding it to its neighbors; and (2) an empty site is available into which the molecule can jump.

The probability of a transition from one site to another is given by the expression :

$$P = P_E \times P_v \ , \qquad (2.77)$$

where P_E is the probability for molecules to obtain sufficient energy to break energy barriers [7,12], and P_v is the probability that there is sufficient local free volume for a jump to occur[13,15].

The general expression given by Macedo and Litovitz[14] for the temperature dependence of the viscosity in a liquid is :

$$\eta = (RT/E_v)^{\frac{1}{2}} (2mkT)^{\frac{1}{2}}/\bar{v}^{2/3} \exp(v_o/v_f + E_v/RT) \ . \qquad (2.78)$$

This equation can fit a wide range of measurements of viscosity (from 10^{-1} cp to 10^{9} cp) versus temperature[14,16].

In equation 2.78, the kinetic properties of liquids have two kinds of behaviors : (1) An Arrhenius behavior, due to the molecule which overcomes a potential barrier; this is a rotational mode. (2) A non-Arrhenius behavior from the free volume effect (molecular translational mode). Within the potential barrier, molecules can undergo free rotations (single valence bond). The translational motion (free volume effect) of a molecule in a liquid is generally pictured as a series jumps by the molecule from one site in the liquid to another. For viscosity considerations, we may think of a molecule as exhibiting free rotations, if it is able to rotate through 360^{o} or more during the translational time[17]. However, if a molecule makes several translational jumps before rotating through 360^{o}, we can say that rotation is restricted to the time scale of the translational relaxation times.

For spherical molecules in liquids, due to the unlimited free rotation around the molecular axis, the viscosity shows a consistent Arrhenius behavior through the whole temperature region. Since the rotational motion is faster, before a translational motion[18-20] occurs, the molecule has rotated a few cycles. Therefore, the viscosity is assumed to have arisen from the rotational motion. For a long chain molecules, at a temperature far above the melting temperature, the rotational motion is still faster than the translational jump motion. It shows a simple Arrhenius behavior. If the temperature is lowered, due to a progressive restriction of

rotation of the molecules in liquids, the viscosity has a non-Arrhenius behavior. The translational motion comparably contributes the resistive force to the viscosity. When the temperature is lowered to the glass or solid phase, the degree of freedom due to rotation[21] occurs only for special cases. An example is the plastic crystal (discussed in section 2.7). At the normal temperature of a liquid, the main contribution to the viscosity arises from the molecular rotational motion. Translational motion contributions (similar to the free volume theory) occur at lower temperatures.

For the free volume effect, the van der Waal volume v_o is taken to be independent of temperature. The free volume is assumed to be equivalent to the total thermal expansion at constant pressure by :

$$v_f = v_o \left\{ \exp\left(\int_{T_o}^{T} \alpha \, dT'\right) - 1 \right\}, \qquad (2.79)$$

where α is the coefficient of thermal expansion, and T_o is the temperature at which the free volume disappears. At higher temperatures, the free volume effect due to the molecular translational motion between equilibrium positions is negligible. Then the viscosity dependence of equation 2.78 reduces to equation 2.72. As T approaches T_o, by substituing equation 2.79 into equation 2.78, we obtain

$$\eta(T) = A \exp[\alpha'/(T-T_o) + E/RT] , \qquad (2.80)$$

where $\alpha' = \alpha \bar{v} / v_o$.

This equation shows a non-Arrhenius behavior from the free volume effect. If $1/\alpha(T-T_o) \gg E/RT$, then equation 2.76 reduces to the free volume limit of equation 2.75. Equation 2.78 is important in the supercooled liquid (section 2.6) and glass state. In this state, the temperature is close to T_o.

2.5 Some Modifications of the Debye Theory

Debye's model for the time dependence of the distribution function f has been successfully used in many cases to interpret experimental data associated with the molecular reorientational motion. However, this equation (2.45) for τ_0 is based on an oversimplified model of the real world. It fails to include the complete picture of motions of molecules in the liquid state. There are at least three facts that should be taken into account in the theory :

(a) Debye's model for the rotation of molecules in liquids is based on a diffusion model of the molecular reorientation caused by infinitesimal fluctuations. However, the reorientation of molecules in liquids is more likely due to discrete angular jumps[22-25] or a distribution of jumps from one point to another. Techniques which measure the susceptibility tensor[26,27] can be used to test whether the diffusion limit or the large jump mechanism is operative for the rotational relaxation kinetics in liquids.

Let us consider the diffusion limit. Basically, the force free distribution function $f(\Omega, t)$ is governed by the general diffusion equation[26-28],

$$\partial f(\Omega, t)/\partial t = D \nabla^2 f(\Omega, t) , \qquad (2.81)$$

where D is chosen as a scalar diffusion constant and depends on the reorientational relaxation time. This constant D is chosen as a scalar instead of a tensor. This implicitly assumes the point of intersection of the major axis of a molecule with the unit sphere which may move in any direction with equal probability. This means that mechanical rotation

about any axis is equally probable.

Let us assume that at $t = 0$, the major rotational axis of the molecule is along the z-axis, then the solution of equation 2.81 is obtained by introducing a trial solution of the form

$$f(\Omega, t) = \sum_{\ell=0}^{\infty} b_\ell P_\ell(\cos\theta)\, g_\ell(t) \quad , \qquad (2.82)$$

where b_ℓ is a constant coefficient, $P_\ell(\cos\theta)$ is the Legendre polynomial function of the ℓ-th order. Substituting equation 2.82 into equation 2.81, we obtain

$$g_\ell(t) = \exp(-t/\tau_\ell/\ell(\ell+1)) \quad , \qquad (2.83)$$

with $\tau_0 \equiv 1/D$.

The relaxation time associated with the ℓ-th Legendre component is

$$\tau_\ell = \tau_0/\ell(\ell+1) \quad . \qquad (2.84)$$

The induced dipole moment for the ℓ-th order susceptibility tensor averaged over all its orientational solid angle is,

$$u_\ell(t) \propto \int d\Omega\, f(\Omega, t)\, P_\ell(\cos\theta) \quad . \qquad (2.85)$$

Substituting equation 2.82 into equation 2.85, from the orthogonality property of the Legendre polynominal, only the ℓ-th component survives. The time dependence of the reorientational motion of the ℓ-th component of the induced moment is given by equation 2.84.

For the dielectric relaxation experiments, the relaxation time of the permanent dipole moment for $\ell = 1$ is

$$\tau_1 = \tau_0/2 \quad . \qquad (2.86)$$

For the depolarized Rayleigh scattering and optical Kerr effect, the second order tensor susceptibility is involved with the reorientational process. The relaxation time in this case is,

$$\tau_2 = \tau_0/6 \quad . \tag{2.87}$$

By comparing equations 2.86 and 2.87, the ratio of two different measured relaxation times in the diffusion limit model is $\tau_1/\tau_2 = 3$.

This model is applicable for a random walk process in which individual reorientational angular steps are small in comparison to the angle θ_0, where θ_0 is defined by the relation[28],

$$P_\ell(\cos\theta_0) = 1/e \quad . \tag{2.88}$$

Using a jump distribution diffusion, the reorientational relaxation time of the ℓ-th rank tensor is derived by Ivanov,[26]

$$\tau_\ell = \tau_0 \left[1 - (2\ell+1)^{-1}\int_0^\pi d\theta \; W(\theta) \sin(\ell+\tfrac{1}{2})\theta/\sin\tfrac{1}{2}\theta\right]^{-1} , \tag{2.89}$$

where τ_0 is the time between jumps, and $W(\theta)$ is the probability of the distribution function of the angular jump θ ($\int_0^\pi d\theta\, W(\theta)=1$).

If one assumes a random distribution of jump lengths, $W(\theta)$ can be obtained by [27,28]

$$W(\theta) = \tfrac{1}{2}\left[1 + (2/\theta_o)^2\right] \sin\tfrac{1}{2}\theta \exp(-\theta/\theta_o) , \quad (2.90)$$

where θ_o is an average angular displacement. Inserting equation 2.90 into equation 2.89, the relaxation time becomes ($\theta_o \ll \pi$) :

$$\tau_\ell = \left[1 + \ell(\ell+1) D_r \tau_o\right]\left[\ell(\ell+1) D_r\right]^{-1} , \quad (2.91)$$

When $\tau_o \ll 1/D_r$, τ_ℓ of equation 2.91 reduces to the simple small angle diffusion equation given by equation 2.84. For large angular jumps, $\tau_o \gg 1/D_r$, and equation 2.91 reduces to $\tau_\ell = \tau_o$ (for all ℓ), τ_ℓ independent of ℓ in the large jump model limit.

(b) The inner frictional force $\mathfrak{f}$ shown in equation 2.44 obtained from Stokes' equation is based on a sphere of radius "a" rotating in liquids with sticking boundary condition. In reality, the molecular shape is in general not a sphere. Moreover, the sticking boundary condition assumed for the molecular motion in the liquid is not totally valid[8]. This modified the coefficient of the inner frictional force which changes the value of the relaxation time.

Moreover in most experiments, such as the dielectric relaxation, depolarized Rayleigh wing scattering, and optical Kerr effect, only one relaxation time is measured in most neat liquids. This single relaxation time in general corresponds to the average of some over-all rotational motion of the molecules[30]. For example, for molecules with C_{2v}

symmetry, such as nitrobenzene, the spectrum from the depolarized Rayleigh wing scattering consists of the sum of two Lorentzians. The intensity of these two Lorentzians depends on the polarizabilities and rotational diffusion coefficients about different molecular axes. The overall relaxation time is given by[30] :

$$\tau_o = (6\theta_s + 2\Delta)^{-1} ,$$

where $\theta_s = (1/3)(\theta_x + \theta_y + \theta_z)$, and

θ_i (i = x, y, or z) is the rotation diffusional coefficient about i-th axis, and $\tau_i = 1/6\theta_i$. Following Bauer et al[30], we obtain

$$\Delta = [(\theta_x - \theta_y)^2 + (\theta_z - \theta_y)x(\theta_z - \theta_x)]^{\frac{1}{2}}$$

Thus the reorientational relaxation time deduced from the depolarized Rayleigh scattering for such molecules depends on a combination of all three rotational diffusion coefficients.

In order to obtain information on the relxation mechanism of each individual axis, one needs to combine two or more experimental quantities. For example, the reorientational relaxation time from an individual axis can be obtained from the Raman linewidth and the spin lattic relaxation time[30] . In this research, we measured an weighted average relaxation time on rotational motion of overall axes of molecules.

In order to give an explicit analysis of the effect of these two factors (boundary conditions and weighted average) on the molecular reorientational relaxation time, one must consider the structure factors of the molecule [31]. The structure factors include three parameters : (1) the moment of inertia about each major axis (obtained from microwave experimental data)[32], (2) the axial ratio of each axis (from space-filling method)[33], and (3) a molecular radius (from the hard sphere radius). The difference in the magnitudes of the axial ratios in each molecule emphasizes the fact that the rotation about each major axis has a characterized steric hinderance. The weighing factors for rotation about each axis are defined by,

$$W_i = q_i^2 \left(\sum_i q_i^2 \right)^{-1} , \qquad (2.92)$$

where q_i denotes the deviation from sphericity of the molecule ($0 \leq q_i \leq 1$). From this argument and the the slip/sticky factor in equation 2.67. A modified Debye equation is given by[34],

$$\tau = (4\pi\eta a^3/3kT)\,\gamma , \qquad (2.93)$$

where γ is a dimensionless parameter which is proportional to the ratio of the mean square intermolecular torques to the square intermolecular forces (a measurement of the coupling between rotation and transition depending on the shape of molecules) and the weighing factor discussed in equation 2.92.

Therefore, the parameter γ is expressed by

$$\gamma = \sum_i W_i \, \theta(q_i) \quad , \qquad (2.94)$$

where $\theta(q_i)$ is the effective slip/sticky ratio[8] for the molecules giving rise to the relaxation. Some typical examples for the measured modified parameter γ in the Debye equation are $\gamma_{\text{nitrobenzene}} \lesssim 0.11^{(2e)}$, $\gamma_{\text{m-nitrotoluene}} \lesssim 0.11^{(2e)}$, and $\gamma_{\text{methyl iodide}} \lesssim 0.35^{(31)}$. In general, γ is small when q^2 is larger.

(c) In the Debye theory, there is no local field correction. In its derivation, Debye assumed that : (1) The internal field at a molecule was replaced by the average value of the internal field over the entire dielectric. and (2) The orientating field was taken to be equal to the internal field.

The first approach which introduce the local field correction to the relaxation equation was through the use of a generalized Lorentz type field : $E_L = E + 4\pi/3 \, P$. The Lorentz field assumed molecules filled up the entire space. For liquids with non-polar molecules and for most pure neat liquids, this assumption is close to reality[3]. Using the Lorentz field, the relaxation time ($\ell = 1$) in equation 2.45 is written by,

$$\tau_{Lorentz} = (\varepsilon_o + 2)/(\varepsilon_\infty + 2)\ \tau_o \quad , \qquad (2.95)$$

where ε_∞ and ε_o are the dielectric constant with high frequency field and static field, respectively; ε_∞ satisfies the Clausius-Mossotti equation and $\varepsilon_\infty = n^2$; where n is the index of refraction. And $\varepsilon_o = \alpha + u^2/3kT$. τ_o is defined in equation 2.45 (τ_{Debye}). For the Onsager theory, the local field was introduced into the Debye equation. This theory assumed : first, a molecule occupied a sphere of radius and its polarizability is isotropic; second, only long range dipole interactions are considered which treat the surroundings of a molecule as a continuum. By introducing a complex dielectric constant, the modified rotational relaxation time for($\ell = 1$) is :

$$\tau_{Onsager} = 3\varepsilon_o/(2\varepsilon_o + \varepsilon_\infty)\ \tau_o \quad , \qquad (2.96)$$

where ε_o and ε_∞ are complex constants.

For example, water has $\varepsilon_o = 81$, $\varepsilon_\infty = 1.8$[36], methanol has $\varepsilon_o = 32$, $\varepsilon_\infty = 1.9$[36], and ethanol has $\varepsilon_o = 26$, $\varepsilon_\infty = 1.85$[37]. By inserting these values into equations 2.95 and 2.96, τ_{On} obtains a better fit to the experimental results than $\tau_{Lorentz}$. Nevertheless, both values are larger than the measured relaxation time. Meanwhile, we still need the modification from the molecular structure factor. From the above modifications, the modified Debye equation only described a single particle rotational relaxation. A study of the pair correlation factor from a general stochastic point view is given in section 2.8.

2.6 Reorientational Relaxation Kinetics in Supercooled Liquids

When liquids are cooled down fast, there is no well defined temperature for freezing in most liquids. Below the melting temperature (which is a well defined temperature from solids to liquids), they still behave like liquids, and follow the simple definition of a liquid : " A liquid is a fluid which if placed in a closed vessel at once conforms to the shape of the vessel without necessary following the whole of its volume."[37,38] Such a liquid, characterized by a high value of viscosity and no definite freezing point is described as a supercooled liquid.

The relaxation mechanism of molecules in liquid has been discussed in sections 2.1 to 2.5. The viscosity of liquids depends on the molecular rotational and translational (free volume effect) motion. We will discuss some properties of liquids in the supercooled and glass regions.

When the temperature of a liquid is far above the temperature, there is less restriction for molecules to rotate internally. The rotationalmode is dominant. When the temperature cools down, there is less free rotational motion. The molecule is no longer able to align itself into the most favorable orientation for making a translational jump. It is possible that although a molecule has sufficient energy to jump, it may not be able to do so. Then the relaxation process of molecules can be decided by the probability that neighboring molecules have opened a sufficient hole to allow

the molecules to jump into it. This is the free volume theory discussed in equation 2.75.

In these two states, there is no well defined temperature from the liquid to the supercooled liquid region and no dramatic difference in the relaxation mechanism of molecules. When the liquid is cooled below the melting temperature, the reorientation effect gradually decreases in magnitude and the free volume effect dominates. The density of the liquid is inversely proportional to the temperature. The variation of specific volume (1/density) with temperature is shown in figure 2.3[33]. The specific volume is smoothly decrasing with the temperature in the liquid or supercooled liquid state. There is an empirical equation[7,16,39] for the density in these states by

$$\rho(T) = \rho_r[1 - a\,(T - 273.2)] \quad ,$$

where ρ_r is the density of a liquid at a reference temperature of 273.2 K, and a is a proportional constant in the order of 0.0005/degree K [39].

Other notations in figure 2.3 are defined below : T_o is a thermodynamic second-order transition temperature which is the fundamental reference temperature for the liquid state. Below T_o, the material would exist in the glass state, while T_g is the experimental glass transition temperature which depends on the rate of cooling. Due to the restriction of rotation mode and lack of the available free volume, it is assumed that there is essentially no orientational motion in the glass state.

The variation of the measured viscosity of liquids with temperature is shown in figure 2.4. In the liquid domain, the dependence of the viscosity in liquids shows an Arrhenius behavior varying as exp(E/RT). At the melting temperature, the behavior of viscosity becomes non-Arrhenius. This is due to the free volume. At the temperature T_g, the material is close to a rigid solid and the viscosity tends to be 10^{12} poises. This defines the glass region.

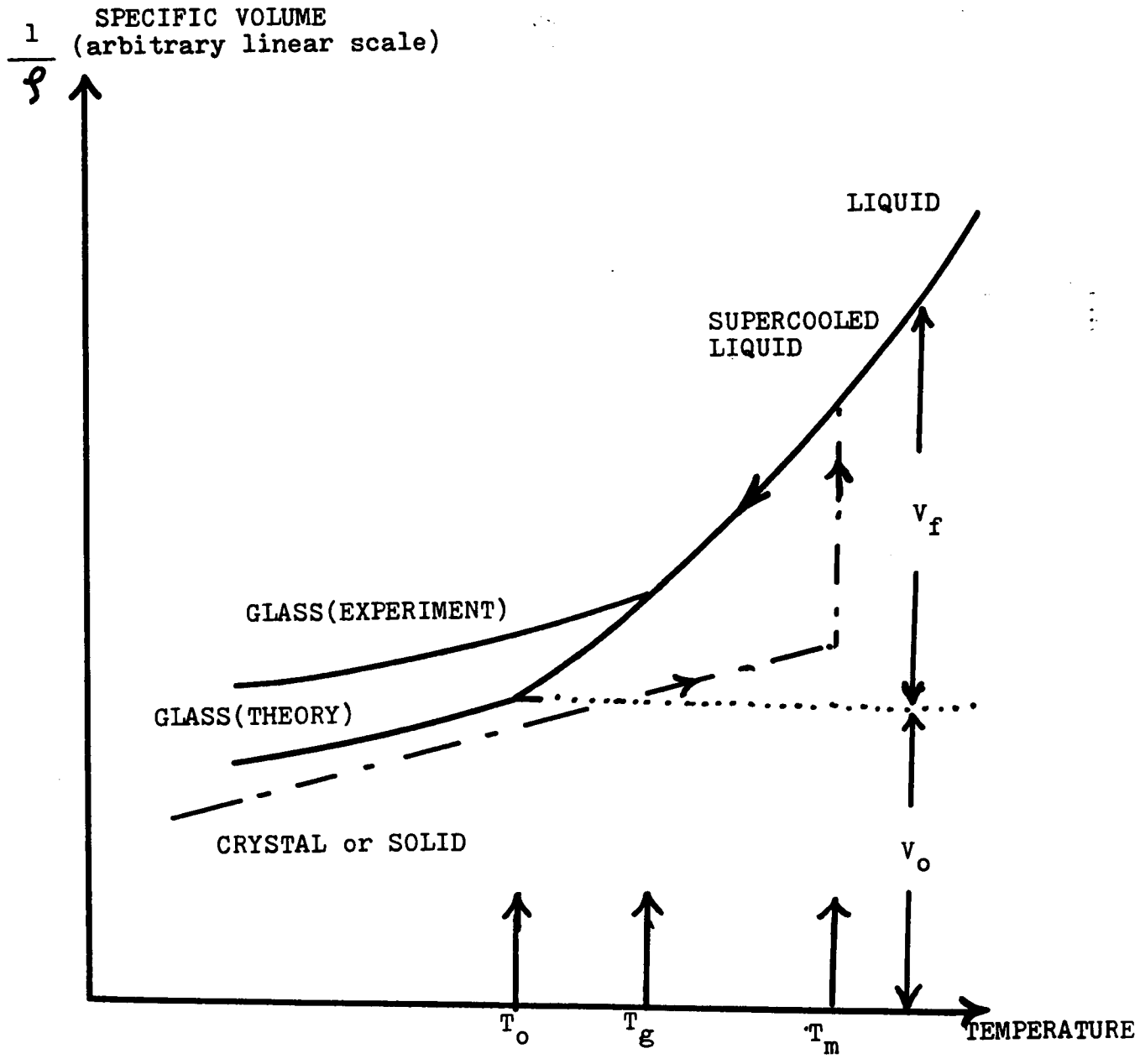

Figure 2.3 A Simple Diagram of the Variation of the Specific Volume of Molecule with Temperature

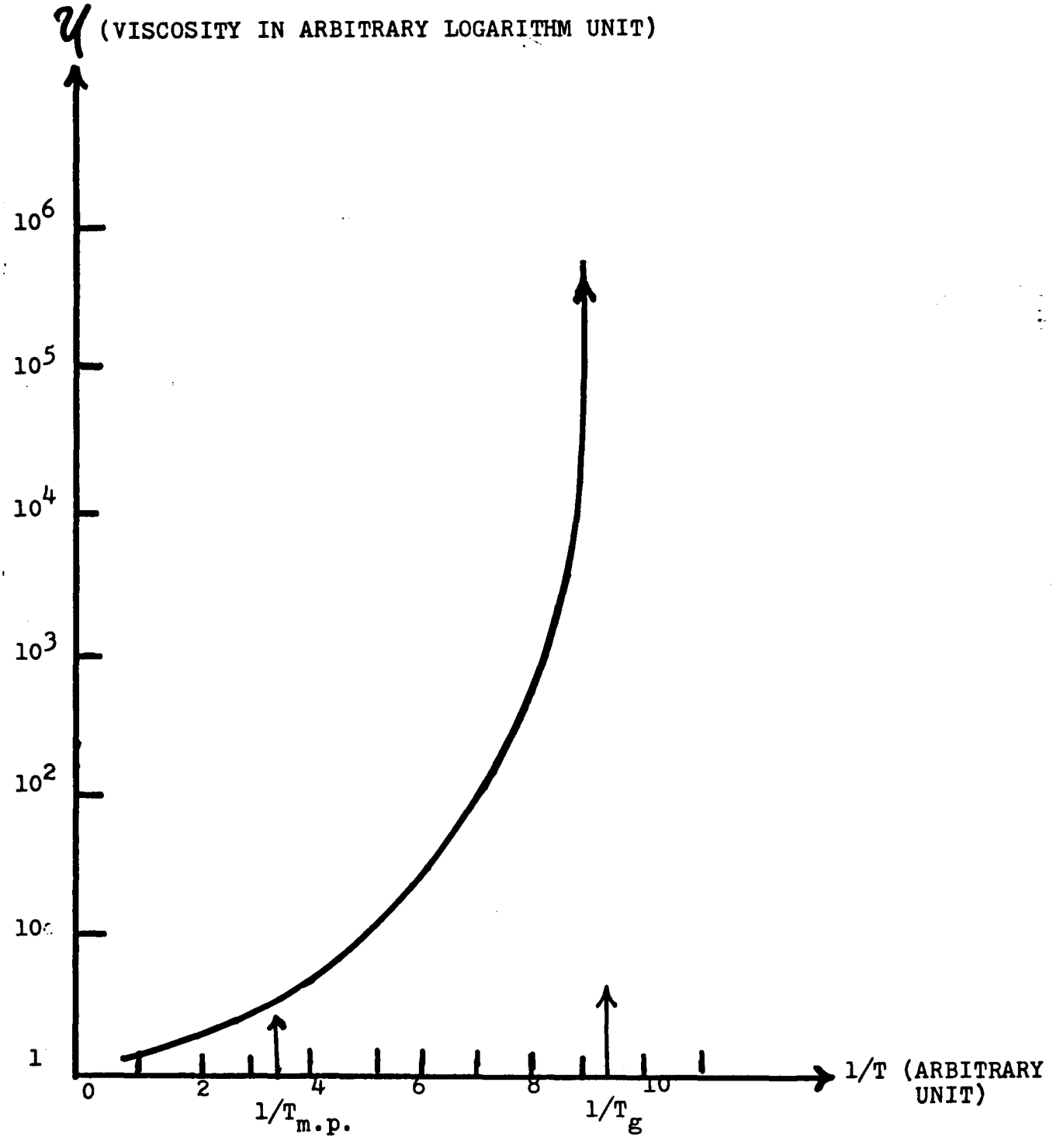

Figure 2.4 The Variation of Viscosity with the Inverse of Temperature

2.7 Reorientational Relaxation in Plastic Crystal

The discussions in the previous sections were concerned with the liquid or liquid-like state such as exists in supercooled liquids or glasses. In this section, we will give a brief description of the reorientational relaxation in solids.

In a liquid, when the temperature drops below the melting temperature of a liquid, the molecules start to crystalize and form a solid. In most substances, both the dielectric constant[40,41] and heat capacity[21,42] experience a sharp drop at the transition temperature from the liquid to solid state. These phenomena can be explained by the restriction of the rotational degrees of freedom in solids. The short-ranged reorientational relaxation is replaced by some regular long-ranged orientational or positional order. However, in some materials, a reorientational degree of freedom remains giving rise to a liquid-like behavior. The relaxation is still expected proportional to exp(E/RT). The reorientation in solids depends on the molecular shape. For spherical symmetrical molecules, such as methane (CH_4), or C_2Cl_6, the molecule can still freely rotate at a crystal site. Due to its wax-like appearance, this type of crystal is called a plastic crystal.

Plastic crystal is a crystal which has liquid-like properties. Its highly symmetrical shape allows most of the crystal to possess a cubic structure. Plastic crystals generally have two crystalline phases. Just below the melting temperature, they are still liquid-like with sufficient large

room to accommadate rotations. The structure of the plastic crystal is in general cubic (one exception is cyclopentane which is a hexagonal). When the temperature is lowered, the dielectric constant increases, and the heat capacity remains essentially constant. As the temperature decreases further, the plastic crystal reaches another phase transition. Now the crystal has a non-symmetrical shape such as triclinic or monoclinic, instead of being cubic. Some examples are given in table 2.1[29]. Below the second transition temperature, there is no evidence of rotational motion in the solid state. The dielectric constant and heat capacity are sharply reduced (see figure 2.6 shown in next page). In some cases, the molecule in the plastic crystal state is not spherical, their reorientational motion is attributed from the molecular isomerication. For example, the reorientational motion of the succinonitrile molecule is accounted for the gauche-trans isomerization.(see figure 2.5).

Table 2.1 Crystal Structures of Plastic Crystals

Substance	Crystal I (Plastic Phase)	Crystal II
CBr_4	cubic	monoclinic
C_2Cl_6	cubic	triclinic
Camphor-D	cubic	orthorhombic
D-Bromcamphor-α	cubic	monoclinic
succinonitrile	cubic ($T < 57^oC$)	monoclinic ($T < -42^oC$)

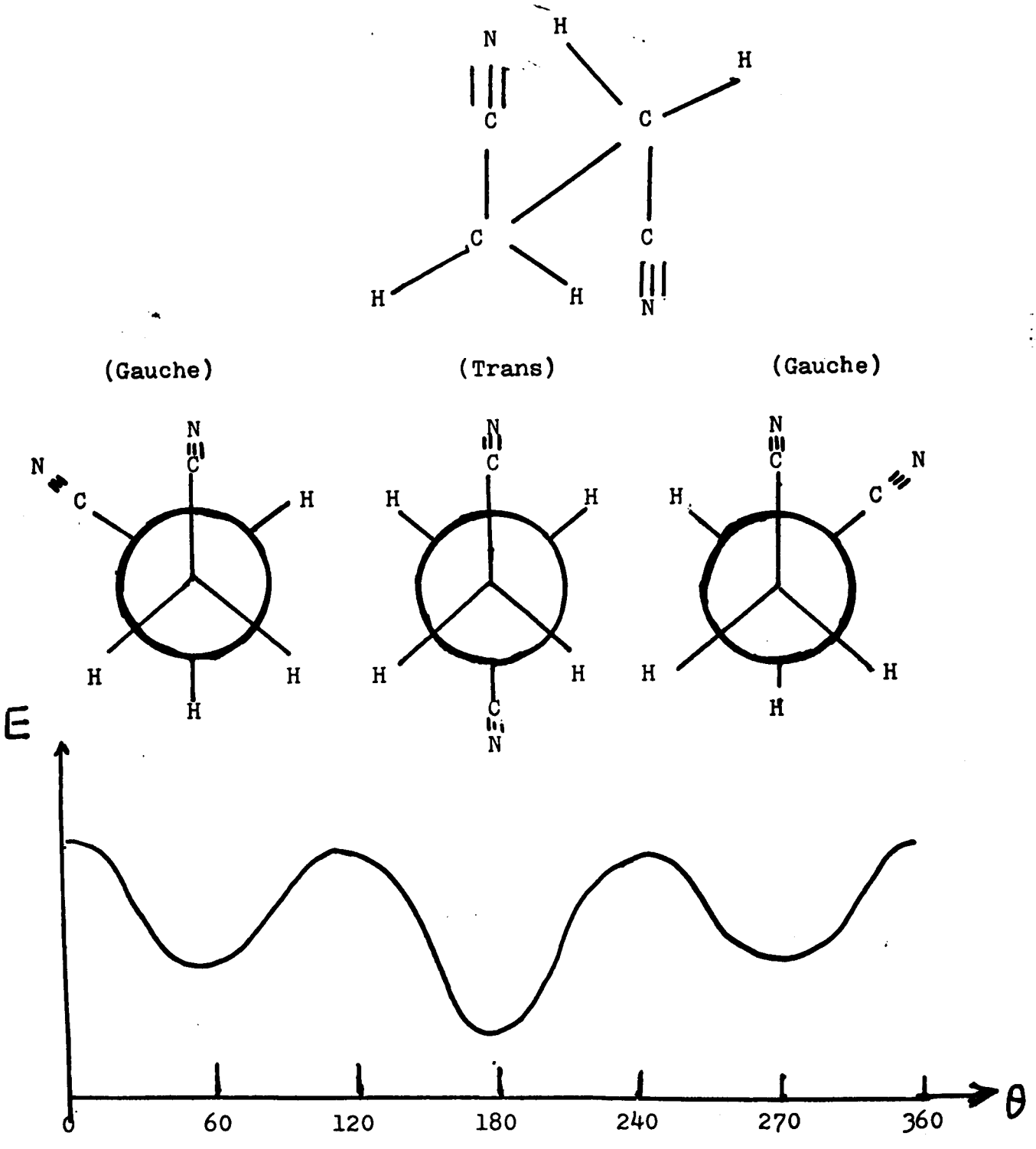

Figure 2.5 Gauche-Trans Isomerization for Succinonitrile

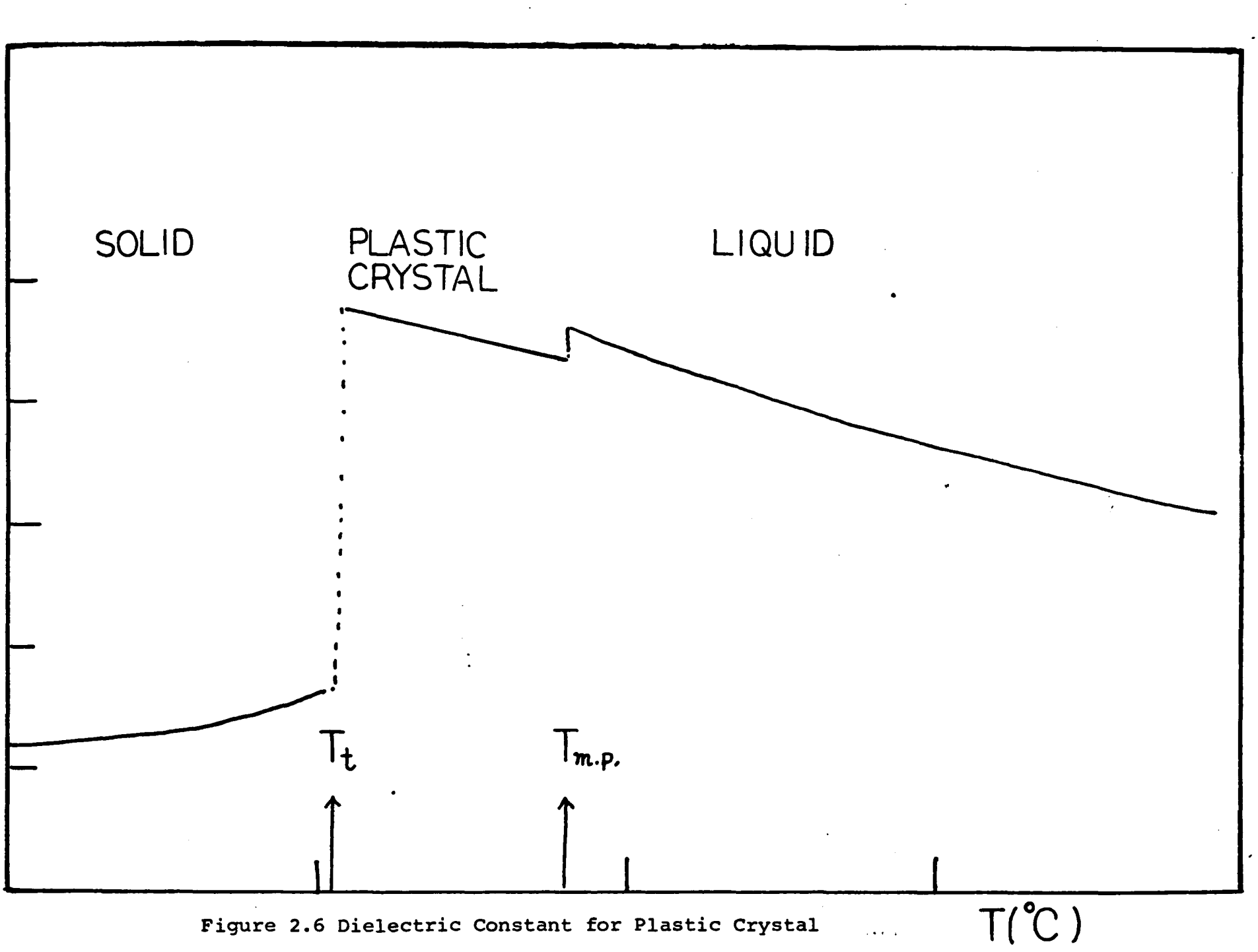

Figure 2.6 Dielectric Constant for Plastic Crystal

The phase chart of a normal substance can be classified into four categories (see figure 2.7) :

Figure 2.7a is a common case with three phase regions : gaseous, liquid(isotropic), and crystal(or solid)

In figure 2.7b, there is an extra phase of anisotropic liquid phase. For some long chain molecules with a prefered orientation axis known as liquid crystal, there is an additional anisotropic liquid phase.

Figure 2.7c indicates that under proper conditions of temperature and pressure, a substance can change phase from solid to gaseous without passing through the liquid phase. This is called sublimation and an example is dry ice.

In figure 2.7d, there are two phases in the solid state. The phase, above the transition temperature, is the plastic crystal phase where the molecules can rotate freely. Below the transition temperature, it is a solid where molecular rotation is restricted.

The diffusional model of molecular orientational relaxation in liquids is not appropriate in plastic crystals. Molecular reorientation in a crystal can be described by a one-molecular model[22,23,41] in which a representative molecule is restricted by a orientational potential energy with various minima formed by the interaction with its neighboring molecules. Debye[(1)] suggested a two-site model in which a molecular dipole could be aligned either parallel (site I) or anti-parallel (site 2) to an external field. Without an external field, these two sites are taken to be of identical probability P_{12} and P_{21} for transitions between them. By applying a constant field to the molecules, the energy is lowered by a parallel alignment of

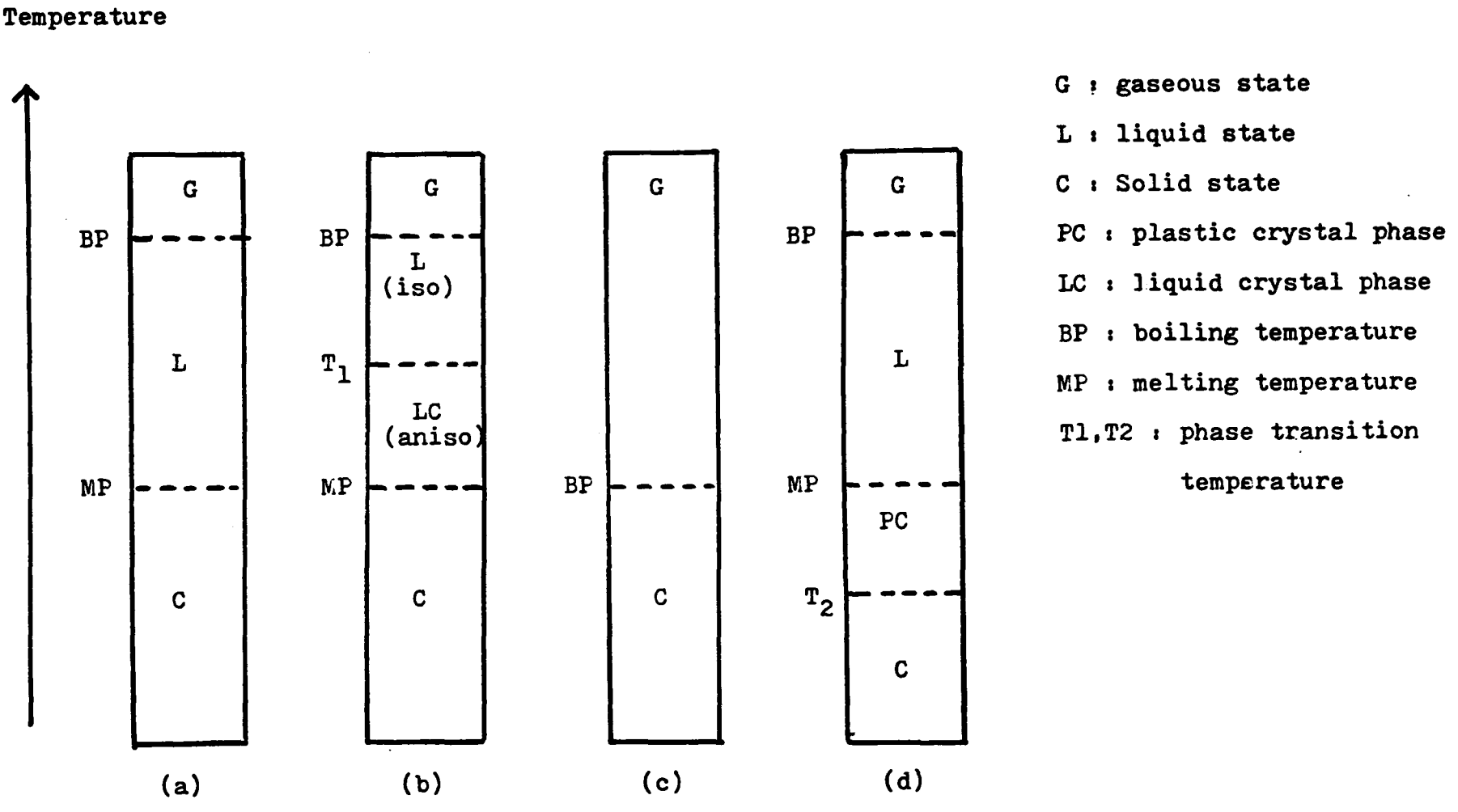

figure 2.7 Phase Diagram for Various Substances

the dipole moments and equilibrium is reached by a net excess of transition from site 2 to site 1. The reorientational relaxation time in solids has a similar temperature dependence as that in liquids and can be expressed by[43]:

$$\tau = A \exp(E/kT) \quad , \tag{2.97}$$

where E is a potential barrier.
A similar equation for a multiple barriers model and multiple relaxation times has also been derived by Hoffman[44].

A more complex "simple defect" model of orientational relaxation in solids was derived by Anderson[45]. This model is based on a completely jump of orientation in a one dimensional Markoff process. At any instant in time, all of the molecules in a hypothetical material can be found in either two distinct environments - state I, or state II. The molecule in either state is either oriented or not oriented. P_A , and P_C are the probabilities of having a molecule in state I and II, respectively, (but not oriented). P_B, P_D are the probabilities of having a molecule in state i and II, respectively (and has oriented). The rate equation for this relaxation model is :

$$\begin{aligned}
dP_A/dt &= -(k_1 + k_3)\, P_A + k_4 P_C \\
dP_B/dt &= k_1 P_A - k_3 P_C + k_4 P_D \\
dP_C/dt &= -(k_2 + k_4)\, P_C + k_3 P_A \\
dP_D/dt &= k_2 P_C - k_4 P_D + k_3 P_B
\end{aligned} \tag{2.98}$$

where the rate constant k_3 and k_4 describe changes between state I and II, and k_1 and k_2 are the decay rates of state I and II, respectively. By assuming the proper initial consitions[45],

the probability P_i can be solved by,

$$P_i = A_{+i} \exp(-\lambda_+ t) + A_{-i} \exp(-\lambda_- t) \quad , \quad (2.99)$$

where $i = A, B, C, D$ and $\lambda_{\pm}$ are the eigenvalues obtained from equation 2.98. $A_{\pm i}$ is determined by setting initial conditions. This is a simplified model for orientational relaxation kinetics in solids.

2.8 Mori's Theory[46]

In this section, we present a general theory to describe the transport, collective rotational motion and Brownian motion for a many-particle system from a unified statistical point of view. An exact description of the motion of molecules in liquids is not possible due to the large number of molecules involved. Mori's theory is derived by rewriting the equation of motion in a generalized form of the Langevin equation in a stochastic theory of Brownian motion. This is achieved by studying the average evolution of a non-equilibrium system or by calculating the linear response function due to a mechanical perturbation. A number of authors[34,47-50] have analyzed Mori's theory to interpret the rotational relaxation processes involved in light scattering[34,47,48] and spin relaxation[49,50]. In this section, a description of Mori's theory is outlined based on the interpretations by Kivelson and his coworkers[34,49].

For a Brownian particle (a particle large compared to the solvent molecules, discussed in section 2.1), an equation of motion (equation 2.7) can be written for times much larger than molecular times by,

$$m\, d\vec{v}/dt = \vec{f}(t) - \alpha\vec{v} + \vec{F}'(t)$$

The key point in Mori's theory of the generalized Langevin equation is the separation of the time scales involved in the motion into a slow time scale associated with the motion of Brownian particle and a fast time scale associated with the molecular motion. The theory has been used to study hydrodynamics and a variety of relaxation and transport phenomena. It represents a statistical mechanical approach to generalized hydrodynamics.

Mori chose a set of dynamical variables which he assumed to form a complete set. For example, the phase point of a liquid of classical molecules can be denoted by $\vec{X}$, which is a collection of all the positions ($\vec{r}$), and momentum ($\vec{p}$). The variables necessary to specify the state of the system : $\vec{X} = \{\vec{r}, \vec{p}\}$. In molecular fluids, $\vec{X}$ contains vibrational and angular orientation variables together with their conjugate momenta. Any dynamical variable of interest can be expressed as a function of $\vec{X}$ variables, e.g. the mass density at a point R is :

$$\rho(R, x) = \sum_i m_i \delta(r_{c_i} - R)$$

where m_i is the mass of the i-th molecules, r_{c_i} is the position of the center of mass of the i-th molecule, and denotes a three-dimensional Dirac delta function. The Hamiltonaian is also an important dynamical variable.

The dynamical variables $A_i(t)$ from the complete set can be represented as a column vector :

$$\vec{A}(t) = \begin{pmatrix} \vdots \\ A_i(t) \\ \vdots \end{pmatrix} . \qquad (2.100)$$

The variables, $\vec{A}(t)$, are always taken such that

$$\langle \vec{A}(t) \rangle = 0 , \qquad (2.101)$$

where the bracket, $\langle\ \rangle$, represents an equilibrium average. The $\vec{A}(t)$ describe a displacement from equilibrium. The projection operator, $\mathbb{P}$, is introduced which projects an arbitrary vector, $\vec{B}$, with the same dimensionality as $\vec{A}$ onto $\vec{A}$, that is

$$\mathbb{P}\, B \equiv \langle \vec{B}\, \vec{A}^{+} \rangle \cdot \langle \vec{A}\, \vec{A}^{+} \rangle^{-1} \vec{A} , \qquad (2.102)$$

where $\vec{A}^{+}$ is the adjoint of $\vec{A}$. In the appropriate Hilbert space, where the set of variables, $\vec{A}$, constitutes a complete set for slowly varying functions. Any function which is orthogonal to all the A_i's should vary rapidly. Thus for an arbitrary vector, $\vec{B}$, its orthogonal component

$(1-P)\vec{B}$, should consist only of rapidly varying terms. Since $\vec{B}$ has both a fast and a slow components, Mori's theory can be successful only if the set of slow varying variables $\vec{A}$ is indeed complete.

The "fast" and slow" function can be chosen as a relative fast and long relaxation process or the fast component as a primary process and the slow component as a secondary process.[48,53] In the molecular reorientational process, the fast mechanism is considered the molecular fluctuations or collisions between molecules and the slow mechanisms are considered the large angular rotation or a given time of molecular jump from one site to another.

The fundamental equation of motion in this theory is the generalized Langevin equation :

$$d\vec{A}(t)/dt = i\vec{\Omega}\cdot\vec{A}(t) - \int_0^t K(\tau)\,\vec{A}(t-\tau)\,d\tau + \vec{\alpha}(t_p) \quad , \quad (2.103)$$

where the time derivative and time dependence of $\vec{A}(t)$ can be expressed in terms of the Liouville operator, $\vec{L}$, of the Hamiltonian, H. In quantum mechanics, $\vec{L}$ is defined by,

$$iL\vec{D} = i/h\,[H,D] \quad , \quad (2.104)$$

where $\vec{D}$ is an arbitrary operator.

The equation of motion in terms of the linear operator L can be written by,

$$\dot{\vec{A}} = i\,L\,\vec{A} \quad , \quad (2.105)$$

$$\vec{A}(t) = e^{iLt}\,\vec{A} \quad , \quad (2.106)$$

$\vec{\Omega}$ is a set of oscillatory frequencies defined by

$$i\Omega \equiv \langle \dot{\vec{A}}\, \vec{A}^{+} \rangle \cdot \langle \vec{A}\, \vec{A}^{+} \rangle^{-1} \quad . \tag{2.107}$$

$\dot{\vec{\alpha}}$ represents the components of the time derivative of $\vec{A}$ which are orthogonal to $\vec{A}$, and are therfore rapidly varying, i.e.

$$\dot{\vec{\alpha}} \equiv (1 - iP)\, \dot{\vec{A}} \quad . \tag{2.108}$$

The time evolution of $\dot{\vec{\alpha}}(t_p)$ is determined by a propagator composed only of those components of the Hamiltonaian, H, which lies outside the subspace determined by the slow variables, i.e.

$$\dot{\vec{\alpha}}(t_p) \equiv \exp\left[t(1 - iP)\, i\, L \right] \dot{\vec{\alpha}} \quad , \tag{2.109}$$

and the subscript p of t_p indicates this projected time dependence : K(t) is a memory function matrix defined as

$$K(t) \equiv \langle \dot{\vec{\alpha}}(t_p)\, \dot{\vec{\alpha}}^{+} \rangle \langle \vec{A}\, \vec{A}^{+} \rangle^{-1} \quad . \tag{2.110}$$

The generalized Langevin equation (equation 2.103) is an identity valid only in the linear response limit, i.e. for small displacements from equilibrium. Therfore, one assigns to it a property similar to that of equation 2.101 :

$$\overline{\dot{\vec{\alpha}}(t_p)} = 0 \quad , \tag{2.111}$$

where the bar denotes an instaneous average in contrast to $\langle\ \rangle$, which indicates an equilibrium average. Assuming a linear response, we can obtain the general transport equation

$$d/dt\ \overline{\vec{A}(t)} = i\vec{\Omega} \cdot \overline{\vec{A}(t)} - \int_0^t K(\tau)\ \overline{\vec{A}(t-\tau)}\ d\tau \, , \tag{2.112}$$

from equation 2.103.

If the variable set $\vec{A}(t)$ is properly chosen to contain all slowly varing terms, then $\dot{\vec{\alpha}}(t_p)$ will be a rapidly varying

function of time, and the memory matrix function, K(t), should decay rapidly to zero.

Keyes and Kivelson[48] have applied Mori's theory to the light scattering for molecular orientational motion. They assumed the dynamical variable Q for the molecular orientational motion as

$$Q = \sum_j Q_j = \sum_j \sum_{m,n} C_{mn} D^{(\ell)}_{mn}(\theta_j, \phi_j, \lambda_j)\, e^{i\vec{k}\cdot\vec{r}_j} \quad , \qquad (2.113)$$

where the sum of j is over all N molecules of interest ; $D^{(\ell)}_{mn}$ is a igner rotation function of order ℓ ; C_{mn} is determined by the symmetry of the molecule; $\vec{r}_j$ is the position of the j-th molecule; and $\vec{k}$ is the propagation vector. The Q is an ordering parameter describing the angular momentum of molecular orientations. The angular function $(\theta_j, \phi_j, \lambda_j)$ of the Wigner or Clesch-Gordan rotation function determines the orientation.

If we assume the cause of the refractive index change for the optical Kerr effect is due to the molecular reorientation, then the relaxation mechanism for the optical Kerr effect depends upon both single and two particle correlations. The total Hamiltonian can be specified. For simplicity, it is assumed that correlation functions are the same for all N molecules. The single particle correlation function is

$$\langle Q_i\, Q_i(t)\rangle \equiv \langle Q_1\, Q_1(t)\rangle. \qquad \text{for all i from N molecules},$$

And the pair correlation functions for a molecule is

$$\langle Q_i\, Q_j(t)\rangle \equiv \langle Q_1\, Q_2(t)\rangle \ , \quad \text{for all i, j from N molecules and } i \neq j \ . \qquad (2.114)$$

where N is the number of molecules and $Q_i(t)$ is a function of the orientation of the i-th molecule at time t.

The correlation function from both single particle and two particles for N molecules in a solution is given by

$$\langle Q\, Q(t)\rangle \equiv \sum_{i}^{N} \langle Q_i\, Q_i(t)\rangle + \sum_{j}^{N} \sum_{\neq i}^{N} \langle Q_i\, Q_j(t)\rangle$$

$$= N\langle Q_1\, Q_1(t)\rangle + N(N-1)\langle Q_1\, Q_2(t)\rangle \quad . \quad (2.115)$$

The self and inter-molecular particle correlation functions for large N in depolarized light scattering was derived and expressed by Keyes and Kivelson[48] :

$$\langle Q_1\, Q_1(t)\rangle = \langle Q_1\, Q_1\rangle\, e^{-\dot{b}t} \quad , \quad (2.116)$$

and

$$\langle Q_1\, Q_2(t)\rangle = \langle Q_1\, Q_1\rangle \left\{ (1/N + f')\, e^{-\left[\dot{t}b(1+Ng')(1+Nf')^{-1}\right]} - 1/N\; e^{-bt} \right\} , \quad (2.117)$$

where $1/\dot{b}$ is the single particle relaxation time ($\cong \tau_{Debye}$), and f' and g' measure the strength of the static and dynamic pair correlation function, respectively. Substiting equations 2.116 and 2.117 into equation 2.115, one obtains the total relaxation function :

$$\langle Q(0)\, Q(t)\rangle / Q_1 Q_1 = (1+f'N)\, e^{-\left[\dot{b}(1+g'N)t(1+f'N)^{-1}\right]} . \quad (2.118)$$

where the relaxation time in depolarized Rayleigh wing scattering is given by $\tau_M = (1+g'N)(1+f'N)^{-1}\, \dot{b}^{-1}$. Equation 2.118 predicts only a single relaxation time for neat liquids in depolarized Rayleigh wing scattering even though the relaxation time depends on both single and two particle correlation functions. While in the nuclear magnetic resonance experiment

there is also only one relaxation time, but this relaxation time ($=1/\dot{b}$) is solely related to the single particle correlation function $\langle Q_i \; Q_i(t) \rangle$[51].

The ratio of the relaxation time between single particle correlation (from NMR) and multi-particle correlation experiments (DRS and OKE) is

$$\tau_M = (1 + f'N)(1 + g'N)^{-1} \tau_D \quad . \qquad (2.119)$$

For example, for a neat nitrobenzene solution, we have $g'N \simeq 0$ and $f'N = 1.3$[52]. and $\tau_M/\tau_D \simeq 2.3$.

Equation 2.119 is important in the study of molecular reorientational kinetics in a concentration dependent experiment.

Since $g'N \simeq 0$, in this research, we have use $\tau_o \backsim (1 + \lambda \; x)\, \tau_{Debye}$ for our data fitting, where $\lambda = f'N$ and $x \equiv N(x)/N_o$ is the mole fraction in mixed binary solutions.

References :

1. P. Debye, "Polar Molecules" (Dover, New York, 1946) .
2. (a) C.P. Smyth, "Molecular Relaxation Process" (Academic Press, New York, 1966) .
   (b) Jackson and Powles, Trans. Farad. Soc. 42A, 101, (1946).
   (c) D.R. Bauer, J.I. Brauman, and R. Pecora, J. Chem. Phys., 63,53, (1975) .
   (d) P.P. Ho and R.R. Alfano, J.Chem., Phys., 67, 1004, (1977) .
   (e) P.P. Ho and R.R. Alfano, Chem., Phys.Lett., 50,74, (1977).
3. E. Hatschek, "Viscosity of liquids" (D. Van Nostrand Co. New York, 1928) .
4. E.N. Andrade "Viscosity and plascity" (Chem. Pub. Co. Inc. New York, 1951).
5. Polymer Science Handbook (1972) .
6. F.W. Sears and M.W. Zmansky "University Phys." (Addison-Wesley Pub. Co. Inc. 1970) .
7. J. Frenkel "Kinetic Theory of liquids" (Oxford, 1946),
8. C.M. Hu and R. Zwanzig, J. Chem. Phys. 60, 4354, (1974).
9. D.R. Bauer, J.I. Brauman, and K. Pecora, J. Am. Chem. Soc. 96, 6840, (1974) .
10. W.H. Gibson and L.M. Jacob. Trans. Chem. Soc., 117,73, (1920),
11. E.N. Andrade, Phil. Mag. 17, 698, (1934).

12. H. Erying, J. Chem. Phys., 3, 107, (1933).

13. M.H. Cohen and D. Turnbull, J. Chem. Phys., 31, 1164, (1959).

14. P.B. Macedo and T.A. Litovitz, J. Chem. Phys., 42, 245, (1965).

15. A.K. Doolittle, J. Appl. Phys., 22, 1471, (1951).

16. A.J. Barlow, J. Lamb, and A.J. Martheson, Proc. Royal Soc. (London), A292, 322, (1966).

17. D.B. Davis and A.J. Matheson, J. Chem. Phys., 45, 1000, (1966).

18. G.J. Clark, J. Chem. Phys., 65, 1403, (1976).

19. S.G. Brush, Chem. Rev., 62, 513, (1962).

20. A.R. Derden and A.J. Matheson, Adv. Mol. Relax. Process, 2, 251, (1972).

21. J. Timmerman, J. Chem. Phys. and Solids, 18, 1, (1961).

22. R.H. Coles, "Progress in Dielectrics", 3, 49, (1961).

23. R.H. Coles, J. Chem. Phys., 42, 637, (1965).

24. C.J.F. Bottcher, "Theory of Polarization" (Elswier Pub. Co. New York, 1952).

25. W. Kauzman, Rev. Mod. Phys., 14, 12, (1942).

26. E.N. Ivanov, Sov. Phys. JETP, 18, 1041, (1964).

27. P.A. Egelstaff, J. Chem. Phys., 53. 2590, (1970).

28. D.A. Pinnow, S.J. Condau, and T.A. Litovitz., J. Chem. Phys., 49, 347, (1968).

29. D. Kivelson, M.G. Kivelson, and J. Oppenheim, J. Chem. Phys, 52, 1810, (1970).

30. D.R. Bauer, G.R. Alms, J.I. Brauman, and R. Pecora, J. Chem. Phys., 61, 2255, (1974).

31. M. Fury and J. Jonas, J. Chem. Phys., 65, 2206, (1976).

32. "Microwave Catalogue" Compiled by B. Starck, Uni. of Ulm, Dept. Spectroscopy and Structural Determination, West Germany.

33. H. Bassow, "Construction and Use of Atomic and Molecular Models" (Pergamon Press, New York, 1968).
"CPK Atomic model", The Ealing Corportion, Cambridge, MA.

34. S.J. Tsay and D. Kivelson, Mol. Phys., 19, 1, (1975).

35. (a) R.H. Coles, J. Chem. Phys., 6, 486, (1938).
(b) H.C. Bolton, J. Chem. Phys., 16, 486, (1948).

36. G. Baz, Physik Z., 40, 394, (1939).

37. D. J. Plazek and J.H. Magill, J. Chem. Phys., 45, 3038, (1960).

38. G. Harrison, "The Dynamic Properties of Supercooled Liquids", (Academic Press, New York, 1976).

39. H.J. parkhurst Jr. and J. Jonas, J. Chem.Phys., 63,2705,(1975).

40. C.P. Smyth, J. Phys. Chem. Solids, 18, 40, (1961).

41. C.P. Smyth, "Dielectric Behavior and Structure " (McGrew-Hill, New York, 1955).

42. L.A.K. Staveley, Ann. Rev. Phys. Chem., 13, 351, (1962).

43. H. Frohlich, "Theory of Dielectrics",(Oxford University Press, London, 1958).

44. J.D. Hoffman, J. Chem. Phys., 23, 1331, (1955).

45. J.E. Anderson, J. Chem. Phys., 47, 4879, (1967).

46. H. Mori, Prog. Theor. Phys. (Japan), 33, 423, (1965).

47. H.C. Anderson and R. Pecora, J. Chem. Phys.,54, 2584, (1971).

48. T. Keyes and D. Kivelson, J. Chem. Phys., 56, 1057, (1972).

49, D. Kivelson and K. Ogan, Adv. in Mag. Res., 7, 71, (1974).

50. J. T. Hynes and J.M. Dertch, "Mathematical Methods", (Academic Press, Physical Chemistry, V11, New York, 1970).

51. E. Zamir, N.D. Gershon, and A. Ben-Reuven, J. Chem. Phys., 55, 3397, (1971).

52. G.R. Alms, D.R. Bauer, J.I. Brauman, and R. Pecora, J. Chem. Phys., 59, 5310, (1973).

53. P. Lallemand, "Photon Correlation and Light Beat Spectroscopy", Ed. by H.Z. Cummins and E.R. Pike, (Plenum Press, 1973).

General Reference Books for Section 2.1

1. F. Reif, "Fundamental of Statistical and Thermal Physics"

2. J.F. Lee, F.W. Sears, and D.L. Trucoltte, "Statistical Thermodynamics", (Addison-Wesley Pub. Co. 1963).

3. C. Kittel, "Elementary Statistical Physics", (John Wiley and Sons Inc., New York, 1958).

4. L.D. Landau and E.M. Lifshitz, "Statistical Mechanics", (Pergamon Press, London, 1959).

CHAPTER 3

Reorientational Relaxation of Molecules in Mixed Binary Liquids

Debye's equation for the reorientation of a single particle in neat liquid is very successful in describing the relaxation time data[1]. Although many experimenters have attempted to fit the molecular reorientational in mixed liquids to the measured viscosity[2,3], their results are not totally consistent. In most of the cases, the relaxation time follow the measured viscosity[2] in accordance to Debye's equation. However, in a few cases, there is no definite relationship between these two measured quantities. It is interesting to find out whether or not the Debye relationship can be used to describe the relaxation time in mixed liquids. In section 3.1, we discuss semi-empirical laws for the measured viscosity in mixed binary liquids. The relationships between τ and η are discussed from different models - one based on semi-empitical relaxation and the second based on Mori's theory.

3.1 Viscosity of Mixed Liquids

There are various empirical equations[4] which describe the viscosity of a mixed solution. Each model expresses the measured viscosity of some mixed liquids in terms of viscosities of the components. At present, there is still no general equation which can completely describe experimental data of many systems. The simplest equation for the viscosity of a binary mixture is given by[5] :

$$\eta_m = x_A \eta_A + x_B \eta_B \quad , \qquad (3.1)$$

where η_m is the viscosity of the mixture, and η_A and η_B are the viscosities of the components A and B neat liquids, respectively; and x_A, x_B represent the fraction $(x_A+x_B=1)$ of the A and B component in the mixture. Different researchers have expressed x as either a volume fraction, weight fraction, or molar fraction.

Bingham[6] used an additive equation for fluidity (1/viscosity) in the mixture which is given by.

$$1/\eta_m = x_A/\eta_A + x_B/\eta_B \quad . \qquad (3.2)$$

While Arrhenius[7] proposed a purely empirical formula,

$$\eta_m = \eta_A^{x_A} \eta_B^{x_B} \quad . \qquad (3.3)$$

Another empirical law was suggested by Drickman[8],

$$\eta_m = \eta_B (\eta_A/\eta_B)^{x_A \epsilon/(\epsilon x_A + x_B)} \quad , \qquad (3.4)$$

with ϵ a fitting parameter.

Another model was used by Balazs[9] :

$$\ln \eta_m = x_A \ln \eta_A + x_B \ln \eta_B - \beta x_A x_B E_{AB}/kT \quad , \quad (3.5)$$

where E_{AB} is the activation energy associated with the transition between A and B species molecules in a mixed liquid. The form of equation 3.5 was based on the following assumptions :

1. The average number of closed neighbors is the same in pure liquids A and B and in their mixture AB, respectively.
2. The ratio of the free volumes of two pure liquids does not differ from unity by more than thirty percent.
3. The isothermal-isobar mixing of these two pure components proceeds without any molecular volume and free volume change.
4. The potential barrier is the sum of contributions from pairs of nearest neighbors.

This model is based on a structureless particle moving in a periodic field of force arising from the nearest neighbors. The field is the average over the nearest neighbor positions.

An important process that occurs in mixtures is the critical point. At this point, the density fluctuations of molecules in liquids is extremely large. At a certain temperature and certain concentration, these molecules in the mixed solutions appear to fuse together and form a cluster. The shear force in liquids is larger when molecules are grouping together. At this critical point, the measured viscosity of the mixture can increase by over one hundred times above its original value[10a]. For example, a mixture of stannic chloride ($SnCl_4$, $\eta \simeq$ 1 cp) and ethyl formate ($HCO_2CH_2CH_3$, $\eta \simeq$ 0.3 cp). at the critical point (30°C and 35% mole fraction of $SnCl_4$), the measured viscosity of this solution is $\eta \simeq$ 60 cp.

There is no definite equation to describe quantitatively of these phenomena. One of the equation to fit the measured viscosity at critical point is[4] :

$$\eta_m = \eta_A v_A (x_A'/x_A - \Delta x)^{C_A} + \eta_B v_B (x_B/x_B + \Delta x)^{C_B}, \quad (3.6)$$

where v_A, v_B are the volume fraction of the two component, with $v_A + v_B = 1$, and c_A, c_B are two components for fitting, Δx is the free volume of the mixture. The critical phenomena adds a complexity to understand the relaxation process in mixtures. In the present thesis research, I have avoided the critical point.

The viscosity for more than two species of molecules in a mixture have studied in the literature[11b]. However, this is beyond the scope of our present research and we will not consider it at this moment.

3.2 Hill's Theory of Molecular Reorientational Process in Mixed Binary Liquids

As mentioned in the beginning of this chapter, the measured reroientational relaxation time in mixed binary liquids can not be totally described by Debye's equation which is proportional to the measured viscosity. Debye's theory discusses the molecular rotational motion in pure liquids in which every molecule is surrounded by molecules of the same kind. Therefore, the interaction between these molecules determines both the viscosity and relaxation time in the liquids. However, in the case of a solute solution of a Kerr active solute in a Kerr non-active solvent, the relaxation time is determined almost entirely by the interaction between the solvent molecules and solute molecules. The viscosity of the solution,on the other hand, is determined almost by the interaction between solvent molecules. So there should not be a simple relationship between the measured viscosity and the relaxation time as describing by Debye's equation (equation 2.45). From numerous experiments, the viscosity dependence does not satisfactory follow the relaxation time. This is because the viscosity experienced by a solute molecule is not the measured viscosity. Applying the concept of a viscosity between the solute and the solvent, Hill[12] has sucessfully shown that the relaxation time of polar molecules in very dilute solution is directly proportional to the mutual viscosity. Hill's model is based on the Andrade theory[13] of viscosity. The following is a review of the Hill theory.

The shear stress is from the momentum transfer of molecules in liquids. Due to collisions between adjacent molecules, this momentum transfer occurs in a viscous liquid between layers moving with different velocities. The viscosity of neat liquids is defined in section 2.3 by,

$$\eta = 1/3\ C\ \nu\ m/\sigma \qquad (3.7)$$

The viscosity in binary mixture is from the momentum transfer due to their different types of collisions[12], which can be represented as CC, BB, and CB, where B is a solute molecules and C is a solvent molecules. The first type (CC) which occurs $1/3\ x_C^2 P_C\ 2\nu_C/\sigma_m^2$ times per second per unit area, and cause a momentum transfer $\frac{1}{2}m_C\ \delta v$ each time, where δv is the drift velocity. This contribution to the shear stress is,

$$1/3\ x_C^2\ (P_C \nu_C\ \ m_C/\sigma_m^2)\ \delta v \qquad (8a)$$

Similary, the second type (BB) collisions contributes a shear stress of,

$$1/3\ x_B^2\ (P_B \nu_B\ m_B/\sigma_m^2)\ \delta v\ . \qquad (8b)$$

The third type (CB) of collisions occur $2/3\ x_C x_B C_{CB} (\nu_C+\nu_B)/\sigma_m^2$ times per second per unit area, and cause a momentum transfer $m_C m_B/(m_C+m_B)\ \delta v$ each time, thus contributing a shear stress of

$$1/3\ 2\ x_C x_B C_{CB} m_C m_B/(m_C+m_B) \cdot (\nu_C+\nu_B)/\sigma_m^2\ \ \delta v\ . \qquad (8c)$$

The total shearing stress is,

$$\left\{x_C\, C_C \nu_C m_C/3\sigma_m^2 + x_B C_B \nu_B m_B/3\sigma_m^2 + 2\, x_C x_B\, C_{CB}(\nu_C+\nu_B) m_C m_B/3\sigma_m^2 (m_C+m_B)\right\}\delta v \tag{3.9}$$

Comparing equations 3.7 and 3.9, the viscosity in mixed binary solution is,

$$\eta_m = x_C^2 \eta_C \sigma_C/\sigma_m + x_B^2 \eta_B \sigma_B/\sigma_m + 2\, x_C x_B\, \eta_{CB}\, \sigma_{CB}/\sigma_m, \tag{3.10}$$

where η_C and η_B are the viscosities of the pure liquids C and B, respectively. The mutual viscosity η_{CB} is defined by,

$$\eta_{CB} \equiv 1/3\, C_{CB}\, (\nu_C+\nu_B)/\sigma_{CB} \cdot m_C m_B/(m_C+m_B), \tag{3.11}$$

where σ_{CB} is the mean distance between a molecules of type C and anadjacent molecule of type B in the mixture ($\sigma_{CB}=[\sigma_C+\sigma_B]/2$).

If the orientational relaxation time measured in a mixed liquid is assumed to arise from the solute molecules only; then the resistance force which causes the angular momentum transfer is only from two types of collisional induced momentum transfers, BB and CB types. Hill followed the analysis of Debye's theory to arrive at the relaxation of the solute molecules in a mixture;

$$\tau = 1/2kT\, \left[x_C\, 6\chi^2 \sigma_{CB}\, \eta_{CB} + x_B(3-2^{\frac{1}{2}})\, 3\, (P_B'/P_B)\, \chi_B^2 \sigma_B \eta_B\right], \tag{3.12}$$

where $\chi^2 \equiv (I_{CB}+I_B)/I_{CB}I_B\ (m_C+m_B)/m_C m_B$.

and I_B is the momentum of inertial of the solute molecule B around its center of mass, and I_{CB} is the momentum of inertia of the solvent molecule C about the center of mass of B molecules, at the instant of collisions. P_B and P_B' are the probability of collisions for B molecules in the absence and presence

of an external field, respectively. P'_B/P_B is found to close to 1[13b].

However, in deriving equation 3.12, Hill only considered a single particle reorientational motion. She did not include the collective mode of molecules in liquid (see section 2.8). Following the discussions of Keyes and Kivelson[16], we empirically introduced a pair correlation term into equation 3.12. A general phenomenalogical expression for relaxation time in mixed binary liquids can be expressed as[3d] :

$$\tau = c_1(a_B) f(x) \gamma_B x + c_2(a_{CB}) \gamma_{CB} (1-x) , \quad (3.13)$$

where x denotes the mole fraction of the solute B component in the solution, $c_1(a_B)$ and $c_2(a_{CB})$ account for the variation in molecular sizes in solution and are dependent on the details of the collisional process (a special form of c's is shown in reference 12). The expression f(x) is specifically inserted to account for the pair correlative effect among the solute molecules. The pair correlative effect between solute and solvent is assumed to be zero. To the first order, f(x) can be approximately as $1 + \lambda x$[16]. As the solute concentration x reduces to zero, the pair correlation factor f(x) clearly approaches one. Equation 3.13 can be written in two adjustable parameters as :

$$\tau = C^* [(1 + \lambda x) x \gamma_B + G (1 - x) \gamma_{CB}] , \quad (3.14)$$

in which $G = c_2/c_1$ is a number not far one, depending on the sizes of the molecules and the correlation between dissimilar molecules. The parameters C* and λ are numerically determined by measuring τ as function of x. The value of γ_{CB} is

determined from the viscosity measurement of equation 3.10. The parameter C* is a measure of the rate of change of the relaxation time with respect to the viscosity at a given temperature; and the parameter λ is a measure of correlation among solute molecules.

The temperature dependent equation for the measured viscosity in mixed binary equation of the Hill model is given by :

$$\eta_m(T) = \frac{x^2}{\sigma_m}\,\sigma_B\,\eta_B(T) + \frac{2x(1-x)}{\sigma_m}\,\sigma_{CB}\,\eta_{CB}(T) + \frac{(1-x)^2}{\sigma_m}\,\sigma_C\,\eta_C(T)\ , \qquad (3.15)$$

where $\eta_B(T) \propto T \exp(E_B/RT)$, (3.16)

and $\eta_{CB}(T) \propto T \exp(E_{CB}/RT)$. (3.17)

Equation 3.17 is discussed in detail by Balazs[9].

From equations 3.14 and 3.15, the temperature dependence of the molecular reorientational relaxation time in a binary liquid is given by[3e] :

$$\tau(T) = C^*/T\ [\,(1 + \lambda x)\ x\ \eta_B(T) + (1 - x)\,\eta_{BA}(T)\,]. \qquad (3.18)$$

The temperature dependence of the Kerr experimental data will be fitted to equation 3.18 in section 2 of chapter 6. These are still empirical equations for τ in mixed liquids.

3.3 Mori-Keyes-Kivelson-Tsay's Theory for Molecular Reorientational Relaxation in Mixed Binary Liquids

In Hill's theory[12] of mixed binary liquids, the measured reorientational relaxation time is accounted for the reorientation of solute molecule about its own axis and about its center of mass. In fact, besides the relaxation process of the solute molecules alone, there should be some kind of coupled resistive forces acting between the solute-solvent molecules which result in a rotation of solvent molecules. In this coupling, it is assumed that there is more than a single relaxation process involved[14,16]. In this section, we discuss the relaxation kinetics of coupled solute and solvent molecules. The theory is based on the fundamental statistical mechanics and projection operators.

From Mori's analysis, the complete set of basis functions for a mixed liquid with two different molecules (species B and C) is represented by

$$\vec{A} = (\vec{A}_B , \vec{A}_C) \quad , \qquad (3.19)$$

where $\vec{A}_B = \sum_i A_{B_i}$,

and $\vec{A}_C = \sum_i A_{C_j}$.

(A_{B_i} , A_{C_j}) are appropriate real linear combination of the second rank wigner rotation functions for molecule i of species B and molecule j of species C, respectively. It is assumed that all the relevent "slow" motions of the liquid can be completely described in a Hilbert subspace. For example. the measured reorientational relaxation time (slow) in neat liquid B is τ_B(due to the interactions BB) and in neat liquid C

is τ_C(due to the interaction CC). The measured relaxtion times in the B and C mixed solution will depend on a complete basis functions by BB, BC, CB, CC interactions. This is a coupled system.

In we can find a complete set of basis functions, then for an arbitrary function G(t) with those parts of G(t) can be described within the "slow" Hilbert subspace are slowly varying functions; whereas those parts of G(t) that lie outside this subspace are rapidly varying functions. The projection operator P, which projects the function G(t) onto the slow subspace is defined in equation 2.102 of section 2.8. PG(t) is a slowly varying function while (1-P)G(t) is a rapidly varying function. The function G(t) is defined by

$$G(t) \equiv P\,G(t) + (1-P)\,G(t)$$
$$\equiv Z(t)\,G(0) + G'(t)\ , \qquad (3.20)$$

where Z(t) describes the time evolution of the projection of G(t). An explicitly form of the time evolution of the slow component of G(t) is written by,

$$P\,G(t) \equiv (\,G(t),\,A^*\,)/(\,A,\,A^*)\;A(0), \qquad (3.21)$$

While the rapidly random fluctuation is given by

$$G'(t) \equiv (1-P)\,G(t)\ . \qquad (3.22)$$

The above descriptions are based on Mori's theory which solves the relaxation phenomena by separating the time scales into two components - fast and slow.

The general Langevin equation (equation 2.112) in the linear response region is,

$$\overline{dG(t)/dt} = i\Omega\cdot\overline{G(t)} - \int_0^t d\tau \; K(\tau)\cdot\overline{G(t-\tau)} \quad , \quad (3.23)$$

where $i\Omega$ and $K(\tau)$ are defined in equation 2.108 and 2.110, respectively.

We carefully choose the slow variable functions of A (equation 3.19), such that A consitutes a complete set of functions in the "slow" Hilbert subspace. That is $\overline{G(t)} = A(t)$ and is a slow functions. This assumption (A is a complete set of slow functions) is equivalent to assume the reorientation of molecules arises from rotational diffusion[20]. In this model, the molecules reoriented by means of free classical rotations : the molecules undergo frequent intermolecular collisions of short durations and their angular momentum are randomized by the impulsive torques associated with the collisions. The rapid motion is by the collisions between molecules, and the slow motion is the molecular reorientation.

Moreover, the frequency matrix Ω represents a fast oscillating or precessing contributions[19] from a chosen set of slow variables A(t). That is, $A(t) \propto \exp(-i\Omega t)\, A'(t)$, where A(t) and A'(t) are slowly varying and Ω is a rapidly varying quantities. In the light scattering and the optical Kerr effect, it is assumed there is no oscillatory effect.[16] Therefore, Ω vanishes,

In addition, since A(t) is a complete set of slow functions, and K(t) is a rapidly function, we can replace A(t-τ) in the equation of motion (3.23) by A(t), and replace the upper limit of integration by $t \to \infty$.

From these approximations, equation 3.23 is rewritten by[19],

$$dA(t)/dt = - \int_0^\infty K(\tau)\, d\tau\, A(t) \quad . \qquad (3.24)$$

The fourier spectrum of K(t) is defined by,

$$K(w) = \int_0^\infty K(t)\, e^{iwt}\, dt \quad , \qquad (3.25)$$

When the variable set A is a complete set of slow variables, then K(w) is approximately independent of frequency. Therefore, we can take w to be an arbitrary number. By taking w = 0, the memory function function matrix K(w) is set equal to K(0)[14]. We define

$$\mathcal{F}^{-1} = K(0) = \int_0^\infty K(\tau)\, d\tau \quad , \qquad (3.26)$$

And the equation of motion from equation 3.24 is replaced by,

$$dA(t)/dt = \mathcal{F}^{-1} A(t) \quad . \qquad (3.27)$$

We now write the equation of motion of the molecular reorientational relaxation for a two-component liquid. There are two variables A_B and A_C in the binary system. The complete basis functions A(t) that chosen for the relaxation process is a 2 x 2 matrices constructed by the variables A_B and A_C. Their relaxation times are coupled and depend on the original relaxation times and the strength of the

interactions between the different species of molecules. From equation 3.27, the transport equation for coupled two-component liquids is derived by[15,16,19]

$$d/dt\begin{bmatrix} \langle A_B(t)A_B^+(0)\rangle & \langle A_B(t)A_C^+(0)\rangle \\ \langle A_C(t)A_B^+(0)\rangle & \langle A_C(t)A_C^+(0)\rangle \end{bmatrix} = \mathcal{F}^{-1}\begin{bmatrix} \langle A_B(t)A_B^+(0)\rangle & \langle A_C(t)A_B^+(0)\rangle \\ \langle A_C(t)A_B^+(t)\rangle & \langle A_C(t)A_C^+(0)\rangle \end{bmatrix} \tag{3.28}$$

where $\langle A_i(t)A_j^+(0)\rangle$ for i, j = B or C, is the correlation function corresponding to the two coupled variables.

A matrix form of $\mathcal{F}$ was explicitly derived by Keyes and Kivelson[16] and Kivelson and Tsay[14]. The coupled reorientational relaxation rates T_+^{-1} for mixed binary liquid is (the notation

$$2\,T_{\pm}^{-1} = (\,K_{BB} + K_{CC}\,) \pm \left[(\,K_{BB} - K_{CC}\,)^2 + 4\,K_{BC}\,K_{CB}\right]^{\frac{1}{2}}, \tag{3.29}$$

where K_{ij} is a matrix element of the relaxation matrix K in Mori's transport equation. The subscripts B and C denote the Kerr active solute molecules and Kerr non-active solvent molecules, respectively. The time T_+ and T_- are the relaxation times for the coupled orientational mode of the system. In this paper, T_+ is chosen to be the fast component and T_- is chosen to be the slow component. The matrix element K_{ij} are defined as follows :

$$K_{BB} = (\,\tau_{BB}^{-1} - \phi^2\tau_{BC}^{-1}\,)\,(\,1-\phi^2\,)^{-1}, \tag{3.30a}$$

$$K_{CC} = (\,\tau_{CC}^{-1} - \phi^2\tau_{CB}^{-1}\,)\,(\,1-\phi^2\,)^{-1}, \tag{3.30b}$$

$$K_{CB} = (\,-\tau_{CC}^{-1} + \phi^2\tau_{CB}^{-1}\,)\,(\,1-\phi^2\,)^{-1}\,e^{-1}\phi, \tag{3.30c}$$

and $$K_{BC} = (\,-\tau_{BB}^{-1} + \phi^2\tau_{BC}^{-1}\,)\,(\,1-\phi^2\,)^{-1}\,e\,\phi\,. \tag{3.30d}$$

where e is a factor depending on the concentration, and Φ is the interspecies coupling parameter. These parameters are defined by,

$$e^2 = x_B (1 + x_B f_{BB}) \left[x_C (1 + x_C f_{CC})\right]^{-1} , \qquad (3.31)$$

and $$\Phi^2 = x_B x_C f_{BC}^2 (1 + x_B f_{BB})^{-1} (1 + x_C f_{CC})^{-1} . \qquad (3.32)$$

The multi-particle correlation times are expressed by,

$$\tau_{ii}^{-1} = \tau_i^{-1} (1 + x_i g_{ii}) (1 + x_i f_{ii})^{-1} , \qquad (3.33)$$

and $$\tau_{ij}^{-1} = (\tau_B \tau_C)^{-\frac{1}{2}} g_{ij}/f_{ij} \qquad (i \neq j) , \qquad (3.34)$$

where all quantities are real, x_i is the mole fraction of the i-th kind of molecules in the mixture ($x_B + x_C = 1$), f_{ij} is the static pair correlation factor which measures the orientational correlation between neighboring molecules and is assumed to be concentration independent[16,17]. The normalized molecular correlation factors f_{BB}, f_{CC}, and f_{BC} are defined by

$$f_{BB} = N \langle A_{B_j}, A_{B_j} \rangle / \langle A_{B_i}, A_{B_i} \rangle ,$$

$$f_{CC} = N \langle A_{C_i}, A_{C_i} \rangle / \langle A_{C_i}, A_{C_i} \rangle ,$$

and $$f_{BC} = N \langle A_{B_i}, A_{C_j} \rangle / \left[\langle A_{B_i}, A_{B_i} \rangle \langle A_{C_j}, A_{C_j} \rangle\right]^{\frac{1}{2}} , \qquad (3.35)$$

where N equal to the number of molecules, and $i \neq j$ in these expressions.

The factor g_{ij} in equation 3.33 is the dynamic pair correlation factor[16] which measures the time evolution of the angular velocity of a molecule relative to that of a neighboring molecule. It is defined by :

$$g_{BB} = N \tau_B \int_o^\infty dt \ \langle e^{i(1-P)L\ t}\ \dot{A}_{B_i},\ \dot{A}_{B_j}\rangle / \langle A_{B_i},\ A_{B_j}\rangle \ ,$$

$$\text{and } g_{BC} = N (\tau_B\ \tau_C)^{\frac{1}{2}} \int_o^\infty dt \langle e^{i(1-P)L\ t}\ \dot{A}_{B_i}, \dot{A}_{C_j}\rangle / \left[\langle A_{B_i}, A_{B_i}\rangle \langle A_{C_j}, A_{C_j}\rangle\right]^{\frac{1}{2}} . \tag{3.36}$$

where τ_i is the single particle reorientational time for i-th type of molecules (i = B or C), τ_B is defined by

$$\tau_B^{-1} = \int_o^\infty dt \ \langle e^{i(1-P)L\ t}\ \dot{A}_{B_i},\ \dot{A}_{B_i}\rangle / \langle A_{B_i},\ A_{B_i}\rangle \ . \tag{3.37}$$

The same analogous relationships hold for τ_{CC}, τ_{CB}, τ_C, g_{CC}, g_{CB}.

The single particle reorientational time τ_i is proportional to the viscosity of the neat liquid of i-th kind of molecules and is possible linearly dependent on the concentration[3d,14,16]. The relaxation time τ_i can be written by[18] :

$$\tau_i = m_i\ x_i + p_i \ , \tag{3.38}$$

where m_i is a parameter proportional to the viscosity of neat liquids of i species and p_i is a parameter related to the internal free rotator time of these molecules[18]. From previous measurements and arguments[3d,14,16,18], g_{ij} is generally small, on the order of zero. In order to simplify our calculation and obtain reasonable data fitting, we have assumed $g_{ij} = 0$ for all i, j = B or C.

Substituting equation 3.30 into equation 3.29, with the assumption $\tau_{ij}^{-1} \propto g_{ij} = 0$, and these defined values for the matrix elements K_{ij}. The equation for the two-component relaxation time that is used in this research to fit the data is reduced to :

$$T_{\pm} = \tfrac{1}{2}(1-\phi^2)^{-1}\left\{\left[\tau_B^{-1}(1 + x_B f_{BB})^{-1} + \tau_C^{-1}(1 + x_C f_{CC})^{-1}\right]\right.$$

$$\left. \pm \left[(\tau_B^{-1}(1 + x_B f_{BB})^{-1} \tau^{-1}(1 + x_C f_{CC})^{-1}) + 4\tau_{BB}^{-1}\tau_{CC}^{-1}\phi\right]\right\}. \qquad (3.39)$$

The theoretical model presented in the beginning of this section indicates that there is always a two-component decay in a mixed binary liquid. A simple diagram to interpret the coupled two-component relaxation times of equation 3.39 is shown in figure 3.1. The relaxation time for the B (solute) and for the C (solvent) components are chosen to be comparable in size. The assumed parameters are given by :

$$\tau_{BB}(x) = (15\, x_B + 5)(1 + 1.5\, x_B) ,$$

and $$\tau_{CC}(x) = (15\, x_C + 5)(1 + 1.5\, x_C) , \qquad (3.40)$$

where $x_B + x_C = 1$, and $f_{BB} = f_{CC} = 1.5$.

Various values are used for the interspecies pair correlation factor, f_{BC}, to calculate the coupled two-component reorientational relaxation times $T_{\pm}$. For $f_{BC} = 0$, there is no coupling term, the relaxation process is described by the uncoupled relaxation times $\tau_{BB}(x)$ and $\tau_{CC}(x)$. As f_{BC} is increased, the curve for the coupled relaxation times $T_{\pm}$ versus x_B starts to separate from the curves for the uncoupled relaxation times $\tau_{BB}(x)$ and $\tau_{CC}(x)$. The relaxation kinetics is mixed. For a given concentration of the solution, there are a two relaxation times in the relaxation kinetics - a fast and a slow decay times. The size of the signal associates with these two relaxation components depend on the strength of the Kerr constants of the mixed liquid. We will discuss this in detail in section 3 of chapter 6.

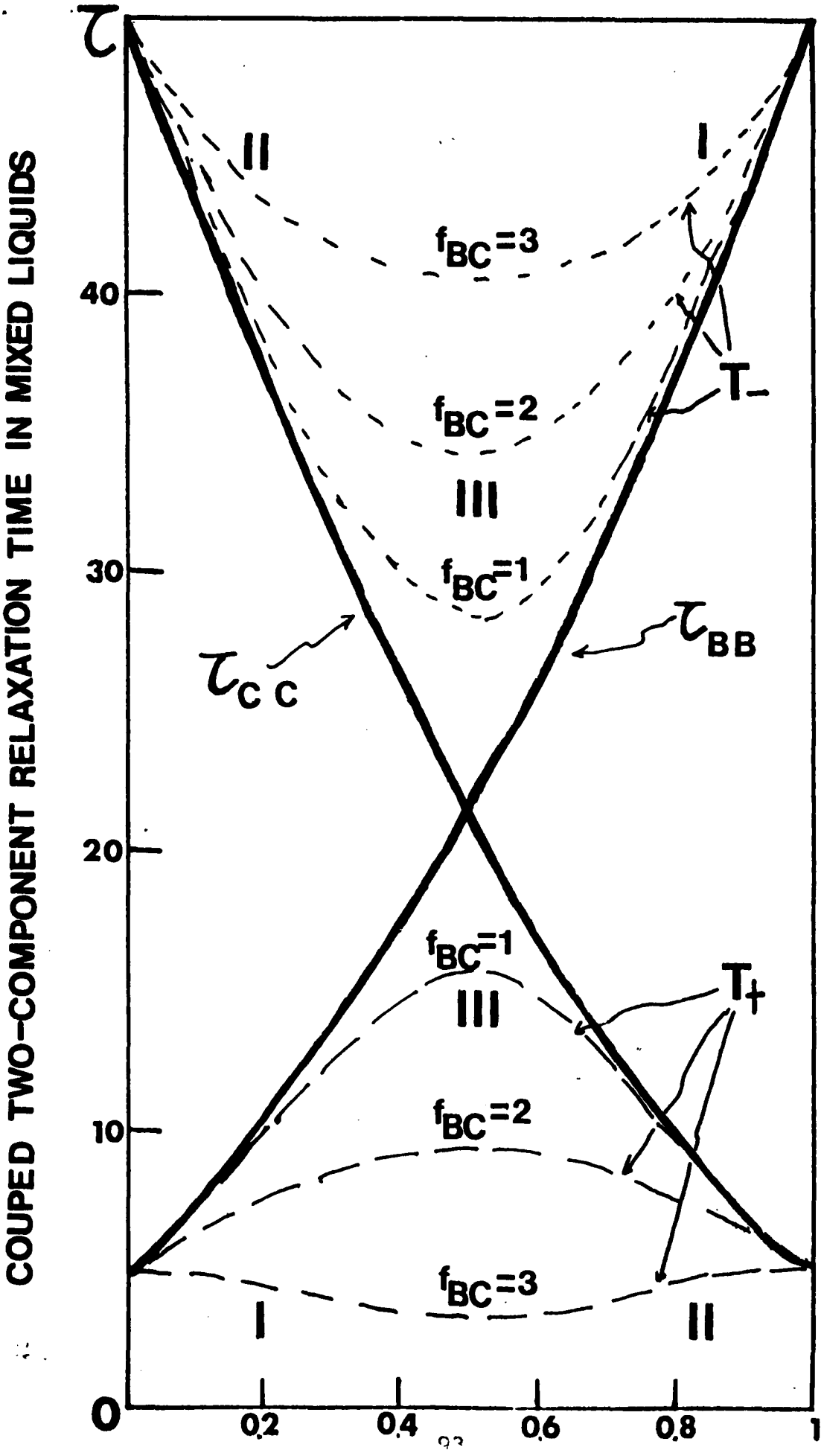
COUPED TWO-COMPONENT RELAXATION TIME IN MIXED LIQUIDS
τ
40
30
20
10
0
0.2
0.4
0.6
0.8
1
X_B
II
I
$f_{BC}=3$
$f_{BC}=2$
III
$f_{BC}=1$
T_-
τ_{BB}
τ_{CC}
$f_{BC}=1$
III
T_+
$f_{BC}=2$
$f_{BC}=3$
I
II

Figure 3.1

References

1. (a) S.T. Bertucci, A.K. Burnham, G.R. Alms, and W.H. Flygare, J. Chem. Phys., 66, 605, (1977).
C.P. Smyth, "Molecular Relaxation Process", (Academic Press, New York, 1967).
D.A. Jackson and J.G. Powles, Trans. Farad. Soc., 42A, 101, (1946).

(b) D.H. Whiffen and H.W. Thompson, Trans. Farad. Soc., 45A, 114, (1949)
A.V. Rakov, Optics Spect., 11, 128, (1959).
N.D. Foltz, C.W. Cho, P.H. Rank, and T.A. Wiggins, Phys. Rev. Lett., 165, 396, (1967).
H.C. Lucas, D.A. Jackson, J.G. Powles, and B. Simic-Glavaski, Mol. Phys., 18, 505, (1970).
P.P. Ho and R.R. Alfano, J.Chem. Phys., 67,1004, (1977).

2. D.H. Whiffen, Trans. Farad. Soc., 45A, 130, (1949).
D.R. Bauer, G.R. Alms, J.I. Brauman, and R. Pecora, J. Chem. Phys.,61,2255,(1974); ibid, 63, 53, (1975).
F.J. Fartali and T.A. Litovitz, J. Chem. Phys., 56 , 404, (1972).
D.R. Jones, and C.H. Wang, J. Chem. Phys, 65, 1835,(1976); ibid, 66, 1659, (1977).
M.M. Malley and G. Mourou, Opt. Comm., 13, 412, (1975).

3. (a) A.J. Curtis, P.L. McGeer, G.R. Rathmann, and C.P. Smyth, J. Am. Chem. Soc., 74, 644, (1952).

(b) H.C. Lucas, and D.A. Jackson, Mol. Phys., 20, 801, (1971).

(c) R.W. Mitchell and M. Eisner, J. Chem. Phys.,33,86, (1970).

(d) P.P. Ho and R.R. Alfano, Chem. Phys. Lett., 37,91, (1976).

(e) P.P. Ho and R.R. Alfano, Chem. Phys. Lett., 50,74, (1977).

4. E. Hatshek, "Viscosity of Liquids", (D.VanNostrand Co., New York, 1928).

5. T. Kendall and K.P. Monroe, J. Am. Chem. Soc.,39,1802,(1917).

6. E.C. Bingham, J. Am. Chem. Soc., 35, 195, (1906).

7. S. Arrhenius, Zeit. Physik Chem., 1, 285, (1887).

8. D.J. Treory and H.G. Drickamer, J. Chem. Phys., 17, 582, (1941).

9. N.L. Balazs, Trans. Chim. Phys-Bas., 70, 412, (1941).

10a. A.E. Dunstan and F.B. Thole, J.Chem. Soc.,95,1556, (1909).

b. N.S. Kurnakow, Zeit. Anorg. Chem., 135, 81, (1924).

c. T.M. Reed III and T.E. Taylor, J.Chem.Phys.,63,58, (1959).

d. G.D. Arrigo, L. Mistura, and P. Tartaglia, J. Chem. Phys., 66, 80, (1977).

11. G.D. Arrigo, L. Mistura, and P. Tartaglia, J. Chem. Phys., 66, 74, (1977).

12. N.E. Hill, Proc. Phys. Soc. (London), 67B, 149, (1954).

13. E.N. Andrade, Phil. Mag., 17, 698, (1934).
E.N. Andrade and C. Dodd, Proc. Royal Soc.,A204,449,(1950).

14. D. Kivelson and S.J. Tsay, Mol. Phys., 29, 29, (1975).

15. H. Mori, Prog. Theor, Phys., 33, 423, (1965).

16. T. Keyes and D. Kivelson, J. Chem. Phys., 56,1057, (1972).

17. D.R. Bauer, J. I. Brauman, and R. Pecora, J. Chem. Phys., 63, 53, (1975).

18. G.R. Alms, G.R. Bauer, J.I. Brauman, and R. Pecora, J. Chem. Phys., 59, 5310, (1973).

19. D. Kivelson and K. Ogan, "Adv. in Mag. Res." 7, 71, (1974).

20. D. Kivelson and T. Keyes, J. Chem. Phys., 57, 4599, (1972).

CHAPTER 4

OPTICAL KERR EFFECT

When an intense linearly polarized light pulse travels through an optically isotropic medium, the material becomes temporarily optically anisotropic. The material behaves optically as it was an uniaxial crystal in which the electric field of the light pulse defines the optic axis. The mechanism responsible for this effect has been attributed to the disturbance from equilibrium of the molecular motions and the distortion of the electron clouds. The induced birefringence in the material is shortlived and last as long as it takes for the system to return to equilibrium. For a typical simple liquid, the relaxation time is less than 1 nanosecond. The theory for this phenomenon was first proposed by Buckingham[1] and was called the optical Kerr effect (OKE). The OKE is different from the traditional electro-optical Kerr effect observed in 1875 by J. Kerr, which uses a d.c. electric field from a voltage source to induce the birefringence in the material.

The first experimental observation of the OKE was reported in 1964 by Mayer and Gires[2] and by Maker et al[3] using a powerful polarized light pulse from a Q-switched nanosecond Ruby laser. The use of a high power (1GW) picosecond ($\leq$ 10 ps) laser pulse to measure the rotational motion of molecules in liquids and the nonlinear change of the index of refraction associated with the OKE was simultaneously made by Duguay and Hansen[4], and by Shimizu and Stoicheff[5]. Recently, fundamental

information on the molecular motions and interactions have been obtained by Ho and Alfano[6,7,8] by measuring the Kerr kinetics in different states of condensed matter.

In this chapter, we present a detail theoretical study of the OKE in liquids induced by picosecond laser pulses. This chapter is divided into eight major sections.

In section 4.1, I outline the nonlinear indices of refraction in liquids calculated by Buckingham[1] and Kielich[9]. In section 4.2, I give a brief description on the mechanisms for the OKE. In section 4.3, I derive a equation of the signal transmitted through the Kerr gate which is calculated by Maker and Terhune[10], by Hellwarth et al[11], and by Wang and Shen[12]. In section 4.4 and 4.5, I discuss the signal and noise transmitted through the Kerr gate, respectively. In section 4.6, calculations are made for the dependence of the OKE on different parameters, such as : temporal and spatial characteristics of the laser pulse, laser power, the length of the sample cell, the wavelength of the probe light, the relaxation time of the sample solution, the concentration of the solution, and the temperature. In section 4.7, deconvolution from the measured relaxation time is plotted. And in section 4.8, I give a brief description on the effect of the distribution of relaxation time in the OKE.

4.1 Theory of the Optical Kerr Effect from Classical Semi-Macroscopic Approach

In 1875, Kerr[13] observed that by applying a steady state electric field to an isotropic medium, it became doubly refracting or birefringent. This birefringence is primarily caused by distortion of the electronic clouds and molecular motions in media through the interactions with external electric field with the polarizability of molecules[9,14]. In 1956, Buckingham[1] generalized this theory by proposing the use of an intense light to induce birefringence in an isotropic medium. The d.c. Kerr effect[13] is equivalent to the optical Kerr effect with frequency at zero.

In the OKE, when an intense light beam passes through an assembly of polarizable molecules, the molecules tend to line up along this electric field. The energy of a molecule in an external field $\vec{E}$ is defined as $U(\tau,\vec{E})$, where τ describes the position and orientation of the molecule at a particular instant,

$$U(\tau,\vec{E}) = U(\tau,0) - \int_0^{\vec{E}} m_\alpha(\tau,\vec{E})\, e''_\alpha\, d\vec{E} \quad . \qquad (4.1)$$

where m^i_α is the dipole moment for the i-th molecule in an external optical electric field, it can be written by a power series expansion :

$$m^i_\alpha = u^i_\alpha + \alpha^i_{\alpha\beta}\,(E_\beta + F^i_\beta) + \tfrac{1}{2}\,\beta^i_{\alpha\beta\gamma}(E_\beta + F^i_\beta)(E_\gamma + F^i_\gamma) + 1/6\,\gamma^i_{\alpha\beta\gamma\delta}\,(E_\beta + F^i_\beta)(E_\gamma + F^i_\gamma)(E_\delta + F^i_\delta) + \cdots \qquad (4.2)$$

where the subscripts α,β,γ, and δ are the coordinate indices of the tensors; u_α is the permanent dipole moment; $\alpha_{\alpha\beta}$, $\beta_{\alpha\beta\gamma}$

$\gamma_{\alpha\beta\gamma\delta}$, etc. represent the various orders of the polarizability[1]; F_α is the local field in liquids due to the molecular charge distribution and is assumed to be constant through out the medium. For simplicity of notation, the superscript i is then dropped and $\vec{E} + \vec{F}^i$ is represented by $\vec{E}$ alone.

The frequency of the light is sufficiently high for the molecule to be unable to follow the alternations. The time average over an optical period of the interactions of the permanent dipole with the field vanishes. The resultant effective energy from equation 4.1 is,

$$\overline{U(\tau,\vec{E})} \equiv 1/T \int_0^T U(\tau,\vec{E})\, dt$$

$$= U^o - \tfrac{1}{4}\, \alpha_{\alpha\beta} e_\alpha e_\beta E_o^2 - 1/64 \gamma_{\alpha\beta\gamma\delta}\, e''_\alpha e''_\beta e''_\gamma e''_\delta E_o^4 - \cdots, \quad (4.3)$$

where $\vec{E} = \vec{E}_o\, e^{iwt}$.

Due to the anisotropic of the polarizability of molecules, these molecules tend to orient to minimize its energy. The axis of maximum polarizability of molecules tends to orient parallel to the direction of the external field. The rotation is not complete because of the thermal energy. When the external field increases from E_α to $E_\alpha + \delta E_\alpha$, the increment in the dipole moment is

$$\delta M_\alpha = (\alpha_{\alpha\beta} + \beta_{\alpha\beta\gamma} E_\gamma + \tfrac{1}{2}\, \gamma_{\alpha\beta\gamma\delta} E_\gamma E_\delta + \cdots)\delta E_\beta$$

$$\equiv \pi_{\alpha\beta} \delta E_\beta \quad . \quad (4.4)$$

The effective molecular polarizability of the i-th molecule determined from the refractive index in the direction of the unit vector e'' and $e^{\perp}$ is $\pi^i_{\alpha\beta} = \partial M_\alpha / \partial E_\beta$. (4.5)

The Classius-Mossotti relation is,

$$(\varepsilon - 1)/(\varepsilon + 2) = 4\pi/3 \sum_i N_i \, \partial\vec{M}/\partial\vec{E} \quad . \qquad (4.6)$$

By combining equations 4.4 and 4.6, we obtain

$$(n_{//}^2-1)/(n_{//}^2+2) - (n_{\perp}^2-1)/(n_{\perp}^2+2) = 4\pi N/3V_m \overline{\langle \pi_{\alpha\beta}(e''_\alpha e''_\beta - e^{\perp}_\alpha e^{\perp}_\beta)\rangle}, \qquad (4.7)$$

where $\overline{\pi_{\alpha\beta}} = 1/T \int_o^T \pi_{\alpha\beta}(\tau,\vec{E})\, dt$

$$= (\alpha_{\alpha\beta} + \tfrac{1}{4}\gamma_{\alpha\beta\gamma\delta}\, e^{\perp}_\gamma e^{\perp}_\delta \vec{E}_o^2)(e''_\alpha e''_\beta - e^{\perp}_\alpha e^{\perp}_\beta) \quad , \qquad (4.8)$$

and the bracket $\langle\ \rangle$ represents an ensemble average which is defined by,

$$\langle \overline{\pi_{\alpha\beta}} \rangle = \int \overline{\pi_{\alpha\beta}(\tau,E)}\, e^{[-U(\tau,E)/kT]} d\tau \Big/ \int e^{-U(\tau,E)}\, d\tau \qquad (4.9)$$

Expanding $\overline{\pi_{\alpha\beta}(\tau,E)}$ as a power series in $\vec{E}$ at $\vec{E}_o = 0$, the coefficient of the first nonvanishing term $(\vec{E}_o^2)$ is :

$$\tfrac{1}{2}\, \partial^2 \langle \overline{\pi(\tau,\vec{E})} \rangle / \partial \vec{E}_o^2 \Big|_{\vec{E}_o=0} = \tfrac{1}{2}\, \partial^2 \overline{\pi(\tau,\vec{E})}/\partial \vec{E}_o^2 \Big|_{\vec{E}_o=0}$$

$$- 1/2kT \left[\partial \overline{\pi(\tau,\vec{E})}/\partial \vec{E}\ \partial \overline{U}/\partial \vec{E}_o + \partial^2 U(\tau,E)/\partial \vec{E}_o^2 \right]\Big|_{\vec{E}_o=0}$$

$$+ (1/k^2T^2)\ \overline{\pi(\tau,\vec{E})}\ (\partial \overline{U}/\partial \vec{E}_o)^2 \Big|_{\vec{E}_o=0} \qquad (4.10)$$

In the limit $E_o \to 0$, with the help of equation 4.10, equation 4.7 is rewritten by,

$$(n_{//} - n_{\perp})/(n_1^2+2)^2 = 4\pi N/V_m \langle \overline{\pi}_{\alpha\beta}(e''_\alpha e''_\beta - e^{\perp}_\alpha e^{\perp}_\beta)\rangle \quad . \qquad (4.11)$$

In measuring the induced birefringence of the OKE, one uses an intense light beam of frequency w_2 to generate the double refraction, then applied a weak linearly polarized light of frequency w_1 to probe the difference between the refractive indices $n_{//}$ and $n_{\perp}$ of the sample parallel and perpendicular to the optical field, respectively (see figure 4.1). The experimental setup is described in detail in chapter 5.

The molecular Kerr constant is defined by[13-17],

$$B = 2\,N\,V_m\,3^{-1}(n_1^2+2)^2(n_2^2+2)^{-2}\lim_{E\to 0}(n_{//}-n_{\perp})/E^2\,, \tag{4.12}$$

where n_1, n_2 are the linear indices of refraction of the sample corresponding to the frequency w_1 and w_2, respectively. In the OKE, n_1 is assumed to be equal to n_2, V_m is the molar volume, and E is the amplitude of the exciting optical field.

Combining equations 4.11 and 4.12, we obtain,

$$B = 2n/3(n^2+2)\;4\pi/3\;\;N\langle\overline{\pi}_{\alpha\beta}(e^{//}_{\alpha}e^{//}_{\beta}-e^{\perp}_{\alpha}e^{\perp}_{\beta})\rangle \tag{4.13}$$

From equations 4.10 and 4.13 (with all odd terms dropping after time average), we have

$$B = 2\pi\,N/27\;\;\langle(\gamma_{\alpha\beta\delta\delta}+1/kT\;\alpha_{\alpha\beta}\alpha_{\delta\delta})\;\;e^{//}_{\alpha}e^{//}_{\beta}(e^{//}_{\gamma}e^{//}_{\delta}-e^{\perp}_{\gamma}e^{\perp}_{\delta})\rangle. \tag{4.14}$$

By trigometric analysis, it is given that

$$\langle e^{//}_{\alpha}e^{//}_{\beta}(e^{//}_{\gamma}e^{//}_{\delta}-e^{\perp}_{\gamma}e^{\perp}_{\delta})\rangle = 1/30\;\{-2\delta_{\alpha\beta}\delta_{\gamma\delta}+3\delta_{\alpha\gamma}\delta_{\beta\delta}+3\delta_{\alpha\delta}\delta_{\beta\gamma}\} \tag{4.15}$$

Thus equation 4.14 reduces to

$$B = 2\pi N/405\;\{2\,\gamma_{\alpha\alpha\beta\beta}+3/kT\;\;(\alpha_{\alpha\beta}\alpha_{\alpha\beta}-3\alpha^2)\}, \tag{4.16}$$

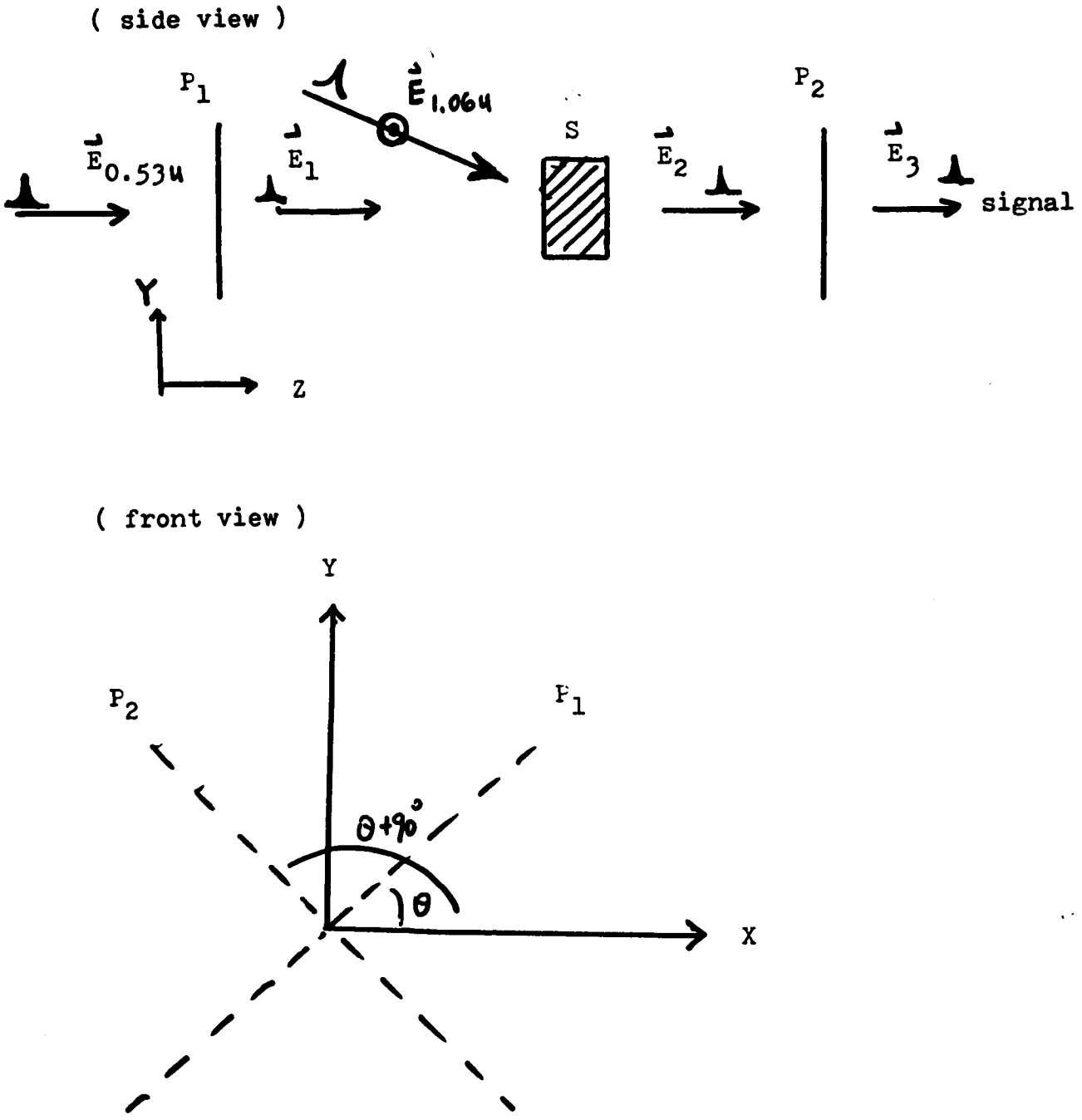

Figure 4.1 Simple diagram of optical Kerr gate

where $\alpha = 1/3\ \alpha_{\alpha\alpha}$, and N is the Avogadro number[1]. The first term is due to the electron cloud distortion of the molecule and is temperature independent. The second term $\alpha_{\alpha\beta}$ is the polarizability tensor of a molecule and is independent of the field strength. Rewriting the $\alpha_{\alpha\beta}$ in terms of the three principle axis components of polarizability α_1, α_2, α_3 ; equation 4.16 is written by :

$$B = 2\pi N/405 \left\{ 2\gamma_{\alpha\alpha\beta\beta} + 3/kT \left[\sum_{s=1}^{3} (\alpha_s)^2 - 3\alpha^2 + \sum_{s,t}^{3} \alpha_s \alpha_t \int\int g_2(\Omega_p, \Omega_q)(3\cos^2\theta_{st}^{pq} - 1) d\Omega_p d\Omega_q \right] \right\} \quad (4.17)$$

where θ_{st}^{pq} denotes the angle between the principle axes s and t of molecules p and q; $g_2(\Omega_p, \Omega_q)$ is the correlation function for pairs of molecules having their principle axes oriented along s and t directions, respectively. This is similar to the pair correlation factor derived by Keyes and Kivelson (see section 2.8).

4.2 Mechanisms for the Induced Polarizability in Liquids

In this section, we will discuss various mechanisms that cause the change in the index of refraction in the optical Kerr effect. These are electronic cloud distortion, molecular reorientational motion, molecular libration, molecular redistribution, electrostriction, and heating. The total change in the index of refraction is the sum of all the possible mechanisms.

a). Electronic cloud distortion :

By applying an external electric field, the electronic structure of a molecule is disturbed produces a net dipole moment. The equation of motion for electrons from the classical theory of the electron oscillation model (Lorentz model)[18];

$$d^2\vec{r}(t)/dt^2 + \gamma\, dr(t)/dt + w_o^2\, \vec{r}(t) + a\, \vec{r}(t)\cdot\vec{r}(t)\, \vec{r}(t) = e\vec{E}(t)/m, \qquad (4.17)$$

where e is the electron charge; $\vec{r}(t)$ is the displacement of the electron from the zero field equilibrium position; m is the electron mass; w_o is the absorption frequency; $1/\gamma$ is the damping time of electrons (this relaxation time is in the order of 10^{-15} seconds[19]); and $a\vec{r}^3$ is the higher order term from the approximation of a binding potential barrier. The solution of electronic displacement (equation 4.17) is related to the molecular polarizability by

$$\vec{P}(t) = N e \vec{r}(t)$$

Thus, the mechanism of this polarization is faster than the light pulse used in this experiment.

b) Molecular reorientational motion :

Molecular orientational motion which has been discussed at length in chapter 2 is a slow mechanism of the order of about 1 ps to 1 us[7,12] depending on the size of the shape of molecules. Since the torque of a permanent dipole is averaged out for an exciting optical field during an optical period, the reorientational motion of a molecule is due to the interaction of the induced polarizability tensor with the optical field. This is the dominant mechanism in our research.

c) Molecular libration :

It is possibly for molecules to oscillate freely in a potential well formed by the local field of the surrounding molecules. This kind of oscillation known as molecular libration or rocking may cause a small jump to a new equilibrium orientation after a time τ_ℓ . Since molecular librations are assumed to be much faster than the molecular orientational time, it add up to produce the net reorientatinnal motion. This occurs mostly likely in solids.

d) Molecular redistribution :

In a dense medium, and intense electric field can cause a mutual interaction between the induced dipoles of molecules. This induced dipole-dipole interaction is proportional to the time average of the square of the electric field and is also a function of the dipole separation (i.e. the density of the medium[20]). In the short range order of the system ($|\vec{r}| < \lambda$), this induced field dependent effect will cause molecules

to redistribute themselves from their zero field distribution and establish a new equilibrium. In liquids, this redistribution motion can be attributed to the product of molecular collisional processes[21]. Therefore, a large anisotropic polarizability can be induced in a fast time.

e) Electrostriction :

Electrostriction is a dielectric medium arises as result of the internal force which is produced from a nonuniform electric field. The net force arising from the interaction of of the induced dipoles is proportional to the gradient of the electric field. The change in refractive index involves a macroscopic density change rather than a local rearrangement of the molecule[22]. This is a relatively slow mechanism which will not respond to picosecond laser pulse excitation.

f) Heating :

The contribution to the nonlinear index of refraction due to heating can be written by[23] :

$$\delta n = \partial n/\partial T \; \delta T \quad , \tag{4.18}$$

where δT satisfies the heat conduction equation :

$$\rho \, c_p \, \partial \delta T/\partial t = Q + \kappa \nabla^2 \delta T \tag{4.19}$$

where $$Q = \alpha \, c/8\pi \, |A|^2 \tag{4.20}$$

The response of the medium due to heating is non-local. Its relaxation time (from equation 4.19) can be approximated as $\tau = r_o^2 \, \rho \, c_p/h$ which is about 10 ns to 1 second depending on r_o. This effect is negligible in the optical Kerr effect.

The total change in the refractive index is the sum of all the possible effects, see table 4.1 below :

Table 4.1: Nonlinear Indices of Refraction and Relaxation Times of Liquids from Different Mechanisms

	n_2(e.s.u.)	τ(sec)
Electronic Deformation	$10^{-13} - 10^{-14}$	10^{-15}
Molecular Reorientation	$10^{-11} - 10^{-12}$	$10^{-9} - 10^{-12}$
Molecular Libration	$10^{-12} - 10^{-13}$	10^{-13}
Molecular Redistribution	$10^{-12} - 10^{-13}$	10^{-13}
Electrostriction	$10^{-11} - 10^{-12}$	10^{-8}
Thermal Change	$10^{-5} - 10^{-8}$	$10^{-8} - 1$

From the strength (n_2) and response time of the mechanism ($\tau_{relaxation}$) to a picosecond pulse excitation shown in table 4.1, the contributions to the optical Kerr effect from these mechanisms can be separated into different cases :

(1). In most cases, electrostriction does not affect the molecular rotation in liquids because it is a relatively slow mechanism. It can only be important if the light pulse is longer than the relaxation time of the molecules. The relaxation time for heating effects are even longer, we have neglected these two mechanisms in this work.

(2). The electronic cloud distortion, molecular libration, and molecular redistribution are rather fast relaxation processes in comparison to the picosecond laser pulse duration. Picosecond pules can not resolve these mechanisms. The birefringence caused by these fast mechanisms (relaxation time faster than the laser pulse duration) only last as the initial pulse duration. The nonlinear index of refraction change will instantaneously follow the excitation pulse in time. The signal transmitted through the Kerr gate for these mechanisms follow the laser pulses as the prompt curve. When the phase retardation $\delta\phi$ (see the discussion in section 4.6) is smaller than one, the Kerr signal vanishes for delay time $t > 30$ ps. An example of carbon disulfide (CS_2) Kerr gate ($\tau_o \leq 1.8$ ps) displays our prompt curve (see figure 6.6.3).

(3). When the relaxation time of molecular reorientational motion is longer than the pulse duration τ_ℓ , and when n_2 is larger enough compared to the prompt response curve, the contribution to the optical Kerr effect is from the molecular reorientational motion. After thirty picoseconds away from the peak signal of the Kerr gate, this slow mechanism is dominant; otherwise, if $\tau_\ell < \tau_o$, the signal merges into the prompt curve. In section 4.7, I will discuss the relaxation time extracted from the Kerr intensity decay profile for laser pulse excitation.

4.3 Theory of Induced Third Order Nonlinear Susceptibility Tensor in Liquids

In an isotropic dense medium, the polarization vector $\vec{P}$ of material under an intense optical electric field $\vec{E}$ can be written by[24-28]:

$$P_i = \chi^{(1)}_{ij}E_j + \chi^{(2)}_{ijk}E_jE_k + \chi^{(3)}_{ijkm}E_jE_kE_m + \cdots , \quad (4.21)$$

where $E_j(t)$ is the component of the electric field along the j-axis, $\chi^{(1)}_{ij}$ is the ordinary linear susceptibility tensor of the medium, and $\chi^{(2)}_{ijk}$, $\chi^{(3)}_{ijkm}$, ... etc. are called the nonlinear susceptibility tensors of rank three, four, etc.. In liquids, due to the property of inversion symmetry, all the even order susceptibility tensors vanish. The lowest order nonlinear susceptibility is $\chi^{(3)}$.

The linear polarization $\chi^{(1)}E$ is responsible for phenomena as the linear refraction and attenuation. Attenuation is caused by the imaginary of a complex $\chi^{(1)}$. When the incident optical field has frequency w, the linear polarization has the same frequency. This field radiates into the medium and modifies the wave propagation. The linear index of refraction n is equal to $(1 + 4\pi\chi^{(1)})^{\frac{1}{2}}$.

The lowest order nonlinear susceptibility in liquids is $\chi^{(3)}$. It gives rise to the third harmonic generation[10] and four waves mixing phenomena. The following are some examples of phenomena caused by $\chi^{(3)}$: 1). The d.c. Kerr effect is caused by sending an optical wave through the medium in the presence of the d.c. field. This leads to a change in the refractive index

which is proportional to the square of the d.c. field. 2). Self-phase modulation[19] is the spectral broadening of a monochromatic wave which travels through a medium due to the modification of $\delta n(t)$. 3). Self-focusing[29] is caused by an intense incident beam profile which produces a spatial distribution of the induced index of refraction in the medium. The medium acts as a positive lens results in the beam to focuse to the propagation axis. 4). In four-photon parametric generation[30-32], some of the additional frequency components from the Stokes and anti-Stokes self-phase modulated light and laser photons are coupled to the laser field via the third order susceptibility $\chi^{(3)}$; originates through the distortion of the atomic configuration inside the medium.

In the following section, we will concentrate on the electromagnetic theory of the optical Kerr effect[4,9,12]. A weak probe beam of frequency w_1 is sent into an isotropic medium which interacts with the induced birefringence caused by the presence of another intense linearly polarized light of frequency w_2 in an isotropic medium.

The nonlinear susceptibility $\chi^{(3)}$ in liquids must be invariant under all spatial symmetry transformation[24,28]. There are twenty-one nonzero elements of which only three are independent out of the total eighty-one elements of the fourth rank tensor. They are :

$$\chi^{(3)}_{1111} : \quad \chi_{xxxx} = \chi_{yyyy} = \chi_{zzzz}$$

$$\chi^{(3)}_{1122} : \quad \chi_{yyzz} = \chi_{zzyy} = \chi_{zzxx} = \chi_{xxzz} = \chi_{xxyy} = \chi_{yyxx}$$

$$\chi^{(3)}_{1212} : \quad \chi_{yzyz} = \chi_{zyzy} = \chi_{zxzx} = \chi_{xzxz} = \chi_{xyxy} = \chi_{yxyx}$$

$$\chi^{(3)}_{1221} : \quad \chi_{yzzy} = \chi_{zyyz} = \chi_{zxxz} = \chi_{xzzx} = \chi_{xyyx} = \chi_{yxxy}$$

and $\chi^{(3)}_{1111} = \chi^{(3)}_{1122} + \chi^{(3)}_{1212} + \chi^{(3)}_{1221}$.

The subscripts 1 and 2 denote the coordinates x, y, or z.

Maxwell's equation in an isotropic medium, free of currents and charges are :

$$\nabla \times \vec{H} = \partial \vec{D}/\partial t = 1/c \quad \partial/\partial t \, (\varepsilon_o \vec{E} + \vec{P}) , \qquad (4.22)$$

$$\nabla \times \vec{E} = - 1/c \quad \partial(u_o \vec{H})/\partial t \qquad (4.23)$$

and $\vec{P} = \vec{P}_l + \vec{P}_{NL} = \vec{P}_l + \vec{P}^{(3)}$, $\qquad (4.24)$

where $P_i^{(3)} = \chi^{(3)}_{ijkm} E_j E_k E_m$

By taking curl of equation 4.23 and substituting it into equation 4.22, these equations combine a form of second order differential equation. With the help of $\nabla \cdot \vec{E} = 0$, it gives

$$\nabla^2 \vec{E} = 1/c^2 \quad \partial^2 \vec{E}/\partial t^2 + 4/c \; \partial^2/\partial t^2 \; \vec{P}_{NL} . \qquad (4.25)$$

The field amplitude in the solution of equation 4.25 is assumed to be a plane wave travelong along the z-axis, this field has several harmonic components all of which are plane

waves travelling in the same direction :

$$\vec{E}(\vec{r},t) = \sum_{j=-N}^{N} \vec{E}(w_j,z)/2 \; e^{i(k_i z - w_j t)} \quad , \qquad (4.26)$$

where $w_{-j} = -w_j$, $k_{-j} = -k_j$, and $\vec{E}(w_{-j},z) = \vec{E}^*(w_j,z)$.
It is also assumed that the variation of the complex field amplitude with z is slowly varied such that

$$dE_i^{(w_p)}/dr \; k_i(w_p) \quad \gg \quad d^2E_i(w_p)/dz^2 \quad .$$

The polarization P is assumed to be expandable in terms of its harmonic components :

$$\vec{P}^{(3)}(\vec{r},t) = \sum_{-M}^{M} \vec{P}(w_p,z)/2 \; e^{i(k_p z - w_p t)} \quad . \qquad (4.27)$$

For example, in the third harmonic generation, by substituting equations 4.26 and 4.27 into equation 4.25, and comparing coefficients of the same harmonics, it is found that[28]:

$$2 i k(3w) \partial E_{3w}/\partial z = - 3 k^2(3w)/n^2(3w) \cdot \chi^{(3)}_{1122}(-3w,w,w,w) E_w E_w E_w e^{i\Delta k z} \qquad (4.28)$$

where $\Delta k \equiv 3 k(w) - k(3w)$. $\qquad (4.29)$

In the optical Kerr effect, an intense linearly polarized laser beam generates a nonlinear polarization in the medium which induces an optical birefringence. A weak light source can be used to probe this induced birefringence. Due to the inversion symmetry of the isotropic medium, such as a liquid or a glass, the odd order of the susceptibility tensors vanishes. The lowest order of the nonlinear polarization for light waves in an isotropic medium is[24,28]

$$P_i^{(3)}(t) = \int_{-\infty}^{\infty}\int_{-\infty}^{\infty}\int_{-\infty}^{\infty} \chi_{ijkm}^{(3)}(t,t_1,t_2,t_3)E_j(t)_1E_k(t)_2E_m(t)_3\, dt_1dt_2dt_3 \,, \tag{4.30}$$

where we have assumed a uniform space and have neglected spatial dispersion effects. After the Fourier transformation from the time space into the frequency space, the induced polarization becomes[10]

$$P_i^{(3)}(w) = D\ \chi_{ijkm}^{(3)}(-w,w_1,w_2,w_3)\ E_j(w)_1E_k(w)_2E_m(w)_3 \times \exp i(n_1w_1 + n_2w_2 + n_3w_3)z/c \quad , \tag{4.31}$$

and $$\chi_{ijkm}^{(3)}(w) = \int_{-\infty}^{\infty}\int_{-\infty}^{\infty}\int_{-\infty}^{\infty}\chi_{ijkm}^{(3)}(t,t,t,t)_{1\ 2\ 3}\ e^{i(w_1t_1+w_2t_2+w_3t_3)}dtdtdt_{1\ 2\ 3} \tag{4.32}$$

where $w = w_1 + w_2 + w_3$, the w_i's are the frequencies of the waves assumed to be propagating along the z-axis, the n_i's are the linear indices of refraction at the i-th frequency w_i, and $E_i^*(w) = E_i(-w)$ is the complex amplitude of the electric field strength. The coefficient D = 1, 3, or 6, depends on whether three, two, or none of the frequencies are the same. Equation 4.31 is invariant to the order of the various field amplitudes. The last three frequencies in $\chi_{ijkm}^{(3)}(-w,w_1,w_2,w_3)$ may be

permuted provided that the corresponding coordinate indices are permuted in the same manner.

For the optical Kerr effect, usually only waves at frequency w_1 and w_2 propagate in a medium. In this discussion, $|E(w_2)| \gg |E(w_1)|$. The material is assumed lossless and isotropic. A schematic diagram of the optical Kerr effect is shown in figure 4.1. The nonlinear polarization at a frequency w_1 induced by the field at a frequency w_2 can be described by[10];

$$\begin{aligned} P_i^{(3)}(w_1) = {} & 6\chi^{(3)}_{1122}(-w_1,w_1,w_2,-w_2)\, E_i(w_1)E_j(w_2)E_j^*(w_2)\, e^{in_1w_1z/c} \\ & + 6\chi^{(3)}_{1212}(-w_1,w_1,w_2,-w_2)\, E_j(w_1)E_i(w_2)E_j^*(w_2)\, e^{in_1w_1z/c} \\ & + 6\chi^{(3)}_{1221}(-w_1,w_1,w_2,-w_2)\, E_j(w_i)E_j(w_2)E_i^*(w_2)\, e^{in_1w_1z/c} \end{aligned} \qquad (4.33)$$

where i and j are the coordinate indices x and y.

The induced polarizability in the medium can be written in terms of the change in the susceptibility tensor $\delta\chi_{ij}$:

$$\begin{aligned} \delta\chi_{ij}(w_1) = {} & 6\,\chi^{(3)}_{1122}(-w_1,w_1,w_2,-w_2)\, E_k^*(w_2)\, E_k(w_2)\, \delta_{ij} \\ & + 6\,\chi^{(3)}_{1212}(-w_1,w_1,w_2,-w_2)\, E_j^*(w_2)\, E_i(w_2) \\ & + 6\,\chi^{(3)}_{1221}(-w_1,w_1,w_2,-w_2)\, E_i^*(w_2)\, E_j(w_2)\,, \end{aligned} \qquad (4.34)$$

where δ_{ij} is a delta function, and $\delta\chi_{ij}$ is defined by the following equation[18];

$$P_i^{(3)}(w_1) = \delta\chi_{ij}(w_1)\, E_j(w_1) \,. \qquad (4.35)$$

In the optical Kerr effect, the measurable parameter is the change of the index of refraction. The relationship between δn and $\delta\chi$ is obtained as follows :
The refractive index in a medium is expressed by

$$n = n_o + \delta n \quad , \tag{4.36}$$

where n_o is the linear index of refraction, and δn is the nonlinear index of refraction. The relationship between the change or susceptibility (equation 4.34) and δn can be obtained from the following definition :

$$n^2 = \varepsilon = 1 + 4\pi\chi \quad . \tag{4.37}$$

The first order approximation to equation 437 for small change in n and χ is :

$$(n_o + \delta n)^2 \simeq 1 + 4\pi (\chi_o + \delta\chi). \tag{4.38}$$

Since $(n_o)^2 = 1 + 4\pi\chi_o$, we obtain δn to the first order

$$\delta n \simeq 2\pi/n_o \, \delta\chi \, . \tag{4.39}$$

From equations 434 and 439, the induced refractive index change parallel and perpendicular to the orienting field E_{w_2} are expressed by,

$$\delta n_{\parallel} = 2\pi/n_o \; 6\left[\chi^{(3)}_{1122} + \chi^{(3)}_{1212} + \chi^{(3)}_{1221}\right](-w_1, w_1, w_2, -w_2)\left|E(w_2)\right|^2 \tag{4.40}$$

and $$\delta n_{\perp} = 2\pi/n_o \; 6\, \chi^{(3)}_{1122}(-w_1, w_1, w_2 - w_2) \left|E(w_2)\right|^2 \quad . \tag{4.41}$$

From equations 4.40 and 4.41, the difference of the nonlinear index of refraction between parallel and perpendicular direction for the optical Kerr effect is given by :

$$\delta n(w_1,w_2) \equiv \delta n_{\parallel} - \delta n_{\perp} = (2\pi/n_o)\left[6\,\chi^{(3)}_{1212}(-w_1,w_1,w_2,-w_2) + 6\,\chi^{(3)}_{1221}(-w_1,w_1,w_2,-w_2)\right] |E(w_2)|^2. \quad (4.42)$$

According to Owyoung et al[12,18], and Wong and Shen[11], the susceptibility tensor in equation 4.4.2 for an isotropic medium can be expressed by :

$$\chi^{(3)}_{1221}(-w_1,w_1,w_2,w_2) = 1/24\ (\sigma + 2\beta)$$

and $$\chi^{(3)}_{1221}(-w_1,w_1,w_2,w_2) + \chi^{(3)}_{1221}(-w_1,w_1,w_2,w_2) = 1/12\ (\sigma + \beta) \quad (4.43)$$

where σ and β are contributions from the electronic and nuclear parts, respectively. In time dependent experiments, Wong and Shen[11] wrote equation 4.43 as :

$$\chi^{(3)}_{1221}(w_1,w_2;t-t') = 1/24\left[\sigma(w_1,w_2)\,\delta(t-t') + 2\beta(w_1,w_2;t-t')\right],$$

and

$$\chi^{(3)}_{1221}(w_1,w_2;t-t') + \chi^{(3)}_{1212}(w_1,w_2;t-t') = 1/12\left[\sigma(w_1,w_2)\,\delta(t-t') + \beta(w_1,w_2;t-t')\right]. \quad (4.44)$$

The $\chi^{(3)}(t)$ can be separated into a fast part where the electronic cloud distortion, molecular libration, and molecular redistribution can be lumped together; and a slow part, such as molecular reorientational mechanism.

The nonlinear polarization $P^{(3)}(t)$ for a time dependent pulse experiment can be written by using the equation 4.10 with the properties discussed by Butcher[24] of causality ($\chi^{(3)}(t) = 0$ when $t_i < 0$) and intrinsic symmetry ($\chi^{(3)}$ is invariant under any permutation of t_i).

$$P_i^{(3)}(t) = \int_0^\infty\int_0^\infty\int_0^\infty dt_1dt_2dt_3 \chi_{ijkm}^{(3)}(t-t_1,t-t_2,t-t_3)\, E_j(t_1)E_k(t_2)E_m(t_3) \quad , \tag{4.45}$$

With the definition of $P_i^{(3)}(w)$ in equation 4.35, its Fourier transformation to the time space is a convoluted function :

$$P_i^{(3)}(t) = \int_{-\infty}^{t} \delta\chi_{ij}(t_1')\, E_j(t-t_1')\ dt_1' \quad . \tag{4.46a}$$

By changing variables $t_1^* = t - t_1'$ and $t_1 = -t_1^*$, we obtain

$$P_i^{(3)}(t) = \int_0^\infty \delta\chi_{ij}\,(t-t_1)\, E_j(t_1)\ dt_1 \quad . \tag{4.46b}$$

By comparing equations 4.45 and 4.46b, we obtain

$$\delta\chi_{ij}(t-t_1) = \int_0^\infty\int_0^\infty dt_2dt_3 \chi_{ijkm}^{(3)}(t-t_1,t-t_2,t-t_3)\, E_k(t_2)\, E_m(t_3) \tag{4.47}$$

Since t_1 is arbitrary in equation 4.47, we can set it $t_1 = 0$ without loss of generality. By changing variable $t_2^* = t - t_2$, and $t_3^* = t - t_3$, $t_2' = -t_2^*$, and $t_3' = -t_3^*$, we have

$$\delta\chi_{ij}(t) = \int_{-\infty}^{t}\int_{-\infty}^{t} \chi_{ijkm}^{(3)}(t\ ,t_2',t_3')\, E_k(t-t_2')\, E_m(t-t_3')\ dt_2'\ dt_3' \tag{4.48}$$

A general form for the time dependent field induced nonlinear refractive index is written by[34]:

$$\delta n(t) = \int_{-\infty}^{t}\int_{-\infty}^{t} f(t,t_2,t_3)\, E(t-t_2)\, E(t-t_3)\, dt_2\, dt_3 \,, \quad (4.48)$$

where $f(t,t_2,t_3) \equiv 2\pi/n_o\, \chi^{(3)}(t,t_2,t_3)$ is a weighting function describing response of the refractive index to a impulse pulse.

There are different mechanisms responsible for the OKE in the picosecond region[8,10,11,14]. At this time, it is believed that these mechanisms are the electronic cloud distortion[8,10,11,14], molecular libration[36,37], molecular redistribution[38], and molecular reorientational motion[6,11,14,39-41]. These mechanisms have different response times. The electronic cloud distortion process is ultrafast; the estimated relaxation time in most media is in a range between 10^{-14} to 10^{-16} seconds[14,34,35]. The relaxation process of the molecular libration or redistribution is fast[36-39] in comparison to the duration of a picosecond pulse. In most cases, the molecular reorientational motion has a response time which is usually slower than the picosecond laser pulse duration[6-12,14].

We can assume the formal response function in equation 4.48 by :

$$f(t,t_2,t_3) = \underbrace{\left[n_2^e\, \delta(t-t_2)\right.}_{\text{(FAST)}} + \underbrace{\left.(n_2^o/\tau_o)\, e^{-t_2/\tau_o}\right]}_{\text{(SLOW)}} \delta(t_2 - t_3) \,, \quad (4.49)$$

where n_2^e represents the contributions from all the fast mechanisms which essentially respond to the laser field instanteously ; n_2^o denotes a slow relaxation process with a relaxation time τ_o ; and $\delta(t_2 - t_3)$ is the property that the event for the two orienting fields E_{w_2}, in the optical Kerr effect is assumed to occur simultaneously.

Inserting equation 4.49 into equation 4.48 of $\delta n(t)$, the induced birefringence becomes :

$$\delta n(t) = n_2^e \langle E_{w_2}^2(t) \rangle + (n_2^o/\tau_o) \int_{-\infty}^{t} \langle E_{w_2}^2(t') \rangle e^{-(t-t')/\tau_o} dt' \tag{4.50}$$

where $\langle \vec{E}^2(t) \rangle = \frac{1}{2} |\vec{E}|^2$.

The reorientational part n_2^o has been described by Kielich[9]:

$$n_2^o = \frac{1}{4} \mathcal{N} (1/15kT) \Delta\alpha^{w_1} \Delta\alpha^{w_2} (n_{w_1}^2 + 2)^2/3 \, (n_{w_2}^2 + 2)^2/3 , \tag{4.51}$$

where $\Delta\alpha^{w_i}$ is the difference between the molecular polarizability parallel and perpendicular to the optical field w_i, and $\mathcal{N}$ is the number density of the Kerr medium. Since the molecules are not completely free to orient themselves due to intermolecular coupling forces, the first order corrected orientational part of the nonlinear index of refraction n_2^o is now defined by[9,14,40,41]:

$$n_2^o = {}_a n_2^o (1 + J) . \tag{4.52}$$

where J is a pair correlation factor depdining on the intermolecular interactions, orientations, and positions; and ${}_a n_2^o$ is an effective orientational Kerr coefficient give in equation 4.50.

The change of index of refraction give by equation 4.50 at time t, $\delta n(t)$, results in a phase retardation $\delta\phi(t)$ between the parallel and perpendicular components of the electric field of the probe pulse w_1 (wavelength λ_1). The phase retardation $\delta\phi(t)$ for a Kerr cell of length L is expressed by :

$$\delta\phi(t) = 2\pi L/\lambda_1 \, \delta n(t) . \tag{4.53}$$

The probe signal $I_t(t,\tau)$ transmitted through the Kerr gate with phase retardation $\delta\phi(t)$ can be written by[4,11]

$$I_t(t,\tau) = \left(1/I_1^o\right) I_1(\tau - t) \sin^2 \delta\phi(t)/2 \quad , \qquad (4.54a)$$

where τ is a relative time difference between the probe light pulse and the orienting pulse; and I_1^o is the total signal of the probe light passes through the system when axes of the two polarizers are oriented parallel to each other which normalize $I_t(t,\tau)$ to one. This equation will be derived in section 4.4. The signal $I_t(t,\tau)$ was recorded by a photodiode. Since the response time of the photodiode is slow; generally, the photodiode integrates the arriving signal in the order of a few nanoseconds. The detection system records the energy of the transmitted signal $I_t(\tau)$ at a relative time τ by the following equation;

$$I_t(\tau) = \int_{T_1}^{T_2} I_t(t,\tau)\, dt \quad . \qquad (4.54b)$$

Because T_1, T_2 are much larger than the time τ (in the order of 10 ps), we can assume $T_1 = -\infty$, and $T_2 = \infty$. The measured transmitted energy at a delay time for the optical Kerr gate is:

$$I_t(\tau) = (1/I_1^o) \int_{-\infty}^{\infty} I_1(\tau - t) \sin^2 \delta\phi(t)/2 \, dt \quad . \qquad (4.54c)$$

4.4 Signal Transmitted Through The Kerr Gate

The optical electric field of the 0.53 um light which is polarized perpendicular to the plane of the table (see figure 4.1) is expressed by :

$$\vec{E}_{0.53} = \tfrac{1}{2} E_o e^{iwt} \hat{y} + c.c. = Re\, E_o e^{iwt} \hat{y} . \quad (4.55)$$

After passing through the first polarizer (figure 4.1), this probe field is polarized at an angle θ, and the electric field of the 0.53 um probe light field is expressed as :

$$\vec{E}_1 = Re\, (E_o \cos\theta \hat{x} + E_o \sin\theta \hat{y}) e^{iwt} . \quad (4.56)$$

At the moment, the exciting 1.06 um light pulse arrives at the Kerr gate S which induces a temporal change in the index of refraction of the liquid. The difference between the index of refraction along the x-axis and y-axis is derived in equation 4.50 as :

$$\delta n(t) = \delta n_{\parallel} - \delta n_{\perp}$$

$$= 2\pi/n_1 \, 6 \int_{-\infty}^{t} \{ \chi^{(3)}_{1212}(-w_1, w_1, w_2, -w_2;\, t-t') + \chi^{(3)}_{1221}(-w_1, w_1, w_2, -w_2; t-t') \} \langle \vec{E}^2_{w_2}(t') \rangle dt' \quad (4.57)$$

At time t_o, the phase difference of the probe electric field E_1 through the sample cell caused by the 1.06 um laser pulse is :

$$\delta\phi(t_o) = 2\pi L/\lambda_1 \, \delta n(t_o) , \quad (4.58)$$

where L is the length of the Kerr cell.

The optical field of the 0.53 um light after the Kerr cell can be written by :

$$\vec{E}_2 = \mathrm{Re}\,(\cos\theta\, e^{i\delta\phi}\,\hat{x} + \sin\theta\,\hat{y})\,E_o\,e^{iwt}\,. \quad (4.59)$$

This field is eliptically polarized for $\delta\phi \neq 0$. The resulatant component of this field which travels through the second polarizer (polarized along the direction of $\theta+90^o$) is,

$$\vec{E}_3 = \mathrm{Re}\,[\cos\theta\, e^{i\delta\phi}\,\cos(\theta+90)\,\hat{A} + \sin\theta\,\sin(\theta+90)\,\hat{A}]\,\vec{E}_o\,e^{iwt}, \quad (4.60)$$

where $\hat{A}$ denotes the direction of P_2.

$\vec{E}_3$ can be expressed as follows :

$$\vec{E}_3 = \mathrm{Re}\,[E_o\cos\theta\sin\theta\,(1 - e^{i\delta\phi})]\,e^{iwt}\,\hat{A}$$

$$= \mathrm{Re}\,[E_o\sin2\theta\,\sin\tfrac{1}{2}\delta\phi\;\; e^{i\frac{1}{2}\delta\phi}(-i)]\;\; e^{iwt}\,\hat{A}$$

$$= E_o\sin2\theta\,\sin\tfrac{1}{2}\delta\phi\;(\cos wt\,\sin\tfrac{1}{2}\delta\phi + \sin wt\,\cos\tfrac{1}{2}\delta\phi)\,. \quad (4.61)$$

The transmitted signal which passes through the Kerr gate is given by :

$$I_t = \langle \vec{E}_3^2 \rangle = E_o^2\sin^2 2\theta\,\sin^2\tfrac{1}{2}\delta\phi\,\langle \cos^2 wt\,\sin^2\tfrac{1}{2}\delta\phi$$

$$+ \tfrac{1}{2}\sin 2wt\,\sin\delta\phi \;\; + \sin^2 wt\,\cos^2\tfrac{1}{2}\delta\phi\rangle \quad , \quad (4.62a)$$

where the bracket $\langle\ \rangle$ represents a time average over an optical period. This average leads $\langle\cos^2 wt\rangle = \langle\sin^2 wt\rangle = \tfrac{1}{2}$, and $\langle\sin 2wt\rangle = 0$. Under this situation, equation 4.62a is rewritten by :

$$I_t = E_o^2\;\sin^2 2\theta\,\sin^2\tfrac{1}{2}\delta\phi \quad . \quad (4.62b)$$

The maximum transmitted intensity is achieved when both polarizers are set at $\theta = 45^o$ and -45^o, respectively. The intensity of light transmitted through the Kerr gate at zero time delay ($\tau = 0$) is;

$$I_t(\theta=45^o) = E_o^2 \sin^2 \tfrac{1}{2}\delta\phi \quad . \tag{4.63a}$$

Equation 4.63a which is identical to equation 4.54a at $\tau = 0$ shows that the transmitted signal for the probe light is proportional to $\sin^2 \tfrac{1}{2}\delta\phi$. For $\delta\phi < 1$, then

$$I_t \propto (\delta\phi)^2 \tag{4.63b}$$

For a slow detection system, with the argument from equation 4.54b, we measured the energy through the Kerr gate by:

$$I_t(\tau) = \int_{-\infty}^{\infty} E^2(\tau - t) \sin^2 \tfrac{1}{2}\delta\phi(t) \quad dt \quad . \tag{4.63c}$$

4.5 Effect of the Permanent Birefringence and Missaligned Polarizers to the Transmitted Kerr Signal

In the discussion of section 4.4, it is assumed that there is no permanent birefringence in polarizers and windows of the Kerr cell, and that the two polarizers are perfectly aligned perpendicular to each other.

If a permanent birefringence exists along the path of the probe beam from windows, etc.. equation 4-63 can be rewritten as :

$$E_2^* = \mathrm{Re}\,(\cos\theta\, e^{i\delta\phi}\, e^{i\,a}\,\hat{x} + \sin\theta\, e^{ib}\,\hat{y})\, E_o\, e^{iwt} \quad , \quad (4.64)$$

where a, b are the phase changes along the x and y directions respectively, due to the permanent strain of matter. This may be caused by a piece of glass changes the polarization of the incident light. The transmitted signal from equation 4.64 is given by;

$$I^* = \overline{E_o^2}\, \sin^2\left[\frac{\delta\phi + (a-b)}{2}\right] \quad . \quad (4.65)$$

Even if $\delta\phi = 0$ (without orienting field), there is still some signal transmitted, which is given by :

$$I^* = \overline{E_o^2}\, \sin^2\frac{(a-b)}{2} \qquad (\delta\phi = 0) \; . \quad (4.66)$$

This gives rise to the noise in the signal.

When the two polarizers are not perfectly crossed, there is light leakage which contributes to the background noise. For example, if P_1 is polarized along θ, and P_2 is polarized along $\theta + 90 + \Delta$, the probe light field of equation 4.66 is

given by :

$$\vec{E}_3 = \mathrm{Re}\ [\cos\theta\ e^{i\delta\phi}\ \cos(\theta+90+\Delta) + \sin\theta\ \sin(\theta+90+\Delta)]\ \hat{A}\ E_o\ e^{iwt}. \tag{4.67}$$

For $\theta = 45^o$, the transmitted intensity through the gate is,

$$I_t = E_o^2\ (\cos^2\Delta\ \sin^2\tfrac{1}{2}\delta\phi + \sin^2\Delta\ \cos^2\tfrac{1}{2}\delta\phi\ ) . \tag{4.68}$$

Now, if $\delta\phi = 0$, the noise signal is :

$$I^*(\delta\phi=0) = E_o^2\ \sin^2\Delta\ . \tag{4.69}$$

The Kerr noise for both effects occur is :

$$I_t = E_o^2\ \sin^2\tfrac{1}{2}[\delta\phi + (a-b)]\cos^2\tfrac{1}{2}\Delta + \cos^2\tfrac{1}{2}[\delta\phi + (a-b)]\ \sin^2\tfrac{1}{2}\Delta\ , \tag{4.70}$$

For $\delta\phi = 0$, the noise is

$$I_t(\delta\phi=0) = E_o^2\ \sin^2\tfrac{1}{2}(a-b)\ \cos^2\tfrac{1}{2}\Delta + \cos^2\tfrac{1}{2}(a-b)\ \sin^2\tfrac{1}{2}\Delta\ . \tag{4.71}$$

In this steady state analysis, the signal to noise can be estimated from the ratio of equation 4.70 to equation 4.71. For typical values of $\Delta = 0.5^o$, and $a-b = 0.5^o$, at $\delta\phi = \pi$, the signal to noise ratio is :

$$S/N = I_{signal}(\delta\phi=\pi)/I_{noise}(\delta\phi=0)$$

$$= \frac{\sin^2(90+0.25)\ \cos^2 0.25 + \cos^2(90+0.25)\ \sin^2 0.25}{\sin^2 0.25\ \cos^2 0.25 + \cos^2 0.25\ \sin^2 0.25}\ ,$$

and $S/N \approx 2.5\times10^4$.

4.6 Characteristics Of The Optical Kerr Gate

The phase retardation $\delta\phi(t)$ of the probe pulse w_1 at time t, goes through the Kerr gate of length L and with the induced index of refraction $\delta n(t)$ is derived in equation 4.53 :

$$\delta\phi(t) = 2\pi\, L/\lambda_1\ \delta n(t) \quad . \quad (4.72)$$

The probe signal $I_t(\tau)$ transmitted through the Kerr gate at delay time τ with phase retardation $\delta\phi(t)$ can be written by[4,12]

$$I_t(\tau) = (1/I_1^o) \int_{-\infty}^{\infty} I_1(\tau - t)\ \sin^2 \delta\phi(t)/2\ dt \quad , \quad (2\text{-}73)$$

where I_1^o is the total signal of the probe light which passes through the system when axes of the two polarizers are oriented parallel to each other.

The following subsections contain discussions on the relevant parameters which affect the Kerr gate. They are : (A) the spatial, temporal and power dependence of the laser pulses; (B) the length of the sample cell; (C) the wavelength of the probe pulse ; (D) the concentration and orientational relaxation time of the solution for the Kerr gate; and (E) the temperature of the solution.

4.6A Dependence Of The Transmitted Signal In The Optical Kerr Effect On The Spatial, Temporal, And Power Of The Laser Pulses

The exact shape of laser pulses in time and space is needed to explicitly calculate the relationship between $\delta n(t)$ and τ_o. Assumptions for the shape of the laser pulses in time are Gaussian,[12,14] symmetrical exponential[6,42], Lorentzian[43], hyperbolic[43], or parabolic[44]. In this section, we have chosen two reasonable shapes for the laser pulse to simplify our analysis : I. a Gaussian time and spatial dependence; and II. a symmetrical exponential decay time profile with a Gaussian spatial dependence. Dispersion effects between pulses in a 1 cm sample solution are neglected[45].

The intensity of the intense orienting laser field can be expressed as follows :

I. Gaussian time and space profile :

$$\langle \vec{E}_{w_2}(r,t) \rangle = I_{2o}\, e^{-(t^2/\tau_2^2)}\, e^{-(r^2/r_o^2)}, \quad (4\text{-}74)$$

where r_o is the beam waist and τ_2 is the $1/e^2$ pulse duration.

II. Exponential time and Gaussian space profile :

$$\langle \vec{E}_{w_2}(r,t) \rangle = I_{2o}\, e^{-|t|/\tau_\ell}\, e^{-(r^2/r_o^2)}, \quad (4\text{-}75)$$

where τ_ℓ is 1/e pulse decay time.

In the case I, the time dependence of the induced index of refraction at center of the beam (r = 0) from equation 4-50 is,

$$\delta n(t) = n_2^e \langle \vec{E}_{w_2}^2(t) \rangle + (n_2^o/\tau_o) \int_{-\infty}^{t} \langle \vec{E}_{w_2}^2(t') \rangle \, e^{-(t-t')/\tau_o} \, dt' \, . \tag{4.76}$$

where $\langle \vec{E}_{w_2}^2(t) \rangle = I_{2o} \, e^{-t^2/\tau_2^2}$

Inserting the dependence of the laser profiles (equation 4.74) into equation 4.76, equation 4.76 reduces to :

$$\delta n(t) = \delta n^e(t) + \delta n^o(t) \tag{4.77}$$

$$= n_2^e \langle \vec{E}_{w_2}^2(t) \rangle + \left[n_2^o I_{2o} \, (\tau_2/\tau_o) \pi^{\frac{1}{2}} \mathrm{erf}\left\{ 2^{\frac{1}{2}} (t/\tau_2 - \tau_2/2\tau_o) \right\} \right.$$

$$\left. \times \, e^{+(t/\tau_o - \tau_2^2/4\tau_o^2)} \right] \quad \text{(for r=0)} \tag{4.78}$$

The time for $\delta n^o(t)$ to reach its maximum value is plotted versus the value of $1/\delta n^o(t_{max})$ in figure 4.2a.

Similarly, for case II, the $\delta n(t)$ for the symmetrical exponential decay time profile is (at r = 0) :

$$\delta n(t) = \delta n^e(t) + \delta n^o(t) \tag{4.79}$$

where $\delta n^o(t) =$

$$\begin{cases} n_2^o \, I_{2o} \, 2\tau_2\tau_o/(\tau_o^2 - \tau_2^2) \, e^{-t/\tau_o} + \tau_2/(\tau_2 - \tau_o) \, e^{-t/\tau_2} & \text{for } t > 0 \quad (4.80) \\ n_2^e \, I_{2o} \, \tau_2/(\tau_2 + \tau_o) \, e^{t/\tau_2} \, , \text{ for } t < 0 & (4.81) \end{cases}$$

$$n^e(t) = n_2^e \, I_{2o} \, e^{-|t|/\tau_2} \tag{4.82}$$

The time for $\delta n^o(t)$ to reach its maximum , $t_{max} = \dfrac{\ln(2\tau_2/(\tau_2 + \tau_o))}{1/\tau_o - 1/\tau_2}$

versus $1/\delta n^o(tmax)$ is plotted in figure 4.2b.

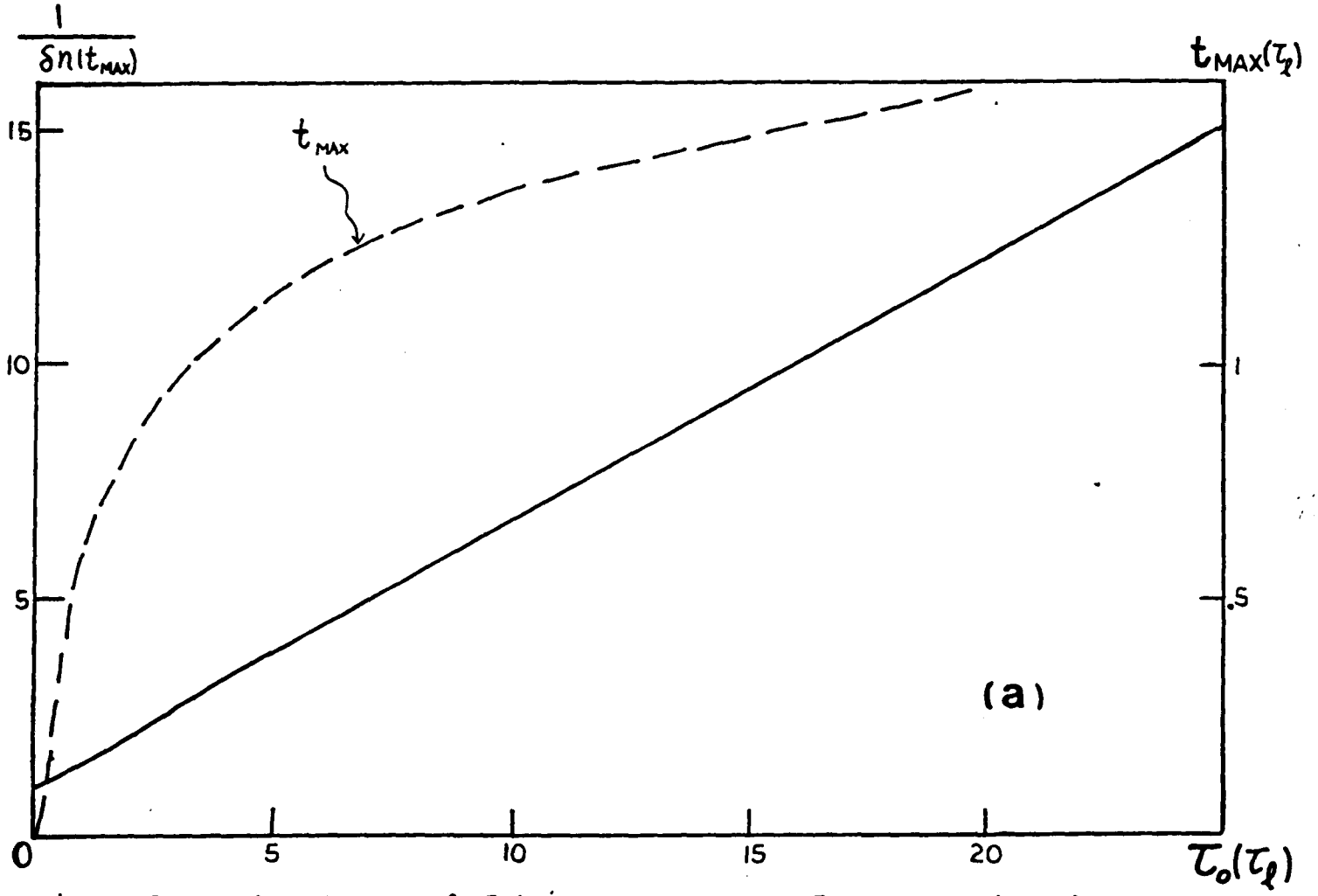

Figure 4.2a The time for the $\delta n(t)$ to reach its maximum value (t_{max}) and the inverse of the maximum nonlinear index of refraction, $1/\delta n(t_{max})$ are plotted versus the relaxation time of the liquid. The time profile of the pulse is Gaussian.

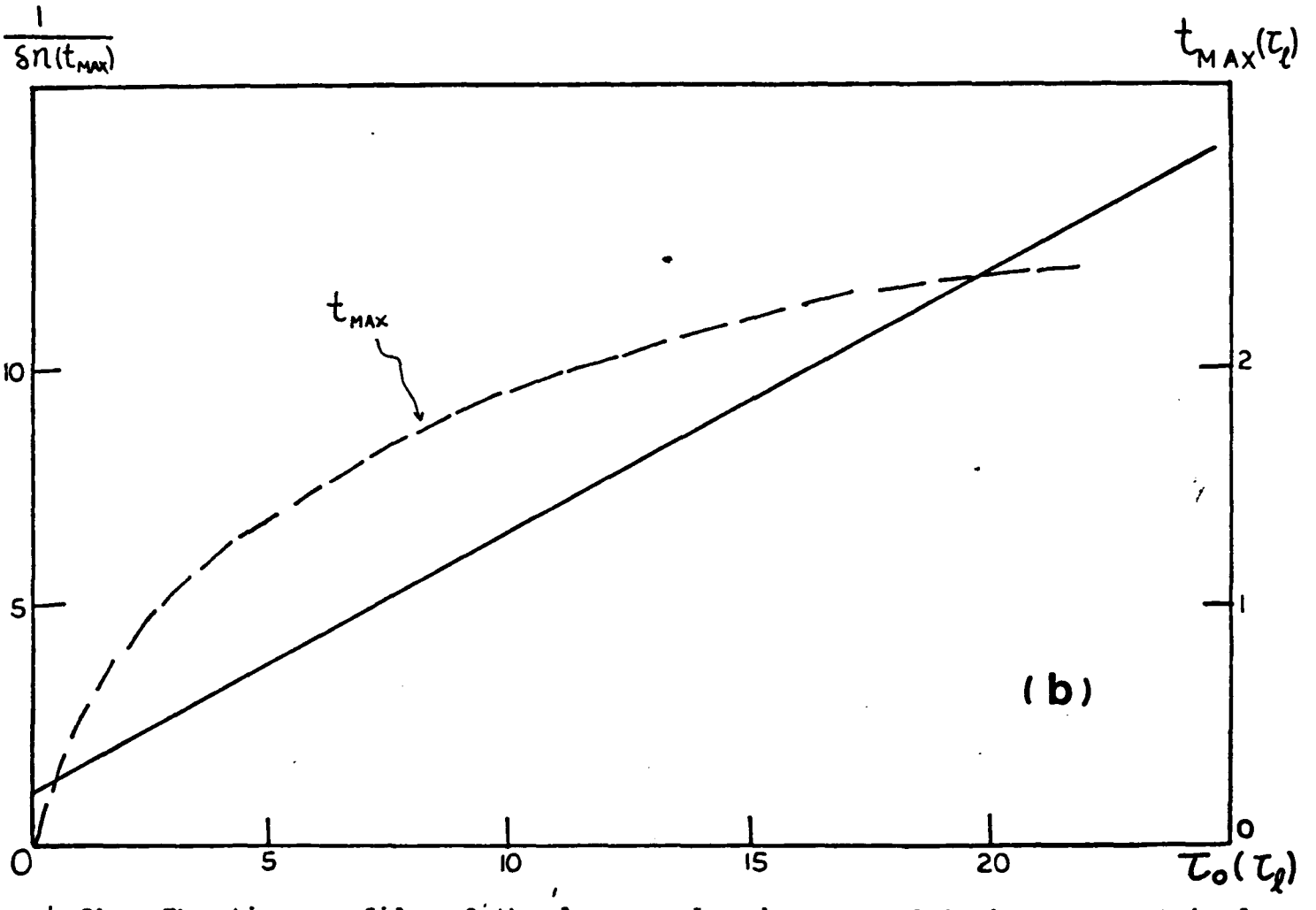

Figure 4.2b The time profile of the laser pulse is assumed to be a symmetrical exponential decay. The rest are the same as figure 4.2a.

A typical example of a calculated intensity decay profile of $\delta n(t)$ (from equations 4.79 and 4.80) for a laser pulse with symmetrical exponential time profile and the relaxation time of a liquid $\tau_o = 7\tau_\ell$ is shown in figure 4.3. Other laser pulse profiles in time such as Gaussian[14], and parabolic[43] show similar characteristics.

The intensity function of the weak probe laser pulse w_1 can be written as :

$$I_{w_1} = I_1(t) \quad e^{-r^2/r_1^2} \quad , \qquad (4.83)$$

w_1 is from the second harmonic generation (SHG) of the exciting laser pulse w_2. This pulse w_1, is time delayed to the orienting pulse by τ. We have assumed the pulse at w_1 has the same spatial and temporal characteristics as the pulse at w_2. Using a small sperture, the center portion of the probe pulse is used in this research. Therefore, the spatial profile of the probe pulses $I_{w_1}(r,t)$ is a square pulse. Under this assumption, equation 4.83 is rewritten by :

$$I_{w_1}(r,t) = I_1(t) \qquad , \quad (r_1 \gg b) \qquad (4.84)$$

where $I_1(t)$ has the same time dependence as the intense orienting pulse w_2, and b is the radius of the aperture.

When the orienting laser pulse has a Gaussian spatial distribution, the photo-detected signal at delay time τ transmitted through the Kerr gate from equation 4.72 is given by :

$$I_t(\tau) = (1/I_1^o) \int_{-\infty}^{\infty} \int_A I_{w_1}(r,\tau-t) \sin^2 \tfrac{1}{2}\delta\phi(r,t) \quad dA \; dt \qquad (4.85)$$

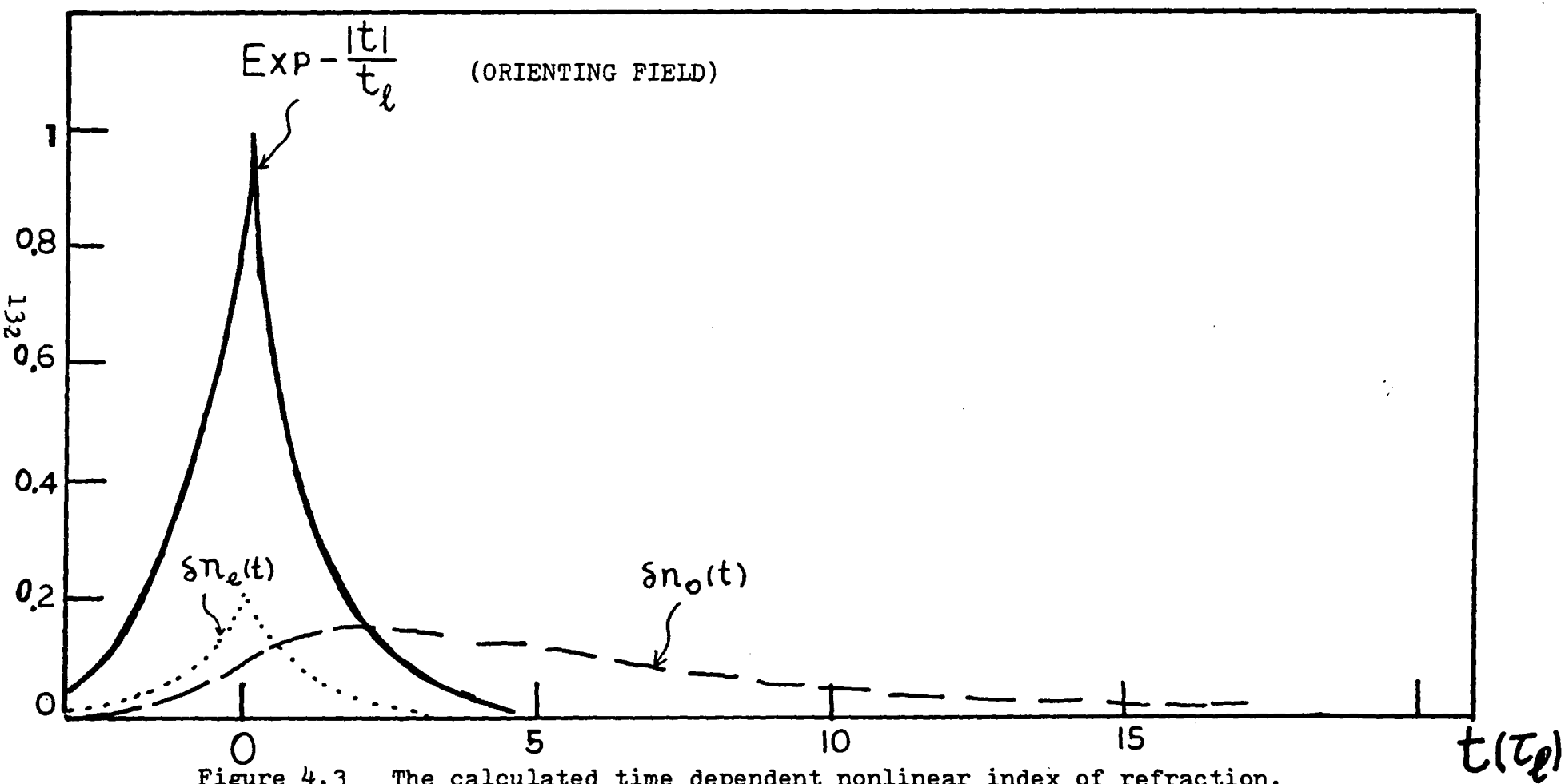

Figure 4.3 The calculated time dependent nonlinear index of refraction.

$$\delta n_o(t) = \begin{cases} 0.8\,(0.293\, e^{-t/7\tau_\ell} - 0.167\, e^{-t/\tau_\ell}) & \text{for } t \geq 0 \\ 0.1\, e^{t/\tau_\ell} & \text{for } t < 0 \end{cases} \quad \text{and} \quad \delta n_e(t) = 0.2\, e^{-|t|/\tau_\ell}$$

where I_{w_1} is described in equation 4.84; $\delta\phi(r,t)$ is the phase retardation of the probe pulse through the Kerr gate at position r and time t; A is the area of the aperture of radius b located in front of the Kerr gate ($A=\pi b^2$); and the normalization intensity I_1^o in equation 4.85 is obtained from :

$$I_1^o \equiv \int_{-\infty}^{\infty}\int_A I_{w_1}(r,t) = A\pi^{\frac{1}{2}}\tau_2 I_{1o} . \qquad (4.86)$$

The probe pulse w_1 in time is given by :

$$I_{w_1}(t) = I_{1o}\, e^{-t^2/\tau_2^2} , \qquad (4.87)$$

where the pulses of w_1 and w_2 are assumed to have the same pulse duration.

The spatial dependence of the phase retardation $\delta\phi(r,t)$ is defined by :

$$\delta\phi(r,t) \equiv \delta\phi(t)\, e^{-t^2/r_o^2} \equiv 2a\, e^{-t^2/\frac{2}{2}}\, e^{-r^2/r_o^2} , \qquad (4.88)$$

where $a \equiv L\pi n_2 I_{2o}/\lambda_1$. (4.89)

Substituting equations 4.86, 4.87, and 4.88 into equation 4.85, we obtain,

$$I_t(\tau) = (A\tau_2\pi^{\frac{1}{2}})^{-1}\int_{-\infty}^{\infty}\int_A e^{-(\tau-t)^2/\frac{2}{2}} \sin^2(a\, e^{-t^2/\tau_2^2}\, e^{-r^2/r_o^2})\,dA\,dt \qquad (4.90)$$

If $a \ll 1$, then $\sin^2(a\cdot e^{-t^2/\tau_2^2}\cdot e^{-r^2/r_o^2})$ can be approximately by $(a\cdot e^{-t^2/\frac{2}{2}}\cdot e^{-r^2/r_o^2})^2$. Equation 4.90 is rewritten by :

$$I_t(\tau) = a^2(A\tau_2\pi^{\frac{1}{2}})^{-1}\int_{-\infty}^{\infty}\int_A e^{-(\tau-t)^2/\tau_2^2}\, e^{-2t^2/\tau_2^2}\, e^{-2r^2/r_o^2}\,dA\,dt.$$

After integration, we obtain

$$I_t(\tau) = (ar_o/b)^2 \ (1 - e^{-2b^2/r_o^2}) \ (24)^{-\frac{1}{2}} \ e^{-(8/9)(\tau/\tau_2)^2} \ . \quad (4.91)$$

Replacing a (for $a \ll 1$) in equation 4.91 with the equation 4.89, we obtain

$$I_t(\tau) = (\pi L n_2/\lambda_1)^2 \ I_{2d}^2 \ (b/r_o)^2 \ (1 - e^{-b^2/r_o^2})^{-1} 24^{-\frac{1}{2}} (1-e^{-2b^2/r_o^2}) e^{-8\tau^2/9} \quad (4.92)$$

where I_{2d} is defined as the power density ($\equiv I_{total}/\text{area}$). For example, the peak transmitted signal $I_t(0)$ calculated from equation 4.92 is about 0.1 in the CS_2 gate, with $b = r_o$, $\tau = 0$, L = 1cm, $\lambda_1 = 0.53$ um, $n_2 = 2\text{x}10^{-11}$ e.s.u., and $I_{2d} = 50$ MW/cm^2 $= 4\text{x}10^5$ e.s.u..

When $a > 1$, the function $\sin^2 a$ can not be approximated to a^2, the time dependence of the transmitted signal in equation 4.90 is given by;

$$I_t(\tau) \equiv \int_A I_t(\tau, r) \ dA, \quad (4.93)$$

where

$$I_t(\tau, r) = (A \tau_2 \pi^{\frac{1}{2}})^{-1} \int_{-\infty}^{\infty} e^{-(\tau-t)^2/\tau_2^2} \ \sin^2(k \ e^{-t^2/\tau_2^2}) \ dt \ , \quad (4.94a)$$

and $$k \equiv a \ e^{-r^2/r_o^2} \ . \quad (4.94b)$$

Taking expansion of the function $\sin^2(k \ e^{-t^2/\tau_2^2})$, the equation 4.94a gives,

$$I_t(\tau, r) \equiv (A\tau_2 \pi^{\frac{1}{2}})^{-1} \int_{-\infty}^{\infty} e^{-(\tau-t)^2/\tau_2^2} \left[(2ke^{-t^2/\tau_2^2})^2/2 + (4k \ e^{-t^2/\tau_2^2})^4/4 + \ldots\right] dt. \quad (4.95)$$

There is no simple analytic expression for the transmitted signal of the Kerr effect for $a > 1$.

The total power I_{total} (≡ energy/duration time) of the intense orienting laser pulse w_2 for a Gaussian spatial profile is defined by :

$$I_{total} = \int_A I_{2o}\, e^{-r^2/r_o^2}\, dA = r_o^2\, I_{2o}\, (1 - e^{-b^2/r_o^2}). \quad (4.96)$$

From equation 4.96, we obtain

$$I_{2o} = I_{2d}\, b^2/r_o^2\, (1 - e^{-b^2/r_o^2})^{-1}\,, \quad (4.97)$$

where I_{2d} and I_{total} are measurable quantities.

In case II of the exponential time and Gaussian spatial profile, we have

$$I_1(t) = I_{1o}\, e^{-|t|/\tau_\ell}\,, \quad (4.98)$$

and $$I_2(r,t) = I_{2o}\, e^{-|t|/\tau_\ell}\, e^{-r^2/r_o^2}\,. \quad (4.99)$$

Inserting equation 4.83 and 4.98 into equation 4.86, we obtain

$$I_t(\tau) = \frac{\int_{-\infty}^{\infty} \int_A I_{1o}\, e^{-|\tau - t|/\tau_\ell} \sin^2 \tfrac{1}{2}\delta\phi(r,t)\, dA\, dt}{\int_{-\infty}^{\infty} \int_A I_1(t)\, dA\, dt}\,. \quad (4.100)$$

The transmitted intensity in equation 4.100 is evaluated with the following two conditions : (a) $\tau_\ell \gg \tau_o$ and (b) $\tau_\ell \ll \tau_o$.

(a) For $\tau_\ell \gg \tau_o$:

We define $$\delta\phi(r,t) \equiv 2\, k\, e^{-|t|/\tau_\ell}, \quad (4.101)$$

where $$k \equiv a\, e^{-r^2/r_o^2}\,. \quad (4.85)$$

Substituting equations 4.98 and 4.101 into equation 4.100, we obtain

$$I_t(\tau) = \frac{\int_{-\infty}^{\infty} \int_A e^{-|\tau - t|/\tau_\ell} \sin^2(k\, e^{-|t|/\tau_\ell})\, dA\, dt}{2\, b^2\, \tau_\ell\, \pi} . \quad (4.102)$$

From equation 4.102, the peak transmitted signal at $\tau = 0$ is :

$$I_t(0) = \tfrac{1}{2}(\pi b^2)^{-1} \int_A \left(1 - \frac{\sin 2k}{2k}\right) dA . \quad (4.103)$$

$$I_t(0) = \frac{1}{2} + (r_o^2/4ab)^2 \left\{ \sin 2a - \sin(2a\, e^{-b^2/r_o^2})/e^{-b^2/r_o^2} + 2a\left[\frac{-(2a)^2(e^{-2b^2/r_o^2} - 1)}{2 \cdot 2!} + \frac{(2a)^4(e^{-4b^4/r_o^4} - 1)}{4 \cdot 4!} + \ldots \right] \right\} \quad (4.104)$$

where $a \equiv \pi L n_2/\lambda_1 = \pi L n_2/\lambda_1 \,(b^2/r_o^2) I_{2d}\, (1 - e^{-b^2/r_o^2})^{-1}$. (4.89)

For $r_o \gg b$, the transmitted signal $I_t(0)$ can be approximated by :

$$I_t(0) \cong \tfrac{1}{2} - \frac{\sin 2a}{4a} . \quad (4.105)$$

This equation is used to fit our data in chapter 6.

For different values r_o at a constant value of input energy or total power, we have calculated different $I_t(0)$ from equation 4.104. These values are displayed in table 4.2.

r_o	a	$I_t(0)$
∞	0.5	0.079
3b	0.528	0.081
2b	0.565	0.082
b	0.79	0.099

Table 4.2 Peak Transmitted Signal of The Optical Kerr Gate At A Constant Power of Exciting Laser Pulse At Various Gaussian Spatial Widths

In table 4.2, we use a same amount of energy of the orienting laser field for the Kerr gate. The peak transmitted signal of an optical Kerr gate varies slightly when $r_o \geq 2b$. When $r_o \leq b$, the spatial profiles must be taken into account for accurate measurements. When $r_o \geq 2b$, we can assume an uniform spatial distribution and the spatial integration in equation 4.85 is simple. Therefore, the transmitted signal is independent of the geometry of aperture. We recommend using a small aperture (compare to the laser beam waist) in front of the Kerr cell.

(b) We now consider the case $\tau_\ell < \tau_o$, and the laser pulse is assumed to be a symmetrical exponential decay time profile with a uniform spatial distribution inside the aperture. Two examples are given below :

(i) For $\delta\phi(0) < 1$, a chosen expression for $I_t(\tau)$ can be obtained from equation 4.72;

$$I_t(\tau) = 1/2\tau_\ell \int_{-\infty}^{\infty} e^{-|\tau - t|/\tau_\ell} \sin^2 \delta\phi(t)/2 \, dt, \quad (4.106)$$

where $\delta\phi(t) \equiv 2\pi \, L/\lambda_1 \, \delta n(t)$. (4.107)

There are two mechanisms contribute to the nonlinear index of refraction as,

$$\delta n(t) = \delta n^e(t) + \delta n^o(t) \quad . \quad (4.108)$$

Equations 4.106, 4.107, and 4.108 are combined into ;

$$I_t(\tau) = 1/2\tau_\ell \int_{-\infty}^{\infty} e^{-|\tau - t|/\tau_\ell} \delta^2 n(t) \, (\pi \, L/\lambda_1)^2 \, dt, \quad (4.109)$$

where $\delta n(t)$ is defined in equation 4.84 (with $I_{2d} = 1$) as;

$$\delta n(t) = \begin{cases} n_2^o \, 2\tau_\ell \tau_o (\tau_o^2 - \tau_\ell^2)^{-1} \, e^{-t/\tau_o} + n_2^e + n_2^o(\tau_\ell - \tau_o)^{-1}\tau_\ell \, e^{-t/\tau_\ell} & \text{for } t \geq 0, \\ \left[n_2^e + \tau_\ell \, n_2^o (\tau_\ell + \tau_o)^{-1} \right] e^{t/\tau_\ell} & \text{for } t < 0. \end{cases} \quad (4.110)$$

We defined these parameters α, β, γ, and a as follows :

$$\alpha \equiv 2 \, \tau_\ell \tau_o \, n_2^o \, (\tau_o^2 - \tau_\ell^2)^{-1}$$

$$\beta \equiv n_2^e + \tau_\ell n_2^o \, (\tau_\ell - \tau_o)^{-1},$$

$$\gamma \equiv n_2^e + \tau_\ell n_2^o \, (\tau_\ell - \tau_o)^{-1},$$

and $a \equiv 1/2\tau_\ell \, (I_{2o} \pi \, L/\lambda_1)^2$. (4.111)

Inserting equation 4.110 into equation 4.109, we obtain

$$I_t(\tau \geq 0) = a \int_\tau^\infty e^{-(t-\tau)/\tau_\ell} \, (\alpha \, e^{-t/\tau_o} + \beta \, e^{-t/\tau_\ell})^2 \, dt$$

$$+ a \int_0^\tau e^{(t-\tau)/\tau_\ell} \, (\alpha \, e^{-t/\tau_o} + \beta \, e^{-t/\tau_\ell})^2 \, dt$$

$$+ a \int_{-\infty}^0 e^{(t-\tau)/\tau_\ell} \, \gamma^2 e^{t/\tau_\ell k} \, dt,$$

Evaluating this;

$$\frac{I_t(\tau \geq 0)}{a} = \alpha^2 \tau_o^2 (\tau_o^2 - 4\tau_\ell^2)^{-1} \, e^{-2\tau/\tau_o/2} + \frac{2 \, \alpha \, \beta \, \tau_o}{\tau_o + 2\tau_\ell} \, e^{-(1/\tau_o + 1/\tau_\ell)\tau}$$

$$+ \beta^2/3 \, e^{-\tau/\tau_\ell} + \frac{\alpha^2 \, \tau_o}{\tau_o - 2\tau_\ell} \, (e^{-2\tau/\tau_o} - e^{-\tau/\tau_\ell})$$

$$+ 2 \, \alpha \, \beta \, \tau_o/\tau_\ell \, (1 - e^{-\tau/\tau_o}) \, e^{-\tau/\tau_\ell} + e^{-\tau/\tau_\ell} \, (1 - e^{-\tau/\tau_\ell})$$

$$+ \gamma^2/3 \, e^{-\tau/\tau_\ell} \, . \quad (4.112)$$

For $\tau < 0$,

$$\frac{I_t(\tau < 0)}{a} = \int_0^\infty e^{-(t-\tau)/\tau_\ell} \, (\alpha \, e^{-t/\tau_o} + \beta \, e^{-t/\tau_\ell})^2 \, dt$$

$$+ \int_\tau^0 \gamma^2 \, e^{-(t-\tau)/\tau_\ell} \, e^{t/\tau_\ell/2} \, dt$$

$$+ \int_{-\infty}^\tau \gamma^2 \, e^{(t-\tau)/\tau_\ell} \, e^{t/\tau_\ell/2} \, dt$$

This integration result is

$$I_t(\tau<0)/a = \frac{\alpha^2 \tau_0 \tau_\ell}{\tau_0 + 2\tau_\ell} e^{\tau/\tau_\ell} + \frac{2\alpha\beta\tau_0\tau_\ell}{2\tau_0 + \tau_\ell} e^{\tau/\tau_\ell} + \frac{\beta^2 \tau_\ell}{3} e^{\tau/\tau_\ell}$$

$$+ \gamma^2 \tau_\ell (1 - e^{\tau/\tau_\ell}) e^{\tau/\tau_\ell}$$

$$+ \frac{\gamma^2 \tau_\ell}{3} e^{2\tau/\tau_\ell}$$

$$= \tau_\ell \left(\frac{\alpha^2 \tau_0}{\tau_0 + 2\tau_\ell} + \frac{2\alpha\beta\tau_0}{2\tau_\ell + \tau_0} + \frac{\beta^2}{3} + \gamma^2 \right) e^{\tau/\tau_\ell} - \frac{2}{3}\gamma^2 e^{2\tau/\tau_\ell} . \quad (4.113)$$

(ii) If $\delta\phi > 1$, then $\sin^2 \delta\phi(t)/2$ can not approximate to $\frac{\delta\phi^2(t)}{4}$. with the help of equations 4.110 and 4.111, equation-4.106 is rewritten as :

$$I_t(\tau) = \begin{cases} 1/2\tau_\ell \int_0^\infty e^{-|\tau - t|/\tau_\ell} \sin^2 a(\alpha e^{-t/\tau_0} + \beta e^{-t/\tau_\ell}) \, dt & (\text{for } t \geq 0) \\ 1/2\tau_\ell \int_{-\infty}^0 e^{-|\tau - t|/\tau_\ell} \sin^2 (a \gamma e^{t/\tau_0}) \, dt , & (\text{for } t < 0) \end{cases}$$

$$= \tfrac{1}{2}\, 1/2\tau_\ell \Bigg\{ \int_\tau^\infty e^{-(\tau - t)/\tau_\ell} \left[\frac{(2a\delta e^{-t/\tau_0} - 2a\beta e^{-t/\tau_\ell})^2}{2!} - \frac{(2a\delta e^{-t/\tau_0} - 2a\beta e^{-t/\tau_\ell})^4}{4!} + \ldots \right] dt$$

(for $t \geq \tau \geq 0$)

$$+ \int_0^\tau e^{\tau - t/\tau_\ell} \left[\frac{(2a\delta e^{-t/\tau_0} - 2a\beta e^{-t/\tau_\ell})^2}{2!} - \frac{(2a\delta e^{-t/\tau_0} - 2a\beta e^{-t/\tau_\ell})^4}{4!} + \frac{(2a\delta e^{-t/\tau_0} - 2a\beta e^{-t/\tau_\ell})^6}{6!} + \ldots \right] dt$$

(for $\tau \geq t \geq 0$)

$$+ \int_\tau^0 e^{\tau - t/\tau_\ell} \left[\frac{(2a\gamma e^{t/\tau_\ell})^2}{2!} - \frac{(2a\gamma e^{t/\tau_\ell})^4}{4!} + \frac{(2a\gamma e^{t/\tau_\ell})^6}{6!} + \ldots \right] dt$$

(for $0 \geq t \geq \tau$)

$$+ \int_{-\infty}^\tau e^{t - \tau/\tau_\ell} \left[\frac{(2a\gamma e^{t/\tau_\ell})^2}{2!} - \frac{(2a\gamma e^{t/\tau_\ell})^4}{4!} + \frac{(2a\gamma e^{t/\tau_\ell})^6}{6!} - \ldots \right] dt$$

(for $0 \geq \tau \geq t$)

(4.114)

4.6B Dependence Of The Transmitted Signal On The Length Of The Kerr Cell

The phase retardation $\delta\phi(t)$ in equation 4.72 of the Kerr gate is linearly proportional to the cell length L. For $\delta\phi < 1$, the transmitted signal through the Kerr gate is proportional to $\delta\phi^2$ varying quadratically with the cell's length.

If we include the group velocity dispersion effect between the probe pulse and orienting pulse, the induced time dependent birefringence from equation 4.50 can be expressed by[45,46] :

$$\delta n(z,t) = \sum_i n_2^{(i)}/\tau_i \int_{-\infty}^{t-z/v} dt' \; \overline{E_{w_1}^2}(z,t') \; e^{[t'-(t-z/v)]/\tau_i} \qquad (4.115)$$

where v is the group velocity of the probe pulse, z is the propagation direction of the laser beam, and i is the sum of all kind relaxation mechanisms. The total phase retardation through the Kerr cell of length L (in equation 4.72) is rewritten by :

$$\delta\phi(t) = 2\pi/\lambda_1 \int_0^L dz \; \delta n(z,t) \; . \qquad (4.116)$$

The time lag caused by the group velocity difference of the two pulses used in the optical Kerr effect over a distance of 1 cm is small in comparison to the laser pulse width. The group velocity dispersion [45] has been neglected in all the calculationsin this thesis.

4.6C Dependence Of The Transmitted Signal On The Wavelength Of The Probe Pulse

For $\phi \ll 1$, the transmitted signal is inversely proportional to the square of wavelength of the probe pulse shown in equation 4.53. This was under the assumption that there is no absorption in the liquid gate. In the research program, there was no electronic transition or vibrational transition process in the region of these frequencies w_1, w_2, and $w_1 \pm w_2$. Each component of $\chi^{(3)}$ in equation 4.45 contains a energy denominator which can become resonance. One possibility of the effect associated of the denominator corresponding to the absorption of one photon with the simultanteous emission of another photon at or near a resonance frequency (especially, a vibrational frequency of molecules). The energy difference is complex. That is,

$$\hbar w_a = \hbar (w_a' - i \Gamma_a) \quad , \tag{4.117}$$

where $\hbar w_a'$ is the real energy and Γ_a is the width of the system's a-th state. Equation 4.31 can be rewritten by[31,32] :

$$P_i^{(3)}(w-w_r) = 6 \chi^{(3)}_{ijkm}[-(w-w_r), w, w-w_r, -w] E_j(w) E_k(w-w_r) E_m^*(w) \times \exp(k_{w-w_r}, r) \quad , \tag{4.118}$$

where w_r is the vibrational energy of the medium. This is called Raman induced Kerr effect. When an intermediate frequency $w_2 - w_1$ is near a Raman frequency w_r of the material, the imaginary part of the resonance contribution to the scattering

cross section[10,47,48]. Equation 4.118 can be written in an apparent form as :

$$\chi^{(3)}_{\text{Kerr}}(-w_1,w_2,-w_2,w_1) = \chi^{(3)}_{\text{NR}}(-w_1,w_2,-w_2,w_1) + \frac{R_S}{w_r - (w_2-w_1) + i\Gamma_r} + \frac{R_A}{w_r + (w_2-w_1) - i\Gamma_r} \quad (4.119)$$

The term $\chi^{(3)}_{\text{NR}}$ is real and smoothly varying. The last two terms are Raman contributed from Stokes and anti-Stokes to the Kerr effect, respectively. The Raman induced Kerr effect induced by picosecond laser pulses can be used to obtain information on the vibrational kinetics in condensed matter.

4.6D Concentration Dependence Of The Nonlinear Index Of Refraction

The Kerr constant in mixed liquids in the steady state measurement described by Kielich[9] is :

$$B = \sum_i x_i B_i^{(1)} + \rho \sum_{ij} x_i x_j B_{ij}^{(2)} + \rho^2 \sum_{ijk} x_i x_j x_k B_{ijk}^{(3)} + \cdots \qquad (4.120)$$

where $B_i^{(1)} \propto \Delta\alpha_i^2 \left(1 + x_i f_{ii} \right)$,

and $B_{ij}^{(2)} \propto \Delta\alpha_i \Delta\alpha_j f_{ij}$ for $i \neq j$.

where x_i is the mole fraction of the i-species molecules, $B^{(i)}$ is :Kerr constant of the i-th species molecules, $B^{(ij)}$, $B^{(ijk)}$ are non-zero constant only for mixtures in which interactions occur both between molecules of the same kind andbetween those of various components, ρ is the number density of molecules in liquids. The relation between the Kerr constant and nonlinear index of refractic is defined by[12,18,17]

$$B = \lim_{E \to 0} n_2/\lambda E^2 \quad , \qquad (4.121)$$

$$\text{or} \quad B = 2\pi (n \lambda_1)^{-1} 12 \left\{ \chi_{1212}^{(3)}(-w_1, w_1, w_2, -w_2) + \chi_{1221}^{(3)}(-w_1, w_1, w_2, -w_2) \right\} \qquad (4.122)$$

Following the derivation of Kivelson and Tsay[49] and section 3.3, the integrated intensity for the two components in the depolarized Rayleigh scattering is :

$$I_{\pm} = (T_{+}^{-1} - T_{-}^{-1})^{-1} \Big\{ \pm \Delta\alpha_B^2 \left[x_B (1 + x_B f_{BB}) (\tau_{BB}^{-1} - T_{\pm}^{-1}) \right] \pm \Delta\alpha_C^2 \left[x_C (1 + x_C f_{CC}) (\tau_{CC}^{-1} - T_{\pm}^{-1}) \right] \pm \Delta\alpha_B \Delta\alpha_C \phi \left[x_B (1 + x_B f_{BB}) x_C (1 + x_C f_{CC}) \right]^{\frac{1}{2}} \left[(T_{\pm}^{-1} - T_{\pm}^{-1}) - (1 - \phi^2)(\tau_{BB}^{-1} - \tau_{CC}^{-1}) \right] \Big\}$$

(4.123)

where $T_{\pm}$ are the fast and slow relaxation times in mixed liquids[49] (see section 3.3), respectively; τ_{ii} is the uncorrelated single particle's relaxation time (defined in section 3.3); $I_{\pm}$ are the integrated light scattering intensities for $T_{\pm}$ component decay processes, respectively; $\Delta\alpha_i \equiv \alpha_{i\parallel} - \alpha_{i\perp}$ where $\alpha_{i\parallel}$ and $\alpha_{i\perp}$ are the components of the polarizability tensor parallel and perpendicular to the symmetry axis of the of the molecules of the i-th species, respectively; x_B and x_C are the mole fractions of the B and C molecular species, respectively; and $x_B + x_C = 1$; f_{BB} and f_{CC} are the pair correlation factors between same kind of molecules; and ϕ is an intermolecular coupling parameter between two different species of molecules which is given by[49] :

$$\phi^2 = x_B\, x_C\, f_{BC}^2\, (1 + x_B\, f_{BB})^{-1}\, (1 + x_C\, f_{CC})^{-1} \quad , \quad (4.124)$$

with f_{BC} as the interspecies pair correlation factor.

The total integrated intensity of the depolarized Rayleigh scattering is given by

$$I = I_+ + I_-$$

$$= \Delta\alpha_B^2 x_B(1 + x_B f_{BB}) + \Delta\alpha_C^2 x_C(1 + x_C f_{CC}) + 2\Delta\alpha_B\Delta\alpha_C x_B x_C f_{BC} . \quad (4.125)$$

The relationship between the intensity of depolarized Rayleigh scattering ,I, and the molecular part of the nonlinear index of refraction of the Kerr effect has been described by Hellwarth[39] as :

$$I_{\pm} \propto n_{2\pm} . \quad (4.126)$$

However, the intensity of light scattering and the size of n_2 expressed by equations 4.123,4.125 are the steady state values. In kinetic experiments, due to the finite response of the molecular reorientation of the molecules to the orienting electric field associated with the laser pulse, the peak of the Kerr intensity is reduced. The peak of the Kerr intensity associated with orientational motion is proportional to :

$$S_{\pm}^2 \propto \left[n_{2\pm} / f(T_{\pm})\right]^2 . \quad (4.127)$$

The peak response function $f(T_{\pm})$ is inversely proportional to the ratio of moleculear orientational relaxation time to the duration time of the laser pulse (see section 4.6A ,p138). This ratio in equation 4.127 corresponds to the amplitude ratio $(S_+/S_-)^2$ for the double exponential decay function (equation 4.127) of the transmitted signal from the experimental data of the mixed binary liquids in the optical Kerr effect:

$$I_t(t) = (S_+ e^{-t/T_+} + S_- e^{-t/T_-})^2 \quad \text{for } t > 0, \quad (4.128)$$

Bauer et at[50] have pointed out that the peak intensity of the depolarized Rayleigh scattering is proportional to I times T. The size of the signal is larger for a slower relaxation process than for a faster one. On the other hand, the opposite is true for the optical Kerr effect. The induced optical Kerr effect by an intense picosecond laser pulse weighs more a faster relaxation component over a slower one. This may be one possible reason to explain some of the inconsistences in the measured relaxation times obtained by these two techniques[6,51] and other methods[52].

4.6E Temperature Dependence Of The Nonlinear Index Of Refraction

The temperature dependence of the transmitted signal arises from molecular contribution $n_2(T)$ (see equation 4.51). If $\phi < 1$, the peak transmitted signal from the Kerr gate is :

$$(I_t(0))^{\frac{1}{2}} = [T\, f(\tau_o(T))]^{-1}\, n_2 \quad , \qquad (4.129)$$

where $f(\tau_o(T))$ is the response function calculated from equations 4.78 and 4.80 and is plotted in figure 4.2. The response function of n_2 is proportional to the inverse of the reorientational relaxation time which is temperature dependent.

If the liquid has a critical transition temperature T_c, such as a liquid crystal[12,41], the Kerr signal is given by :

$$(I_t(0))^{\frac{1}{2}} \propto n_2\, [(T - T_c)\, f(\tau_o(T))]^{-1} \, . \qquad (4.130)$$

According to the argument by Kielich[9], the pair correlation factor J defined in equation 4.52 is temperature dependent with

$$J(T) = A\, e^{E/RT} \quad , \qquad (4.131)$$

where A is a proportional constant, and B is a parameter of intermolecular energy involving the orientational motion between two molecules. Thus n_2 in equation 4.129, 4.130 is also a function of T.

Taking into account equation 4.131 for $\phi < 1$, the temperature dependent relationship between the square root of the transmitted signal and the nonlinear index of refraction of equation 4.129 can be written as :

$$(I_t)^{\frac{1}{2}} = C\left[{}_a n_2^o\,(1 + J(T))\,(T\,f(\tau_o(T))^{-1} + n_2^e\right], \quad (4.133)$$

where C is a proportional constant, n_2^e is the nonlinear index of refraction arisinng from the electronic process which is assumed to be temperature independent[7,9,14] and ${}_a n_2^o$ is defined in equation 4.53as a constant arising from molecular reorientational motion.

In mixed binary liquids, the temperature dependence of the nonlinear index of refraction can be expressed by[49,53],

$$n_2 = x_B n_{2B}^e + x_C n_{2C}^e + I_+(T)\left[T\,f(\tau_+(T))\right]^{-1} + I_-(T)\left[T\,f(\tau_-(T))\right]^{-1}, \quad (4.134)$$

where I_+ and I_- are the total integrated intensity of the fast and slow molecular orientational processes in mixed binary liquids[49,53], and τ_+ and τ_- are the corresponding fast and slow molecular orientational relaxation times which have been discussed in section 3.3. The above analysis, we have neglected the contributions from molecular libration and molecular redistribution. These two mechanisms are fast and temperature dependent. However, with the resolution of our experimental techniques, we can not distinguish them from the electronic process and we have lumped it into the prompt response curve.

4.7 Deconvolution Of The Measured Relaxation Time

The experimental measured relaxation time τ_{exp} is extracted from the transmitted decay profile of the dynamic Kerr effect. The Kerr decay profile is the measured transmitted signal through the gate at different decay times between the orienting and the probing pulses. This profile in the convolution of the laser pulses and the relaxation kinetics of the sample liquids (see equation 4.54). If the exciting laser pulse and the probe laser pulse both are a δ-function in time, then the Kerr decay profile will be the relaxation time of the sample. After the time convolution (see equations 4.50, 4.54, and 4.80), the experimental measured decay time τ_{exp} extracted from the transmitted signal is not equal to the true molecular reorientational relaxation time τ_o. When $\tau_o \rightarrow 0$, the decay profile of the transmitted Kerr signal will resemble to the shape of the laser pulse.

Numerical calculations have been made for the convoluted signal of equation 4.54 for various ratios of τ_o/τ_ℓ. The calculated $I_t(\tau)$ is plotted on a semi-logarithm paper as a function of time. The slope is the predicted relaxation time τ_{exp}.

In figure 4.4, the theoretical predicted values τ_{exp}/τ_ℓ versus the true reorientational relaxation time, τ_o/τ_ℓ, are plotted for two different pulse shapes. The dynamic range used here is about 1000 to 1 which is close to the real experimental situation. In figure 4.4a, both of the laser pulses - orienting

and probing are assumed to be Gaussian in time profile, that is

$$I(t) = e^{-(t^2/\tau_\ell^2)\ln 2} \quad , \qquad (4.134)$$

where $2\tau_\ell$ is the FWHM of the laser pulse. And the molecular reorientational relaxation function is assumed a single exponential decay. The zero time is the exciting pulse arriving the sample which coincident to the probe pulse.

$$I_o(t) = \begin{cases} e^{-t/\tau_o} & \text{for } t \geq 0 \\ 0 & \text{for } t < 0 \end{cases} \quad . \qquad (4.135)$$

The convoluted plot in figure 4.4a indicates that the measured relaxation time τ_{exp} can be taken as the true molecular reorientational time τ_o with a negligible error ($< 5\%$) for $\tau_o > \tau_\ell$.

In figure 4.4b, both of the laser pulses are assumed to be a symmetric exponential decay profile :

$$I(t) = e^{-|t|/\tau_\ell} \quad . \qquad (4.136)$$

This pulse convoluted with the relaxation function (equation 4.135) shows that for $\tau_o \leq \tau_\ell$, the measured relaxation time τ_{exp} is a representation of the laser pulse widths. For $\tau_o > 2\tau_\ell$, the deviation factor between τ_{exp} and τ_o is less than 10%. Therefore, the relaxation time can be extracted from the decay profile without much error ($< 10\%$), if $\tau_o > 2\tau_\ell$, where τ_ℓ is the 1/e power of the laser width.

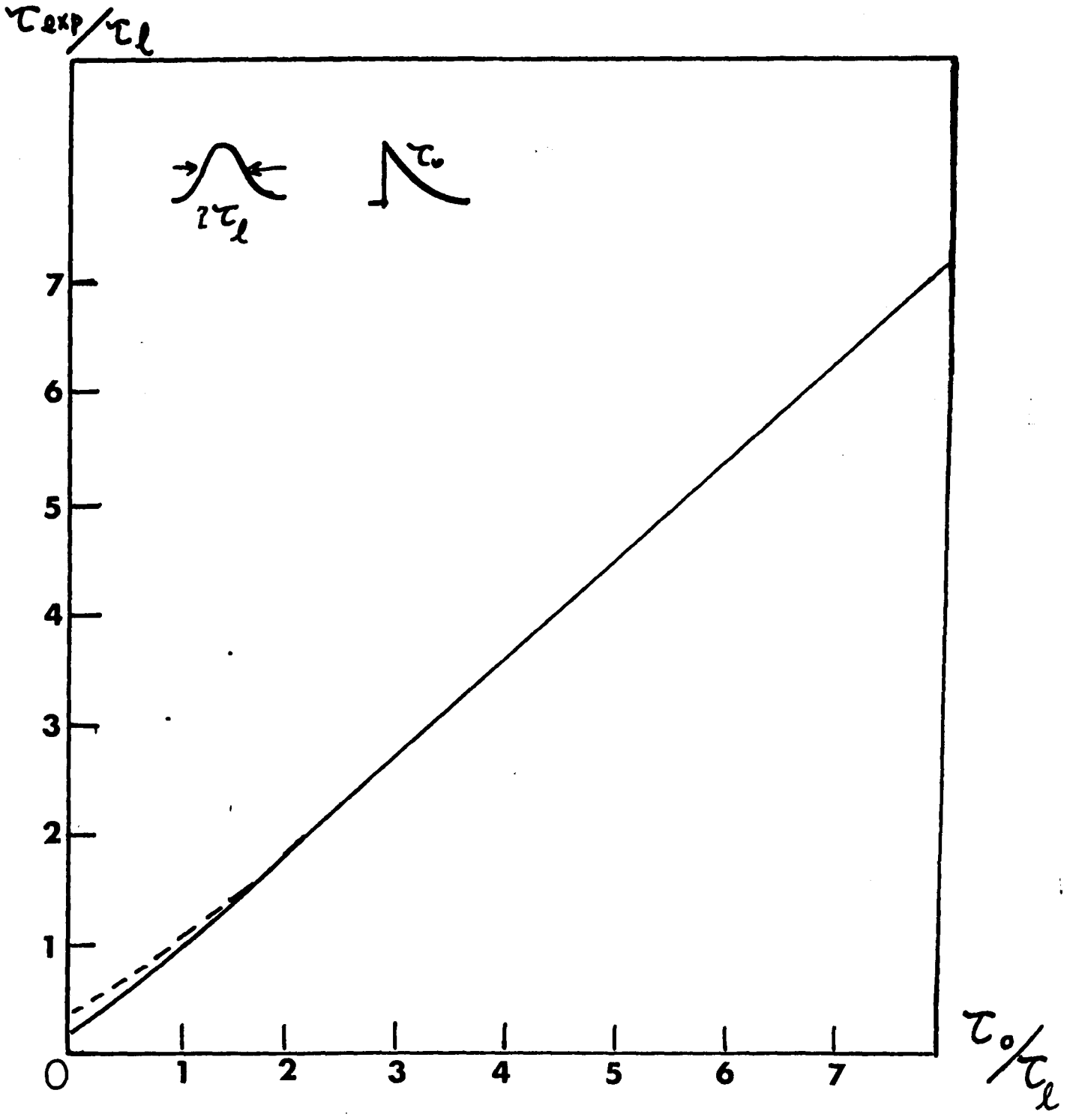

Figure 4.4a A plot of the measured Kerr relaxation time, τ_{exp}, extracted from the tail of the convolution of an exponential decay curve with a Gaussian shape laser pulse of duration, $2\tau_l$, (F.W.H.M.) versus the molecular orientational relaxation time, τ_o. The τ_{exp} is obtained from the slope of tail at $t > \tau_l$. The solid line obtained from $\delta n(t)$, and the dashed line is from $I_t(\tau)$.

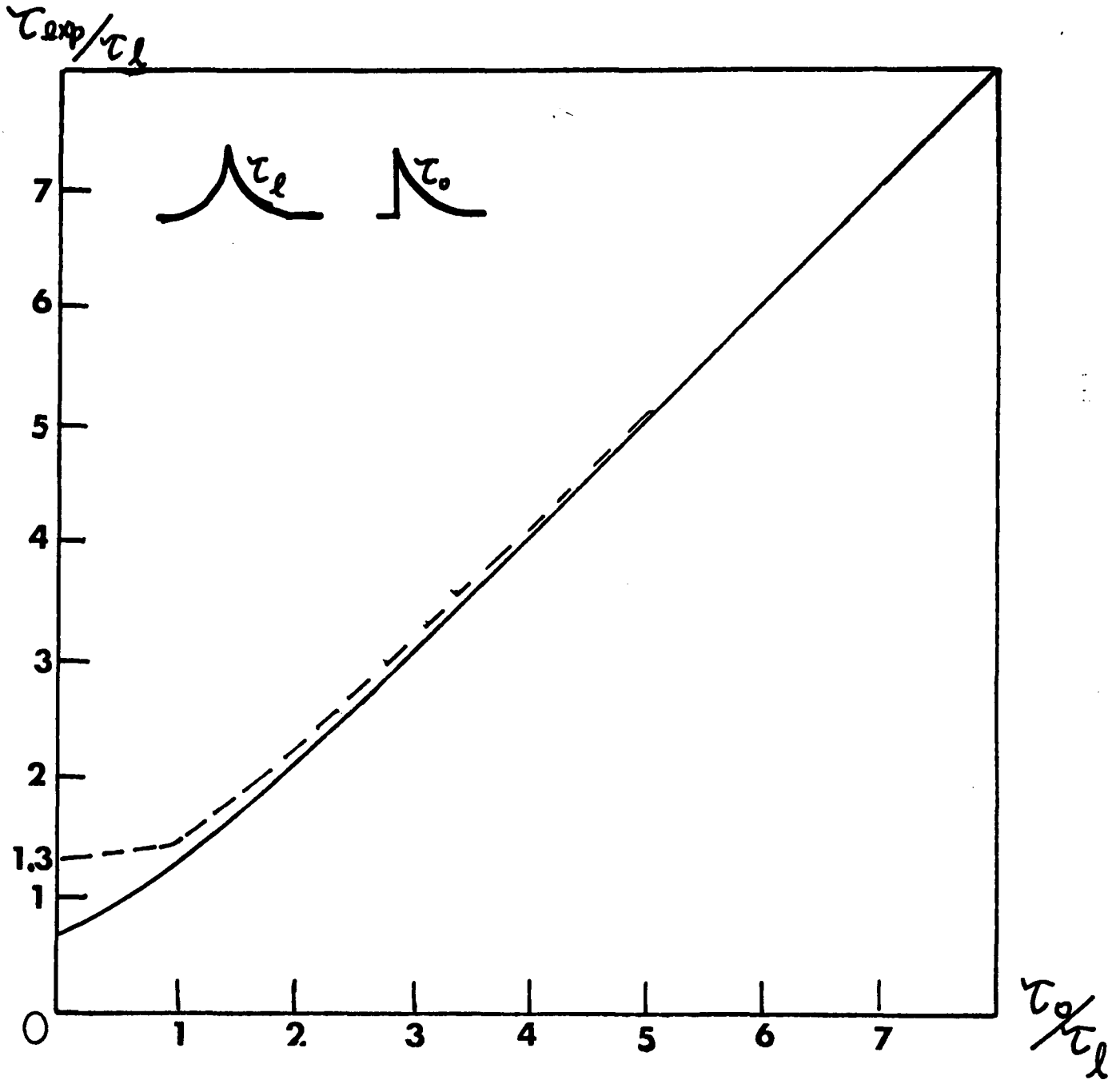

Figure 4.4b A plot of the measured Kerr relaxation time, τ_{exp}, extracted from the tail of the convolution of an exponential decay curve with a full exponential shape laser pulse of τ_l (1/e time), versus the molecular orientational relaxation time τ_o. The τ_{exp} is obtained from the slope of tail at $t > \tau_l$. The solid line is obtained from $\int n(t)$, and the dashed line is obtained from $I_t(\tau)$.

4.8 Effect of Distribution Relaxation Time for Molecular Reorientational Motion

In the condensed state, the magnitude and direction of the interaction force between molecules varies from point to point and at different times. At a certain moment, the molecule at its own position has its own intrinsic relaxation time. In general, there is a spread of relaxation time distributed around a most probable value τ_o. In the experimental relaxation decay time from the optical Kerr effect (OKE), we have assumed a single relaxation time τ_{exp} in neat liquids to fit our data. It is a measurement of the average value over all the possible relaxation processes. The form of the distribution function of the relaxation times in condensed state has been given by Schester[54] as a simple gaussian function $G(\tau) = A \exp\{-(\tau - \tau_o)^2/b^2\}$; and by Kirkwood and Fuoss[55] as a function $G(\tau) = \{2\cosh(\tau/\tau_o) + 2\}^{-1}$.

If we apply such kind of distribution of relaxation time into the OKE, the nonlinear index of refraction is rewritten by ;

$$\delta n(t) \equiv \int \delta n(t,\tau)\, d\tau \qquad (4.138)$$

where $\delta n(t,\tau) \equiv \frac{1}{\tau}\int_{-\infty}^{t} n_{2\tau} E^2(t') e^{-(t-t')/\tau} dt'$

$$\propto n_{2\tau}(e^{-t/\tau})/\tau \quad , \qquad (4.139)$$

and $n_{2\tau} \equiv n_2 G(\tau)$ is the magnitude of the nonlinear index of refraction of molecules which relaxes with a time τ .

There is no simple closed form for equation 4.138 with either gaussian, Lorentzian, hyperbolic cosine, square relaxation time distributions. There is a common property

for all the possible distributions. For a symmetrical distribution function $G(\tau)$ in τ , due to the factor $1/\tau$ in $\delta n(t,\tau)$, the overall relaxation time extracted from $\delta n(t)$ versus t fitted with a single exponential decay curve will be less than the most probable relaxation time τ_o. For example, we take a simple discrete distribution relaxation times for equation 4.138 :

$\tau_o = 10\tau_\ell$ and $n_{2\tau_o} = 1$; $\tau_{-1} = 7.5\tau_\ell$ and $n_{2\tau_{-1}} = 0.6$;

$\tau_1 = 12.5\tau_\ell$ and $n_{2\tau_1} = 0.6$; $\tau_{-2} = 5\tau_\ell$ and $n_{2\tau_{-2}} = 0.3$;
and $\tau_2 = 15\tau_\ell$ and $n_{2\tau_2} = 0.3$; where τ_ℓ is the laser pulse width. The relaxation times τ_o, $\tau_{\pm 1}$, $\tau_{\pm 2}$, are the possible relaxation times of molecules in liquids with a magnitude of nonlinear index of refraction $n_{2\tau_i}$.

The best fit for a single exponential relaxation time in the experiment τ_{exp}, for the sum of these five possible decay times is about $9\tau_\ell$. This is about 90% of the most probable relaxation time τ_o. If we use another experimental technique, such as the inverse linewidth of the depolarized Rayleigh wing scattering (DRS) to measured τ_{exp}. The data deduced from DRS is favorable to measure longer relaxation time in a distribution relaxation times. The measured relaxation time from a single Lorenzian fit to the data of the DRS has a tendence longer than the most probable value τ_o. This is one possible reason why τ_{exp}(from OKE) is faster than τ_{exp}(from DRS). Take nitrobenzene as an example. From the measured value deduced from the OKE, τ_{exp} lies between 28 ps to 36 ps[56], while the measured value deduced from the DRS is mostly in the region of 36 ps to 44 ps[57].

References

1. A.D. Buckingham, Proc. Phys. Soc.(London), B69,344 (1956).
2. G. Mayer and R. Gires, C.R. Acad. Sci.(Paris),258, 2039 (1963).
3. P.D. Maker, R.W. Terhune, and C.W. Savage, Phys. Rev. Lett., 12, 507, (1964).
4. M.A. Duguay and J.W. Hansen, Appl. Phys. Lett.,15,192 (1969).
5. F. Shimizu and B.P. Stoicheff, IEEE, QE-5, 544, (1969).
6. P.P. Ho, W.Yu, and R.R. Alfano, Chem. Phys. Lett.,37,91, (1976).
7. P.P. Ho and R.R. Alfano, J. Chem. Phys., 67, 1004, (1977).
8. P.P. Ho and R.R. Alfano, Chem. Phys. Lett., 50, 74 (1977).
9. S. Kielich, Acta. Phys. Polon., 30, 683 (1966).
10. P.D. Maker and R.W. Terhune, Phys. Rev., 137, A801 (1965).
11. G.K.L. Wong and Y.R. Shen, Phys. Rev.,A10, 1277 (1974).
12. R.H. Hellwarth, A. Owyoung, and N. George, Phys. Rev., A4, 2343 (1971).
13. J. Kerr, Phil. Mag., 50, 337 (1875).
14. K. Sala and M.C. Richardson, Phys. Rev., A12, 1036 (1975).
15. M. Born, Ann. Phys. Lpz., 55, 177, (1918).
16. Ottenbein, Phys. Zeit., 35, 209, (1935).
17. A.D. Buckingham and R.E. Raab, J. Chem. Soc., 2341 (1957).
18. A. Owyoung, Ph.D. Thesis, (California Inst. Tech., 1972).
19. R.R. Alfano and S.L. Shapiro, Phys. Rev. Lett., 24, 592, (1970); ibid, 24, 1219 (1970).
20. R.W. Hellwarth, Phys. Rev., 163, 205 (1967).
21. W.S. Gornel, H.E. Howard-Lock, and B.P. Stoicheff, Phys. Rev. A1, 1288 (1970).
22. Y.R. Shen, Phys. Lett., 20, 378, (1966).

23. A.G. Litvak, JETP Lett., 4, 230 (1966).

24. P.N. Butcher "Nonlinear Optical Phenomena" (Ohio State University Press, 1965).

25. N. Bloemberger, "Nonlinear Optics", (Cambridge, 1964).

26. O. Svelto, "Prog. in Optics", Ed. by Wolf, XII, 3 (1974).

27. A. Yariv, "Quantum Electronics", (John Wiley and Sons, New York, 1975).

28. S.A. Akhmanov and R.V. Khokhlov, "Problems in Nonlinear Optics", FTD-MT-24-259-69, (1964).

29. Y.R. Shen and M.M. Loy, Phys. Rev., A3, 2099 (1971).

30. R.Y. Chiao, P.L. Kelly, and E. Garman, Phys. Rev. Lett., 17, 1158 (1966).

31. E. Garmire, F. Pandarese, and C.H. Townes, Phys. Rev. Lett., 11, 160 (1963).

32. R.R. Alfano and S.L. Shapiro, Phy.. Rev. Lett.,24, 584 (1970).

33. R.R. Alfano, L.L. Hope, and S.L. Shapiro, Phys. Rev., A6, 43 (1972).

34. F. Shimuzu, Phys. Rev. Lett., 19, 1097 (1967).

35. P. Lallemand, Appl. Phys. Lett., 8, 276, (1966).

36. A.C. Cheung, D.M. Rank, R.Y. Chiao, and C.H. Townes, Phys. Rev. Lett., 20, 786 (1968).

37. R. Polloni, C.A. Sacchi, and O. Svelto, Phys. Rev.,A2,1955 (1970).

38. R.W. Hellwarth, J. Chem. Phys., 52, 2188 (1970).

39. R.W. Rentzepis, M.R. Topp, R.R. Jones, and J. Jortner, Phys. Rev. Lett., 25, 1742 (1970)

40. T. Keyes and D. Kivelson, J. Chem. Phys., 56, 1057 (1972).

41. T.D. Glerke and W.H. Flygare, J. Chem. Phys., 61, 2231(1974).

42. D.von der Linde, A. Laubereau, and K. Kaiser, Phys. Rev. Lett., 26, 954 (1971).

43. R.R. Alfano, GTE technical Report, TR 72-2301 (1972).

44. J.H. Marburger, "Progess in Quantum Electronics" 4, 35 (1975).

45. M.R. Topp and G.C. Orner, Opt. Comm., 13, 276 (1975).

46. T.W.Strouve, Opt. Comm. 21, 216 (1977).
C.A.G.O. Verma and P.M. Rentzepis, 58, 5237 (1973)

47. P.Heiman, R.W. Hellwarth, M.D. Levenson, and G. Martin, Phys.Rev. Lett., 36, 189 (1976).

48. H. Lotem and R.J. Lynch Jr., Phys. Rev. Lett., 37, 334 (1976).

49. D. Kivelson and S.J. Tsay, Mol. Phys. 29, 29 (1975)

50. D.R. Bauer, J.I. Brauman, and R.Pecora, J.Chem. Phys.,63,53(1975)

51. G.R. Alms, D.R. Bauer, J.I. Brauman, and R. Pecora, J. Chem. Phys., 59, 5310 (1973).

52. C.P. Smyth, "Molecular Relaxation Processes", (Academic Press, New York, 1966).

53. P.P.Ho and R.R.Alfano, J. Chem. Phys., (to be published).

54. E. Von Schweidler, Ann. Physik, 24, 711 (1907).

55. J.G. Kirkwood and R.M. Fuoss,J. Chem. Phys., 9, 329 (1941).

CHAPTER 5

EXPERIMENTAL TECHNIQUES

5.1 Experimental Apparatus - Laser

The experimental apparatus used in the research program is shown in figure 1. It is similar to the designs shown in the references 1 to 5.

The laser (see figure 1a) consists of a Korad K-1 series laser head surrounded by a flash lamp, a K-1 power supply with a 400 uf capacitor, and a Owen-Illinos (ED-2.3) Nd:glass rod Brewster-Brewster cut $7\frac{1}{2}$" long by $\frac{1}{2}$" diameter situated in a laser cavity. The laser head,with its xenon flash lamp, is water cooled. The Korad KWC-3 cooler employs a deionizer to maintain low electrical conductivity to prevent shorting of the electrodes in the laser head. A flow rate of 2 gal/min and pressure 7 psi is recommended. The temperature of the water is controlable from the range of 15^{o} to 30^{o}C with 0.2^{o}C accuracy. The temperature was set at 22^{o}C in the experiments. The firing rate is about once per minute with a pump energy of about 2,000 joules.

The laser cavity consists of a rear wedged ($\frac{1}{2}^{o}$) curve mirror at 100% reflection at 1.06 um. The output mirror is a wedged ($\frac{1}{2}^{o}$) flat mirror with a 55% reflection for 1.06 um. Both dielectric coated mirrors were purchased from the Laser Energy Company. A 1 cm long dye cell serves a dual purpose : it improves the shot to shot reproducibility of the laser trains and it eliminates satellite pulse. The mode-locking dye solution consists of Kodak 9860 dye dissolved in 1,2-dichloroethane solution at

transmission for 1.06 um of about 66% to 74% at normal incidence. The transmission was measured by placing the cell into a close box with a constant light source. This signal was recorded by a selenium photodetector and a microvolt meter. The one cm long dye with pyrex windows was placed in the cavity at Brewster's angle with respect to the direction of the laser beam.

The pumping voltage from the K-1 power supply is set about 10V to 30V above the threshold voltage for laser action. This was necessary in order to obtain a single reproducible train (amplitude fluctuation from shot to shot is about 10%) without satellite pulses and multiple trains. When the pumping voltage is too high, the discriminating action of the mode-locking dye is reducing, this allows another train to built up inside the cavity. When the pumping voltage is too close to the threshold voltage, the pulse train frequently fails to built up. The most stable laser trains were obtained at a dye concentration between 70% to 73% transmission for 1.06 um at normal incidence at 20 volts above the threshold.

The laser output train was analyzed by the detection systems as shown in figure 1. It consisted of (1) a Hadron model 105C with S1 surface fast photodetector together with a Tektronix 519 fast response oscilloscope; (2) a Joule meter from the GEN-TEC Company model EN-100; (3) a two-photon fluorescence[7] (TPF) setup; and (4) a ½ meter Jarall-Ash spectrometer. The fast photodiode and oscilloscope were used to check the shape of the output train. Each train consists of

about 100 pulses (see figure 2a). The joule meter with sensitivity of 50 uJ was used to measure the total energy of the train. The typical energy of each pulse in the train at 1.06 um is about 5 to 15 mJ depending on the concentration of the mode-locking dye.

The average pulse duration of the 1.06 um pulse was obtained (see figure 2b) by using the technique of TPF with a supersaturable solution of Rhodamine 6G dye dissolved in methanol. The pulse duration of the 1.06 um pulse was measured to be 9.5 ± 2 ps.

The spectral width of the laser pulses was analyzed by a ½ meter spectrometer with a 50 um wide input slit with a resolution of 1.6 Å. Most of the data in determining the spectral width were taken at the wavelength of the 0.53 um laser pulse using the polaroid film. The 0.53 um laser light is generated by the second harmonic generation[9] (SHG) from the laser output wavelength of 1.06 um. The band width of both the 1.06 um (1.0632 um) and 0.53 um (0.5316 um) laser pulses is about 80 cm^{-1} (see figure 2c for example). The SHG 0.53 um light was obtained by passing the 1.06 um pulse through a KDP crystal 1 inch in length. The KDP crystal was mounted in a cartridge with anti-reflection coated windows and is surrounded by a index matching fluid. The conversion efficiency is about 10%. This crystal was purchased from the Lasermetrics

Company. The pulse duration time of the 0.53 um laser was measured by TPF technique with a supersaturable dye solution of 7-diethylamino 4-methyl coumarin dissolved in ethanol. The mean pulse duration of 0.53 um laser was about 8 $\pm$ 2 ps.

5.2 Some Characteristics of the Mode-locked Laser Pulses

The high power picosecond laser pulses are generated by placing a saturable dye solution in the laser cavity[2,8]. The dye has a wide absorption band ($\leq$ 200 Å) with its peak absorption wavelength near the emission wavelength of the laser medium. Moreover, the dye solution has a recovery time $\sim$ 10 ps which is faster than the laser cavity's round trip time (7.2ns). The absorption characteristic of this dye is nonlinear; that is, the absorption at laser frequency decreases with light intensity above a critical intensity (see figure 3). With these properties, the saturable absorber dye can filter the noise and reflections generated inside the laser cavity. The light in the cavity initially consists of a messy noiselike signal with random amplitude and phase fluctuations. The short pulse is built up out of this random distribution of noise pulses by the bleachable dye. The largest fluctuation in the initial fluorescence intensity pattern of the laser medium is selected out and preferentially amplified. As the light bounces back and forth in the cavity, the bleachable dye acts as a time varying attenuator, opening and closing at a frequency equal to the difference in frequency of two adjacent modes. Through this action the fields of the oscillating modes interfere, therefore coupling each of two adjacent modes together, and a definite relationship among the oscillating modes is achieved. The dye is used to absorb the smaller amplitude pulses and attenuates the wings of the more intense pulse and producing a much sharper pulse. This pulse sharpening proceeds until the maximum number of modes are coupled together typically 10^3 modes (this is limited by the band width of the gain medium). After hundreds

of passes through the laser cavity, combination of the nonlinear absorption of the dye and amplification by the laser medium results in an intense pulse circulating in the cavity (see figure 2a). Upon reflecting on the output mirror, about 45% of the pulse escapes through the mirror, resulting in a periodic train of ultrashort pulses. These pulses are separated by the round trip time in the laser cavity (=2L/c ~ 7.2 ns).

The generation of satellite pulses in the laser output is possible. The satellite pulses are smaller pulses which pass through the dye solution when the dye is bleached by an intense pulse in the opposite direction. The dye is opened for the recovery time of the dye molecules. During this time, and weak pulse which are not intense enough to bleach the dye by itself can be transmitted if they are travelling in the opposite direction. These weak pulses are then amplified by the laser gain medium forms an additional pulse circulating in the cavity. This generates a satellite pulse train. This pulse is separated from the main output pulse by the time of $n(2d/c)$, where d is the distance from the backmirror of the laser cavity to the dye cell ($d \sim 30$cm), and n is an integer number ($= \pm 1, \pm 2, \pm 3, \cdots$) which represents the order of the satellite pulse.

There are two methods which can be used to eliminate the satellite pulses from the basic laser output pulses. The first method uses a contact dye cell at the backmirror. When $d = 0$, the satellite pulse can no longer exists. The second method uses a long dye cell. It takes a pulse 33 ps to travel a distance of 1 cm in air. The optical length of the dye cell

divided by the speed of light is about three times as long as the recovery time of the dye molecules. With such a long dye cell, the intense pulse bleaches only a fraction of the dye molecules in the dye cell, the rest of the dye cell still acts as a filter for the weaker pulses which tend to pass through the cell in the opposite direction. The disadvantage of this method is that the duration time of the output pulse is slightly longer than that from a thinner dye cell by ~ 2 ps.

The characteristics of a pulse in the laser pulse train (100 pulses) obtained in this experiment are :

(a) The energy of each pulse is about 10 mJ and pulse duration time is about 10 ps at a dye concentration of about 70% transmission at 1.06 um. The power output at 1.06 um is about 1 GW.

(b) The relationships between the dye concentration (measured transmitivity for 1.06 um light at normal incidence) versus the 1) spectral width, 2) intensity of the spectral peak (from spectrometer with an optical multichannel analyzer), 3) total energy (from energy meter), and 4) time duration (from TPF) are shown in figure 4. From the fast oscilloscope (Tektronix 519), after about 5 initial intense pulses, each pulse in the train has about the same amplitude. The signals recorded corresponds to the sum of 100 pulse measurements, if the relaxation time of the sample is much smaller than the pulse separation time. Therefore, these results are the statistical mean average of 100 pulses. Moreover, each error bar in figure 4 is an average of five laser shots. There is a jump from these values around 83% dye concentration. Above this transmitivity, the laser

output is not mode-locked. This is verified by the pictures from the Tektronix 519 oscilloscope. The band width Δw and pulse duration time, $\Delta\tau$, do not vary too much with respect to the different dye concentrations in the region studied. However, the intensity at each spectral output increases linearly with the dye concentration (the sum of all spectral intensity is the total energy). Sometimes, multiple trains appeared in the experiment resulting in larger energy measurements (this data were eliminated).

(c) The laser output became more stable and spectral width narrowed, when a SHG crystal[11] or a 1 mm thickness dielectric coated mirror of arbitrary reflectivity was placed in the laser cavity. Weisman and Rice[11] showed that the spectral width is narrowed and the pulse duration remained the same when a SHG crystal is placed in the cavity. When we placed a 1 mm thickness mirror of 20% reflection for 1.06 um into the cavity, the measured spectral width reduced to 5 cm^{-1} while the pulse duration increased to 20 ps. We found the larger the reflectivity of the mirror, the narrower the spectral width and the longer the pulse duration. In figure 5, characteristics of the laser output (TPF and spectra measurements) for a 28% reflectivity 1 mm thickness mirror in the cavity. The pulse train was checked by the Tektronix 519 oscilloscope for proper pulse shape(figure 5a). In this case, the pulse duration is $\lesssim$ 15 ps and the spectral width is about 6 cm^{-1}.

5.3 Sample Preparations

All the chemicals used in the experiments were purchased from the Eastman Kodak Company and Fisher Scientific Company of the puriest grade available.

In the temperature dependent experiments the sample cell was situated in a glass dewar with strain free windows. The Kerr effect of the windows, and sample cell was measured to be less than one hundredth of the samples. A thermocouple was cleaned and immersed in the sample. After sealing the cell, the temperature was controlled by flowing cooled nitrogen gas into the dewar and surrounding the sample cell holder with heater tape. The sample temperature was controlled to $\pm$ 1 K. The temperature variation across the sample region was measured to be less than 1 K. A simple schematic diagram of this setup is shown in figure 6.

The viscosity of the samples was measured by an Ostwald type Cannon-Fenske viscometer (see figure 7) in a temperature controlled water reservoir. With four viscometers of different capillary radius, we can cover the viscosity range from 0.2 cp to 35 cp with an 1% accuracy. Generally, a capillary viscometer has a dynamic range about 10. Only one size of viscometer was needed to measure a series in a temperature dependent measurement of the viscosity. For example, nitrobenzene has a measured viscosity of 1.25 cp at 60°C and 2.9 cp at 3°C. The measured viscosity was obtained from the following equation :

$$\eta_m(cp) = K \rho_x t_x$$

where K is a proportional constant which is a function of radius

and length of the viscometer, ρ is the density of the x liquid, and t_x is the time for x liquid travelled in the viscometer from Z_1 to Z_2 (see figure 7). Distilled water of a viscosity equal to 1 cp and density equal to 1 gm/cm^3 at 20°C were chosen as a standard for the calibration of the viscometer. time for water through the capillary viscometer was about 130 seconds. Using the values from water, K was deduced.

In the supercooled liquid state experiment, salol was used as the Kerr medium. The melting temperature of salol is 42°C. Under proper conditions, salol can stay in a liquid form at room temperature. The powder crystal salol was heated up to about 100°C. At this temperature, water and low boiling point alcohols impurities were removed from the sample. This liquid was quickly sealed into a clean, dry, and nitrogen gas filled sample cell. In a slow cooling rate (= 1°C/min), the sample started to crystalize below -30°C. This is due to some impurities left inside the sample.

In the plastic crystal phase experiment, succinonitrile (SN) was chosen as the Kerr medium. The single crystal SN was grown by using Bridgman-Stockbarger methods[6]. A schematic diagram of this technique is shown in figure 8. The melting temperature of SN is 57°C. The wax sample SN was placed in a 15 cm long by 1.5 cm diameter test tube with a Conical tip. The sample was heated up to 100°C to eliminate the possible water and low boiling point organic chemical impurities. Then the sample tube was sealed. The sample tube was placed into a temperature reservoir with two different temperature zones. The upper region of the reservoir was set at 70°C and the lower portion of this reservoir was set at room temperature. The sample tube was slowly dropped from the upper zone (liquid

state) down to the lower zone with a constant speed. After passing the temperature gap, the sample started to crystallize. In order to obtain a good quality single crystal, the following requirements must be met : (1) A sharp vertical temperature gradient at the boundary of these two temperature zones; (2) An uniform temperature distribution across the sample tube in each zone; (3) A slow growing rate. In this experiment, pump oil and water were chosen for the upper and lower zones, respectively. A two feet long 10 ohms heating tape with 10 volts was used to obtain 70°C for the upper zone. The lower zone was set at room temperature. By choosing a clock motor, the growing speed was controlled to be about 1 mm/hour. All other effect tended to disturb the melt-interface of the growing crystals, such as temperature fluctuation, mechanical shock, and erratic descent were avoided. A 10 cm long by 1.5 cm diameter single SN crystal was obtained in this method.

Crystal x-ray diffraction pattern was obtained by using both the Laue method and rotating-crystal method. This was done with the help of Dr. Paul Wang in Polytechnic Institute of New York and Prof. J. Steiner of The City College of New York.

5.4 Prism Delay Multi-shot Optical Kerr Gate Technique

The technique used to obtain most of the Kerr kinetics data on the molecular relaxation processes in this research is described here.

The output beam at 1.06 um from the laser was weakly focused by a 1 meter focal length lens (L1 in figure 1) to compensate for the divergence of the output beam. This beam was passed through a KDP crystal for SHG. About 10% of the 1.06 um light was converted to the 0.53 um light. The beam splitter (M4 in figure 1) transmitted 90% at 1.06 um and reflected 99% at 0.53 um. The 0.53 um pulses which were used as the probe beam in the optical Kerr effect was passed through a movable prism for optical delay. The 0.53 um pulses was directed through two crossed polarizers (Polaroid HN 22) polarized along $+45^{o}$ and -45^{o}, respectively. For steady state measurements, the transmission of a non-polarized light (at wavelength $\simeq$ 0.53 um) through these two polarizers $\leq$ 10% when their axes parallel and $\leq$ 5×10^{-4}% when their axes were set perpendicular.

In this experiment, the Kerr samples were placed in a 1 cm cell with strain free windows. A 3/32" diameter aperture was placed in front of the cell. The transmitted signal through the Kerr gate was measured by a S4 RCA IP39 phototube. With a 500 ohms resistor, the detector was found to be linear from 1 mV to 1V.

The exciting 1.06 um light which was linearly polarized parallel to the plane of the table surface was focused into the sample cell by a lens (L3, f=50cm) to a beam diameter of 3mm. The 1.06 um was directed at an angle of incidence of three

degrees with respect to the plane of the table. The optical delay between the 1.06 um and 0.53 um pulses was achieved by a prism in the 0.53 um light path (1cm delay = 67ps). Inside the 1cm long sample cell, the probe beam and the exciting beam were collinear and almost totally overlapped. The intensity of the exciting laser pulse was varied by inserting different neutral density filters (Hoya) along the 1.06 um beam path. The highest intensity used in this study was about 2.5 GW/cm^2. The maximum dynamic range for the Kerr gate reached in this study was about $5x10^3$. This is the ratio of the peak transmitted signal when the gate is opened to its maximum value when it is closed (exciting pulse blocked or the probing pulse not overlapping the exciting pulse). The power of the pump laser at 1.06 um was measured before and after the sample gate (D3, D1 in figure 1) to assure correct optical alignament and no lost from absorption or nonlinear effects in the samples. The maximum energy of each probe pulse was less than 10 uJ. The probe beam was not focused. An example of the nitrobenzene gate is displayed in figure 9.

The operation of the Kerr gate is fully described in chapter 4. The induced birefringence in the isotropic medium is caused by orienting and redistributing the anisotropic molecules and disturbing the electron clouds in liquids through the interaction of the linearly polarized optical electric field of the laser pulse with the polarizability of the molecules.

5.5 Single Shot Kerr Technique

Recently, a single shot picosecond laser Kerr gate technique was developed[5,10]. If offers both convenience and accuracy in measuring the kinetics of the optical Kerr effect over the multi-shot technique (section 5.4). Except the dynamic range was limited to about 100. This range was due to the dynamic range of detection and read out system and thermal noise of the PAR optical multichannel analyzer I.

A schematic of the essential parts of the experimental appratus for measuring the Kerr relaxation time was shown in figure 10. An intense 1.06 um laser pulse with 10 ps duration induced the Kerr birefringence in the sample solution which was situated between a pair of crossed polarizers. Upon passing a second harmonic pulse of 8 ps duration through a dilute milky solution. The energy of each 0.53 um pulse was about 1 mJ. The 0.53 um beam travels through the milky solution was observed to be about 3mm in height by ½ mm in width inside this cell. This was achived by sending the 0.53 um beam through a regular lens (f = 50 cm) to reduce its diameter, then passing through a cylindrical lens (f =25 cm) to reduce the width of the probe beam. This ½ mm width of the scattered light introduced an additional 2.2 ps uncertainty of the actual laser pulse which was negligible in comparision to the 10 ps pulse duration of the 1.06 um pulse. The 0.53 um light along the path was unifromly scattered into a continuous series of delayed pulses. This milky solution was placed in the 4 cm long rectangular cell for scattering

the light. The solution was made by adding cream powder into a water-alcohol (90%-10%) solution. The concentration of the milky solution was checking by a photodetecting system in which 10% of the light was lost after traversing through this 4 cm long milky solution. The scattered light of the probe beam at 90° was almost uniform.

The scattered light at 90° formed an oblique wave front and was directed into a 1 cm long sample cell. In this manner, the scattered light which was variably delayed with respect to the 1.06 um exciting pulse was used to interrogate the time evolution of the induced transitory birefringence of a sample solution in a single laser shot. The 1.06 um pulse was incident at an angle of approximately three degrees with respect to the plane of incidence of the scattered 0.53 um pulse and was focused (f=100 cm) to a diameter of about 5mm into the sample cell. In addition, an aperture of 5mm diameter was placed in front of the sample cell. At the sample cell, the maximum intensity used for the exciting laser pulse was 1 GW/cm^2. The track of the 0.53 um scattered light from the milky solution was imaged and demagnified (2.25x) by a camera lens (f/2.8, 13.5 mm) onto the target face of an optical multichannel analyzer (OMA I). The active face of SIT (silicon intensified tube) of OMA is 12.5 mm x 2.5 mm. The subtraction mode of the OMA SIT target face was not used.

The alignment procedure for the single shot's Kerr gate is described as follows : First, we used an He-Ne alignment laser which followed the shape and beam path of the 0.53 um laser pulses. Second, the axes of these two polarizers were set in a parallel direction. The scattered light from the

He-Ne laser was imaged on the OMA target surface. The image was uniform across the whole detection region of the OMA. Third, a diffraction slide with four thin slits (each slit is 100 um in width and is separated by 5 mm between each other) was placed in front of the milky solution cell. We adjusted the distance from lens to the OMA until we obtained sharp images with equal intensity from the scattered light from these slits. The final step was to check the uniformity and the images of the slits with the 0.53 um pulse.

The triggering unit from the OMA to the laser pulses train was arranged as follows :

When the accumulation buttom of the OMA was pressed down, there were two actions in the OMA console. First, a 5v triggering signal from OMA console (TTL remote program pin 1 and pin 7 to pin 29 in figure 11) turned on a coil switch. When the switched closed, pin 4 and pin 5 of the K-1 power supply of the laser were shorted together. This short automatically fired the laser within 1 ms. Second, simultaneously, the signal accumulation process of the signal on SIT target in the OMA was not started for two full cycles (32 ms x 2 delay time). Then, the OMA started to collect and remove the signal from the first channel of the SIT detector target. These two processes allowed the total optical signal to reach the target face of the SIT detector before the OMA console started to remove the signal and accumulate the data. Five scans of the SIT detector face removed most of stored voltages.

The induced light intensity profile passing through the Kerr gate was detected by the OMA which has 500 channel detectors over length 12.5 mm and height 2.5 mm. The signal was processed in the OMA I system and the decay profile stored in the OMA's memory. The effect of lag[12] of the SIT detector was minimized by scanning most of the charge off the SIT vidicon. Usually, five scans were used. Using more scans, the background signal was larger. In the five scans mode, the system was linear to within 5% over the dynamic range used in the experiment ($\approx$ 100).

The time axis of the OMA was calibrated by moving a prism in the 0.53 um laser beam path. A one cm delay in prism with respect to the 1.06 um pulse corresponded to 66.7 ps delay time. The length of the track imaged on the detector determined the time span investigated. Typically, a time display of about 127 ps [= 12.5mm(width of the detector face)x2.25(demagnification factor) x 1.35 (refractive index of milky solution) x 10/3 (ps/mm)] was investigated on a single shot. A signal to background ratio $\approx$ 100 was achieved. The intensity profile was then recorded by a xy-recorder and replotted on a semi-logarithm graph paper. The relaxation time was extracted from the slop of the measured intensity profile. Deconvolution was not necessary when the Kerr relaxation times of these liquids were longer than the prompt experimental decay of CS_2 Kerr intensity profile ($\approx$5ps).

References

1. M. Duguay and J. Hansen, Appl. Phys. Lett., 15, 192, (1969). F. Shimizu and B.P. Stoicheff, IEEE, QE-5, 544, (1969).
2. R.R. Alfano and S.L. Shapiro, Scientific American, 228, 43, (1973).
3. P.P. Ho and R.R. Alfano, J. Chem. Phys., 67, 1004, (1977).
4. P.P. Ho, W. Yu, and R.R. Alfano, Chem. Phys. Lett., 37, 91, (1976).
5. P.P. Ho and R.R. Alfano, Chem. Phys. Lett., 50,74,(1977).
6. W.D. Lawson and S. Nielson, "Preparation of Single Crystals" (Butterworths, London, 1958).
7. J.A. Giordmaine, P.M. Rentzepis, S.L. Shapiro and K.W. Wecht, Appl. Phys. Lett., 11, 216, (1967).
8. A.J. DeMaria, D.A. Stetser, and W.H. Glenn Jr., Science, 156, 1557, (1967).
9. J.A. Giordmaine, Phys. Rev. Lett., 8, 19, (1961).
10. M.A. Duguay and A.T. Mittick, Appl. Optics, 10, 216, (1971).
11. B.B. Weisman and S.A. Rice, Spect. Lett., 8, 329, (1975).
12. RCA "Electro Optics Handbook" EOH-11, (1974).

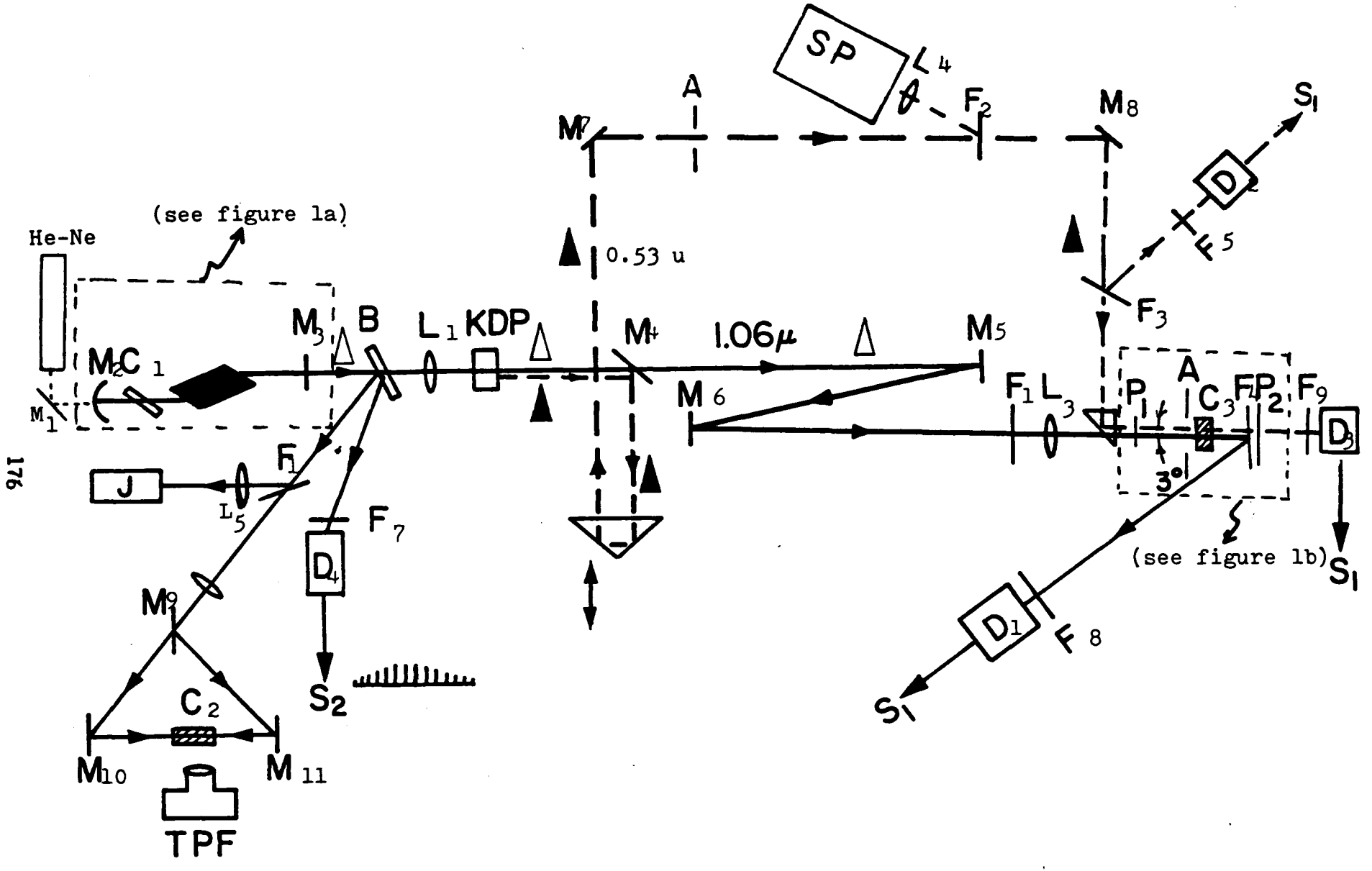

Figure 1. Experimental Setup

Figure 1, The experimental setup

A : 3/32" aperture,

B : 1/2° wedged beam splitter,

C1: 1 cm long Pyrex cell with Kodak dye 9860 in 1,2-dichloroethane solution,

C2 : TPF cell with Rhodomine-6G dye in methanol solution.

C3 : 1 cm long optical cell,

D1 : S1 surface slow response photodiode,

D2,D4 : S4 surface slow response photodiodes,

D4 : S1 surface fast response photodiode.

F1,F6,F7,F8 : Corning 7-99 filters,

F2,F4 : Corning 4-96 filters,

F3 : Corning 3-69 filter,

F5,F9 : Ditric 3-C narrow band filters,

J : energy meter,

L1 : 100 cm focal length AR coating at 1.06 um lens,

L2,L3 : 50 cm focal length AR coating at 1.06 um lens,

L4 : 15 cm lens,

L5 : 25 cm lens,

M1 : metal mirror,

M2 : 1/2° wedged and curved 100% reflection at 1.06 um mirror,

M3 : 1/2° wedged and plane mirror, 55% reflection at 1.06 um,

M4 : 99% reflection at 0.53 um and 90% transmission at 1.06 um mirror at 45° incidence angle.

M5,M6,M10,M11 : 100% reflection at 1.06 um at normal incidence,

M7,M8 : 100% reflection mirror at 0.53 um at normal incidence,

M9 : 50%-50% 1.06 um laser beam splitter,

(figure 1 continue)

P1, P2 : Polaroid HN 22 polarizers, polarized along the direction 45° and -45°, respectively : its extinction ration is 2×10^{4}.

S1 : dual beam Tektronix 556 oscilloscope,

S2 : Tektronix 519 oscilloscope,

SP : $\frac{1}{2}$ meter Jarall-Ash spectrometer.

Using a movable prism along the 0.53 um light path, the 1.06 um and 0.53 um laser beams arrive at the sample cell at different times. Moving the prims by 1 mm corresponds to a 6.67 ps delay time of the probe 0.53 um pulse with respect to the exciting 1.06 um pulse. Using this technique, the transmitted signal of the probe pulse at different delay times is measured. In this measurement, the sample Kerr kinetics is obtained. The maximum power density of 1.06 um used for the gate is about $2.5\ GW/cm^{2}$.

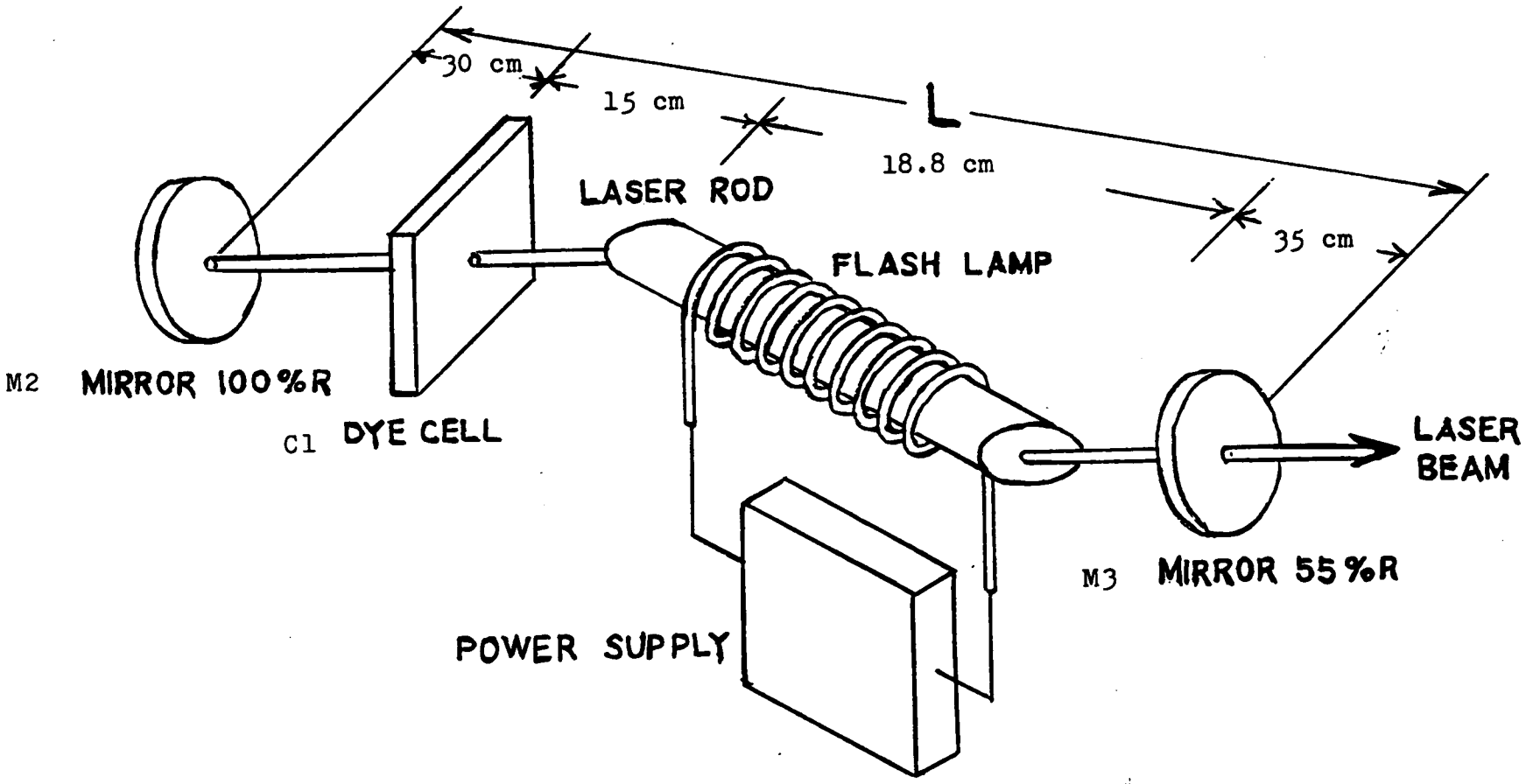

Figure 1a. A Schematic Diagram of the Laser Cavity Design

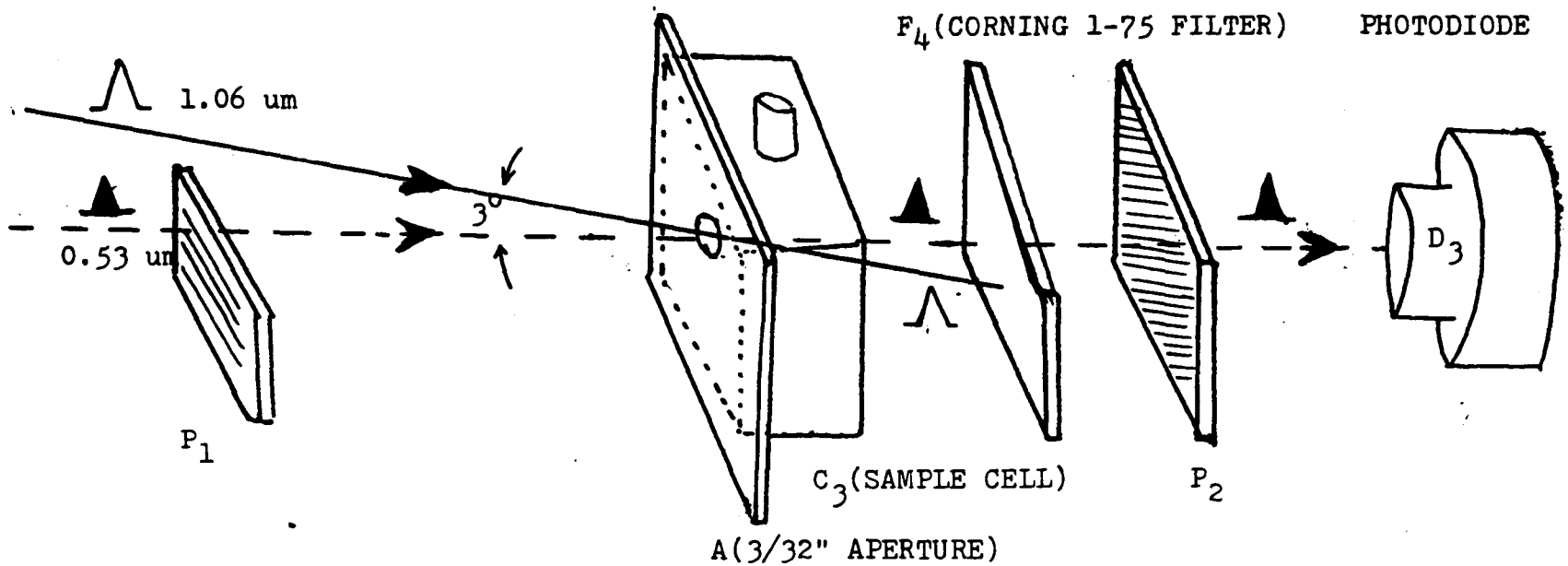

Figure 1b. Optical Kerr Gate

Figure 2a. Laser output train at 1.06 um. The horizontal scale is 100 ns/cm.

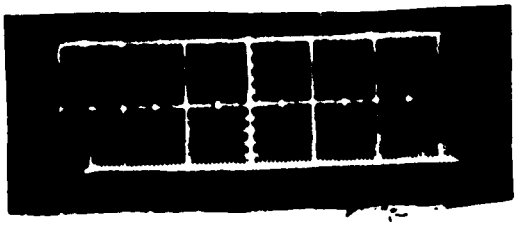

Figure 2b. TPF picture from 1.06 um pulse. Assuming a gaussian time profile of the laser pulse, the pulse duration is estimated by $t = \frac{(\Delta d)\, n\, 2^{\frac{1}{2}}}{c}$. where n is the index of refraction of the TPF solution (=1.36), c is the speed of light, the magnification of this picture is 1, and Δd is the full width of TPF. The pulse duration $\Delta\tau$ is 9ps.

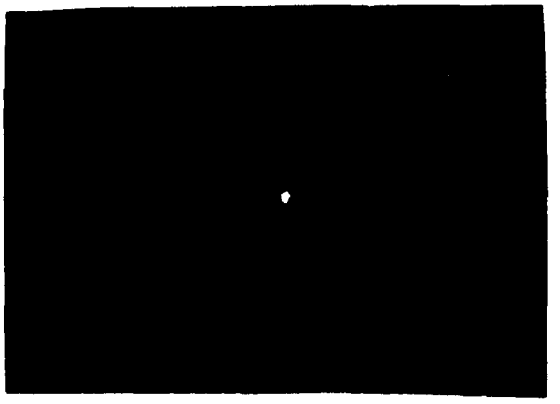

Figure 2c. Spectrograph picture of 0.53 um laser pulse. 1 mm = 32 Å. $\Delta\lambda_{F.W.H.M.}$ = 40 Å. This picture is overexposed for copying.

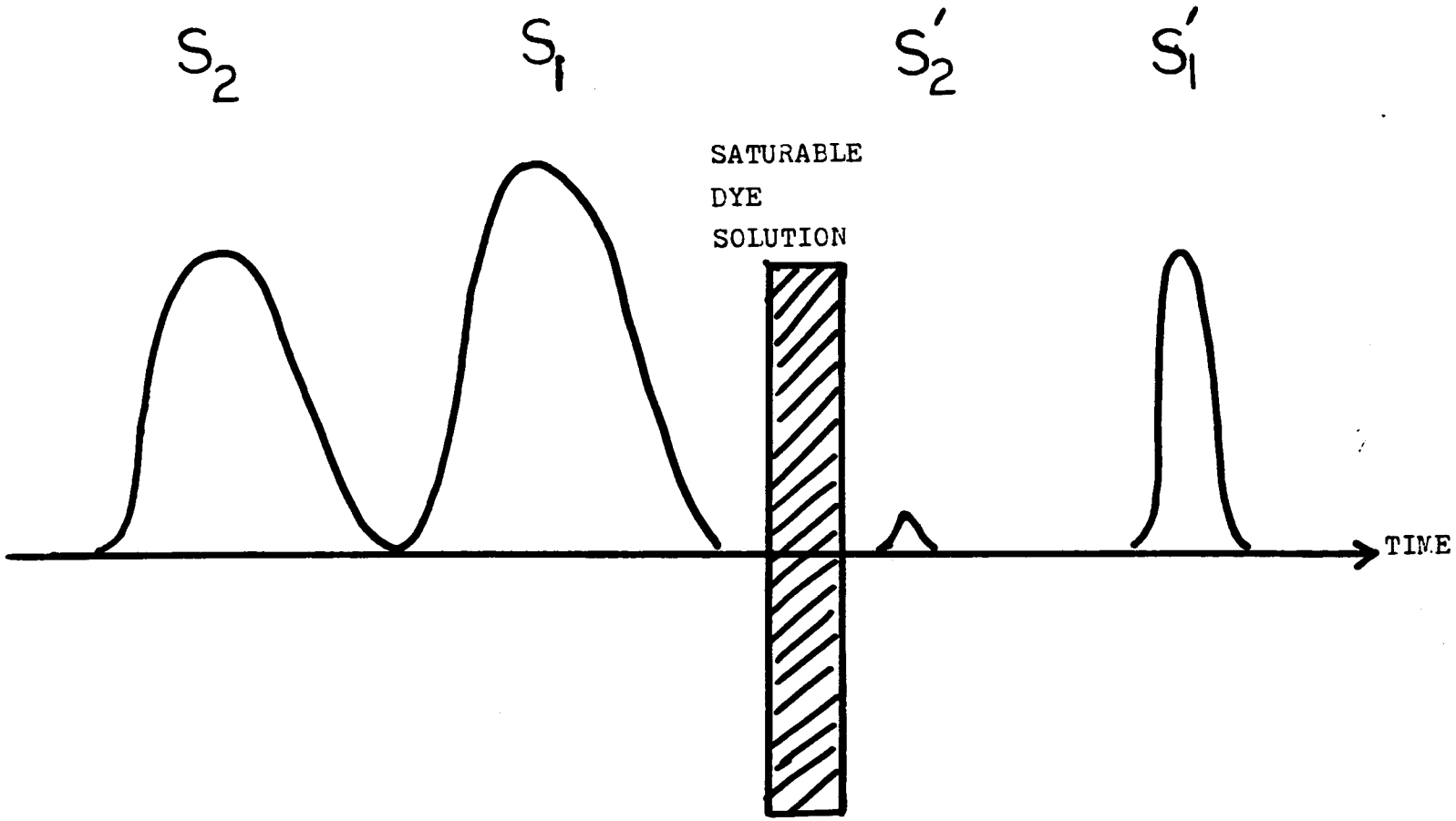

Figure 3. Interaction of Short Pulses with A Saturable Dye Solution

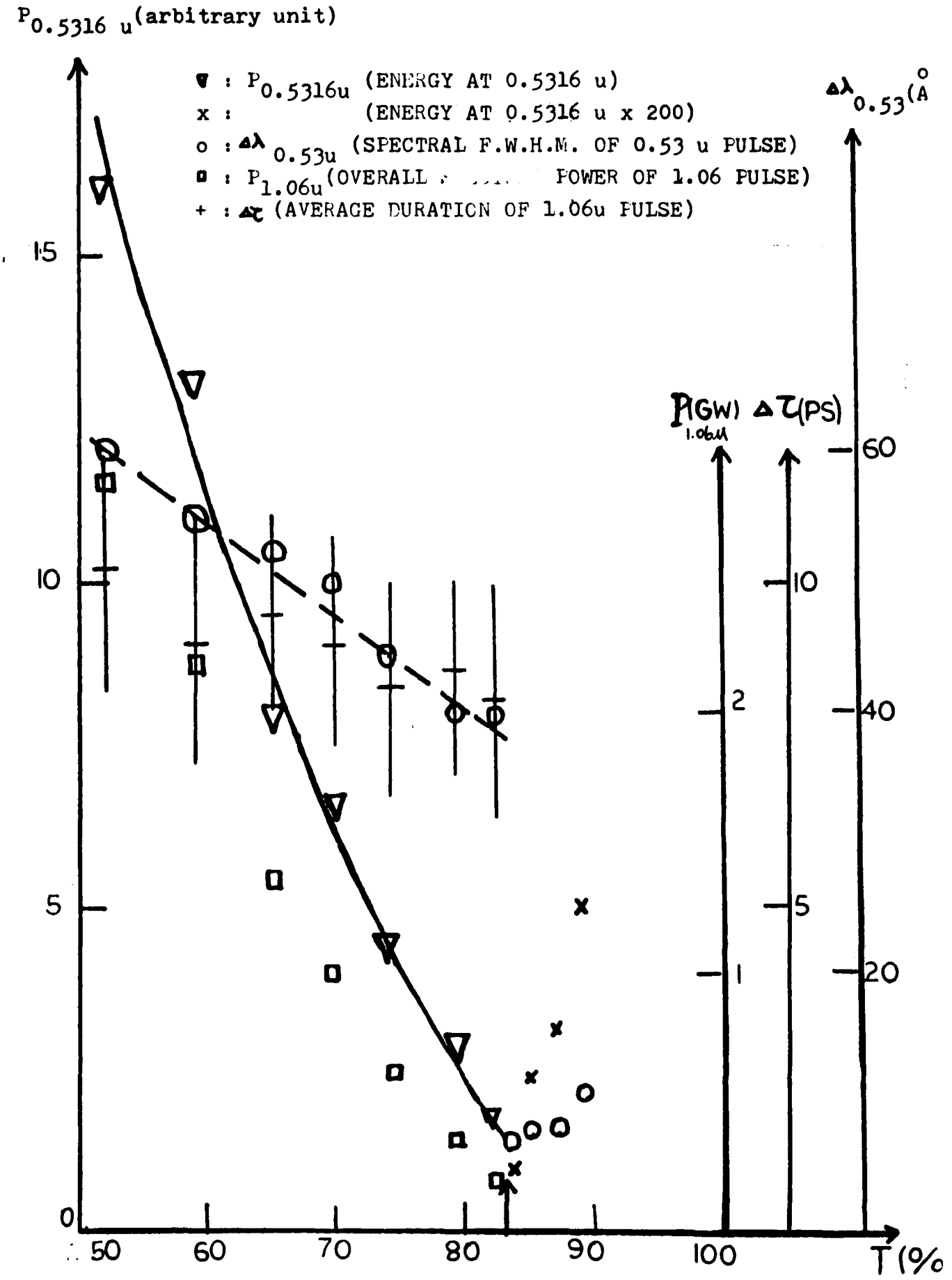

Figure 4. Dependence of the Laser Output Characteristics on the Transmission of Saturable Dye

Figure 5. Spectral Narrowing Experiment

A 1 mm thichness 28% reflection dielctric coating mirror at 1.06 um is placed inside the laser cavity at about 30^{o} to the propagation direction of the laser beam.

(a) laser output train at 1.06 um. The horizonatal scale is 50 ns/cm.

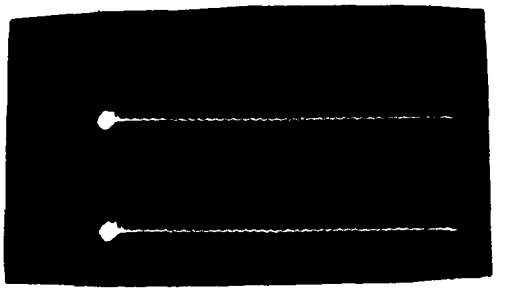

(b) TIF picture. The magnification of this picture is 1. The pulse duration $\Delta\tau$ = 15 ps.

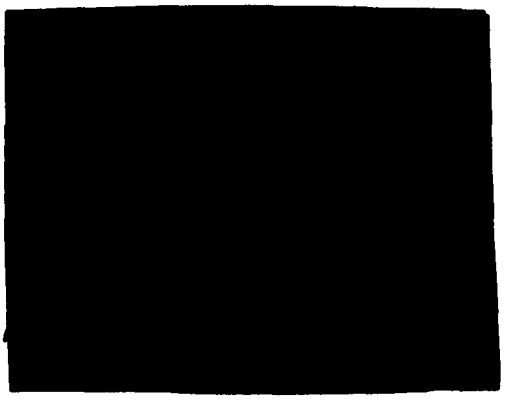

(c) Spectrograph picture of 0.53 um laser. 1mm = 32 $\mathring{A}$. $\Delta\lambda_{F.W.H.M.}$ = 2 $\mathring{A}$. This picture is overexposed for easy copy.

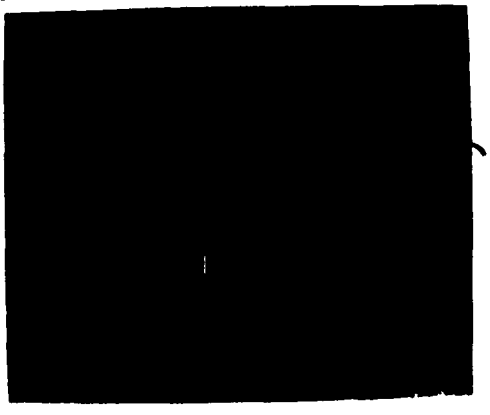

A : 3/32" aperture
T : thermocouple
M : microvolt meter
W : ice water
H : heater tape
V : voltage variac
P : pressure gauge
L : liquid
G : gas

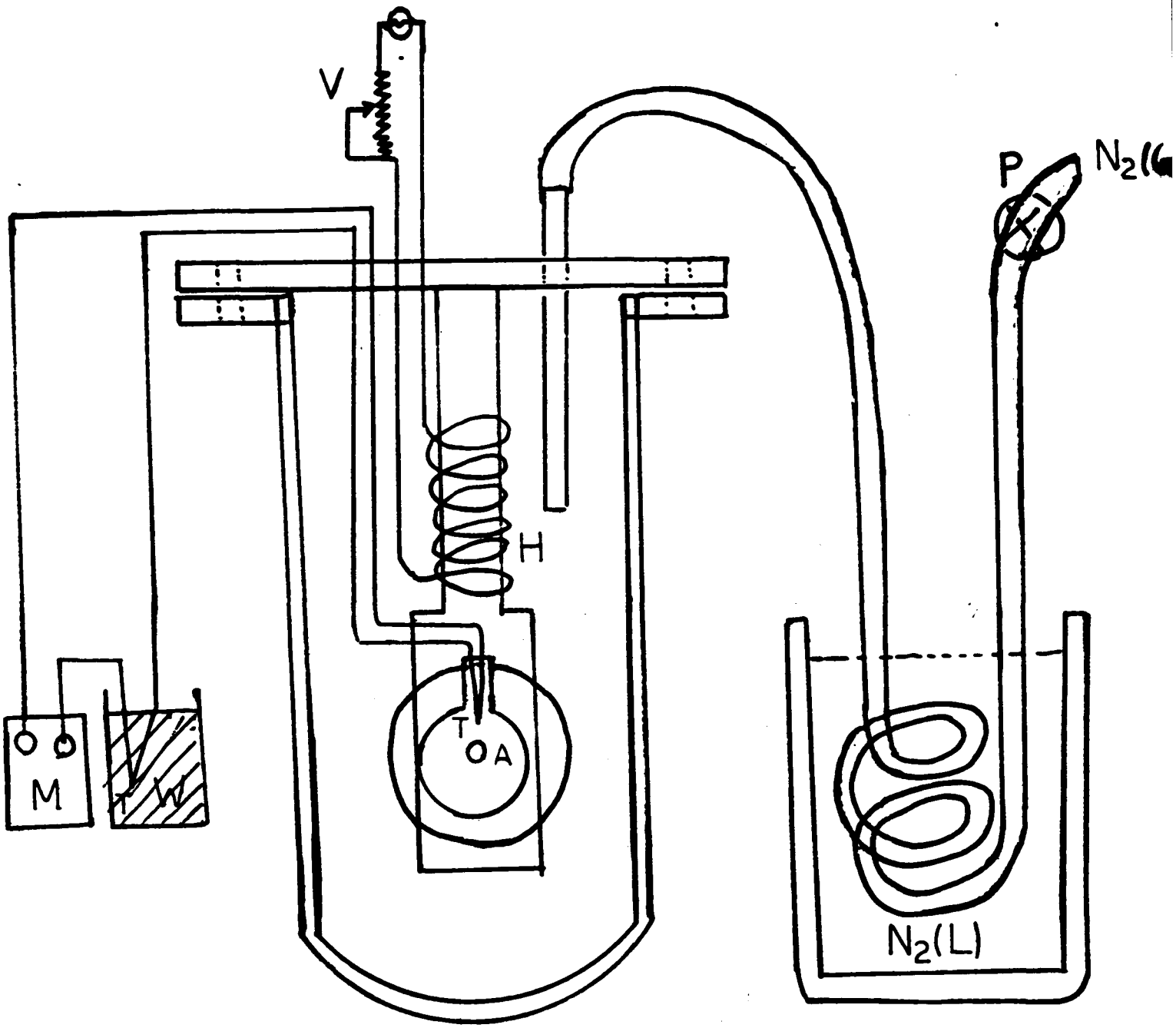

Figure 6 Temperature Controlled Dewar

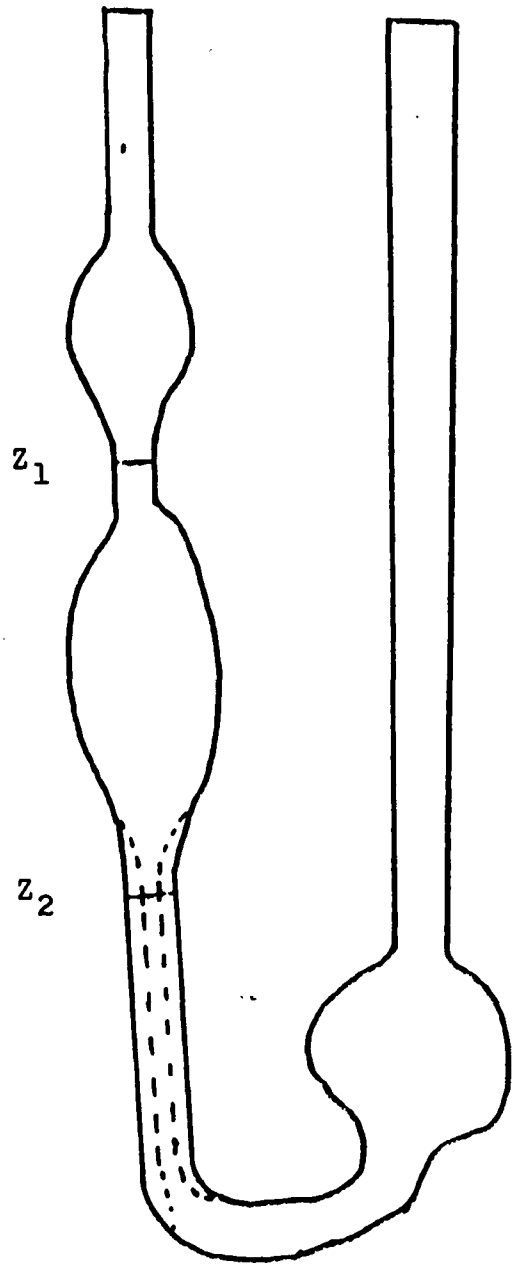

OSTWALD CANNON-FENSKE VISCOMETR

Figure 7

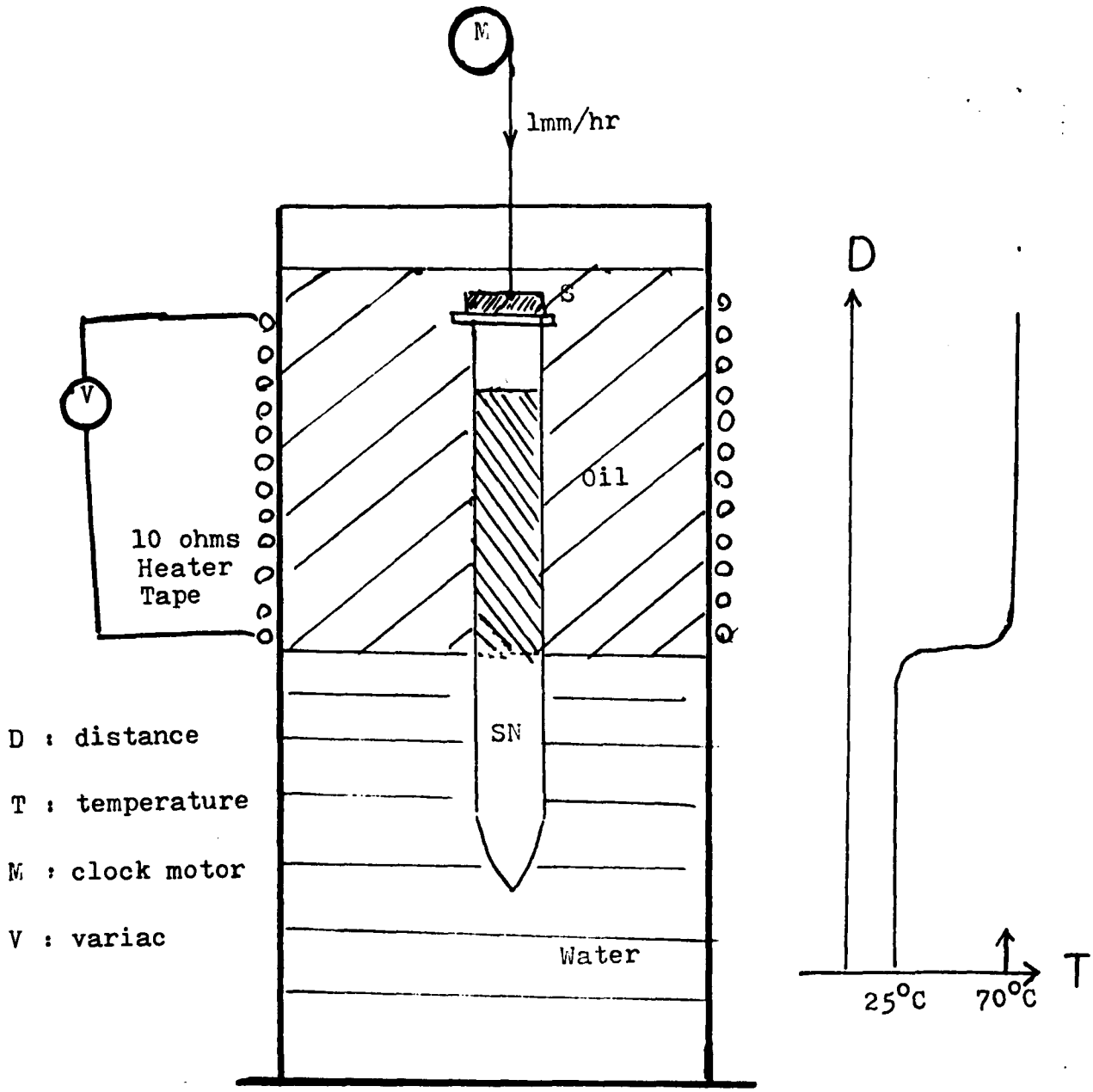

Figure 8 SN Crystal Growth Setup

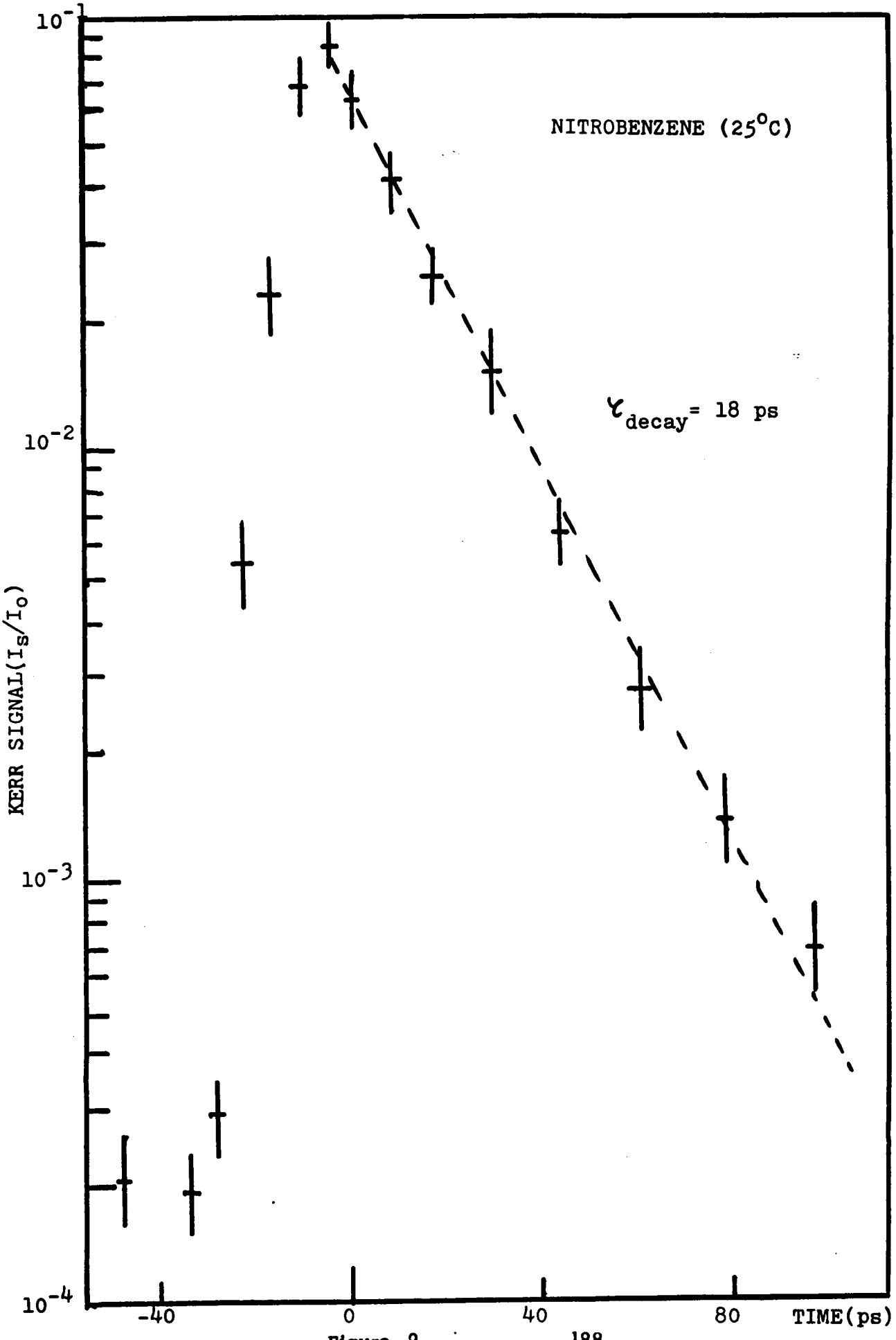
NITROBENZENE (25°C)
τ_{decay} = 18 ps
KERR SIGNAL(I_s/I_o)
10^{-1}
10^{-2}
10^{-3}
10^{-4}
-40
0
40
80
TIME(ps)

Figure 9

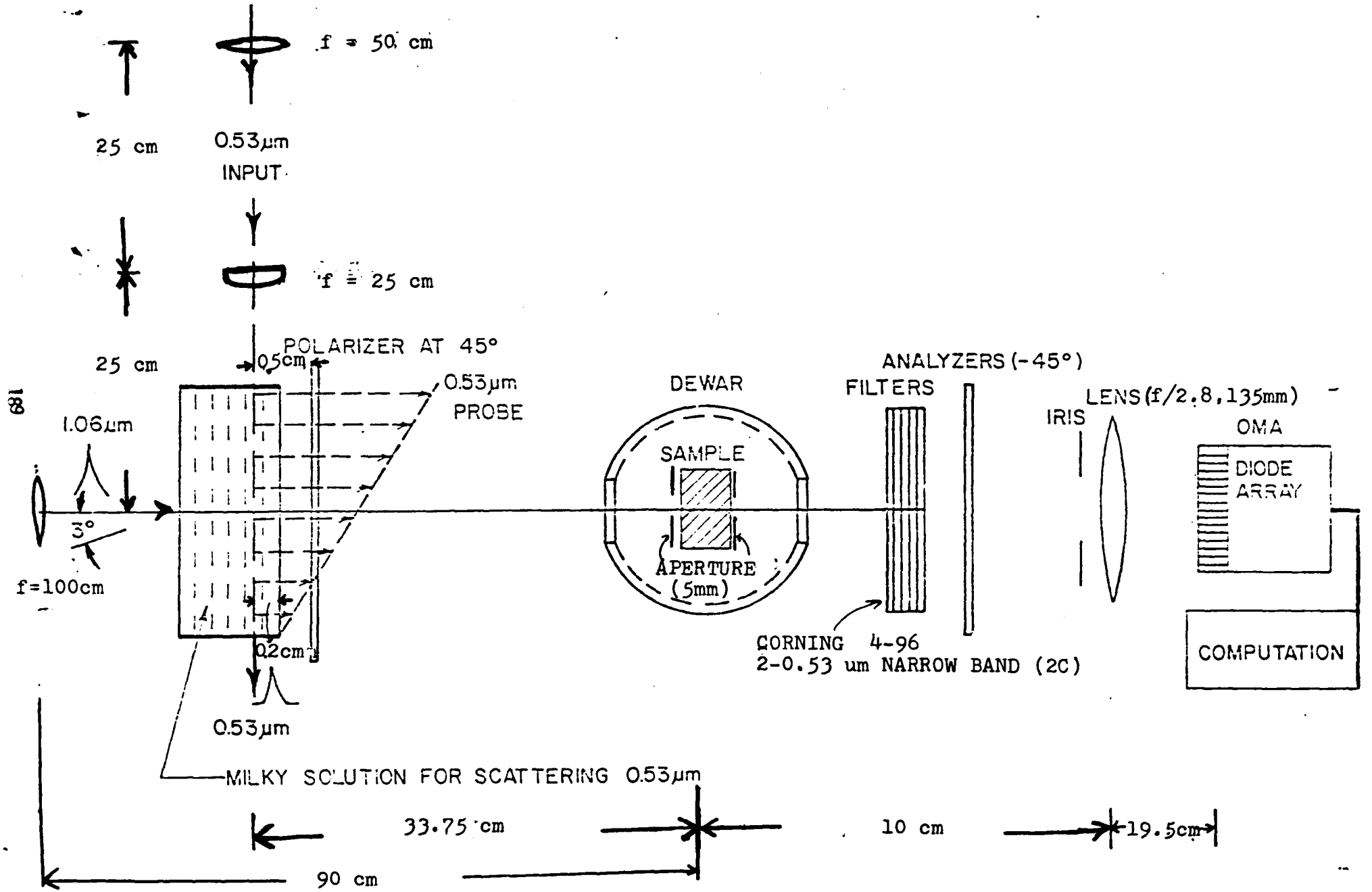

Figure 10. Single Shot Optical Kerr Gate

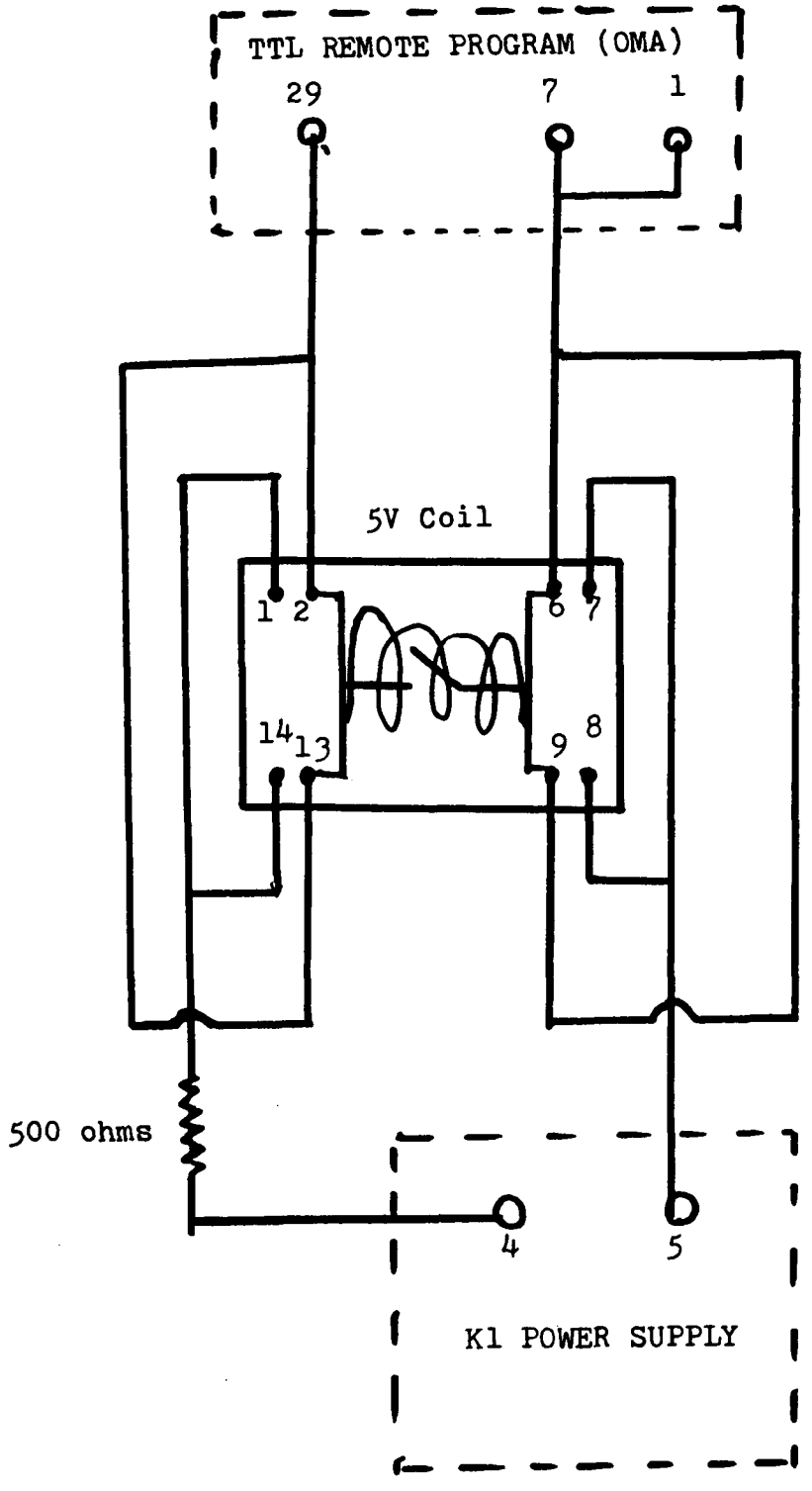

Figure 11. Wire Diagram of the Trigger Switch from OMA to Laser

CHAPTER 6

EXPERIMENTAL PROGRAM - RESULTS AND DISCUSSIONS

In this chapter, I will present my experiment results in six sections on the direct measurements of the relaxation time of polyatomic molecules in different states of condensed matter using the picosecond optical Kerr effect. These results will be discussed using the theoretical models presented in the previous chapters.

In section 6.1, the relaxation time of the optical Kerr effect of nitrobenzene, m-nitrotoluene, and hexadecane in different mixtures with carbon tetrachloride and various alcohols was determined by measuring the kinetics of the Kerr effect using picosecond laser techniques. These measurements yield information on the rotational motion of molecules in liquids. The relaxation time data are interpreted in terms of an effective local viscosity effect and pair correlation effect.

In section 6.2, the relaxation times of the optical Kerr effect of nitrobenzene and m-nitrotoluene have been measured as a function of temperature in neat and mixed binary liquids. The activation energy of molecular reorientational motion for various solutions has been determined from the Kerr effect and viscosity measurements. A modified Hill's theory for the relaxation times provides satisfactory agreement with the experimental measurements for the mixed liquids.

In section 6.3, the measured relaxation times from the optical Kerr effect in mixed liquids are discussed based on the

theory of coupled two-component reorientational relaxation from Mori's generalized Langevin equation. By choosing proper parameters, the equation derived by Mori-Keyes-Kivelson-Tsay is used to fit the intensity decay profile from the dynamic optical Kerr gate. The difference between section 6.3 and sections 6.1 and 6.2 is the dynamic range of the experiment has increased by more than ten times. This allows us to observe an additional slow decay component.

In section 6.4, the relaxation kinetics of the supercooled liquid - salol is investigated. The Kerr intensity profile versus time is found to decay with two components. The mechanisms responsible for this effect is attributed to the nonlinear index of refraction arising from mechanisms which includes the electronic cloud distortion and molecular librations, and a slow molecular reorientational motion of the salol molecules. In the supercooled region, we reorientational relaxation time at temperature from the melting temperature ($42^{o}C$) down to $-5^{o}C$. The activation energy deduced from the temperature dependent relaxation time by the optical Kerr effect is found to be smaller than the value obtained from the viscosity measurement.

In section 6.5, the relaxation kinetics of succinonitrile $(CH_2CN)_2$ is measured in the liquid and plastic crystal phases. The Kerr intensity decay profile of the plastic crystal indicates that two different relaxation mechanisms are operative - a fast mechanism (electronic and molecular librational) and a slow molecular reorientational motion. The temperature dependence

study of the succinonitrile's relaxation time in the plastic crystal phase yields an activation energy of 2.6 $\pm$ 0.7 Kcal/mole. The reorientation motion of the succinonitrile molecules in the plastic crystal phase is due to the gauche-trans isomerization.

In section 6.6, a detail experimental study on the parameters which affect the optical Kerr effect is investagated following the theoretical discussions in section 4.6. The various parameters are : the intensity of the orienting laser pulse, the time and spatial distribution of the pulse profile, the wavelength of the probing and orienting pulses, the relaxation time and concentration of the Kerr solution, temperature of the Kerr gate, pair correlation factor, and bond strength as a vector sum of all bonds in a molecule. These experimental measurements are compared to the theory presented in section 4.6.

6.1 Relaxation Of The Optical Kerr Effect Of Anisotropic Molecules In Mixed Liquids

Knowledge of the internal motions of molecules in liquids, such as the rotational motion, is indispensable for the full understanding of the Physics of the liquid state. A variety of experimental techniques can be used to probe the dynamics of molecular motions. Dielectric relaxation[1], microwave absorption[2], infrared[3] and Raman[4] spectroscopy, nuclear[5] and electronic[6] spin relaxation, depolarization of fluorescence[7] and depolarized Rayleigh wing scattering[8], and neutron[9] scattering have all been employed to study the molecular rotation in liquids. Recently, picosecond laser techniques have become available for directly measuring the time dependence of the Kerr effect in pure organic liquids[10], and of the dichroism of dye solutions[11]. Almost all of the above mentioned experiments measure the relaxation phenomena of the change of the dielectric or paramagnetic property of matter. The relaxation times may vary depending upon the rank of the observed polarizability (or susceptibility) tensor, and upon the detail of the rotaional Brownian motion in liquids[12,13].

In this section we report the direct measurement of the relaxation times of the optical Kerr effect of nitrobenzene, m-nitrotoluene, and hexadecane in mixed liquids by measuring the kinetics of the optical Kerr effect using picosecond laser pulses. In these anisotropic molecules, the relaxation of the Kerr effect is primary due to the molecular reorientational motion and its coupling with the collective mode of motion

in the liquid, such as the angular momentum correlation. The distribution to the optical Kerr effect due to the electronic cloud distortion or the librational motion of the molecules is either too small or too fast to be resolved with longer than picosecond pulses. In this experiment the relaxation times are measured as functions of concentration and viscosity of the solution. By varying the concentration of the Kerr-active solute in the solution, we are able to deduce the effect of pair correlation in liquids. By appropriately choosing the viscosity of the solution, we found that the relevant parameter to describe the viscosity dependence of the relaxation time in mixed liquids in an effective local viscosity which is essentially the measured viscosity excluding the contribution from solvent molecules. Comparing the results of this experiment and those from light scattering with the data obtained from dielectric relaxation experiment, our data support the conclusion that the characteristic angular step of the rotation by a small molecule in ordinary liquids is in such a size that neither rotation by simple diffusion through small angles nor rotation by a singularly large jump is an adequate picture in describing the rotational motion.

The experimental apparatus for measuring the relaxation time of the Kerr has been previously reported[10,11] which is similar to the discussion in section 5.1. It consists of a mode-locked Nd:glass laser, a potassium dihydrogen phosphate second harmonic crystal, and a Kerr gate (1 cm sample cuvette situated between crossed polarizers). Two laser beams are used in the experiment. An intense 1.06 um pulse with ~10 ps duration is used to induce the Kerr birefringence in the

sample solution. The birefringence is caused by partially orienting the anisotropic molecules in the liquid through the interaction of the optical electric field of the laser pulse with the polarizability of the molecules. A second harmonic 0.53 um pulse with ~8 ps duration, variably delayed with respect to the 1.06 um exciting pulse, is used to probe the time evolution of the induced transitory birefringence in the sample solution. The intensity profile formed in this manner is a convolution in time of the 1.06 um pulse, 0.53 um pulse, and the induced birefringence. The light signal passing through the Kerr gate is :

$$I(\tau) \propto \int_{-\infty}^{\infty} I_{0.53um}(t-\tau) \sin^2 \tfrac{1}{2}\delta\phi(t) \; dt \; , \qquad (6.1.1)$$

where $\delta\phi(t) = (2\pi/\lambda)\, n_2 (L/\tau_k) \int_{-\infty}^{t} \overline{E^2_{1.06um}}(t')\, e^{-(t-t')/\tau_k} \; dt'$

(6.1.2)

is the phase retardation between the parallel and perpendicular components of the 0.53 um beam after passing through an L distance in the Kerr cell, n_2 is the nonlinear index of refraction, τ_k is the Kerr relaxation time, $I_{0.53}$ is the intensity profile of the 0.53 um beam, and $\overline{E^2_{1.06}}$ is the time averaged electric field of the 1.06 um beam in the Kerr cell. The relaxation time can be extracted from the measured intensity decay profile by deconvolution. In the deconvolution, an exponential time profile for the laser pulse is assumed. In the experiment we have studied the rotational relaxation times of nitrobenzene, m-nitrotoluene, and hexadecane. Carbon tetrachloride, a symmetrical nonpolar molecule, is essentiall non-Kerr-active. The alcohols, whose Kerr effect was determined to be less than one hundredth of that of nitrobenzene and

m-nitrotoluene, were chosen for providing the variation of solution viscosity.

As the solute concentration was decreased, the peak transmitted signal of the 0.53 um light was observed to decrease quadratically. This is expected from equation 6.1.1 for $\phi \ll 1$ which limits the solute concentration to about 20% in this experiment. All experiments were performed at room temperature at 23 $\pm$ 2°C. The measured relaxation time of nitrobenzene, m-nitrotoluene, and hexadecane are plotted as function of mole fraction in the solution in figure 6.1.1 through figure 6.1.5. The viscosity of these measure were measured and also plotted on the correspondent graphs. The salient feature of the data presented in these figures is that the relaxation time <u>decreases</u> with decreasing concentration, even with <u>increasing</u> solution viscosity (in particular, see figure 6.1.4).

Debye's classical theory of dielectric relaxation[15] is generally applicable to single particle rotational relaxation in pure polar liquids. The relaxation time is shown to be proportional to the viscosity of liquids as :

$$\tau = (4\pi a^3/kT)\,\eta_m , \qquad (6.1.3)$$

where a is the molecular radius of a spherical molecule, T is the temperature, and k is the Boltzmann constant. In reality, liquid molecules hardly behave as a single particle. In solution one further finds that viscosity dependence appeared in equation 6.1.3 is not followed by the relaxation time[16]. This

is simply because the viscosity experienced by a solute is not the measured viscosity. Applying this concept of a mutual viscosity between the solute and the solvent molecules, Hill[17] has successfully shown that the relaxation time of a series of polar molecules in a very dilute solution is directly proportional to the mutual viscosity as discussed in section 3.2. A general phenomenological expression for the rotational relaxation time of a solute molecule in a binary liquid can be expressed by;

$$\tau = c_1(a_B)\, f(x)\, \eta_B x + c_2(a_{BC})\, \eta_{BC}\, (1-x) , \quad (6.1.4)$$

where x denotes the mole fraction of the solute molecule B component in the solution, η_B is the viscosity of the solute B molecules in neat liquid, η_{BC} is the mutual viscosity between the solute B and the solvent C molecules. The expression $c_1(a_B)$ and $c_2(a_{BC})$ account for the variation in molecular sizes in solution and are dependent on the details of the collisional process (a special form of c's has been calculated by Hill, see section 3.2). The expression f(x) is specially inserted here to account for the pair correlative effect among the solute molecules. To the first order, f can be represented as $(1 + \lambda x)$ [18]. As the solute concentration x reduces to zero, the correlation term f clearly approaches one. Equation 6.1.4 can now be written as

$$\begin{aligned} \tau &= c_1(a_B)\, f(x)\, \eta_B x + c_2(a_{BC})\, \eta_{BC}(1-x) \\ &= C'\left[(1+\lambda x) x \eta_B + G(1-x)\eta_{BC} \right] , \end{aligned} \quad (6.1.5)$$

in which $G=c_2/c_1$, is a number not far from one, depending on

the sizes of the molecules and the correlation between dissimilar molecules, and C′ and λ are two parameters which can be numerically determined by measuring τ as function of x. The parameter C is a measure of the rate of change of the relaxation time with the respect to the viscosity at a given temperature. The parameter λ is a measure of correlation among solute molecules.

From the measured values of the viscosity as a function of x, the mutual viscosity η_{BC} can be calculated from the expression

$$\eta_m = (x^2/\sigma_m)\eta_B a_B + [2x(1-x)/a_m]\eta_{BC} a_{BC} + [(1-x)^2/a_m]\eta_C a_C \quad , \qquad (6.1.6)$$

where the subscript m denoted mixture, and the η's, $\underline{a}$'s are viscosities, and intermolecular distances (calculated from $\underline{a}=(M/\rho N_o)^{1/3}$; where M=molecular weight, ρ=density, N_o=Avogadro number). The mutual viscosity η_{BC} at 23 ± 2^{o}C is determined to be 1.20 for nitrobenzene and carbon tetrachloride, 1.26 for nitrobenzene and n-propanol, 0.9 for m-nitrotoluene and carbon tetrachloride, and 1.50 for m-nitrotoluene and n-decanol, and 1.9 for hexadecane in CCl_4. The value η_{BC} for nitrobenzene and carbon tetrachloride is in excellent agreement with the value quoted in Hill's paper [17].

The correlation parameter λ and the constant C′ can now be determined from the data in figure 6.1.1 through figure

6.1.5 according to equation 6.1.5. The results are for nitrobenzene λ = 1.55 and 1.2, and C'= 6.1 and 7.3 ps/centipoise in carbon tetrachloride and n-propanol, respectively; and for m-nitrotoluene, λ = 1.64 and 2.56, and C' = 6.9 and 5.5 ps/cp, in carbon tetrachloride and n-decanol, respectively; and for hexadecane in carbon tetrachloride : λ = 2 and C' = 28 ps/cp. In the data reduction, G = 1 is assumed. It should be emphasized here that the empirical approach employed in this paper to relate the viscosity and correlation with the relaxation time differs from the other method[19] by : (1) employing an effective local viscosity $\eta_{eff} \propto x\,\eta_B + (1-x)\,\eta_{AB}$ for a given solute molecule instead of the measured viscosity; (2) the correlation term is only attached to the η_B term in η_{eff}. This formulation enabled us to interpret the data consistently, including those of m-nitrotoluene in n-decanol. Evidently, the relaxation time of m-nitrotoluene in n-decanol is not simply proportional to the measured viscosity.

In figure 6.1.1, the data obtained from depolarized Rayleigh wing scattering experiment by Alms et al.[19] is plotted along with the result of this experiment. It is gratifying that both results have a similar dependence on x. The light scattering data were deduced by Alms et al.[19] according to the relation $\tau = (1+\lambda x)/(1+gx) \cdot (c\eta_m + \tau_o)$. The data can also be be fitted and successfully interpreted by equation 6.1.5.

The rotational motion of a liquid molecule can be visualized as an oscillatory librational motion about an equilibrium position disrupted by a quick angular displacement caused by collisions. It is this latter part of the molecular motion, the Brownian motion, for which this experiment and other light scattering or

absorption experiments intend to explain. The usual approach to the Brownian motion problem is that of random walk method. It is well known that the random walk problem is reduced to a diffusion problem, provided the time interval during which the total displacement is taken place is sufficiently long[20]. For small molecules such as nitrobenzene and m-nitrotoluene, the rotational step can become relatively large such that the diffusional approach is inadequate. It is therefore of interest if experimental evidence can be obtained to explain the nature of the characteristic rotational step in a liquid. In a general approach to the problem of the theory of the rotational Brownian motion, Ivanov [12] has shown that the relaxation time of the measured quantity depends on the rank (k) of the related polarizability tensor. When diffusion is applicable, the relaxation time for a spherical molecule is

$$\tau_k = \tau_o/k(k+1) \quad , \qquad (6.1.7)$$

where τ_o is the time interval which the molecule in the local equilibrium position. In case of large angular step, since each large step causes complete randomization, the relaxation time should be independent of the rank. We have

$$\tau_k = \tau_o \quad , \quad \text{for all } k \quad . \qquad (6.1.8)$$

In this experiment, according to the th ory of the optical Kerr effect of an anisotropic molecule[21], the rank of the related polarizability tensor is k = 2, which is the same as that used for light scattering experiments (Rayleigh and Raman);

and for absorption experiments (dielectric relaxation, microwave and infrared absorption) the rank k = 1. Using the relaxation time data obtained from the dielectric relaxation measurement τ_1 = 48 ps[22], from the Rayleigh scattering measurement τ_2 = 36 ps[19a] or 39 ps[19b], and from the Kerr effect τ_2 = 32 ps for nitrobenzene the calculated ratio are $\tau_1/\tau_{2,Kerr} \simeq 1.5$ and $\tau_1/\tau_{2,LS} \simeq 1.3$ where the subscript LS denotes the light scattering measurments. In an analysis for various aromatic liquids[23] : τ_1/τ_{LS} has also been shown to be between 1.1 to 1.5. Therefore, the analysis of experimental data suggests that the rotational motion of small molecules (molecular weight $\simeq$ 100) in a liquid of moderate viscosity ($1 < \eta_m < 5$) is not likely describable by diffusion through small angular jumping steps ($\tau_1/\tau_2 = 3$ following equation 6.1.7), nor by large jumping steps ($\tau_1 \simeq \tau_2$). Rather, the rotational motion is probably characterized either by jumps of intermediate size, or more likely by a distribution of the jump angles.

In summary, we have measured the Kerr relaxation time of nitrobenzene, m-nitrotoluene, and hexadecane in mixed liquids by observing the kinetics of the picosecond laser pulse induced Kerr effect. The relaxation time data are interpreted in terms of an effective viscosity of the mixed liquid and the effect of pair correlation. From the dependence of the relaxation time on the rank of the polarizability tensor, the experimental result has provided new evidence in the understanding of the nature of the rotational motion in liquid.

References

(1) C.P. Smyth, Molecular Relaxation Processes (Academic Press, New York, 1966).

(2) D.H. Whiffen, and H.W. Thompson, Tran. Faraday Soc., 42A, 114 (1946).

(3) W.G. Rothschild, J. Chem. Phys., 53, 990(1970).

(4) M.F. Crawford, H.L. Welsh, and J. H. Harrold, Can. J. Phys., 30, 81 (1952); W.R.L. Clements, and B.P. Stoicheff, Appl. Phys. Lett., 12, 246 (1968).

(5) N. Bloembergen, E.Purcell, and R.V. Pound, Phys. Rev., 73, 679 (1948);

R.W. Mitchell, and M. Eisner, J. Chem. Phys., 33, 86 (1960).

(6) N.S. Angerman, and R.B. Jordan, J. Chem. Phys., 54, 837 (1971).

(7) R.F. Chen, in Fluorescence: theory, Instrumentation, and Practice G. Guilbault ed. (Dekker Inc. New York, 1967).

(8) D.R. Bauer, G.R.Alms, J.I. Brauman, and R.Pecora, J.Chem. Phys., 61, 2255 (1974);

H.C. Craddock, D.A. Jackson, and J.G. Powles, Mol. Phys., 14, 373 (1968);

S.L. Shapiro, and H.P.Broida, Phys.Rev., 154, 129 (1967);

E.Zamir, N.D.Gershon, and A.Ben-Reuven, J.Chem. Phys., 55, 3397 (1971).

(9) L.A. deGraaf, Physica 40, 497 (1969);
V.F.Sears, Can. J.Phys. 45, 237 (1967).

(10) M.Duguay, and J. Hansen, Appl. Phys. Lett. 15, 192 (1969); Opt. Comm 1, 254 (1969).

(11) T.J. Chuang and K.B. Eisenthal, Chem. Phys. 11, 368 (1971);
K.B.Eisenthal and K.H. Drexhage, J.Chem. Phys. 51, 5720 (1969).

(12) E.N. Ivanov, Sov. Phys. JETP 18, 1041 (1964).

(13) E.A. Egelstaff, J. Chem. Phys., 23,2590, (1970).

(14) W.Yu and R.R.Alfano, Optoelectronics 6, 243 (1974).

(15) P. Debye, Polar Molecules (Dover, New York 1929).

(16) A.J.Curtis, P.L.McGveer, G.B.Rathman, and C.P. Smyth, J.Amer. Chem. Soc. 74, 644 (1952).

(17) N.E. Hill, Proc.Phys.Soc. (London) 67B 149 (1954).

(18) T. Keyes, and D.Kivelson, J.Chem. Phys. 56, 1057 (1972).

(19)(a) G.R. Alms, D.R.Bauer, J.I. Brauman, and R.Pecora J.Chem. Phys.59, 5310 (1973);

(b) G.I.A. Stegegman,and B.P. Stoicheff, Phys.Rev. A7, 1160 (1973).

(20) S.Chandrasekhar, Rev. Mod. Phys. 15,1 (1943).

(21) S.Kielich, Acta Phys. Pol. 30, 683 (1966).

(22) C.P.Smyth, Dielectra Behavior and Structure (McGraw Hill, New York,1955).

Figure Caption

Kerr Relaxation time is plotted as a function of mole fraction of solute molecules. The crosses are data point; the solid curve is the measured viscosity; and the dash curve is calculated from

$$\tau = C'\left[(1 + \lambda x) \times \eta_B + (1 - x)\ \eta_{BC}\right] \quad .$$

Figure 6.1.1 Nitrobenzene in carbon tetrachloride.

$$\tau = 6.1\ \left[(1 + 1.55\, x) \times \eta_B + (1 - x)\ \eta_{BC}\right] .$$

The circles are obtained from Alm et al light scattering data[19a].

Figure 6.1.2 Nitrobenzene in n-propanol.

$$\tau = 7.3\ \left[(1 + 1.2\ x) \times \eta_B + (1 - x)\ \eta_{BC}\right] \quad .$$

Figure 6.1.3 m-nitrotoluene in carbon tetrachloride.

$$\tau = 6.9\ \left[(1 + 1.64\ x) \times \eta_B + (1 - x)\ \eta_{BC}\right] .$$

Figure 6.1.4 m-nitrotoluene in n-decanol.

$$\tau = 5.5\ \left[(1 + 2.56\ x) \times \eta_B + (1 - x)\ \eta_{BC}\right] .$$

Figure 6.1.5 Hexadecane in carbon tetrachloride.

$$\tau = 28\ \left[(1 + 2x\ ) \times \eta_B + (1 - x)\ \eta_{BC}\right] \quad .$$

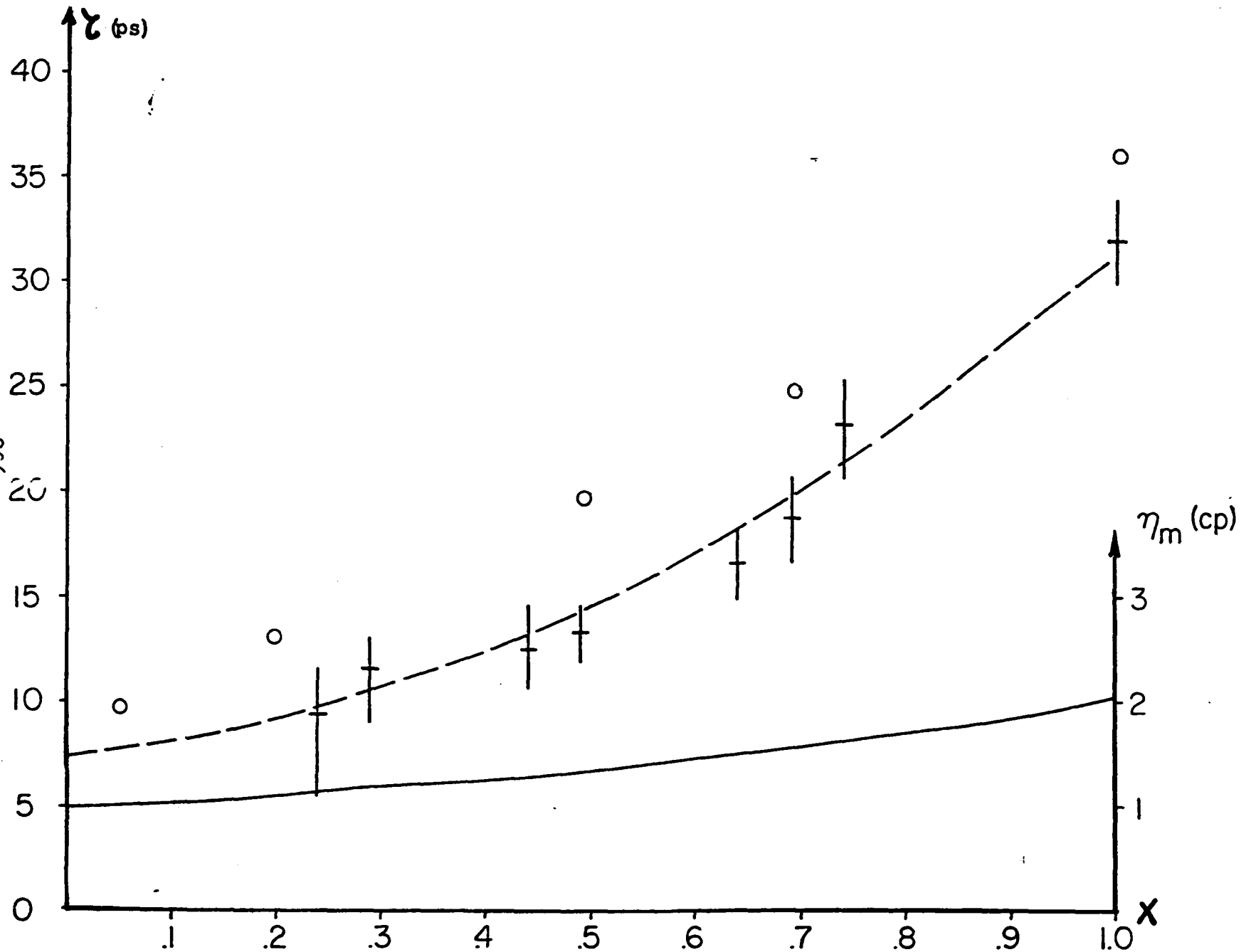

Figure 6.1.1 Nitrobenze in carbon tetrachloride

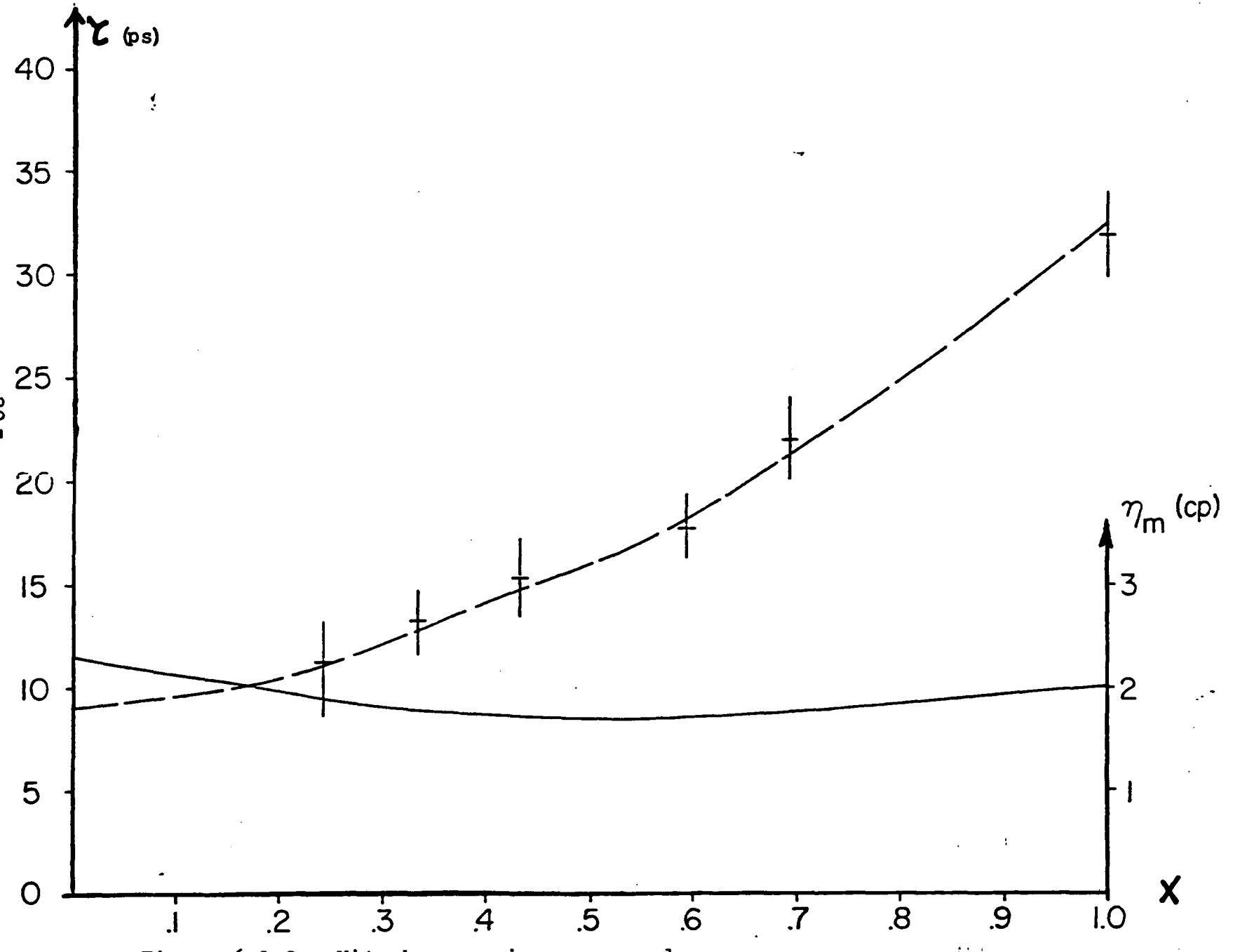

Figure 6.1.2 Nitrobenzene in n-propanol

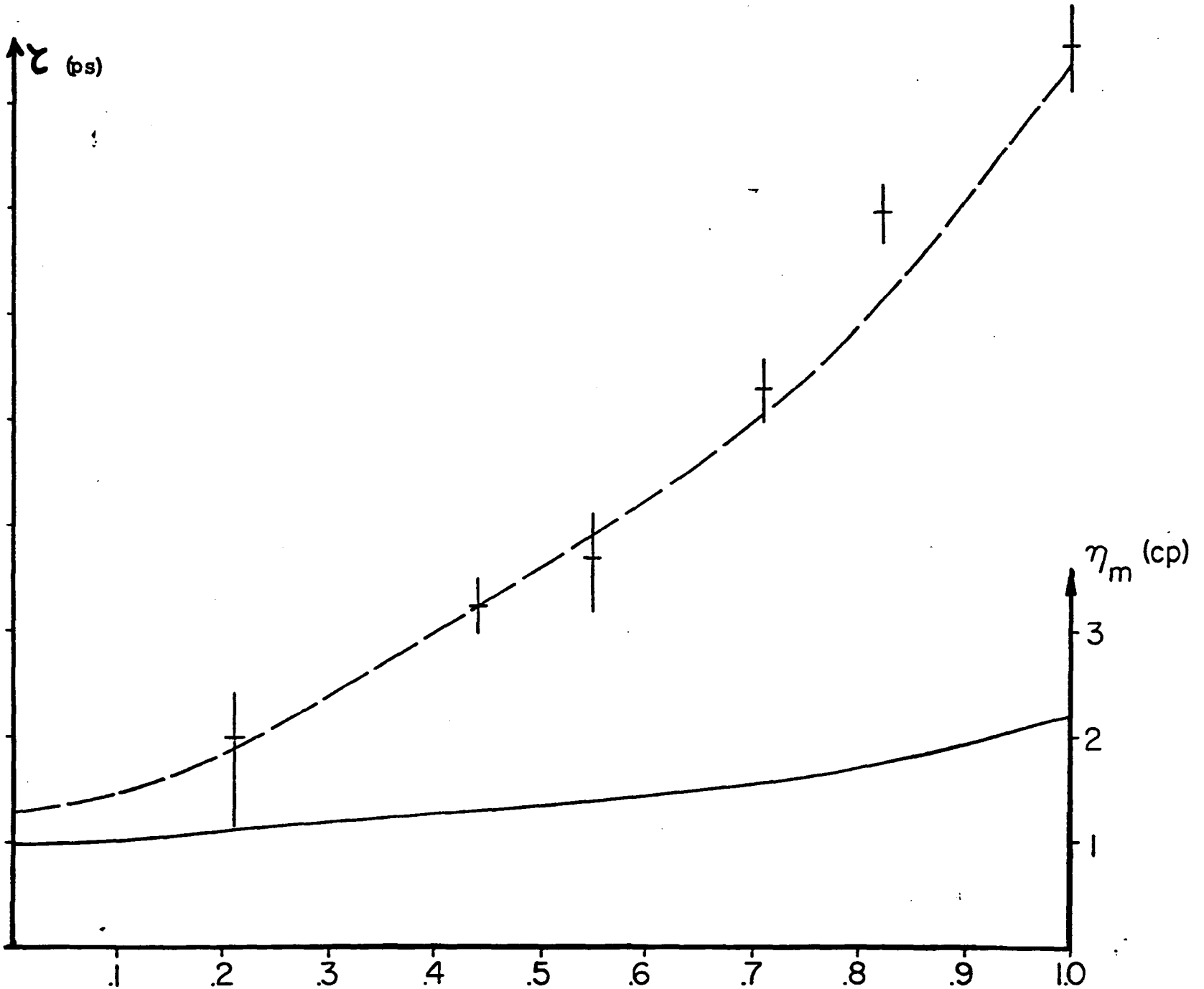

Figure 6.1.3 m-nitrotoluene in carbon tetrachloride

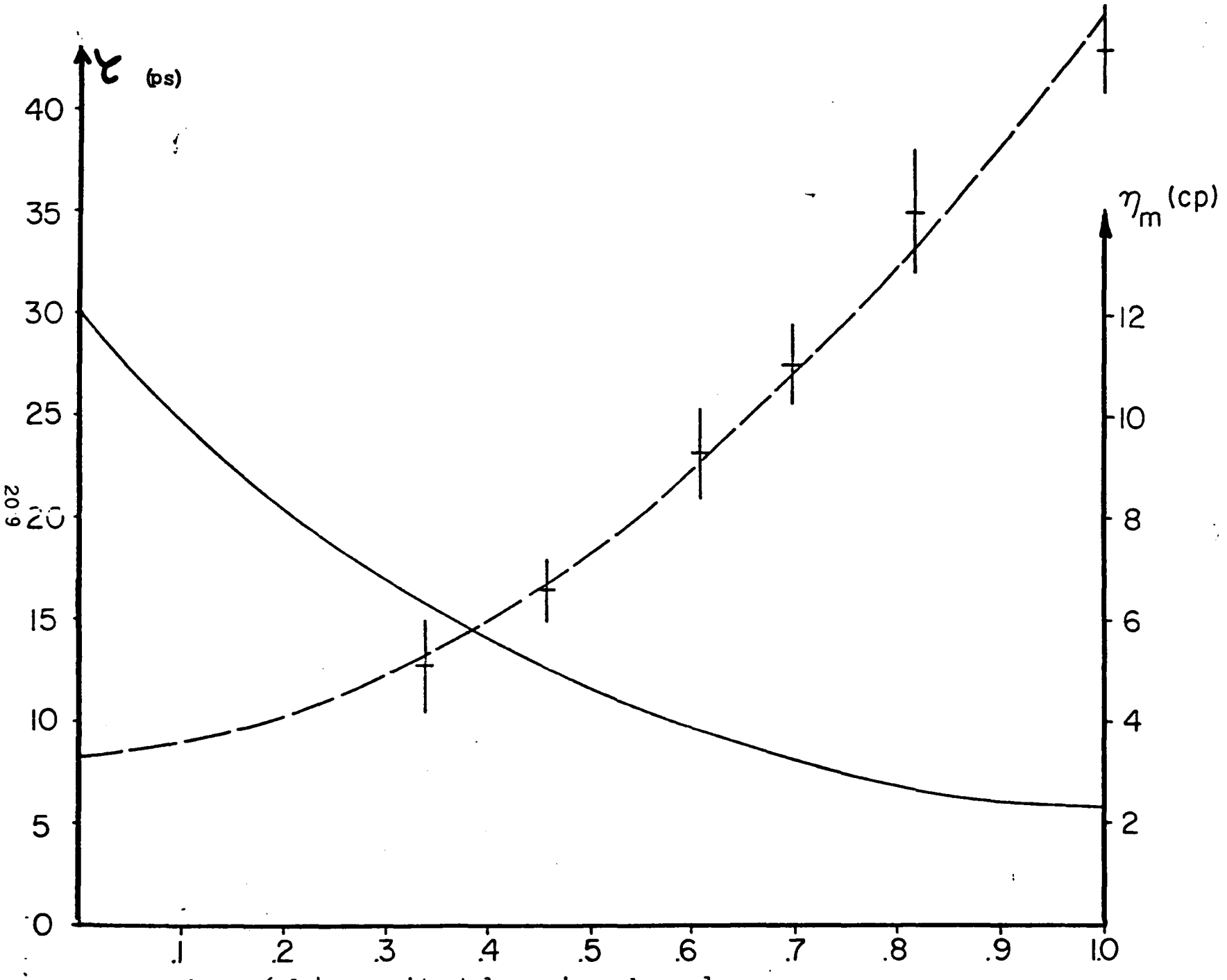

Figure 6.1.4 m-nitrotoluene in n-decanol

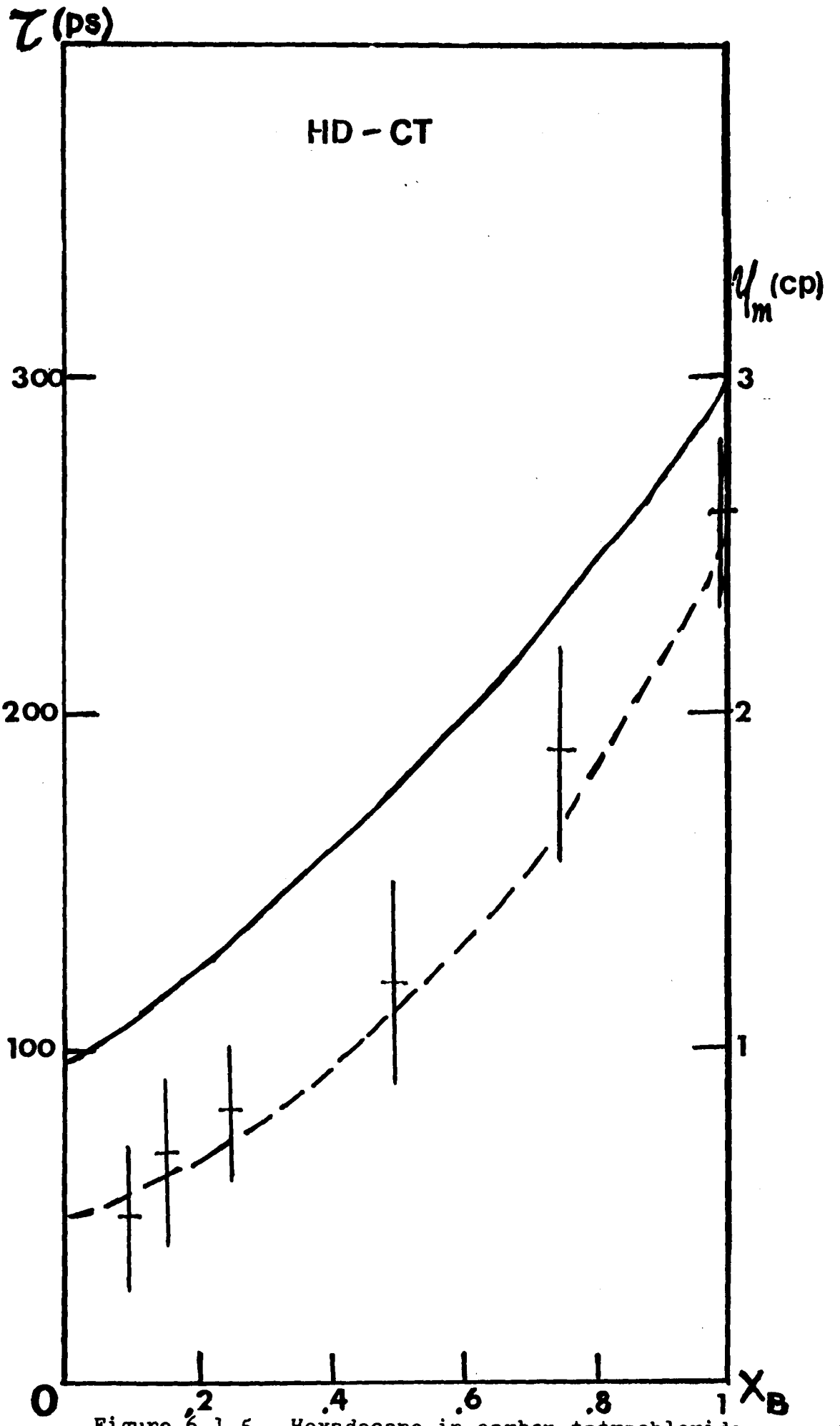

Figure 6.1.5 Hexadecane in carbon tetrachloride

6.2 Temperature Dependence Of The Rotational Relaxation Times Of Anisotropic Molecules In Neat And Mixed Binary Liquids

In this section, we extend our research in section 6.1[1] by measuring the temperature dependence of the relaxation time of the optical Kerr effect for nitrobenzene (NB) and m-nitrotoluene (mNT) molecules in neat and mixed binary liquids. For anisotropic molecules, the dominant mechanisms responsible for the optical Kerr effect are the molecular reorientational motion and electronic cloud distortion[2]. The electronic mechanism is temperature independent and is so fast ($< 10^{-14}$ seconds) that its time dependence cannot be resolved by picosecond techniques. The measurement of the temperature dependence of the Kerr relaxation time will yield information on the kinetics of the reorientational motion of the molecules. The relaxation time corresponds to an overall rotation of the motion of the molecule[3]. Just like the relaxation time obtained from the depolarized Rayleigh wing scattering, the Kerr relaxation time is a combination of the rotations about the individual axis of the molecules. The relaxation time is more strongly weighted by the reorientation about the axis which is associated with the largest polarizability change upon rotation[3] (see section 4.8 also).

We confirm within experimental error that the temperature dependence of the relaxation time depends on the measured viscosity in neat liquids as suggested by Debye[4], and on the effective viscosity in mixed liquids as suggested by Hill[5]. These measurements give credence to the use of effective

viscosity dependence in the equation for relaxation time for mixed liquids[1]. The form of the effective viscosity was empirically introduced previously[1] from Hill's[5] theory on the mutual viscosity between solute and solvent molecules and arises from the solute-solute and solute-solvent interactions. This is a reasonable model since it only takes into account the solute molecule interaction with its neighbors. The Debye equation for the rotational relaxation time which depends on the measured viscosity, accounts for an additional interaction between solvent-solvent molecules in mixed liquids.

The single shot picosecond laser technique[6-8] offers both convenience and accuracy in measuring the kinetics of the optical Kerr effect over the multiple shor technique. A schematic of the experimental apparatus used for measuring the Kerr relaxation time is shown in figure 9 of chapter 5. The sample Kerr cell was situated in a glass dewar with strain free windows. After sealing the cell, the temperature was controlled by flowing cooled nitrogen gas into the dewar and surrounding the sample cell holder with heating tape. The sample temperature was controlled to $\pm$ 1^{o}K. The temperature variation across the sample region was measured to be less than 1^{o}K. The lowest temperature used in the experiment was about 20 degrees below the freezing temperature of the liquid. At this temperature, the liquids was supercooled. The highest temperature reached was about 350^{o}K. Above this temperature, the relaxation time was too fast to be deconvoluted reliably from the Kerr decay profile. The viscosity of the sample was messured by an Ostwald type Cannon-Fenske viscometer in a temperature controlled water reservoir. The temperature was

controlled to within one degree. The viscosities were measured within a 2% error and were in good agreement with the viscosities listed in the standard tables. A typical single shot Kerr intensity profile versus delayed time for NB at 297°K is displayed in figure 6.2.1. The measured relaxation times and viscosities of NB, mNT, and the mixture of mNT with carbon tetrachloride (CT) and decyl alcohol (DA) are plotted as function of temperature in figures 6.2.2 to 6.2.5 . The relaxation time data presented in these figures are the average of decay times extracted from five to ten different intensity profile curves. The typical error in relaxation time is $\leq$ 20%. The salient feature of the data presented in figure 6.2.2 to 6.2.5 is that the relaxation times decrease approximately exponentially as 1/T. The data in figure 6.2.5 shows a curvature at the high temperature end.

The modified Debye model for molecular rotation relaxation time which is generally applicable for single particles rotational motion in pure polar liquid is [4,10] :

$$\tau = 4\pi a^3 (\zeta/3) \eta_m(T)/kT \quad , \qquad (6.2.1)$$

where τ is the relaxation time; k, is the Boltzmann constant; T is the absolute temperature; $a = (M/\rho N)^{1/3}$ is the radius of a spherical molecule ; ζ is a dimensionless parameter which is proportional to the mean square intermolecular torques to the mean square intermolecular force[10]; and $\eta_m(T)$ is the measured viscosity viscosity at temperature T. In mixed liquids, it has been observed[1,11] that measured viscosity dependence

given in equation 6.2.1 is not followed by the measured relaxation time as discussed in section 6.1. Applying the concept of the mutual viscosity introduced by Hill[5], the expression for the the temperature and concentration dependence for the molecular rotational relaxation time of solute molecules in a binary liquid is obtained[1]:

$$\tau(T) = C'/T \left[(1 + \lambda x)\ x\ \eta_B(T) + (1 - x)\ \eta_{BC}(T)\right], \quad (6.2.2)$$

where x is the mole fraction of solute molecues B which has a much larger Kerr effect than the solvent molecule C in this experiment; η_B is the pure solute viscosity; η_{BC} is the mutual viscosity between solute B and solvent C molecules; C' is a constant parameter to account for the pair correlation effect among the solute molecules at different concentrations. Values for C' and λ were numerically determined in section 6.1 on the concentration dependence of the relaxation time at room temperature. The parameters are $C'_{mNT+CT} = 7.3\ (296)$ K sec/cp[12], $\lambda_{mNT+CT} = 2.0$ (slightly changed due the correction of mNT measurement); $C'_{mNT+DA} = 5.5\ (296)$ K sec/cp, and $\lambda_{mNT+DA} = 2.56$. A similar formula to equation 6.2.2 was used by Kivelson and Tsay[13].

Using Hill's model for mixed liquids, the temperature dependence equation for the measured viscosity is given by :

$$\eta_m(T) = x^2/a_m\ a_B\eta_B(T) + 2\ x(1-x)/x\, a_{BC}\eta_{BC}(T) + (1-x)^2/a_m a_C\eta_C(T)$$

These parameters have been discussed in section 6.1. The temperature dependence of the measured viscosity is assumed to arise from the viscosities $\eta_B(T)$, $\eta_C(T)$, and $\eta_{BC}(T)$. All other terms are assumed to be constant with respect to the

temperature variation. The temperature dependence of the viscosity in neat liquids can be expressed[14,15] by

$$\eta_m(T) = (RT/E)^{\frac{1}{2}}(2mRT)^{\frac{1}{2}} v^{-2/3} P_v^{-1} \exp(R/RT) \quad , \quad (6.2.4)$$

where E is the potential barrier or activation energy; R is the gas constant; m is the molecular mass; v is the volume of a molecule; and P_v is the probability that there is a sufficient local free volume for transition to occur. When the temperature is changed, the viscosity of the pure liquids of the solute and the solvent will be varied as $T \exp(E_i/RT)$. The mutual viscosity [16] between the solute and the solvent molecules is assumed to vary similarly :

$$\eta_{BC}(T) \propto T \exp(E_{BC}/RT) \quad , \quad (6.2.5)$$

where E_{BC} is the potential energy barrier between the poistions of the solute and solvent molecules. From the measurements of the viscosities $\eta_B(T)$, $\eta_C(T)$, and $\eta_m(T)$, the mutual viscosity $\eta_{BC}(T)$ can be calculated from equation 6.2.3.

A list of activation energies calculated from different measurements is displayed in table 6.1 for various solutions. The first column shows the activation energies obtained from measuring the viscosity as a function of temperature. Using equations 6.2.3 and 6.2.4, the activation energies between solute and solvent molecules are calculated; $E_{mNT+CT}(x=0.75)$ =2.2 kcal/mole and $E_{mNT+DA}(x=0.72)$ = 3.8 kcal/mole. These are listed in column 2. The third column in the table is obtained by fitting the measured Kerr relaxation times displayed

Table 6.1 Activation Energies of Neat Liquids and Mixed Binary Liquids

(Activation Energy E : kcal/mole ± 10%)

	1	2		3
	E_{Debye} (Viscosity Measurement)	E_{Hill}		E_{Kerr} (Measured Arrhenius)
		Solute-Solute	Solute-Solvent	
NB	3.0	3.0	—	3.0
mNT	3.6	3.6	—	3.6
mNT+CT(x=0.75)	2.9	3.6	2.2	3.2
mNT+DA(x=0.72)	4.2	3.6	3.8	3.0
CT	2.5	—	—	—
DA	6.2	—	—	—

in figures 6.2.2, 6.2.3, 6.2.4, and 6.2.5 to a simple Arrhenius behaviour of the form :

$$\tau = A \exp(E/RT) \quad . \qquad (6.2.6)$$

The energies listed in columns 1 and 2 of the table are used for curve fitting the relaxation time data displayed in figures 6.2.2 to 6.2.5. The data of Hill's relaxation time are calculated from equation 6.2.2 using the previously measured (see section 6.1) parameter C' and λ, the measured $\gamma_B(T)$, and the calculated $\gamma_{BC}(T)$ (or $E_{BC}(T)$). The Debye's relaxation times are calculated from equation 6.2.1 by using $\gamma_m(T)$, $\eta_{NB} = 0.1$, and $\eta_{mNT} = 0.1$. These values are plotted in figures 6.2.2 to 6.2.5. As shown in figures 6.2.2 and 6.2.3, the calculated curve from Debye's and Hill's models give excellent fits to the relaxation data for neat liquids. Also these models agree well with the temperature dependence of τ for the mixture of mNT and CT (figure 6.2.4). This is reasonable, since the effective and the measured viscosities are about the same at different temperatures. This is not so for the mixture of mNT and DA. The dashed curve in figure 6.2.5 is a plot of the relaxation time calculated from equation 6.2.1 of Debye's model using the measured value of $\gamma_m(T)$ and the calculated values of a^3 and η_{mNT} from the neat liquids. Using $\eta_{mNT} = 0.1$, this curve does not agree with the data. Even if we force fit Debye's equation for τ to the data point of figure 6.2.5 at $T = 296^{\circ}K$ by changing $\eta = 0.023$, the slope of the curve from the Debye equation is still of by 40% with the slope of the data (see figure 6.2.6). On the other hand, Hill's model provides a better fit to the experimental

data which is only about 20% off at the higher temperature end. The deviation of the data at high temperature from a linear dependence in figure 6.2.5 may arise from a low intensity slow relaxation component which merges with the main fast component as the temperature is increased. A possible mechanism which may cause such a component is the reorientation of a solvent molecule by the field of the neighboring solute molecules. At this time, from the concentration and temperature dependence Kerr relaxation experiments, Hill's model seems to be a reasonable model to explain the molecular reorientational time in mixed liquids. However, in next section (6.3), with an increase signal to noise of the Kerr gate, an additional decay component is present. This complicates the problem further.

References

1. P.P. Ho, W. Yu, and R.R. Alfano,Chem.Phys.Lett., 37,91,(1976).
2. O. Svelto, Progress in Optics, XII, 23, (1974).
   K. Sala and M.C. Richardson, Phys. Rev., A12, 1036, (1975).
3. D.R. Bauer, G.R. Alms, J.J. Brauman, and R. Pecora,
   J. Chem. Phys., 61, 2255, (1974).
4. P. Debye, Polar Molecules, (Dover, New York, 1929).
5. N.E. Hill, Proc. Phys. Soc. (London), 67B, 149, (1954).
6. M.A. Duguay and A.T. Mittick, Applied Optics,10,2162,(1971).
7. M.R. Topp and P.M. Rentzepis, J.Chem. Phys.,56, 254,(1972).
8. G. Mourou and M.M. Malley, Opt. Comm., 13, 412, (1975).
9. Internal Critical Table, V5, (1972).
   Landolt-Bornstein Tables V5, (Springer Verlag, Berlin, 1969).
10. D. Kivelson, M.G. Kivelson, and I. Oppenheim, J. Chem. Phys.,
    52, 1810, (1970).
11. A.J. Curtis, P.G. McGreer, G.R. Rathman, and C.P. Smyth,
    J. Am. Chem. Soc., 74, 644, (1952).
12. From section 6.1, we determined C'/T = 7.3 ps/cp at 296^{o}K,
    this imply C' = 7.3(296) ^{o}K ps/cp.
13. D. Kivelson and S.J. Tsay, Molecular Physics, 29,29, (1975).
14. H.D. Weymann, Kolloid Z., 181, 131, (1962).
15. P.B. Macedo and T.A. Litovitz, J. Chem. Phys.,42, 245,(1965).
16. N.L. Balaze, Rec. Trav. Chim. Pays-Bas., 70, 412, (1951).

Figure Captions

Figure 6.2.1. Intensity profile of the optical Kerr effect of NB at 25°C versus time. The zero time is arbitrary and the peak transmission is about 10%. The rise time is 5.3 ps and the decay time is 15.2 ps. This decay time corresponds to a molecular orientational time of 30.4 ps.

Figure 6.2.2. The Measured Kerr relaxation time versus 1/T of NB. The data • are the measured viscosities in cp, and the data + are the measured relaxation times (psx2). The solid line is the theoretical fit to Debye's model.

$$\tau = 4\pi/3\, a^3\, \eta_m(T)/T = 5.2\times10^{-9}(^{\circ}K \text{ sec/cp})\, \eta_m(T)/T .$$

Figure 6.2.3. Kerr relaxation time vs 1/T of pure mNT. The data • are the measured viscosities in cp, and the data + are the measured Kerr relaxation times (psx2). The solid line is the theoretical fit to Debye's model.

$$\tau = 4\pi/3\, a^3\, \eta_m(T)/T = 5.7\times10^{-9}(^{\circ}K \text{ sec/cp})\, \eta_m(T)/T .$$

Figures 6.2.4. Kerr relaxation time Versus 1/T for 75% mole fraction of mNT and 25% mole fraction of CT. The solid line is the theoretical fit of Hill's model.

$$\tau_{Hill} = (6.9)(296)/T \left[(1+2x)\, x\, \eta_{mNT}(T) + (1-x)\, \eta_{mNT+CT}(T)\right],$$

where $x = 0.75$. Debye's model for τ is almost identical to $\tau_{Hill}(T)$.

Figure 6.2.5 Kerr relaxation time versus 1/T for 72% mole fraction of mNT and 28% mole fraction of DA. The solid line is

$$\tau_{Hill} = (5.5)(296)/T \left[(1 + 2.56x) \times \gamma_{mNT}(T) + (1-x)\, \gamma_{mNT+DA}(T)\right],$$

and the dashed line is:

$$\tau_{Debye} = (5.7)10^{-9}\ (^{o}K\ sec/cp)\ \gamma_{m}(T)/T\ .$$

Figure 6.2.6 Comparision of modified of modified Hill, Debye, and Arrhenius forms for the relaxation time of mNT in DA. The solid line is

$$\tau_{Hill} = (5.5)(296)/T \left[(1 + 2.56x) \times \gamma_{mNT}(T) + (1-x)\, \gamma_{mNT+DA}(T)\right],$$

and the dashed line is

$$\tau_{Debye} = (1.2)10^{-9}\ (^{o}K\ sec/cp)\ \gamma_{m}(T)/T\ ,$$

where the value 1.2×10^{-9} is chosen to force the curve lie on the data point of $296^{o}K$. The dotted line is the best fit by assuming an Arrhenius behavior :

$$\tau_{Arrh.} = (9.1)10^{-14}\ (sec\ )\ \exp(1500/T)\ .$$

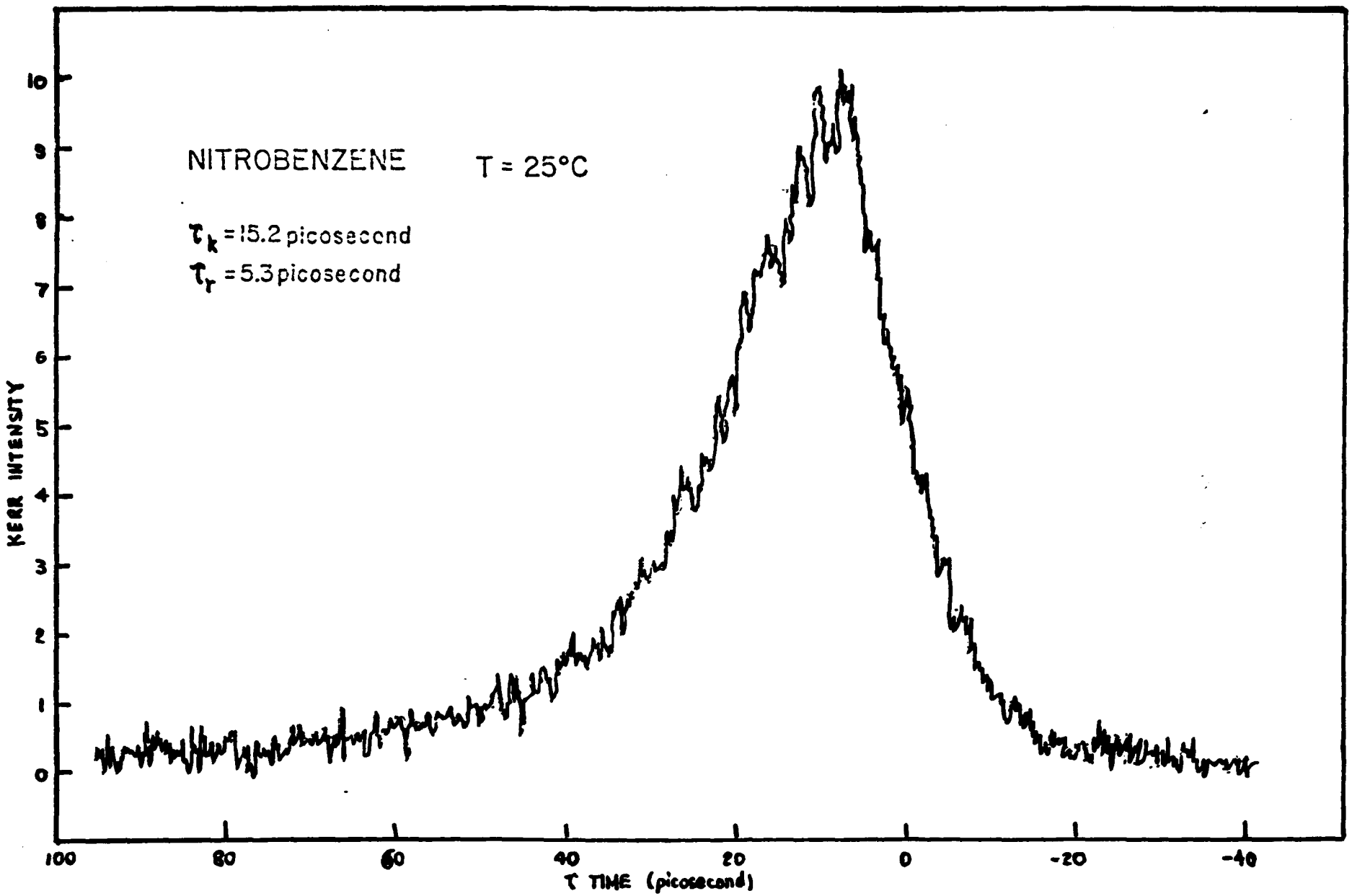

Figure 6.2.1 Single Shot Kerr Relaxation Curve of NB

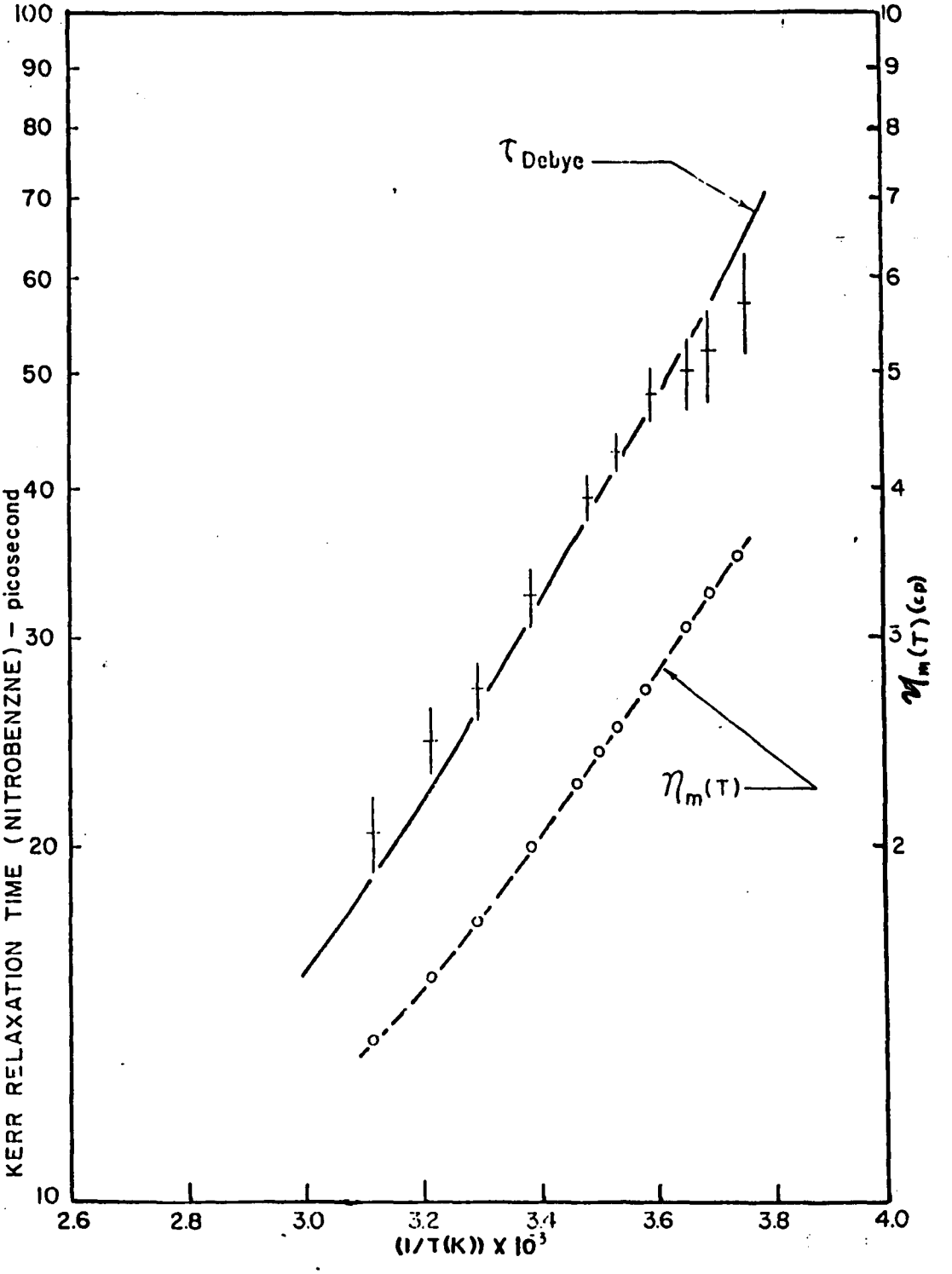
100
90
80
70
60
50
40
30
20
10
KERR RELAXATION TIME (NITROBENZNE) – picosecond
τ_{Debye}
$\eta_{m(T)}$
10
9
8
7
6
5
4
3
2
$\eta_{m(T)}$ (cp)
2.6
2.8
3.0
3.2
3.4
3.6
3.8
4.0
(1/T(K)) X 10^3

Figure 6.2.2

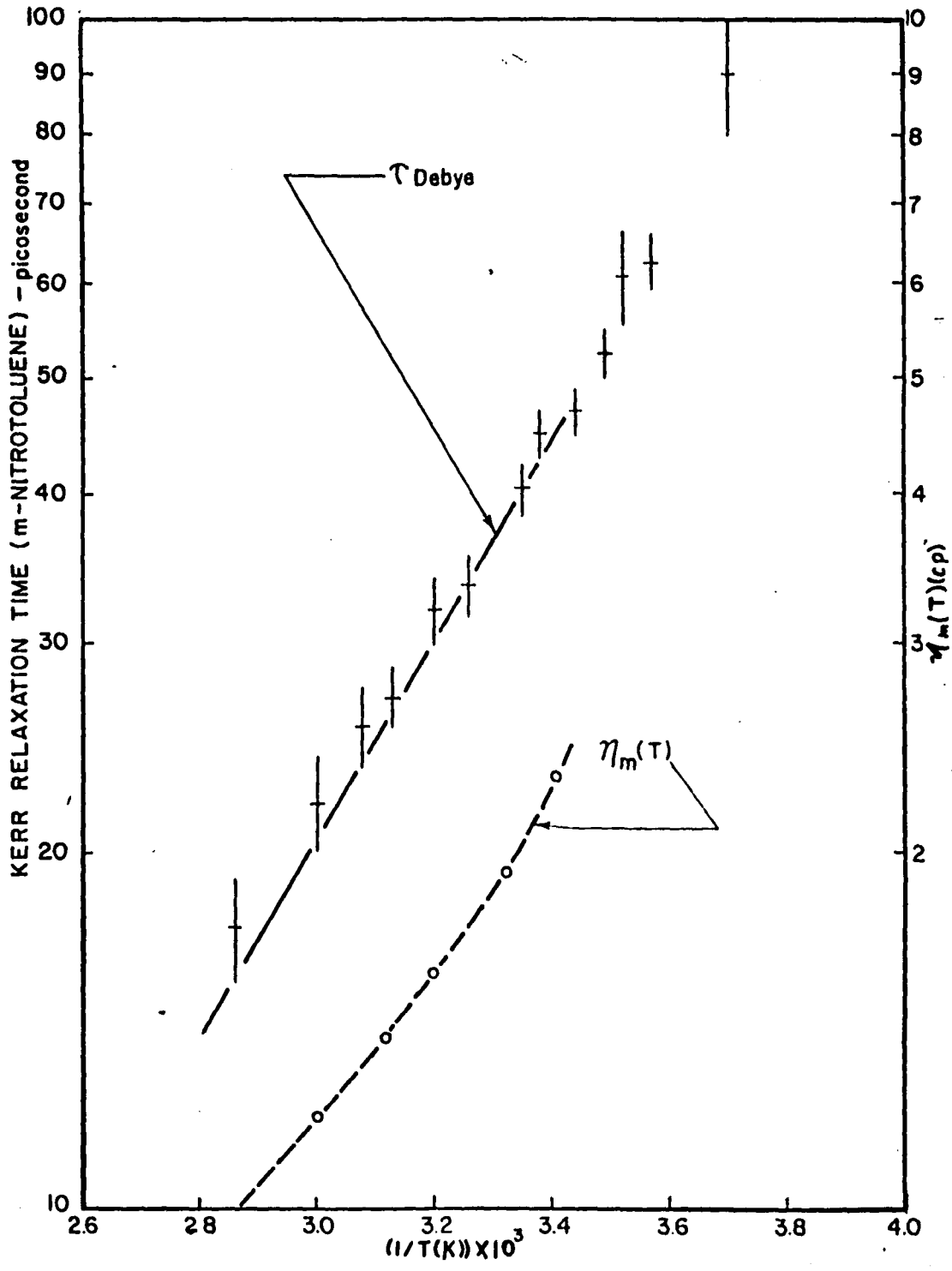
KERR RELAXATION TIME (m-NITROTOLUENE) - picosecond
100
90
80
70
60
50
40
30
20
10
τ Debye
$\eta_m(T)$
$\eta_m(T)$(cp)
10
9
8
7
6
5
4
3
2
2.6
2.8
3.0
3.2
3.4
3.6
3.8
4.0
(1/T(K)) X10^3

Figure 6.2.3

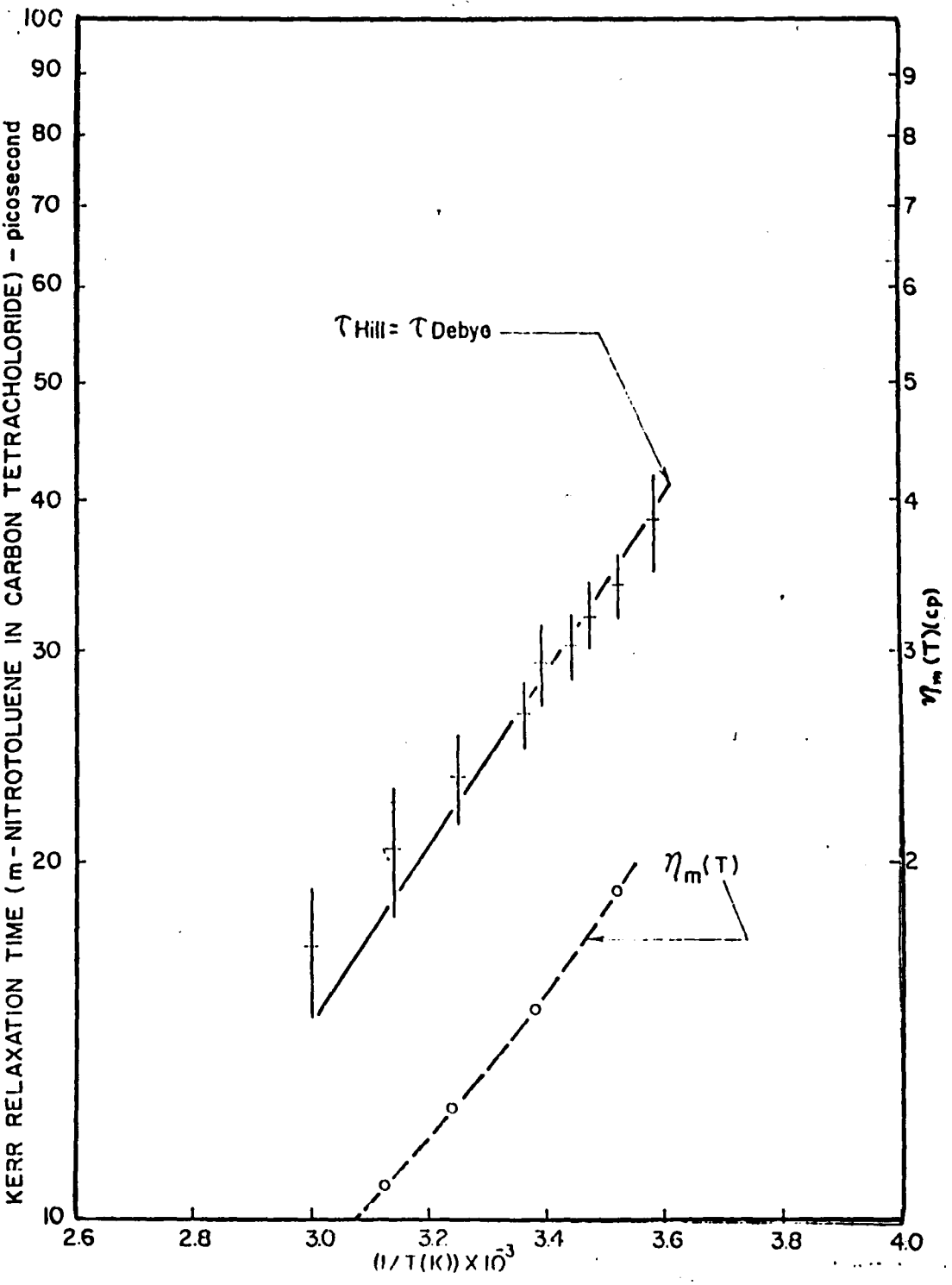
KERR RELAXATION TIME (m-NITROTOLUENE IN CARBON TETRACHOLORIDE) - picosecond
100
90
80
70
60
50
40
30
20
10
$\tau_{Hill} = \tau_{Debye}$
$\eta_m(T)$
$\eta_m(T)$(cp)
9
8
7
6
5
4
3
2
2.6
2.8
3.0
3.2
3.4
3.6
3.8
4.0
$(1/T(K)) \times 10^{-3}$

Figure 6.2.4

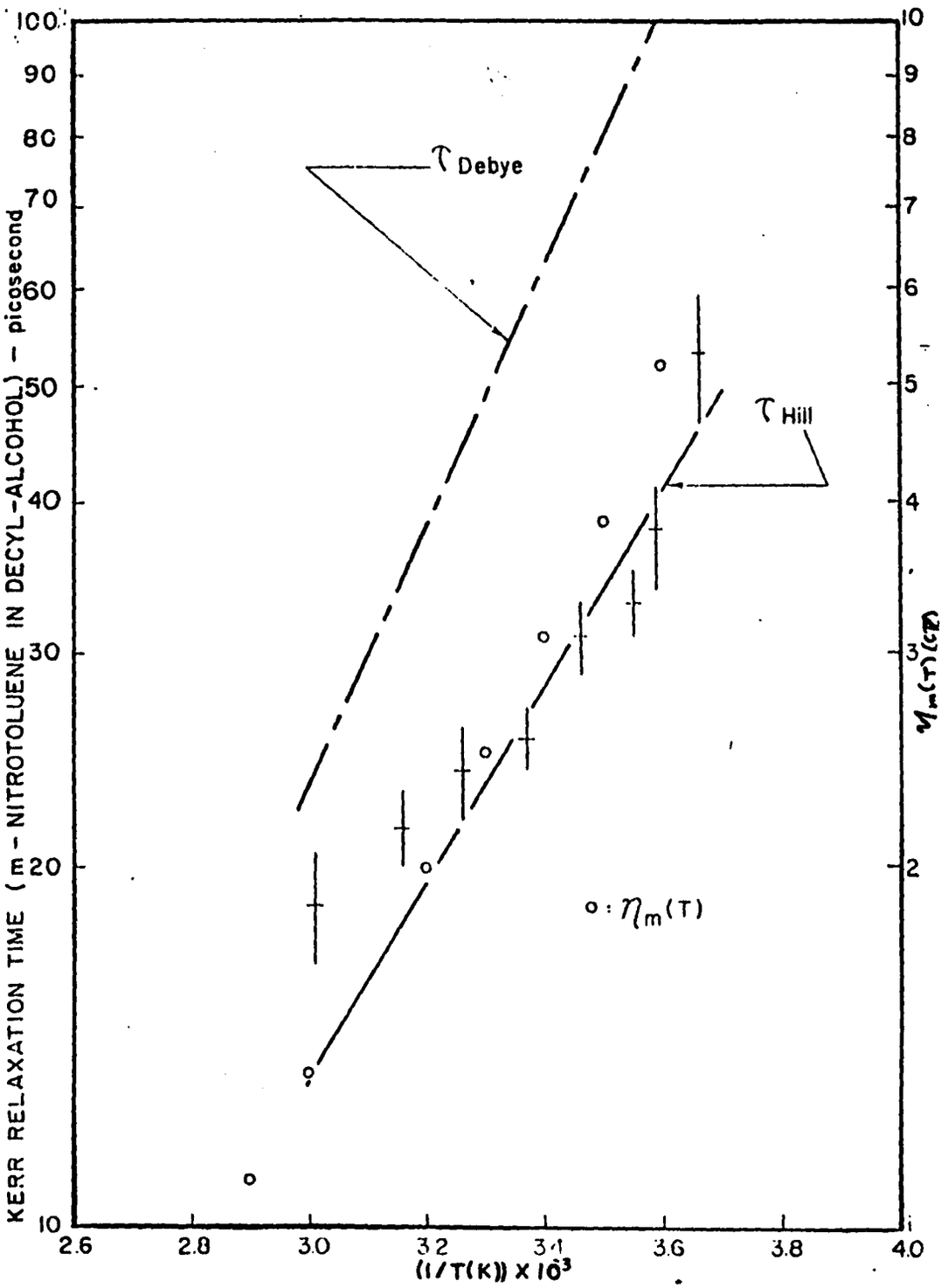
KERR RELAXATION TIME (m-NITROTOLUENE IN DECYL-ALCOHOL) - picosecond
100
90
80
70
60
50
40
30
20
10
τ Debye
τ Hill
o : $\eta_m(T)$
$\eta_m(T)$(cp)
10
9
8
7
6
5
4
3
2
1
2.6
2.8
3.0
3.2
3.4
3.6
3.8
4.0
(1/T(K)) X 10^3

Figure 6.2.5

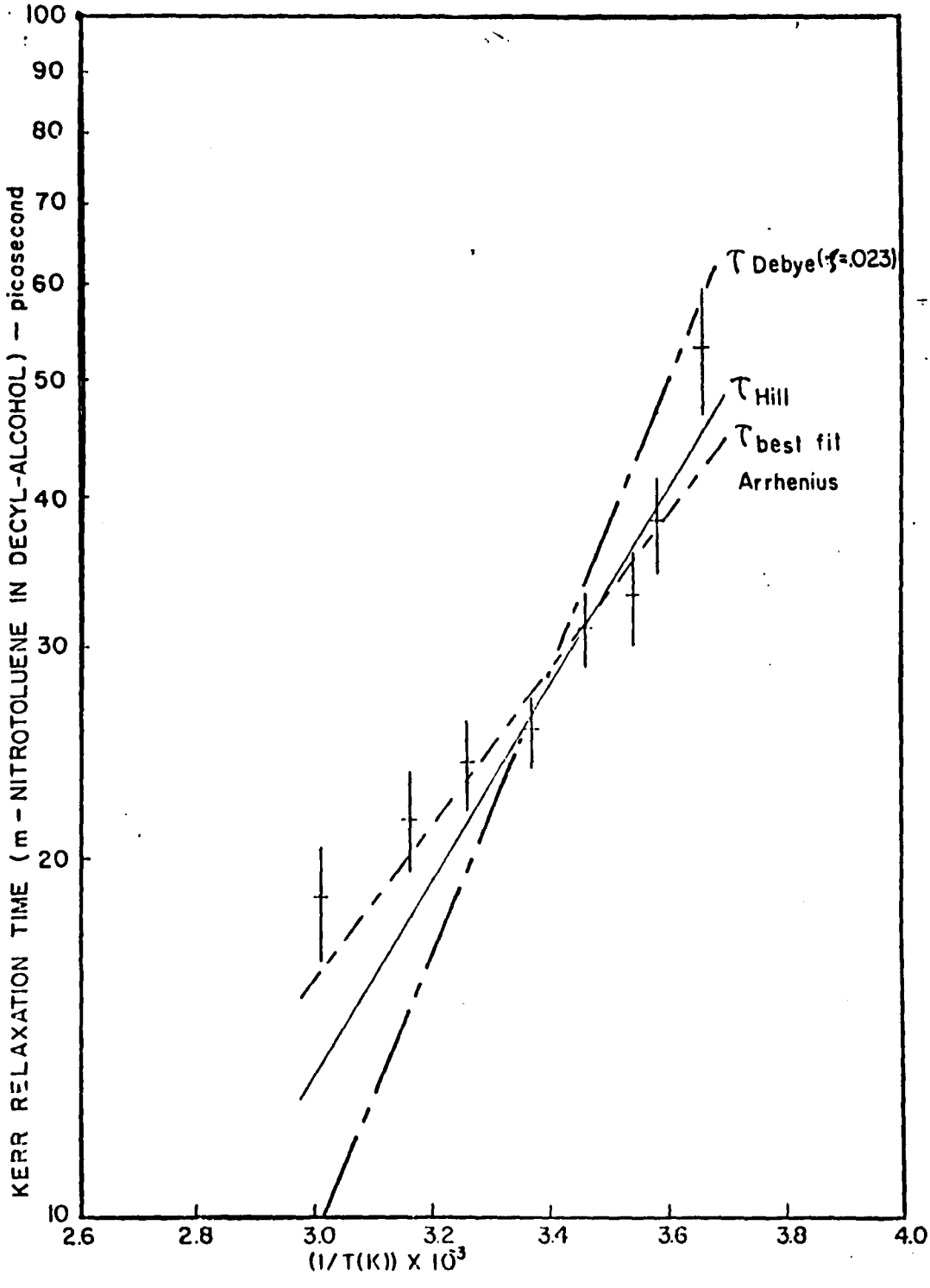
KERR RELAXATION TIME (m-NITROTOLUENE IN DECYL-ALCOHOL) — picosecond
100
90
80
70
60
50
40
30
20
10
2.6
2.8
3.0
3.2
3.4
3.6
3.8
4.0
(1/T(K)) X 10³
τ Debye(f=.023)
τ Hill
τ best fit
Arrhenius

Figure 6.2.6

6.3 Coupled Molecular Reorientational Relaxation Kinetics In Mixed Binary Liquids

The reorientational relaxation time has been described by Debye[1] as a function of molecular volume, viscosity, and temperature. The experimental results of the Kerr reorientational relaxation time of neat liquids can be interpreted by this theory[2,3]. However, in a binary mixture of Kerr active and nonactive liquids, there are difficulties in applying Debye's theory to fit the experimental Kerr kinetic data[2,3,4]. Previously, an effective viscosity was introduced[2,3,5] to fit the Kerr kinetic data in these mixtures. In this section, we have concentrated our research on the direct measurement of the relaxation kinetics of the Kerr effect in binary mixtures of liquids and on describing the data using the coupled two-component theory of Kivelson and Tsay[6]. The data can be fitted to the theo y.

The Kerr intensity decay profile of viscous solutions is generally found to be a non-single exponential decay which can be fitted by the addition of two exponential functions - a fast and a slow component. It now appears that the Kerr relaxation kinetics of binary solutions (Kerr active plus Kerr non-active liquids) is not just the reorientation of the Kerr active solute molecules about their own axes but the reorientation of the coupled solute-solvent system. In this section, the Kerr intensity decay profile is believed to arise from the reorientation of the solute-solvent system which includes the reorientation of Kerr non-active solvent molecules (the solvent molecules are coupled to the solute molecules).

6.3 Coupled Molecular Reorientational Relaxation Kinetics In Mixed Binary Liquids

The reorientational relaxation time has been described by Debye[1] as a function of molecular volume, viscosity, and temperature. The experimental results of the Kerr reorientational relaxation time of neat liquids can be interpreted by this theory[2,3]. However, in a binary mixture of Kerr active and nonactive liquids, there are difficulties in applying Debye's theory to fit the experimental Kerr kinetic data[2,3,4]. Previously, an effective viscosity was introduced[2,3,5] to fit the Kerr kinetic data in these mixtures. In this section, we have concentrated our research on the direct measurement of the relaxation kinetics of the Kerr effect in binary mixtures of liquids and on describing the data using the coupled two-component theory of Kivelson and Tsay[6]. The data can be fitted to the theo y.

The Kerr intensity decay profile of viscous solutions is generally found to be a non-single exponential decay which can be fitted by the addition of two exponential functions - a fast and a slow component. It now appears that the Kerr relaxation kinetics of binary solutions (Kerr active plus Kerr non-active liquids) is not just the reorientation of the Kerr active solute molecules about their own axes but the reorientation of the coupled solute-solvent system. In this section, the Kerr intensity decay profile is believed to arise from the reorientation of the solute-solvent system which includes the reorientation of Kerr non-active solvent molecules (the solvent molecules are coupled to the solute molecules).

Previously,[2,3] our data in section 6.1 and 6.2 on the reorientation of solute molecules in mixed liquids were fitted by using a model based on the Hill theory[5] of an effective viscosity combined with the Keyes and Kivelson theory[6] of pair correlations in the liquid state. This model only considers the reorietation of solute molecules caused by the molecular interactions between solute-solute and solute-solvent molecules. In that case, the Kerr intensity decay profiles were measured over a dynamic range of about one hundred and were fitted to a single exponential. Reasonable agreement between this model and the experimental results was found by adjusting two parameters. Now, with an improved signal to noise ratio, we have observed a "new" weak and slowly decaying component in the Kerr intensity profile in viscous solutions ($\eta_m > 2$ cp). In this section, these two components (fast and slow) are attributed to the reorientation of the solute and solvent molecules. All the data can be fitted to the recent coupled two-component reorientational relaxation theory of Kivelson and Tsay[6] by adjusting seven parameters.

The equation for the two-component relaxation time that is used in this paper to fit the data is reduced to :

$$T_{\pm} = \tfrac{1}{2}(1-\phi^2)^{-1}\left\{\left[\tau_B^{-1}(1+x_B f_{BB})^{-1} + \tau_C^{-1}(1+x_C f_{CC})^{-1}\right] \pm \left[(\tau_B^{-1}(1+x_B f_{BB})^{-1} - \tau_C^{-1}(1+x_C f_{CC})^{-1})^2 + 4\tau_{BB}^{-1}\tau_{CC}^{-1}\phi\right]\right\} \quad (6.3.1)$$

This equation is derived in section 3.3. The relative peak intensity in the two-component decay curve is another relation

which has been used simultaneously with equation 6.3.1 to interpret our data. Following the derivation of Kivelson and Tsay[6], the integrated intensity for the two components in the depolarized Rayleigh scattering is as follows :

$$I_{\pm} = (T_{+}^{-1} - T_{-}^{-1})^{-1} \Big\{ \pm \Delta\alpha_B^2 \left[x_B (1 + x_B f_{BB}) (\zeta_{BB}^{-1} - T_{\pm}^{-1}) \right] \pm \Delta\alpha_C^2 \left[x_C (1 + x_C f_{CC}) (\zeta_{CC}^{-1} - T_{\pm}^{-1}) \right] \pm \Delta\alpha_B \Delta\alpha_C \phi \left[x_B (1 + x_B f_{BB}) x_C (1 + x_C f_{CC}) \right]^{\frac{1}{2}} \left[(T_{\pm}^{-1} - T_{\pm}^{-1}) - (1-\phi^2)(\zeta_{BB}^{-1} - \zeta_{CC}^{-1}) \right] \Big\} \tag{6.6.2}$$

where $I_{\pm}$ are the integrated light scattering intensities for $T_{\pm}$ component decay processes, respectively. The difference in polarizability is $\Delta\alpha_i = \alpha_{i//} - \alpha_{i\perp}$ where $\alpha_{i//}$, and $\alpha_{i\perp}$ are the components of the polarizability tensor parallel and perpendicular to the symmetry axis of the molecules of the i-th species, respectively.

The relationship between the intensity of depolarized Rayleigh scattering, I, and the molecular part of the nonlinear index of refraction of the Kerr effect has been described by Hellwarth[7] as :

$$I_{\pm} \propto n_{2\pm} . \tag{6.6.3}$$

However, the intensity of light scattering and the size of n_2 expressed by equation 6.3.2 are the steady state values. In kinetic experiments, due to the finite response of the molecular reorientation of the molecules to the orienting electric

field associated with the laser pulse, the peak of the Kerr intensity is reduced. The peak of the Kerr intensity associated with orientational motion is proportional to[7,12],

$$S_{\pm}^2 \propto \left[n_{2\pm} / f(T_{\pm}) \right]^2 \quad . \qquad (6.3.4).$$

The peak response function $f(T_{\pm})$ is inversely proportional to the ratio of moleculear orientational relaxation time to the duration time of the laser pulse (see section 4.6A).

Bauer et al[9] have pointed out that the peak intensity of the depolarized Rayleigh scattering is proportional to I times T. The size of the signal is larger for a slower relaxation process than for a faster one. On the other hand, the opposite is true for the Kerr effect. The optical Kerr effect induced by an intense picosecond laser pulse weighs more heavily on a faster relaxation component over a slower one. This may be one possible reason to explain some of the inconsistences in the measured relaxation times obtained by these two techniques.

The theoretical model presented in section 3.3 indicates that there is always a two-component decay in a mixed binary liquid. The relative sizes of two-component decay depend on the parameters given in the complex equation 2. In general, if $\tau_{BB}(x)$, $\tau_{CC}(x)$, f_{BB}, f_{CC}, f_{BC}, and changes in polarizabilities $\Delta\alpha_i$ are known, equations 1 and 2 can be used to evaluated $T_{\pm}$ and $n_{2\pm}$. Calculated curves for the coupled two-component relaxation processes $T_{\pm}$ and $n_{2\pm}$ are shown in figure 1 and 2 under different conditions. The parameters chosen are reasonably close to the experimental situation.

In figure 1, the relaxation time for the B (solute) and for the C (solvent) components are chosen to be comparable in

size. The assumed parameters are given by :

$$\tau_{BB}(x) = (15\, x_B + 5)\, (1 + 1.5\, x_B),$$
$$\text{and } \tau_{CC}(x) = (15\, x_C + 5)\, (1 + 1.5\, x_C), \qquad (6.3.5)$$

where $x_B + x_C = 1$ and $f_{BB} = f_{CC} = 1.5$.

In figure 1a, various values are used for the interspecies pair correlation factor, f_{BC}, to calculate the coupled two-component reorientational relaxation times $T_{\pm}$. For $f_{BC} = 0$, there is no coupling term, the relaxation process is described by the uncoupled relaxation times $\tau_{BB}(x)$ and $\tau_{CC}(x)$. As f_{BC} is increased, the curve for the coupled relaxation times $T_{\pm}$ versus x_B starts to separate from the curves for the uncoupled relaxation times $\tau_{BB}(x)$ and $\tau_{CC}(x)$. Calculated values of the two component Kerr constants $n_{2\pm}$, versus the mole fraction are shown in figure 1b. In figure 1b-1, by assuming $n_{2B} = n_{2C} = 2.5$ and $f_{BC} = 2$, the contribution to the nonlinear index of refraction from solute-solute (B-B), solvent-solvent (C-C) and solute-solvent (B-C) molecular interactions are shown. These contributions were calculated from equation 2. In figure 1b-2, the parameters $n_{2B} = n_{2C} = 2.5$ and $f_{BC} = 0$ are chosen and equation 2 is used to calculate $n_{2\pm}$ for the different contributions. In figure 1b-3, the parameters $n_{2B} = 2.5$, $n_{2C} = 0.1$, and $f_{BC} = 2$ are chosen and used to calculate the different contributions to the nonlinear index of refraction $n_{2\pm}$. These are examples of coupled systems of two kinds of liquids which have comparable orientational relaxation time in neat solutions but different

interspecies coupling parameters and Kerr constants. Taking the values for $n_{2\pm}$ shown in figure 1b-1, the $T_{\pm}$ curves in figure 1a can be separated into different regions. The index $n_{2\pm}$ measures the strength of the $T_{\pm}$ signals. Region I is called the solute-like zone where the relaxation time of the system is proportiona to the parameters of neat solute kinetics. Region II is called the solvent-like zone where the relaxation mechanism of the system is similar to the reorientation of solvent molecules. Region III is the mixed zone where relaxation depends on both species of molecules and the coupling strength between the solute and solvent molecules.

Mixing two neat liquids, one with a rather long relaxation time in comparison to the other, results in a different type of coupling curves. The relaxation times and Kerr constants for the coupled two-component relaxation of such a system are plotted in figure 2 versus the mole fraction x_B by assuming the equations :

$$\tau_{BB}(x) = (15x_B + 5) (1 + 1.5x_B) \quad ,$$
$$\text{and } \tau_{CC}(x) = (x_C + 0.1) (1 + 1.5x_C) \quad , \qquad (6.3.6)$$

where $x_B + x_C = 1$ and $f_{BB} = f_{CC} = 1.5$.

The two-component relaxation times $T_{\pm}$ for various f_{BC} are shown in figure 2a. The size of $n_{2\pm}$ for the two component at f_{BC} for various combinations of Kerr constants are plotted versus mole fraction x_B in figure 2b (in figure 2b-1, it is assumed that

$n_{2B} = n_{2C} = 2.5$; in figure 2b-2, it is assumed that $n_{2B} = 2.5$ and $n_{2C} = 0.1$; and in figure 2b-3, it is assumed that $n_{2B} = 0.1$ amd $n_{2C} = 2.5$). As long as $f_{BC} \neq 0$, there is always a small mixing in the curves resulting in three zones as described before; however, the distributions are different. In figures 2b-1 and 2b-3 the relaxation process for the fast component T_+ is mostly due to C-species molecules.

A schematic of the experimental apparatus [11] for measuring the relaxation kinetics of the optical Kerr effect is shown in figure 5.1 of chapter 5. A dynamic range of 5×10^3 in the transmitted 0.53 um signal was obtained in this experiment. The single shot technique [3] offers convenience; however, the dynamic range was limited to about 10^2.

In the experiment, Kerr active solute molecules nitrobenzene (NB) and m-nitrotoluene (mNT) were separately mixed with Kerr non-active solvents such as pentane (PN), carbon tetrachloride (CT), cyclooctane (CO), hexyl alcohol (HA), and cyclohexanol (CHA). The peak transmitted signal measured with the neat solvent Kerr gate is less than one hundredth of the neat solute gate. The transmitted signal from the neat solvent Kerr gate vanishes for times beyond 30 ps away from the peak. The size of the solute and solvent molecules are roughly the same, with their mole fraction and volume fraction differing by 4%. The chemicals used in this experiment was purchased from the Eastman Kodak Company and the Fisher Scientific Company.

In the temperature dependent part of this experiment, a 1 cm cuvette was placed in a glass dewar with strain free windows. A thermocouple was cleaned and immersed in the cuvette. The temperature was changed by adjusting the flow rate of cooled nitrogen gas into the dewar and by applying voltage to heater tape which surrounded the sample cell holder. The temperature was controlled to within one degree. All other experiments were performed at room temperature at 25 $\pm$ 2^{0}C. The viscosity of the samples were measured by an Ostwald type Cannon-Fenske viscometer in a temperature controlled water reservoir. The viscosities were measured with a 2% error and are in good agreement with the viscosities listed in the standard tables [12].

The Kerr intensity decay profile of 10% NB in various solvents are shown in figure 3.

The Kerr intensity decay profiles of the neat solvents and of mNT in PN, CT, CO, HA, and CHA at various concentrations are shown in figure 4. The Kerr intensity decay profiles of the mixture of 35% mNT and 65% CHA at three different temperatures are shown in figure 5. The salient features of these curves are (1) the slope of the earlier time portion ($t \leq 40$ ps) decays faster as the concentration of solute is reduced; and (2) a weaker slow decay component appears later in time as the solution becomes more viscous (figures 4c to 4e).

The four major mechanisms responsible for the optical Kerr effect in the picosecond time domain are the electron cloud distortion, molecular libration, molecular redistribution, and molecular reorientational motion[13,14,7,8]. The relaxation time of the electronic effect ($\tau_e \leq 10^{-14}$ seconds)[8] and molecular libration and redistribution ($\tau \simeq 10^{-13}$ seconds)[14] are very fast and can not be resolved by picosecond pulse techniques. When the reorientational relaxation time is slower than the laser pulse width, the molecular reorientational motion can be distinguished from these fast processes. The induced refractive index due to the molecular reorientational motion n_2^o is usually much larger than the nonlinear index of refraction from the fast processes n_2^e. For the solutes used in this experiment ($n_2^o \geq 4n_2^e$)[8,15]. For mNT solution, the reorientational relaxation time in neat liquids is 50 ps. The Kerr intensity decay profile of the mNT gate is a single exponential over the whole intensity range studied. Moreover, in the mNT and NB neat liquids, the electronic and librational contribution will essentially decay away with the prompt pulse shape, vanishing beyond 20 ps from the peak. The prompt Kerr intensity profile versus time is measured by using CS_2 liquid where τ_o = 2 ps[16] (see figure in P302). The relaxation kinetics of mNT and NB liquids are dominated by the molecular reorientational motion. For neat solvent liquids, the transmitted Kerr signal is mainly due to the electronic distortion and molecular librations. The transmitted signal from various solutions displayed in figures 3 to 5 are assumed to arise from the molecular reorientational motion.

In the data reduction, the measured Kerr signal curves are fitted to the data by a double exponential decay function of the form :

$$I_s(t) = \left[S_+ \exp(-t/T_+) + S_- \exp(-t/T_-)\right]^2 \qquad (t>0) \quad (6.3.7)$$

where the zero time (t=0) is taken to be the time of the maximum transmitted signal; T_+ and T_- denote the relaxation times of the two-component liquid described by equation 2; and S_+ and S_- are parameters to fit the data points which correspond to the strength of the decay process T_+ and T_-, respectively. The values of $T_{\pm}$ and $S_{\pm}$ are chosen to fit the whole decay intensity profile within the mean deviations of the data points. From equation 11, the ratio of S_+ and S_- can be expressed as,

$$S_+ / S_- = (I_+/I_-) \left[f(T_-)/f(T_+)\right], \qquad (6.3.8)$$

where I_+ and I_- are proportional to the coupled nonlinear index of refraction $n_{2\pm}$ in binary solutions. The square in equation 7 is a characteristic of the Kerr gate[11] (see section 4.6A).

In this section, the relaxation times and the peak transmitted signal at various concentrations which are extracted from the experimental data. in figures 4 and 5 are compared to the values calculated from the theoretical equations 1 and 2.

The parameters used in the calculations are displayed in table 1. The viscosities η_m of neat liquids were measured at room temperature. The nonlinear index of refraction for mNT and CT in the neat liquids was estimated by comparing its value to that of the carbon disulfide (CS_2) gate ($n_2 = 2\times10^{-11}$ e.s.u.)[11,12]. The values of n_2 (orientational Kerr constant) for PN, CO, HA, and CHA were estimated from equations 2 and 8, and from data fitting. The parameters f_{ij}, m_i, and p_j, where i,j = B (mNT) or C (solvent), were chosen to fit the data. The parameters f_{BB}, f_{CC}, and f_{BC} were chosen to fit the measured relaxation times of the concentration dependent experiments. These values are reasonable estimates for values obtained from similar materials[10]. The values of p_i are assumed to be the free rotator relaxation times as $x_B \rightarrow 0$. Our estimated values for p_i are slightly larger than the measured values of a few picoseconds[10]. It is reasonable that values obtained from the data fitting of the measured Kerr decay curves are overestimated on account of the minimum experimental time resolution of $\simeq$ 10 ps.

The mechanism responsible for the Kerr decay curves shown in figures 4a to 4e (except x_B = 1 and 0) is assumed to arise solely from the coupled molecular orientational motion of the two types of molecules. At low concentration of mNT (in figures 4c to 4e), there is definitely a slow second decay component present

in the Kerr gate intensity profile. This does not appear in the neat solute or solvent gate. One point should be emphasized with respect to the present and previous[1,2,3] reports. The signal to noise ratio in the present experiments has been improved by at least ten times over the previous measurements[2,3]. This is the main reason why we have observed the weak slower decay component.

In figure 6, the measured two-component relaxation times obtained from the data of figure 4e are plotted and compared with the calculated curve from equation 1 and the parameters listed in table 6.2. The calculated relaxation times reasonably follow the measured values. Using equation 2, the calculated values $T_{\pm}$ in figure 6, and the parameters listed in table 6.2, the contributions to the two-component nonlinear index of refraction $n_{2\pm}$ at various concentrations of mNT and CHA mixtures are calculated and plotted in figure 7a and 7b. In figure 7a, the size of the nonlinear index of refraction n_{2+} (solid line) is mainly due to the solute-solute interactions (dashed line). In figure 7b, the size of the nonlinear index of refraction n_{2-} (solid line) is the sum of three different sources : solute-solute (B-B, dashed line), solvent-solvent (C-C, dotted line), and solute-solvent (B-C, dotted-dashed line) interactions. In the solute-rich solutions ($x_B > 0.6$), the solute-solute interaction dominates; in the region of $0.3 < x_B < 0.6$, the solute-solvent interaction is larger; while in the solvent-rich solution ($x_B < 0.3$), the solvent-solvent interaction contributes more to n_{2-}. The calculated values of $n_{2\pm}$ are in reasonable

agreement with the measured peak transmitted Kerr signals (see table 6.3).

In figure 6, the Kerr relaxation times of the system $T_{\pm}$, at different concentrations have different characteristics. In the solute-rich region I, the relaxation mechanism of T_- behaves more like the neat solute liquid. In the solvent rich region II, the relaxation mechanism of T_- has the characteristic of the neat solvent liquid. The relaxation mechanism of T_+ behaves like the neat solute throughout the concentration region studied. This is mainly due to n_{2+} arising from the solute-solute interactions (see figure 7a). These agreements can be checked by a temperature dependent study. In figure 8, the relaxation times of T_+ and T_- obtained from the data in figure 5 and section 6.2(3) are plotted against the inverse of temperature. According to Debye's equation[1], the relaxation time for the rotation of a single molecule is :

$$\tau(T) = \frac{V\eta(T)}{kT} \quad , \qquad (6.3.9)$$

where V is the effective molecular volume, $\eta(T)$ is the measured viscosity, k is the Boltzmann constant, and T is the temperature. The temperature dependence of the viscosity can be expressed by the Arrhenius form[17] :

$$\eta(T) = A \exp(E/RT) \quad , \qquad (6.3.10)$$

where E is the activation energy of the liquid.

The activation energies estimated from the slope of these curves (see figure 8) are E_+ (from T_+) = 3.2 Kcal/mole [3] and E_- (from T_-) = 10 Kcal/mole. In reference 14, from the mixture of 72% mNT and 28% decanol and the mixture of 75% mNT and 25% CT, their activation energies are 3 Kcal/mole and 3.2 Kcal/mole, respectively. These activation energies are close to the values obtained from the viscosity measurement [12] for the neat liquids (E_{mNT} =3.6 Kcal/mole and E_{CHA} =10.5 Kcal/mole).

Using equation 1 and the parameters in table 6.2, the calculated values of the relaxation times ($T_\pm$) and strength of Kerr effect ($n_{2\pm}$) of the two-component solution of mNT in CO are plotted versus the mole fraction of mNT in figures 9 and 10. The measured two-component relaxation times obtained from the data displayed in figure 4c are plotted in figure 9 and compared with the calculated curves. These curves are similar to the theoretical curves described in figures 1a and 1b-3. These two liquids have comparable reorientational relaxation times in neat solution. The Kerr constant of mNT is sixty times larger than CO. In figure 9, the fast component arises from the solute-solute interactions; it is zone I, For the slow decay process, for $x_B > 0.2$, the solute-solute (zone I) interactions are dominant. Whereas, for $x_B < 0.2$ the slow component curves arise from all three kinds of interactions. As $x_B \to 0$, the solvent-solvent interaction is dominated (zone II). The measured relaxation times and the ratio of the two Kerr constants (n_{2+}/n_{2-}) are in good agreement with the calculated values.

In figures 4a and 4b, mNT is mixed with PN and CT, respectively. There is only a single exponential decay observed over the entire experimental region covered. This can be explained, since the relaxation time of the solvent is faster than the relaxation time of the solute (estimated from the viscosity of the neat liquid and reference 18,). Also the size of n_2 fo the solvent is much smaller than that of the solute. In this case, it would be very difficult to clearly observe the two-component decay. The behavior shown in figures 4a and 4b can be described by the theoretical curves shown in figures 2a and 2b-2.

NB and CS_2 are also investigated in this study as solute molecules mixing with these five solvents. Similar results were observed in the NB mixtures. This is reasonable, since mNT and NB have similar molecular structure, Kerr constant, and the orientational relaxation time (τ_{NB} = 40 ps[10,11], τ_{mNT} = 50 ps). 10% NB gate is shown in figure 3.

In the CS_2 mixture, the fast decay curve dominates, the slower decay curve is near the noise level and is hard to measure. To estimate the size of the slow component, consider a 1-1 mixture of CS_2 in CHA, this is the case of figure 2b-3. Applying equation 2 and assuming $f_{CS_2\text{-}CS_2}$ = 1, $f_{CS_2\text{-}CHA}$ = 1, the ratio of the two Kerr constant n_{2+}/n_{2-} = 2. This indicates the ratio of fast to slow peak transmitted signal of the Kerr effect is about $[n_{2+}\, f(T_-)]^2/[n_{2-} f(T_+)]^2 \simeq 2x9/1x1 \simeq 3x10^2$. Therefore, the amplitude of slower relaxation mechanism is just about the noise level by 10. Nevertheless, in the DRS experiment, the peak signal of the spectrum is proportional to $I_+T_+/I_-T_- \simeq 3x10^{-2}$. And the slower component dominates.

In figure 11, the relaxation times of various neat liquids, τ_o and T_+, T_- of mNT mixture are plotted versus the measured viscosity. In figure 11a, there is no simple relation between T_+ and η_m. This is reasonable since the contributions to n_{2+} (for example, see figure 7a and 10a) arises mainly from the solute-solute (B-B) interaction, while the measured viscosity arises from the internal resistive force from all kinds of interactions between the molecules of the mixture. In figure 11b and 11c, the relaxation times of neat liquids τ_o and T_- of mNT mixtures is shown to vary with the measured viscosity for $\eta_m < 5$cp. In moderately viscous solutions, the measured viscosity and the orientational relaxation times, τ_o and T_- arise from similar molecular interactions (see figures 7b and 10b). The relaxation mechanism of T_- in mNT mixtures arises from three different types of molecular interactions. However, in very viscous solutions ($\eta_m > 5$cp), the measured reorientational relaxation times, τ_o and T_-, do not exactly follow the measured viscosity. This is a common characteristics for very viscous solutions[19] near the melting temperature ($mp_{CHA} = 25^oC$) and for supercooled liquids[19]. This has been attributed to the progressive restriction of the different rotational degrees of freedom of the molecules about different axes with decreasing temperature[20,21]. The Kerr relaxation data most likely arises from the kinetics of particular rotational degrees of freedom of the molecule whose motion only contributes partly to the overall measured viscosity.

In figures 6, 7, 9, and 10, the two-component relaxation times $T_{\pm}$ are calculated from the coupled equations of $\tau_{BB}(x)$ and $\tau_{CC}(x)$. When the interspecies coupling parameter $f_{BC} = 0$ ($\phi = 0$), the system will relax as $T_+(x) = \tau_{BB}(x)$ depending only on B species molecules and as $T_-(x) = \tau_{CC}(x)$ depending on C species molecules. However, if $f_{BC} \neq 0$, there will be three sources contributing to the relaxation processes of T_+ and T_- arising from B-B, C-C, and B-C interactions. This is displayed in figure 6 and figure 9. There is only one relaxation to be observed in figures 4a and 4b. It is T_- (see figure 2b-2). This decay time is also proportional to the measured viscosity[10]. In all our cases studied, the component T_- is proportional to the measured viscosity. Furthermore, as shown in figures 7 and 10, the nonlinear index of refraction n_{2-} of mNT in CHA and CO solutions is larger than n_{2+}. The dependence of the relaxation time T_- on the measured viscosity is more easily observed in light scattering experiments.

In conclusion, the kinetics of the reorientational relaxation of molecules in mixed binary liquids have been measured directly using picosecond laser techniques. The theory for coupled two-component liquids is applied to described the Kerr relaxation data in the binary solutions. The Kerr orientational relaxation mechanism for the binary mixture is attributed to the reorientation of the solute-solvent system. This theory is more fundamental than Hill's theory which we used to fit our experimental data in sections 6.1 and 6.2. However, there are too many parameters (at least seven) to adjust from this two-component theory to fit the experimental data. It also depends

on a series of assumptions. For example, Mori's theory requires a complete set of slow variables to be chosen in the system. We have only chosen one slow relaxation time for each component in the mixture. In fact, there are a distribution of relaxation time of each relaxation process (see section 4.8), and the relaxation times of molecular reorientation about each individual axis are different (see section 2.5). Moreover, in the data fitting, we have assumed the dynamic pair correlation factor to be zero. This is not universally true, either. Hill's theory is a rather simplified empirical model which is not too far from the reality in most cases. If the solute-solvent interactions is small and the solvent effects can be neglected, Hill's theory gives a similar representation of the molecular reorientational motion in liquids. I hope this work will stimulate more theoretical and experimental research.

Table 6.2 Parameters for the Coupled Orientational Relaxation in mNT Mixtures Used for Data Fitting

Liquid	η_m (cp)	$\frac{n_2\ (10^{-12}\text{e.s.u.})}{1 + f_{ii}}$	f_{ii}	f_{BC}	$\tau_{ii} = (1 + x_i f_{ii})\tau_i$ (ps)	$\tau_i = m_i x_i + p_i$ (ps)
mNT	2.05	12	1.5		$(1 + 1.5x_B)\tau_B$	$12x_B + 8$
PN	0.34	≤ 0.5				
CT	0.91	≤ 0.5				
CO	2.17	0.5	0	1		$50x_C + 10$
HA	4.05	1	2	1.5	$(1 + 2x_C)\tau_C$	$25x_C + 10$
CHA	50	1.25	2	1.5	$(1 + 2x_C)\tau_C$	$60x_C + 15$

Table 6.3 Nonlinear Index of Refraction for Binary Liquids.

Comparison of the ratio of the transmitted signal for the two components S_+ and S_- for the experimental and calculated values. Estimated error in experimental values are about 30%.

Mixture	x_B	$\frac{S_+}{S_-}$ (experimental)	$\frac{n_{2+}}{n_{2-}} \frac{f(T_-)}{f(T_+)}$ (theory)
mNT + CHA	0.8	0.9	0.6
	0.6	1.9	3
	0.3	3.6	4.8
	0.23	3.8	4.9
	0.1	6	4.8
mNT + CO	0.6	0.63	0.54
	0.33	3.3	5.5
	0.23	3.1	4.3
	0.1	4.5	3.8
mNT + HA	0.23	3.3	3.3
	0.1	5.5	3.9

Reference

1. P. Debye, "Polar Molecules", (Dover, New York, 1946).
2. P.P. Ho, W. Yu, and R.R. Alfano, Chem. Phys. Lett., 37, 91, (1976) and section 6.1.
3. P.P. Ho and R.R. Alfano, Chem. Phys. Lett., 50, 74, (1977) and section 6.2.
4. A.J. Curtis, P.L. McGreer, G.B. Rathman, and C.P. Smyth, J. Am. Chem. Soc., 74, 644, (1952).
5. N.E. Hill, Proc. Phys. Soc. (London), 67B, 149, (1954).
6. D. Kivelson and S.J. Tsay, Mol. Phys., 29, 29, (1975).
7. R.W. Hellwarth, J. Chem. Phys., 52, 2128, (1970).
   F.B. Martin and J.R. Lalanne, Phys. Rev., A4, 1275, (1971).
8. P.P. Ho and R.R. Alfano, J. Chem. Phys., 67, 1004, (1977).
   K. Sala and M. Richardson, Phys. Rev., A12, 1036, (1975).
9. D.R. Bauer, J.I. Brauman, and R.Pecora, J.Chem. Phys., 63, 53, (1975).
10. G.R. Alms, D.R. Bauer, J.I. Brauman, and R. Pecora, J. Chem. Phys., 59, 5310, (1973).
    T.D. Glerke and W.H. Flygare, J. Chem. Phys., 61, 2231, (1974).
    E. Zamir, N.D. Gershon, and A. Ben-Reuven, J. Chem. Phys., 55, 3397, (1971).
11. M. Duguay and J. Hansen, Appl. Phys. Lett., 15, 192, (1969).
    F. Shimizu and B.P. Stoicheff, IEEE, QE-5, 544, (1969).
12. Landau-Bornstein Tables, (Spring Verlag, Berlin, V5).
13. S. Kielich, Acta. Phys. Polon., 30, 423, (1965).
14. R.W. Hellwarth, "Quantum Optics", (R.Glauber ed., Academic Press, New York, 1969).

15. R.W. Hellwarth, A.Owyoung, and N. George, Phys. Rev., A4, 2343, (1971).
16. S.L. Shapiro, PH.D. thesis, (University of California,1967).
17. J. Frenkel, "Kinetic Theory of Liquids", (Oxford, 1946).
18. J.A. Bucaro and T.A. Litovitz, J.Chem.Phys.,55,3385,(1971).
19. H.J. Hennelly,W.H. Heston, and C.P. Smyth, J. Am. Chem. Soc., 70, 4102, (1948).
20. D.B. Davis and A.J. Matheson, J.Chem.Phys., 45,1000,(1966).
21. A.R. Derden and A.J. Matheson, Adv.Mol.Relax.Proc.,2,251,(1972).

FIGURE CAPTIONS

Figure 1. The calculated curves of a two-component relaxation process for mixed binary liquids. Assuming the following relaxation times and parameters:

$$\tau_{BB}(x) = (15x_B + 5)\ (1 + 1.5x_B)\ ,$$

$$\tau_{CC}(x) = (15x_C + 5)\ (1 + 1.5x_C)\ ,$$

where $x_B + x_C = 1$, and $f_{BB} = f_{CC} = 1.5$.

(a) The two-component molecular orientational relaxation times $T_{\pm}$ versus the mole fraction x_B of B-species molecules at various interspecies pair correlation factor (f_{BC}). The solid lines are $\tau_{BB}(x)$ and $\tau_{CC}(x)$. The dashed lines are $T_{\pm}$ for different f_{BC} values.

(b) The Kerr constant $n_{2\pm}$ of two-component relaxation corresponding to the relaxation times $T_{\pm}$ is plotted versus the mole fraction of B-species molecules for :

1) $n_{2B} = n_{2C} = 2.5$, and $f_{BC} = 2$,
2) $n_{2B} = n_{2C} = 2.5$, and $f_{BC} = 0$, and
3) $n_{2B} = 2.5$, $n_{2C} = 0.1$, and $f_{BC} = 2$.

Equations 7 and 8 are used to calculate these curves. The units of n_2 and time are arbitrary.

Figure 2. The calculated curves of two-component relaxation process for mixed binary liquids. Assuming the following relaxation times and coupling parameters:

$$\tau_{BB}(x) = (\ 15x_B + 5\ )\ (\ 1 + 1.5x_B)\ ,$$

$$\tau_{CC}(x) = (\ x_C + 0.1\ )\ (\ 1 + 1.5x_C\ ),$$

where $x_B + x_C = 1$, and $f_{BB} = f_{CC} = 1.5$.

(a) The two-component molecular reorientational relaxation times $T_{\pm}$ versus the mole fraction of B-species molecules x_B at various interspecies pair correlation factor (f_{BC}). The solid lines are $\tau_{BB}(x_B)$ and $\tau_{CC}(x_C)$, and the dashed lines are $T_{\pm}$ for different values of f_{BC}.

(b) The Kerr constant $n_{2\pm}$ of two-component relaxation corresponding to the relaxation times $T_{\pm}$ is plotted versus the mole fraction of B-species molecules at $f_{BC} = 2$ for various combination of n_{2B} and n_{2C}.

1) $n_{2B} = n_{2C} = 2.5$,

2) $n_{2B} = 2.5$, $n_{2C} = 0.1$,

and 3) $n_{2B} = 0.1$ and $n_{2C} = 2.5$.

Equations 7 and 8 are used to calculate these curves. The units of time and n_2 are arbitary.

Figure 3. Kerr transmitted signal of 10% NB in various solvents. The solid line is a theoretical fit to the data points.

$$I_s(t) = [S_+ \exp(-t/T_+) + S_- \exp(-t/T_-)]^2 .$$

o (PN) : $I_s = [0.4(\exp(-t/10)]^2$,

Δ (CT) : $I_s = [0.35 \exp(-t/11)]^2$,

x (CO) : $I_s = [0.18\exp(-t/8) + 0.07\exp(-t/40)]^2$,

□ (HA) : $I_s = [0.14\exp(-t/10) + 0.045\exp(-t/70)]^2$,

+ (CHA): $I_s = [0.13\exp(-t/10) + 0.05\exp(-t/120)]^2$.

The maximum power density of 1.06 um pulse used for the Kerr gate is about 2 GW/cm^2.

Figure 4. Kerr kinetic data for different liquid mixtures. Transmitted signal of the 0.53 um probe laser pulse through the sample Kerr gate at various delay times. Each error bar corresponds to the average of four to six data points. The solid lines are a theoretical fit to the data points.

$$I_s(t) = \left[S_+ \exp(-t/T_+) + S_- \exp(-t/T_-) \right]^2 .$$

where S_+ and S_- are the strength of Kerr constant, and T_+ and T_- are the corresponding orientational relaxation times in the binary solution. The square is a characteristic of the Kerr gate[11]. The background signal has been subtracted from the data point[13]. The error bar of each data point not shown is about 20%. Typical error in the extracted relaxation time is ≈ 15%.

(a) mNT (B) mixed with PN

□ : $x_B = 0.6$, $I_s = [0.6 \exp(-t/24)]^2$,

× : $x_B = 0.23$, $I_s = [0.24 \exp(-t/14)]^2$,

○ : $x_B = 0.1$, $I_s = [0.35 \exp(-t/10)]^2$,

● : $x_B = 0$.

(b) mNT (B) mixed with CT

+ : $x_B = 1$, $I_s^* = [0.28 \exp(-t/50)]^2$,

□ : $x_B = 0.6$, $I_s^* = [0.15 \exp(-t/30)]^2$,

× : $x_B = 0.23$, $I_s = [0.27 \exp(-t/15)]^2$,

○ : $x_B = 0.1$, $I_s = [0.35 \exp(-t/10)]^2$,

● : $x_B = 0$.

(c) mNT (B) mixed with CO

+ : $x_B = 0.6$, $I_s^* = [0.1 \exp(-t/20) + 0.16 \exp(-t/40)]^2$,

□ : $x_B = 0.33$, $I_s = [\, 0.3 \exp(-t/17) + 0.09 \exp(-t/45)\,]^2$,

X : $x_B = 0.23$, $I_s = [\, 0.23 \exp(-t/13) + 0.073 \exp(-t/50)\,]^2$,

O : $x_B = 0.1$, $I_s = [\, 0.2 \exp(-t/10) + 0.045 \exp(-t/55)\,]^2$,

● : $x_B = 0$.

(d) mNT (B) mixed with HA

X : $x_B = 0.23$, $I_s = [\, 0.33 \exp(-t/14) + 0.1 \exp(-t/80)\,]^2$,

O : $x_B = 0.1$, $I_s = [\, 0.22 \exp(-t/10) + 0.04 \exp(-t/90)\,]^2$,

● : $x_B = 0$.

(e) mNT (B) mixed with CHA

+ : $x_B = 0.6$, $I_s = [\, 0.35 \exp(-t/24) + 0.18 \exp(-t/85)\,]^2$,

□ : $x_B = 0.3$, $I_s = [\, 0.20 \exp(-t/17) + 0.055 \exp(-t/125)\,]^2$,

X : $x_B = 0.23$, $I_s = [\, 0.15 \exp(-t/13) + 0.04 \exp(-t/150)\,]^2$,

O : $x_B = 0.1$, $I_s = [\, 0.12 \exp(-t/10) + 0.02 \exp(-t/185)\,]^2$,

● : $x_B = 0$.

* 1.06 um exciting laser intensity is attenuated to only 30% of the original intensity.

Figure 5. Kerr kinetic data of the mixture of 35% mNT and 65% CHA at different temperatures.

□ : T = 24 C, $I_s = [\, 0.25 \exp(-t/17) + 0.07 \exp(-t/95)\,]^2$,

X : T = 40 C, $I_s = [\, 0.25 \exp(-t/13) + 0.25 \exp(-t/40)\,]^2$,

O : T = 54 C, $I_s = [\, 0.15 \exp(-t/11) + 0.5 \exp(-t/22)\,]^2$,

Figure 6. The orientational relaxation times of two-component liquid mNT in CHA is plotted at various mole fraction of mNT (x_B). The solid lines are $\tau_{BB}(x)$ and $\tau_{CC}(x)$ which are calculated as in section 33. The dashed lines are $T_{\pm}$ which are calculated from equation . + represents the measured relaxation times extracted

from figure 4e. The dotted line is the measured viscosity of mNT in CHA at various concentrations. The parameters in table are used to calculated these curves.

Figure 7. The Kerr constant of two-component liquid mNT in CHA from different liquid components versus the mole fraction of mNT.

solid line : total nonlinear index of refraction,

dashed line : contribution from solute molecules only,

dotted line : contribution from solvent molecules only,

dotted-dashed line : contribution from coupled solute-solvent molecules.

(a) n_{2+} . and (b) n_{2-}.

These curves are calculated by equation 1 and the parameters in table 6.2. The scale of n_2 was determined by using $n_2(CS_2)$ as a standard

Figure 8. The relaxation time of 35% and 65% CHA solution is plotted versus the inverse of temperature. + is T_-. o is T_+. The solid lines are the theoretical fits to Debye's equations :

$$T_- = (6\times10^{-10}\ \text{ps·K/cp})\ \eta_{CHA}/T\ ,$$

$$T_+ = (24\times10^{-10}\ \text{ps·K/cp})\ \eta_{mNT}/T\ .$$

The dashed line is the measured viscosity of CHA, and the dashed -dotted line is the measured viscosity of mNT.

Figure 9. The orientational relaxation time of two-component liquid mNT in CO is plotted versus the mole fraction of mNT. The solid lines are τ_{BB} and τ_{CC} which are calculated from section 3.3 and the parameters in table 6.2 The dashed lines are

$T_{\pm}$ which are calculated from equation 1 and the parameters in table 6.2 The dashed line is the measured viscosity. + represents the measured relaxation time extracted from figure 4c.

Figure 10. The nonlinear index of refraction of two-component liquid mNT in CO versus the mole fraction x_B of mNT.

solid line : total nonlinear index of refraction,

dashed line : contributions from solute molecules only,

dotted line : contributions from solvent molecules only,

dotted-dashed line : contributions from coupled solute-solvent molecules.

(a) n_{2+} and (b) n_{2-}.

These curves are calculated by equation2 and the parameters in table 6.2.The scale of n_2 was determined by using $n_2(CS_2)$ as a standard

Figure 11. The measured Kerr relaxation times versus the measured viscosity for various solutions.

(a) Fast relaxation time (T_+) from various mNT mixtures.

+ : $x_B = 0.6$, ◻ : $x_B = 0.23$, o : $x_B = 0.1$.

(b) Slow relaxation time (T_-) for various mNT mixtures.

(c) Relaxation time of neat liquids, τ_o , obtained from the optical Kerr effect.

The relaxation time of CS_2 and benzene were obtained from reference 10, CO and CHA were obtained from fitting the Kerr data of the mixtures and extrapulating to $x_B = 0$.

HA (hexadecane), OA (n-octanol), DA (n-decanol).

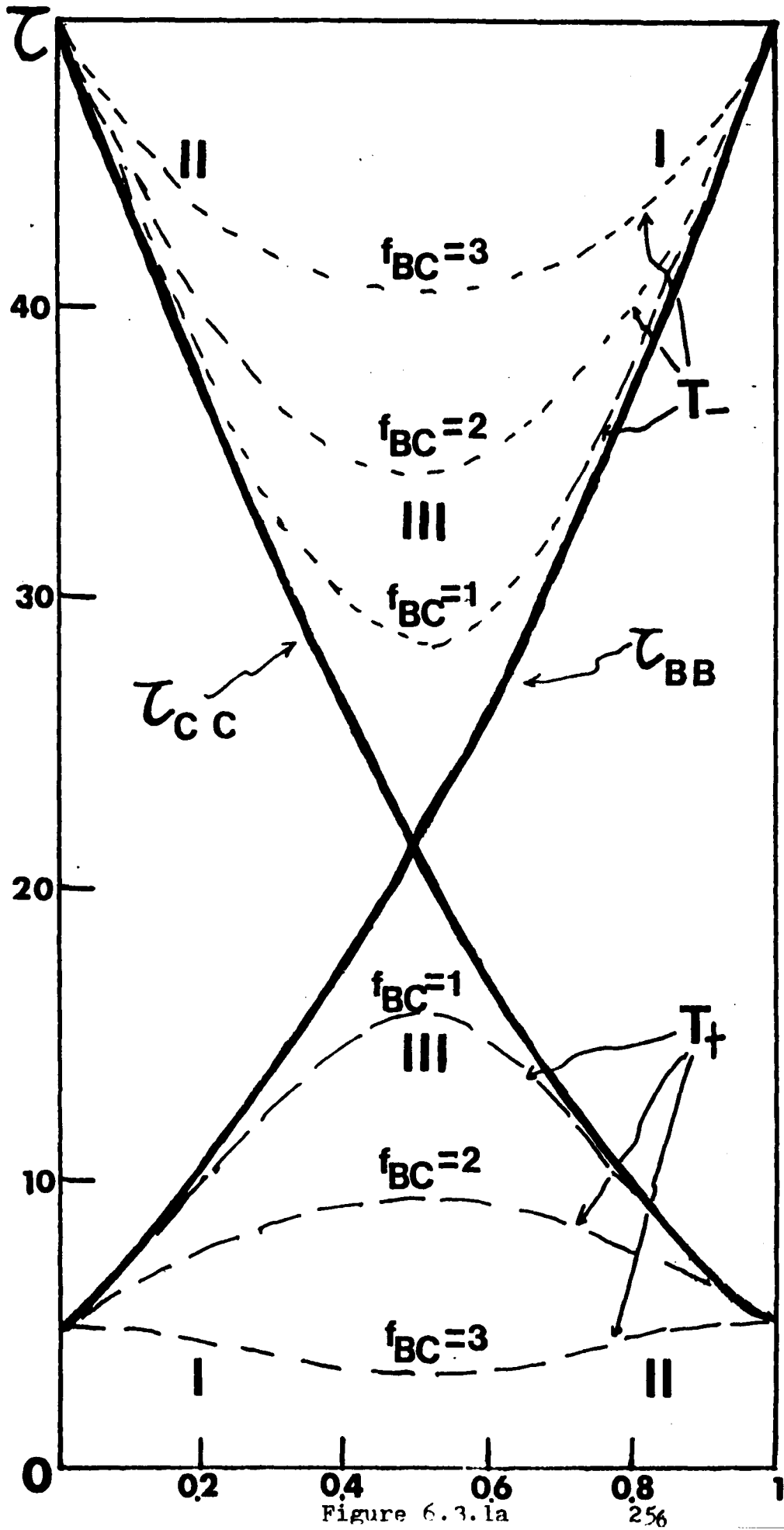
(a) COUPED TWO-COMPONENT RELAXATION TIME IN MIXED LIQUIDS
τ
40
30
20
10
0
II
I
$f_{BC}=3$
$f_{BC}=2$
III
$f_{BC}=1$
T_-
τ_{BB}
τ_{CC}
$f_{BC}=1$
III
T_+
$f_{BC}=2$
$f_{BC}=3$
I
II
0.2
0.4
0.6
0.8
1
X_B

Figure 6.3.1a

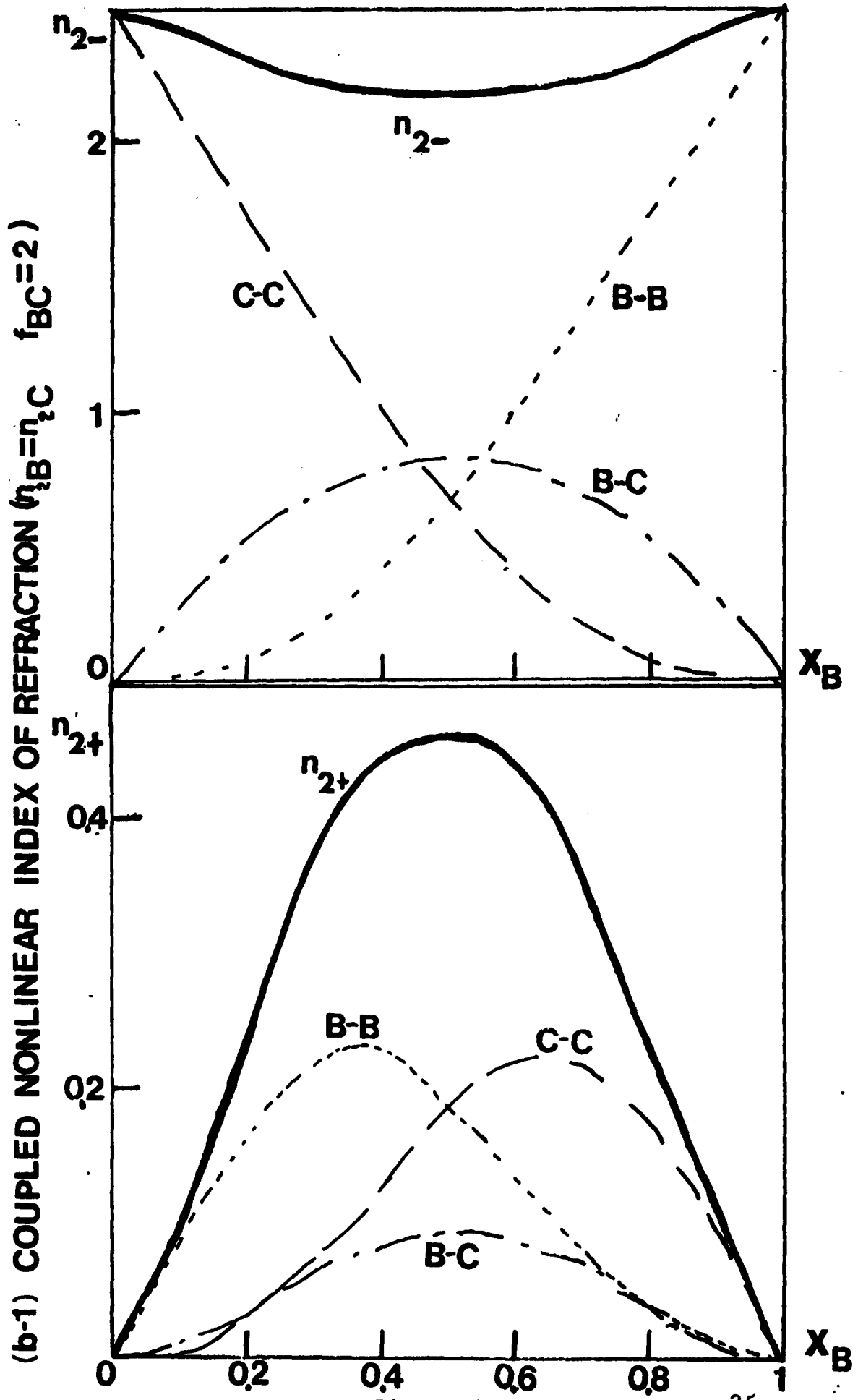

Figure 6.3.1b-1

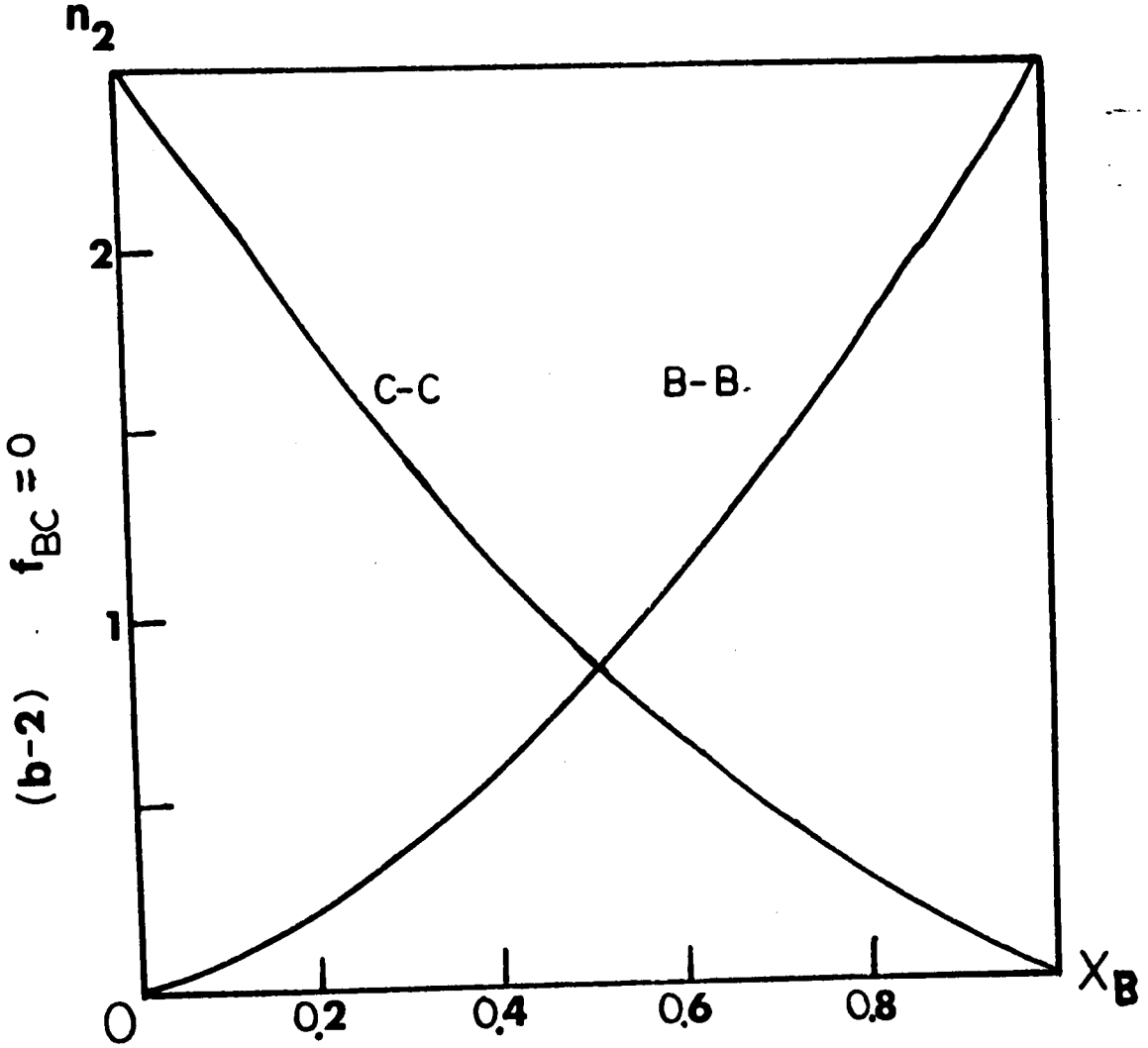

Figure 6.3.1b-2

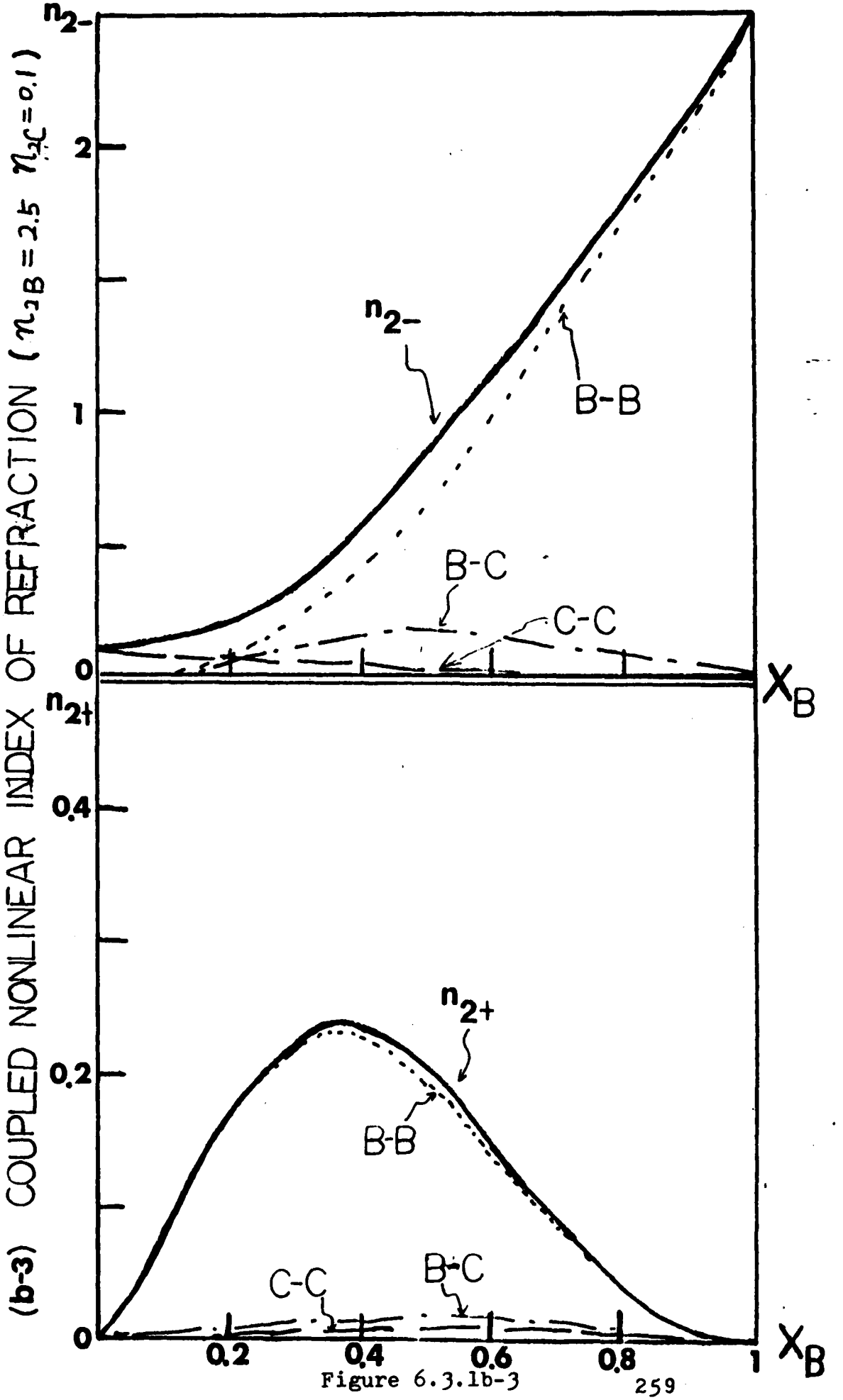

Figure 6.3.1b-3

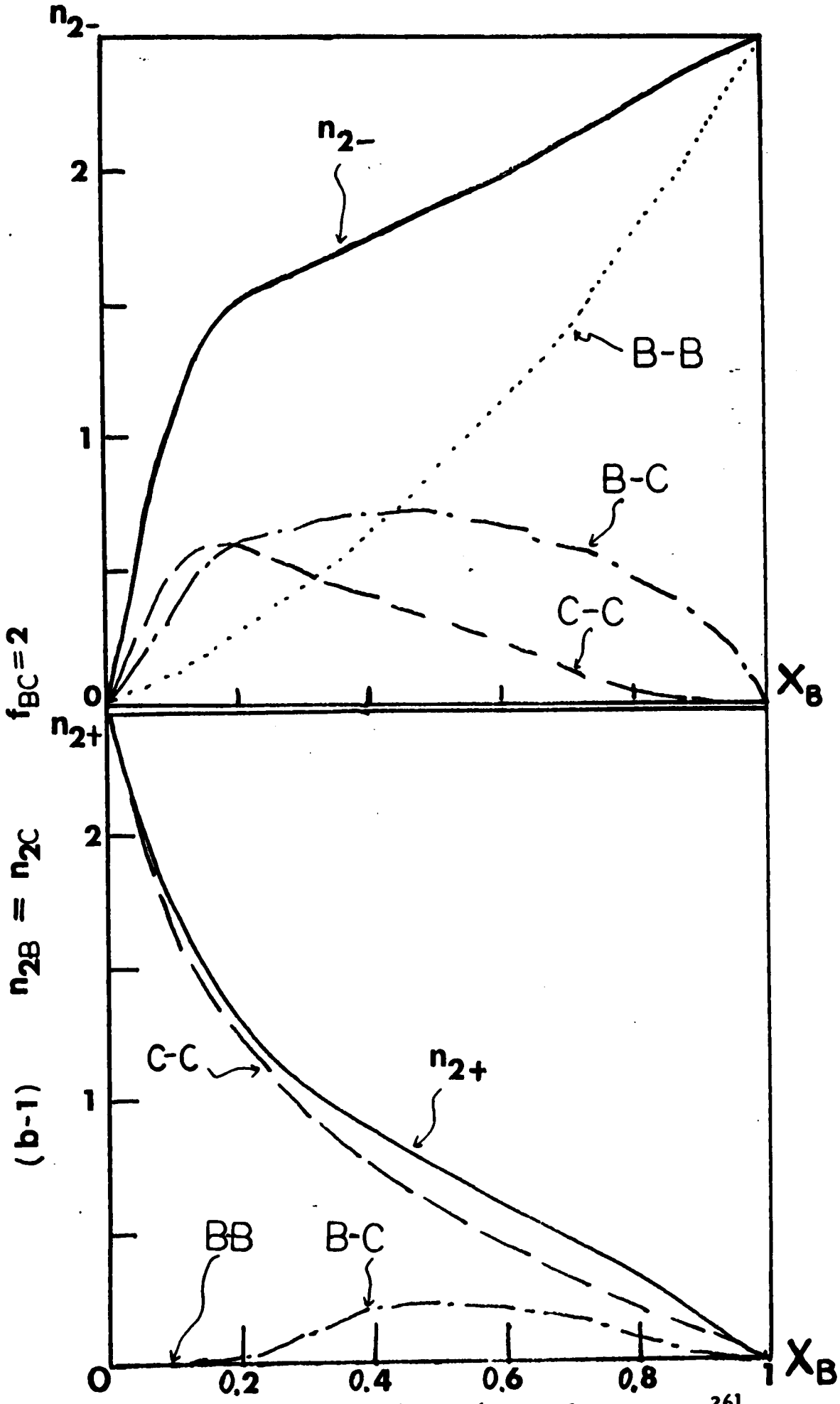

Figure 6.3.2b-1

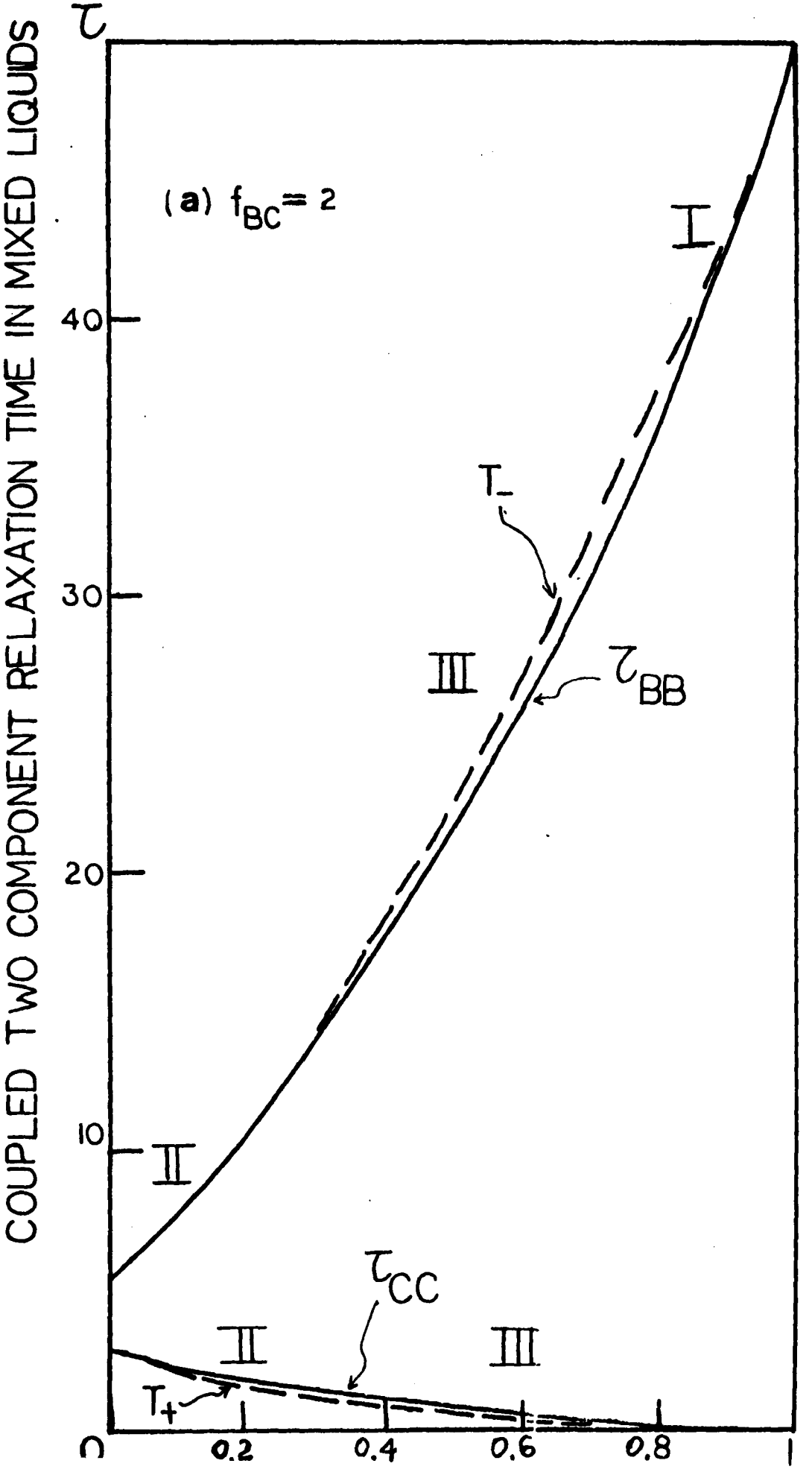
COUPLED TWO COMPONENT RELAXATION TIME IN MIXED LIQUIDS
τ
(a) f_{BC} = 2
I
II
III
II
III
T_-
τ_{BB}
τ_{CC}
T_+
40
30
20
10
0
0.2
0.4
0.6
0.8
1
X_B

Figure 6.3.

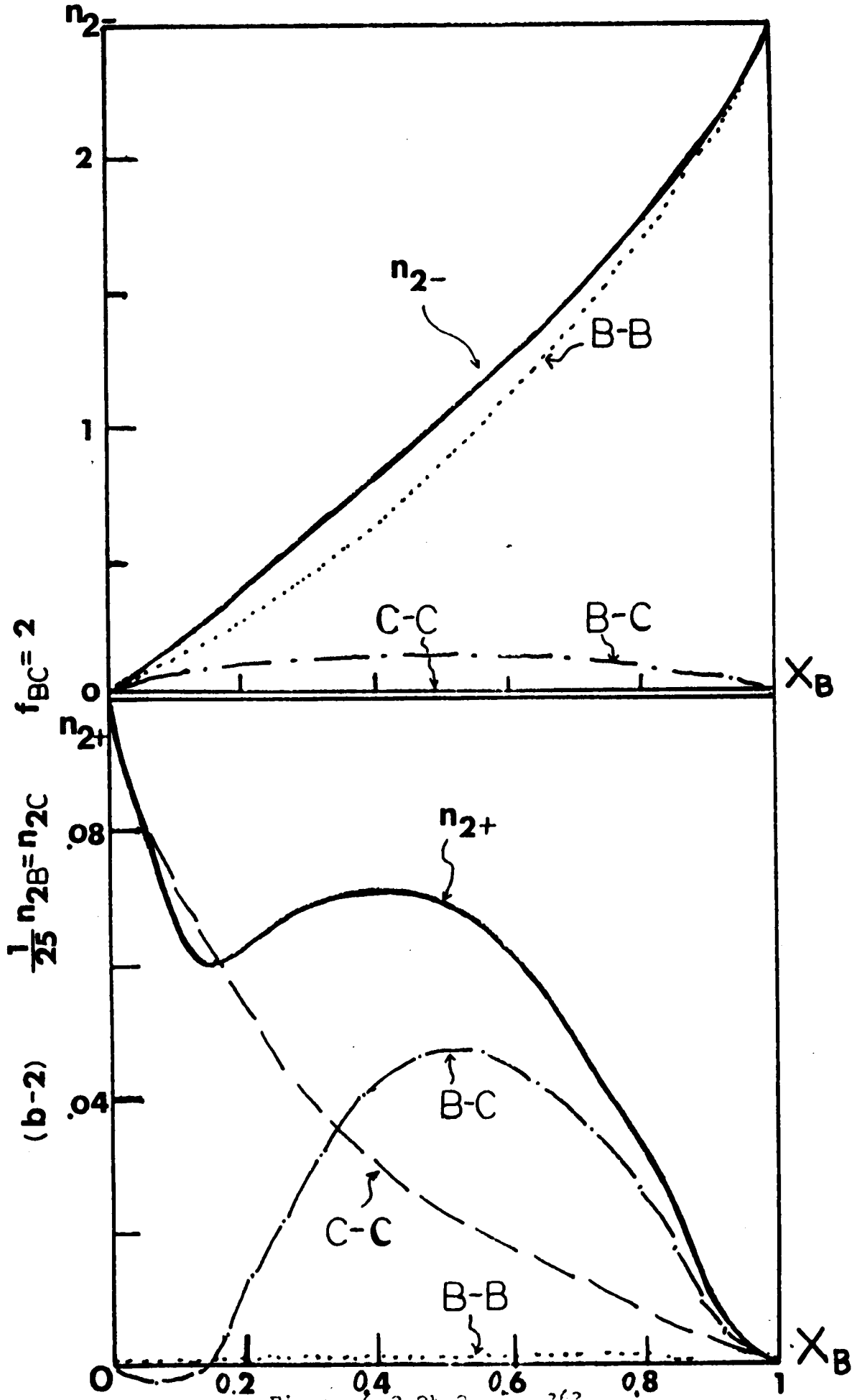
n_{2-}
2
1
0
n_{2-}
B-B
C-C
B-C
X_B
$f_{BC}=2$
n_{2+}
.08
.04
0
n_{2+}
B-C
C-C
B-B
X_B
0.2
0.4
0.6
0.8
1
$\frac{1}{25} n_{2B}=n_{2C}$
(b-2)

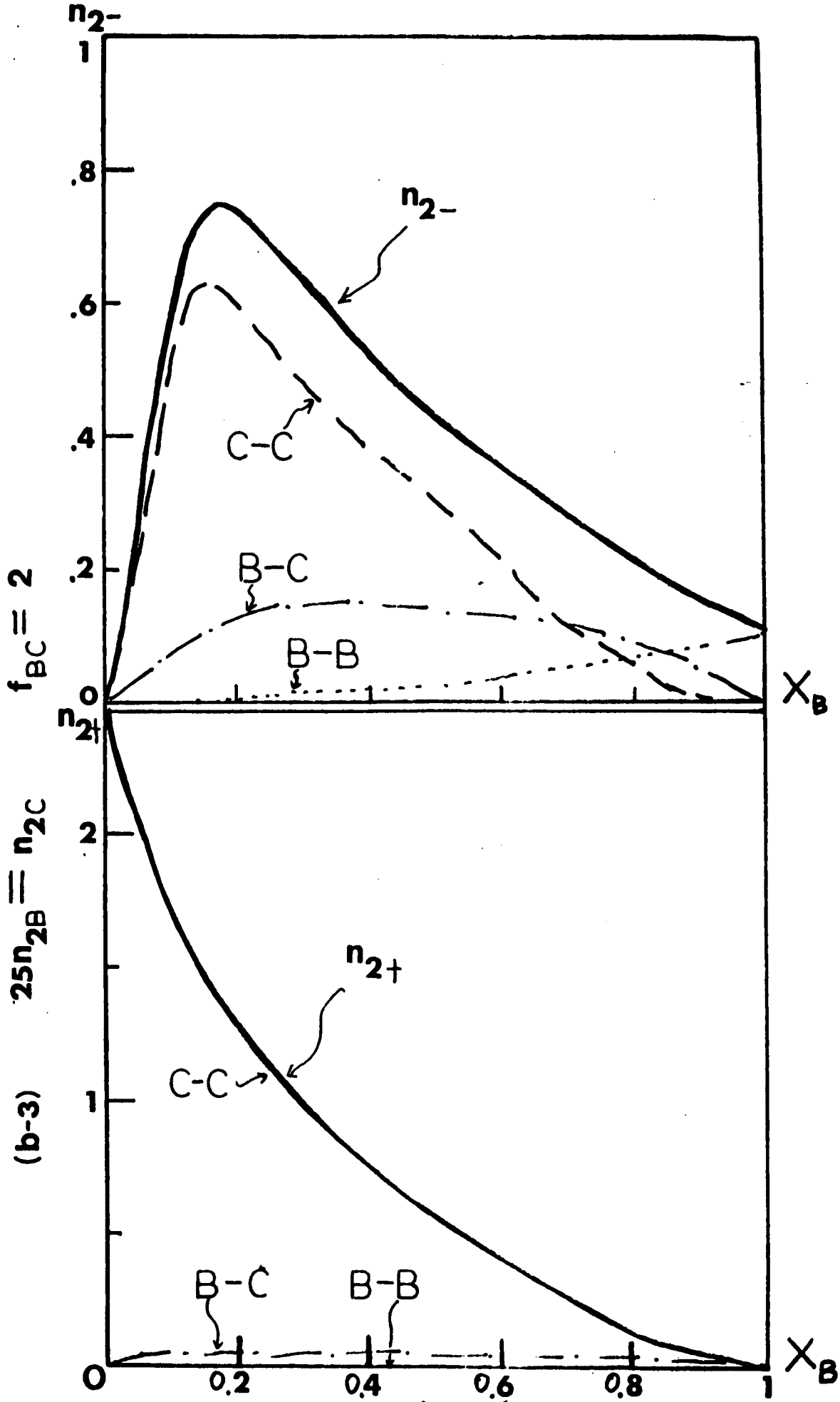

Figure 6.3.2b-3

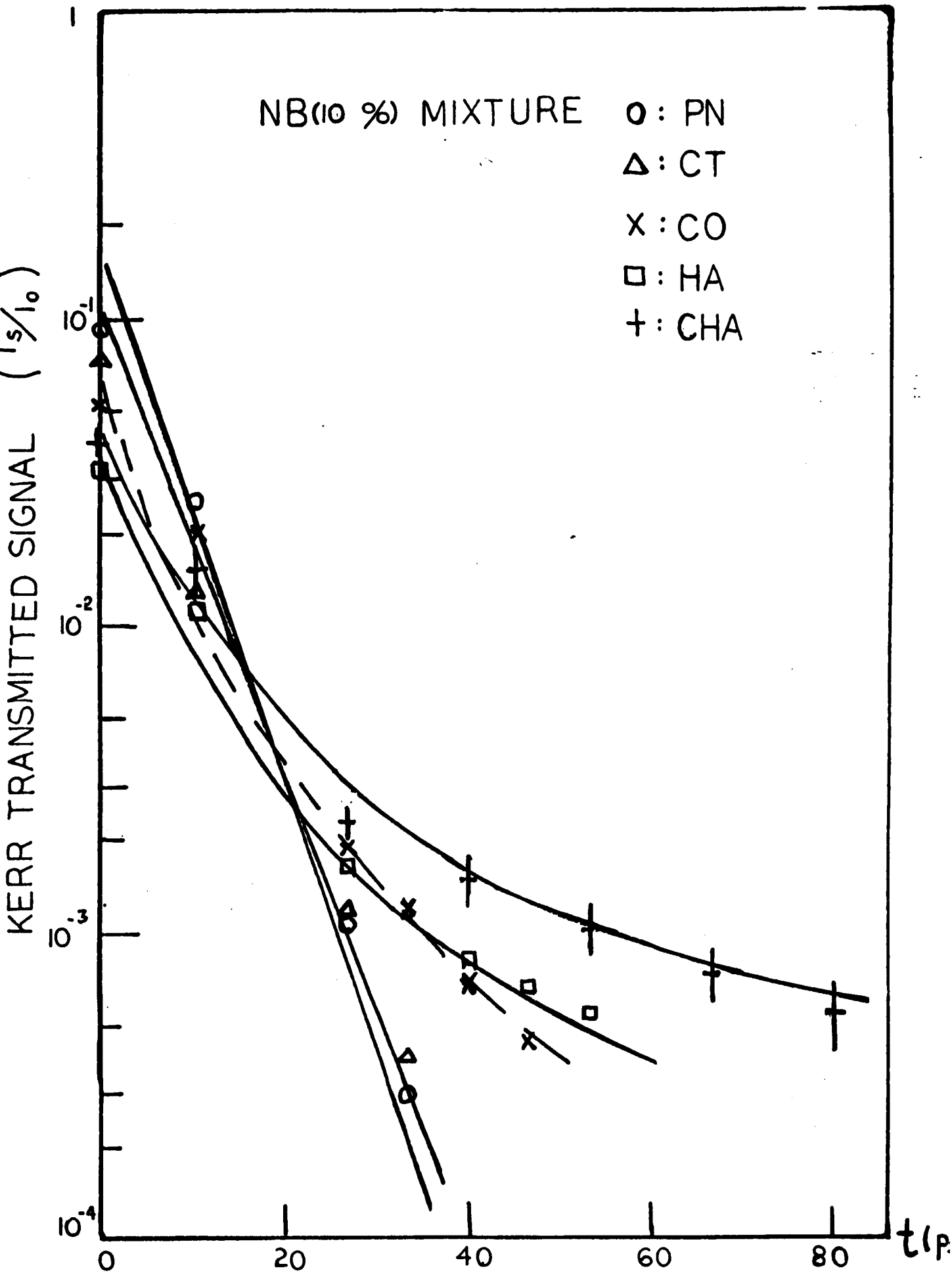
NB(10 %) MIXTURE
O : PN
Δ : CT
X : CO
□ : HA
+ : CHA
KERR TRANSMITTED SIGNAL (Is/Io)
1
10⁻¹
10⁻²
10⁻³
10⁻⁴
0
20
40
60
80
t(p

Figure 6.3.3

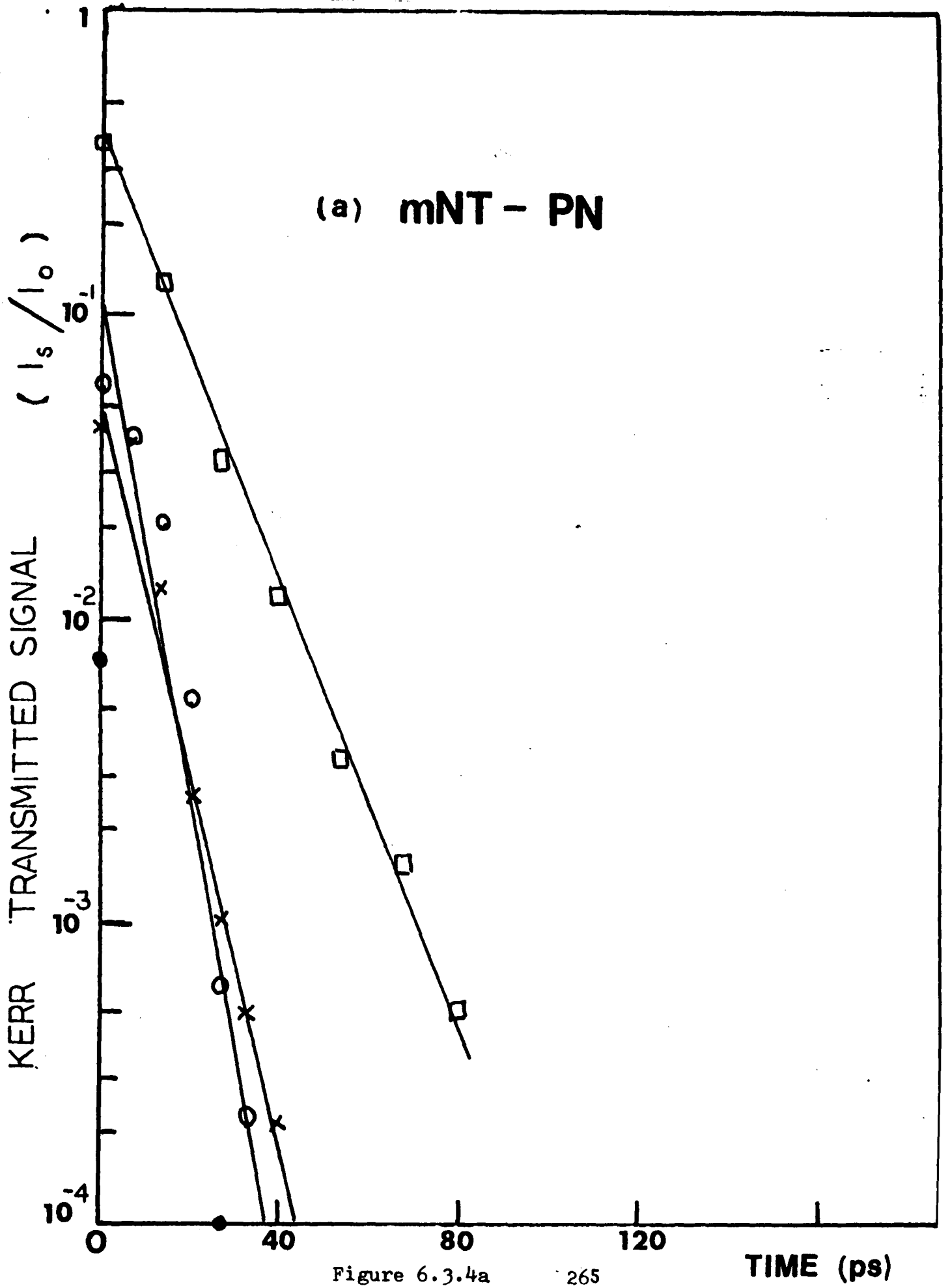
(a) mNT - PN
KERR TRANSMITTED SIGNAL (I_s / I_o)
1
10^{-1}
10^{-2}
10^{-3}
10^{-4}
0
40
80
120
TIME (ps)

Figure 6.3.4a

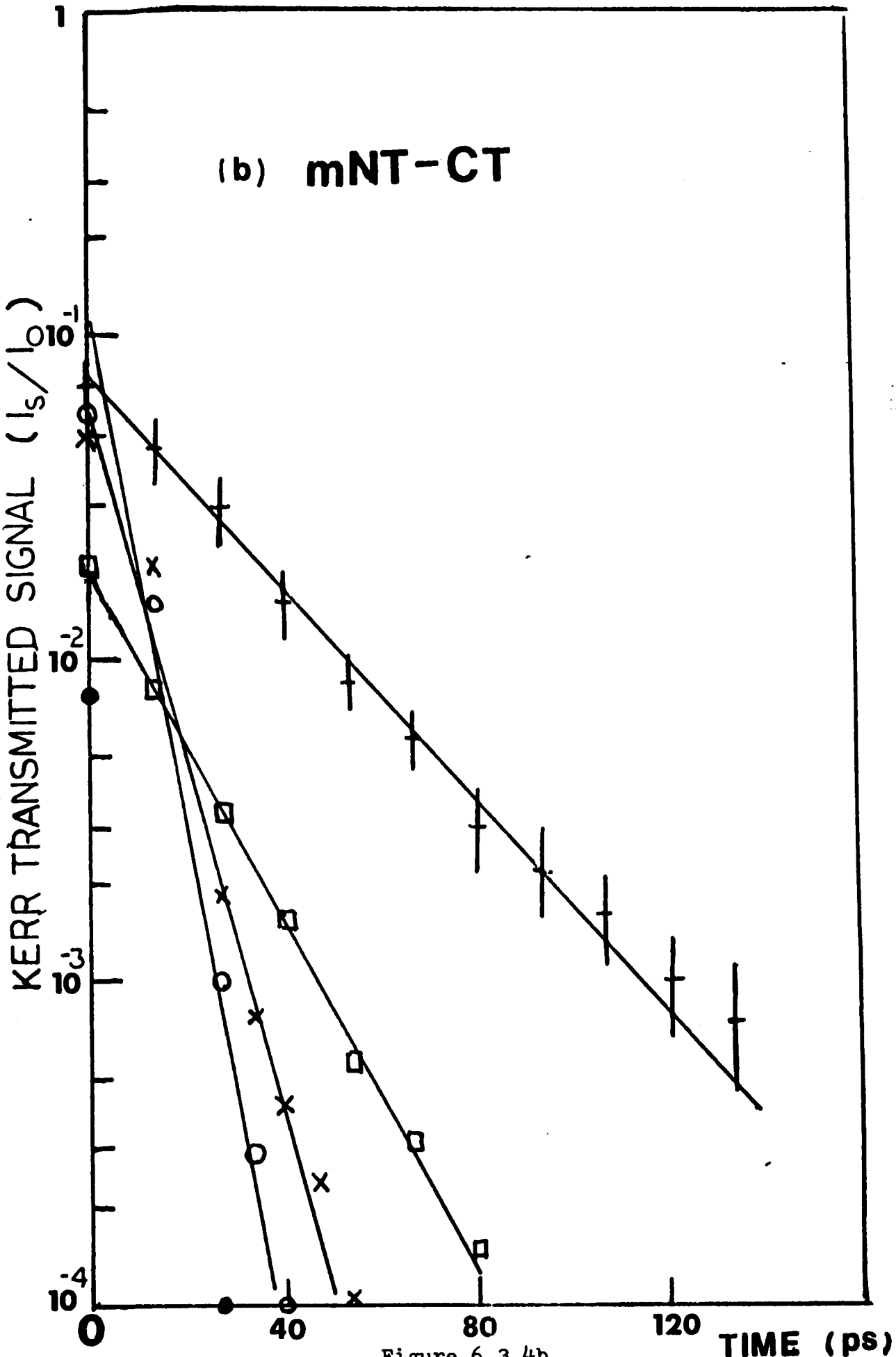
(b) mNT-CT
KERR TRANSMITTED SIGNAL (I_s/I_o)
1
10^{-1}
10^{-2}
10^{-3}
10^{-4}
0
40
80
120
TIME (ps)

Figure 6.3.4b

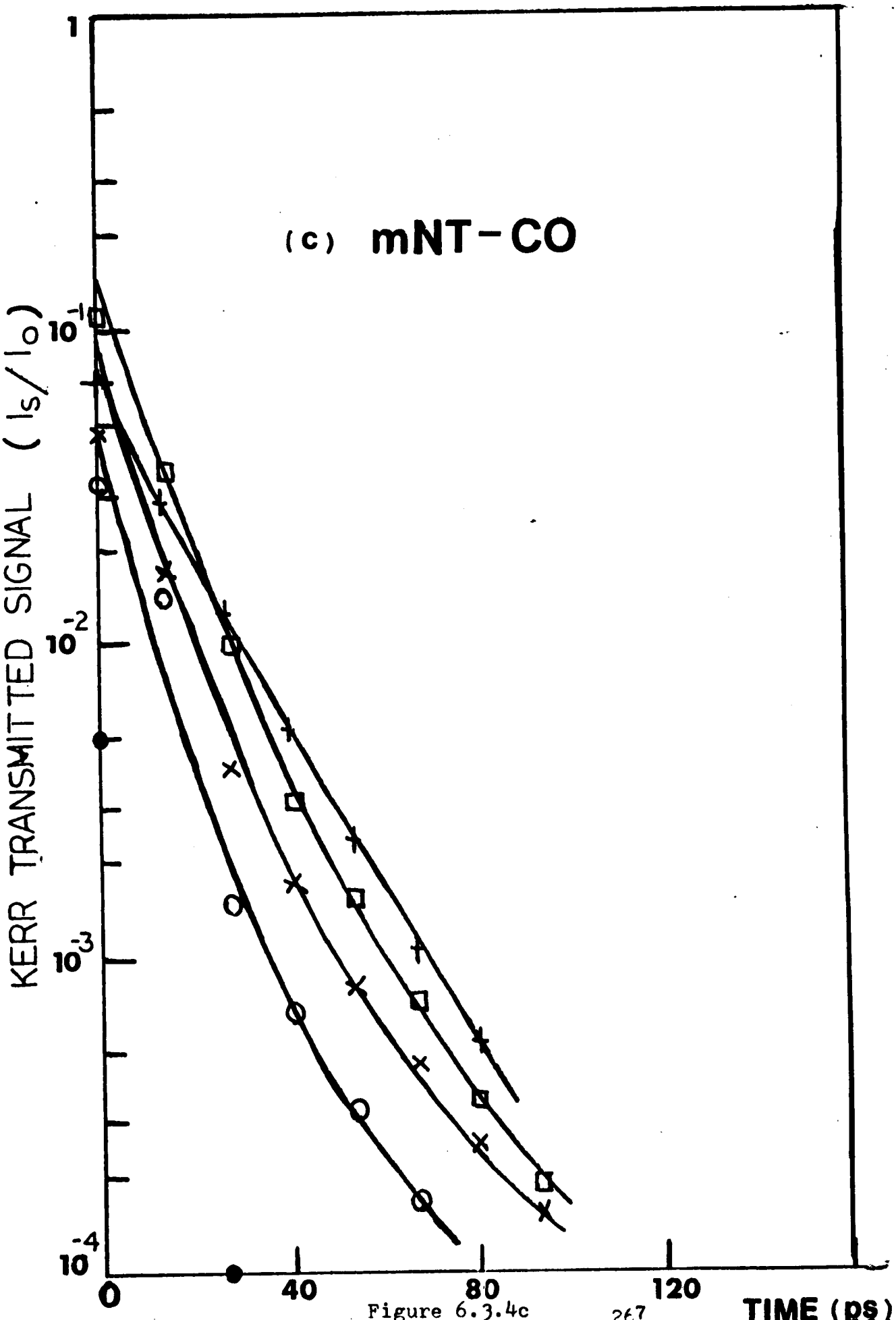
(c) mNT-CO
KERR TRANSMITTED SIGNAL (Is/ Io)
1
10-1
10-2
10-3
10-4
0
40
80
120
TIME (PS)

Figure 6.3.4c

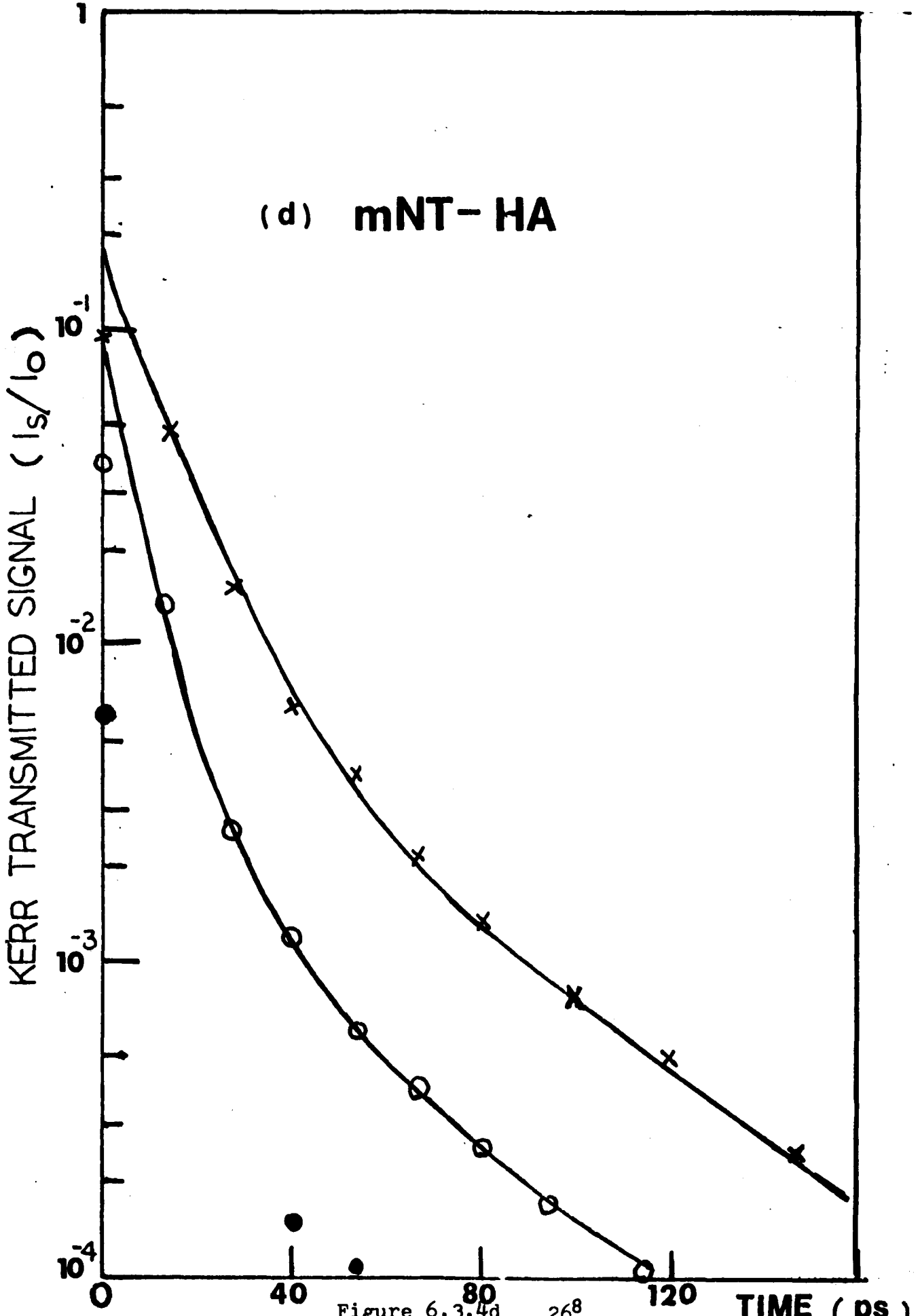
(d) mNT-HA
KERR TRANSMITTED SIGNAL (Is/Io)
1
10-1
10-2
10-3
10-4
0
40
80
120
TIME (ps)

Figure 6.3.4d

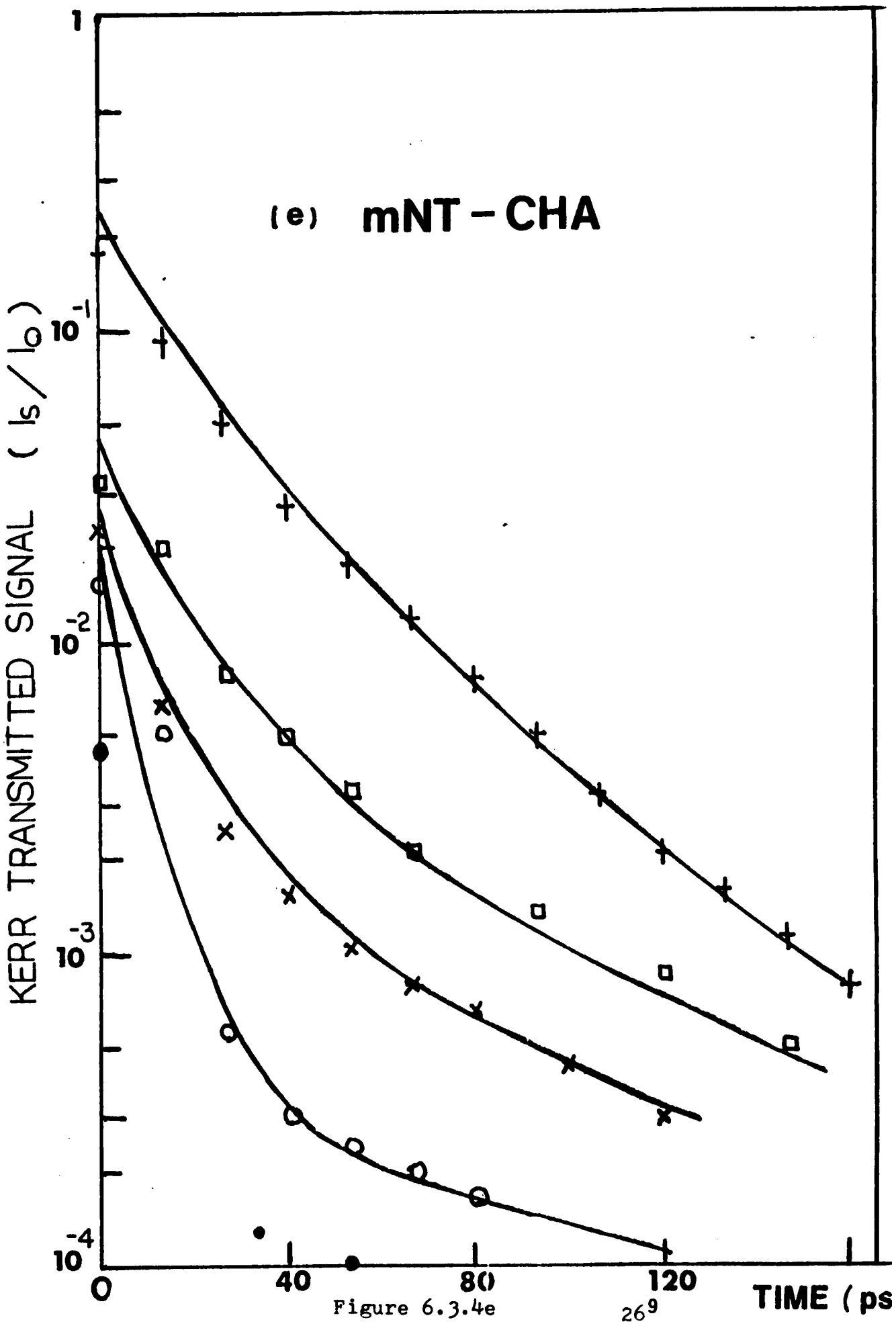
(e) mNT – CHA
KERR TRANSMITTED SIGNAL (Is / Io)
1
10-1
10-2
10-3
10-4
0
40
80
120
TIME (ps

Figure 6.3.4e

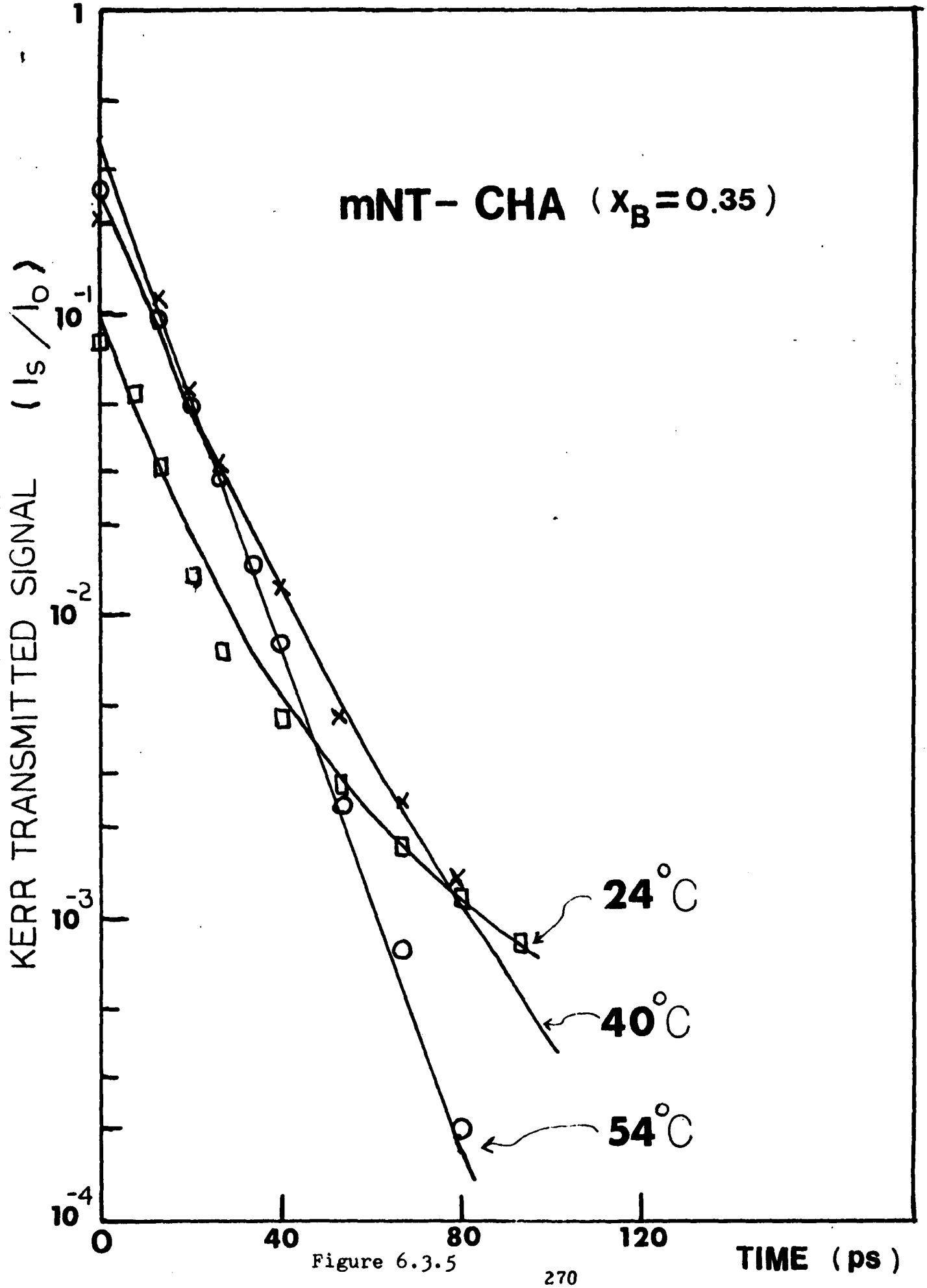
mNT- CHA (x_B=0.35)
KERR TRANSMITTED SIGNAL (I_s / I_o)
1
10^{-1}
10^{-2}
10^{-3}
10^{-4}
0
40
80
120
TIME (ps)
24°C
40°C
54°C

Figure 6.3.5

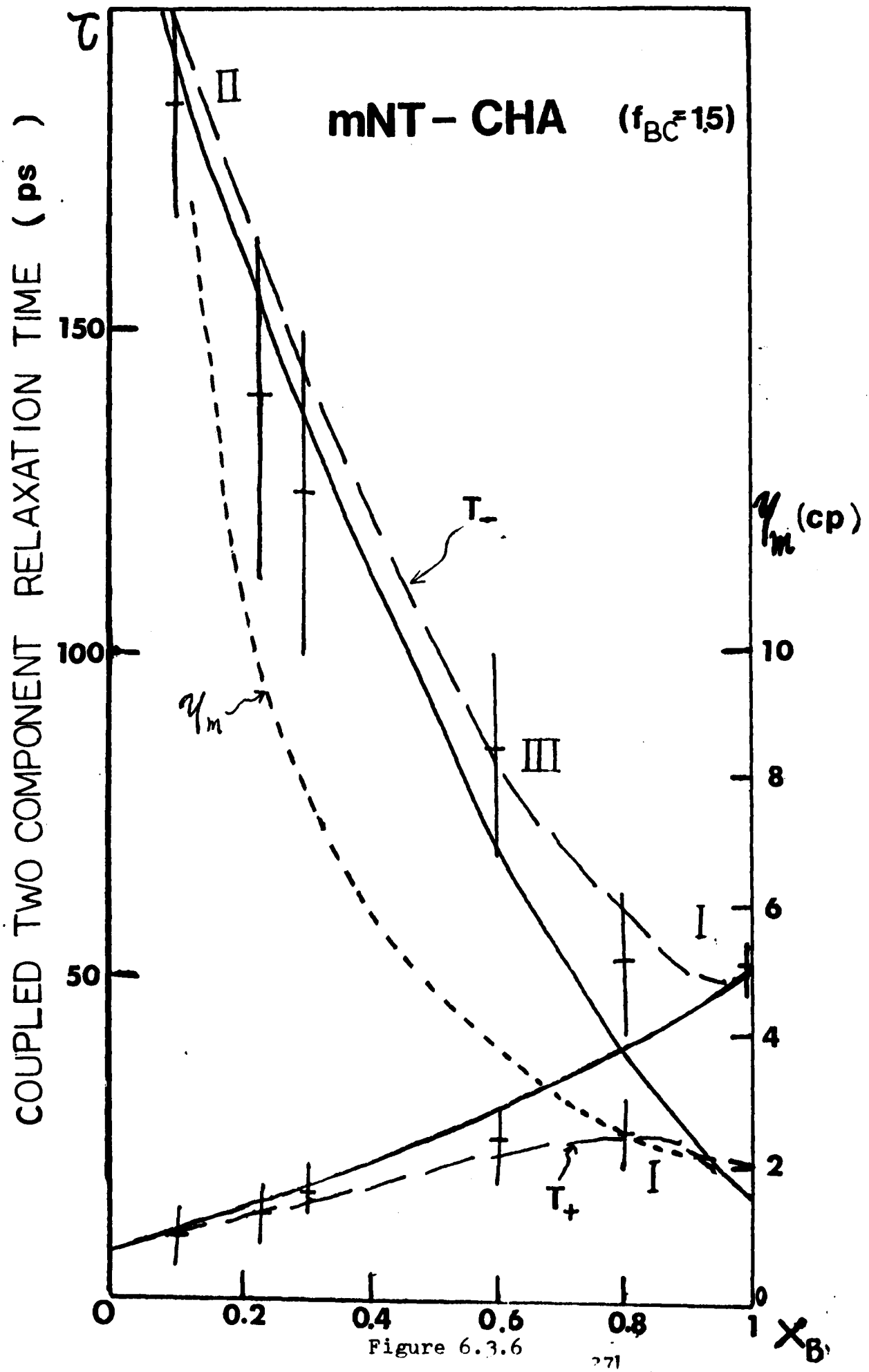
τ
mNT - CHA (f_BC = 1.5)
COUPLED TWO COMPONENT RELAXATION TIME (ps)
150
100
50
0
0.2
0.4
0.6
0.8
1
X_B
II
III
I
T_
T+
η_m
η_m (cp)
10
8
6
4
2
0

Figure 6.3.6

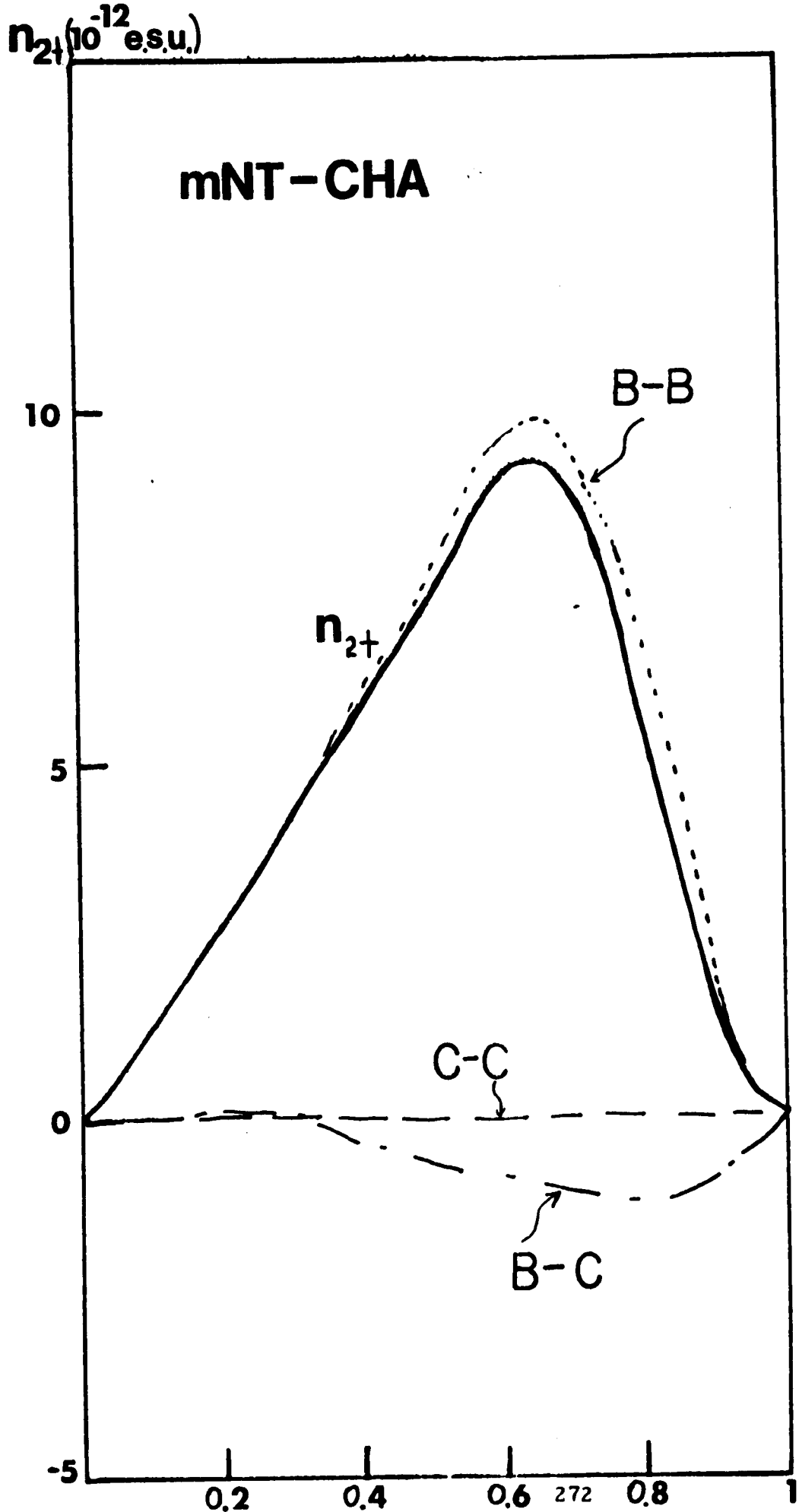

(a)

Figure 6.3.7a

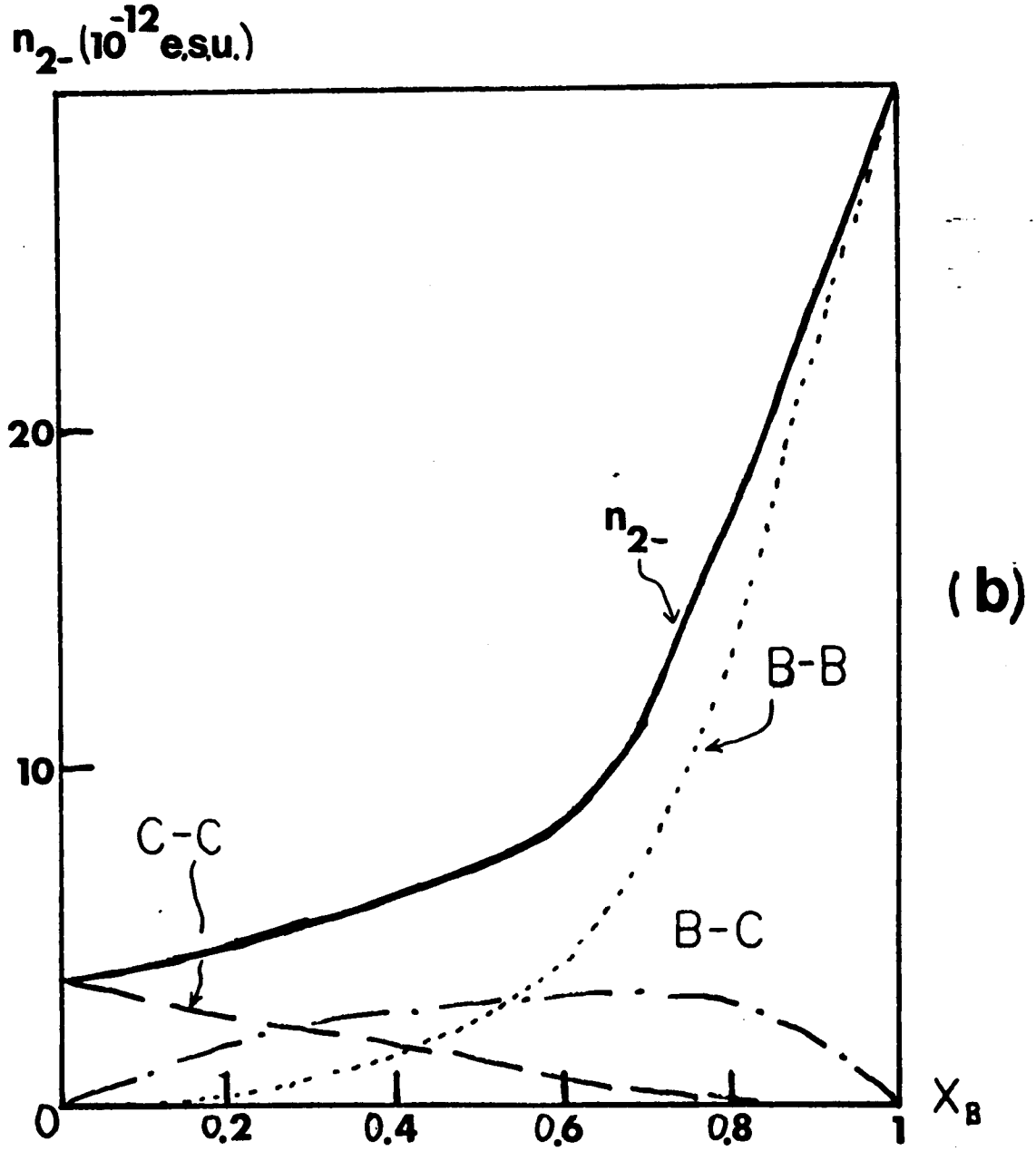

Figure 6.3.7b

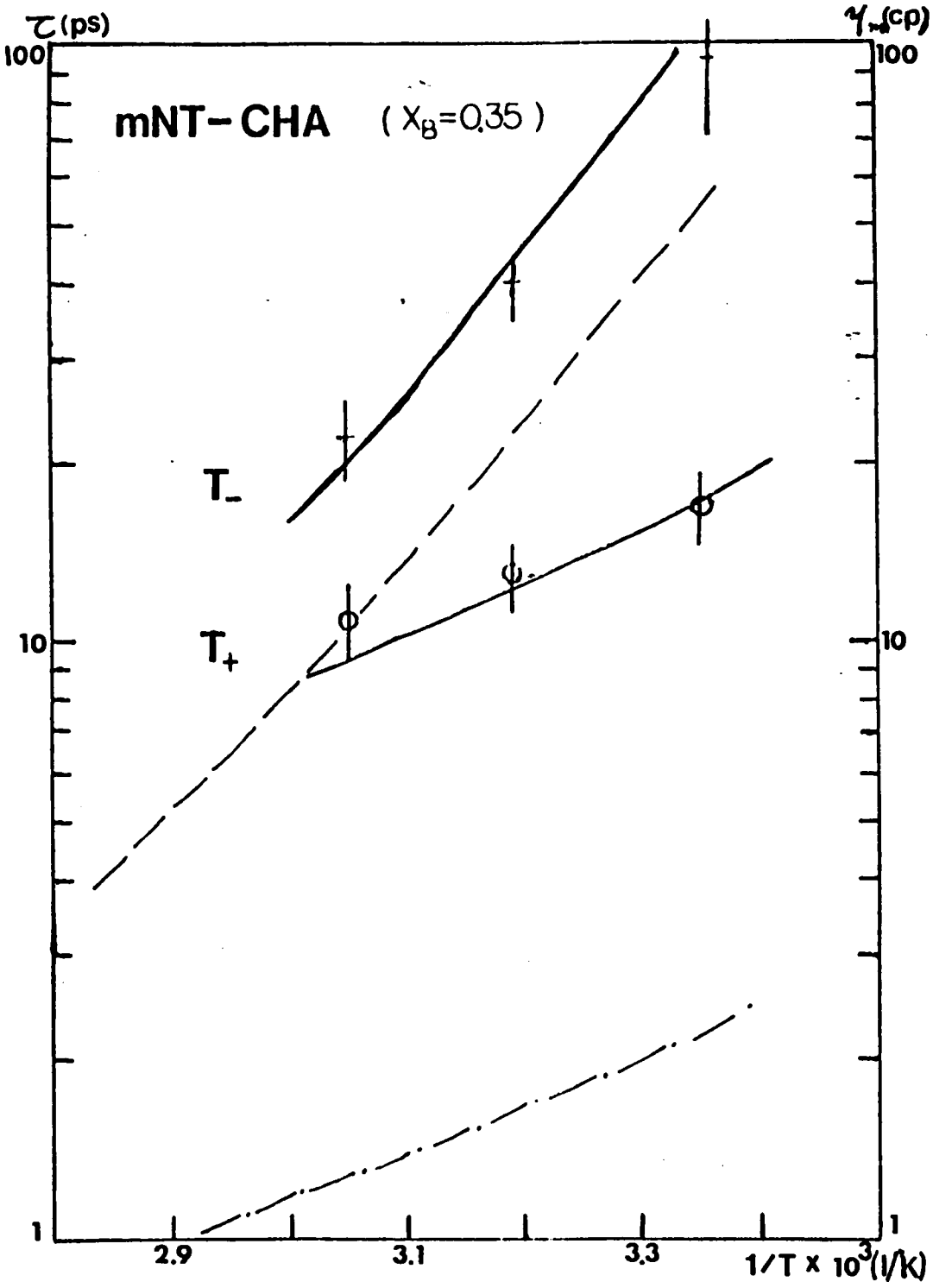

Figure 6.3.8

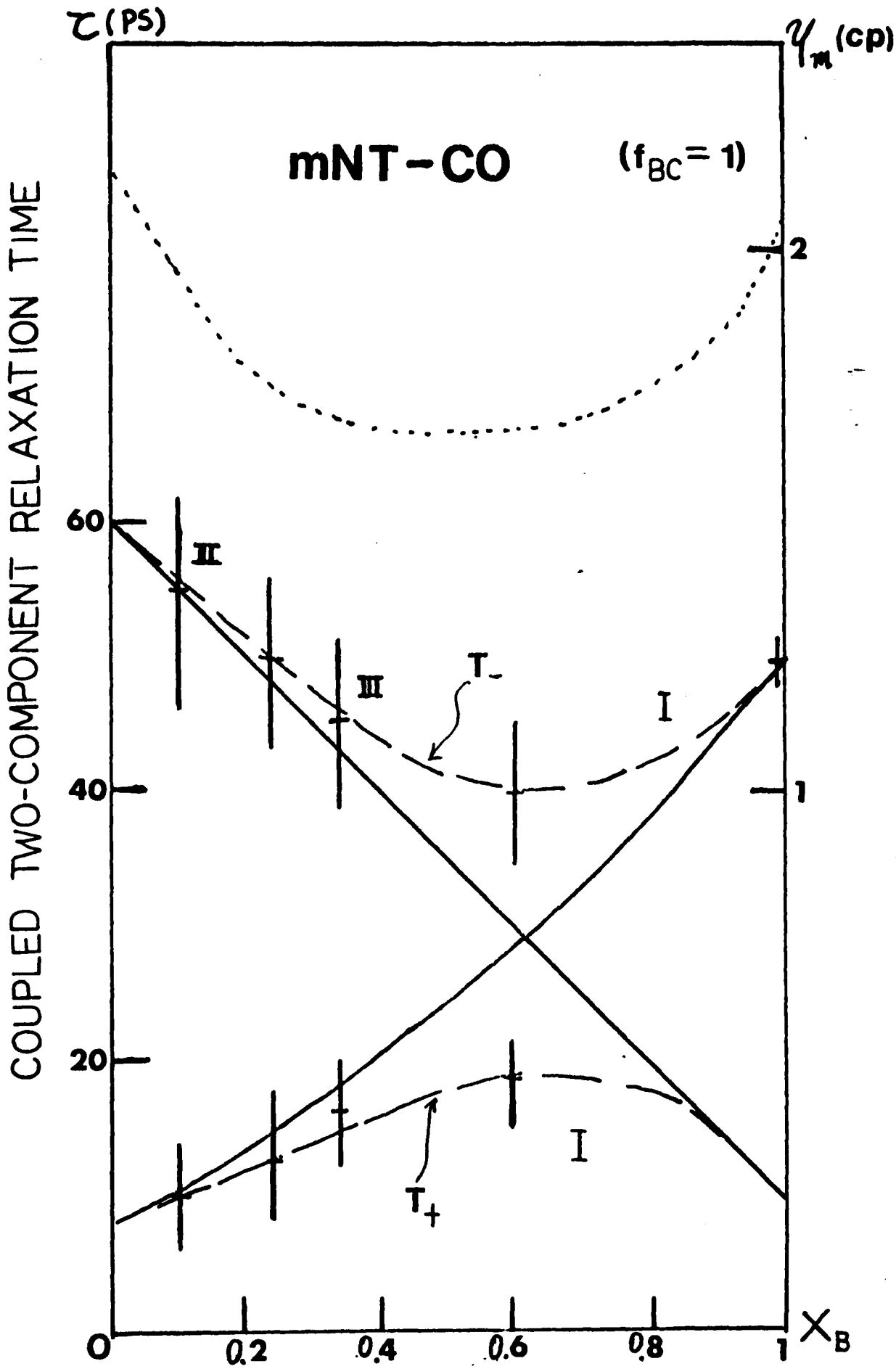
τ (PS)
η_m (cp)
mNT-CO
(f_{BC} = 1)
COUPLED TWO-COMPONENT RELAXATION TIME
60
40
20
0
2
1
II
III
T_-
I
I
T_+
0.2
0.4
0.6
0.8
1
X_B

Figure 6.3.9

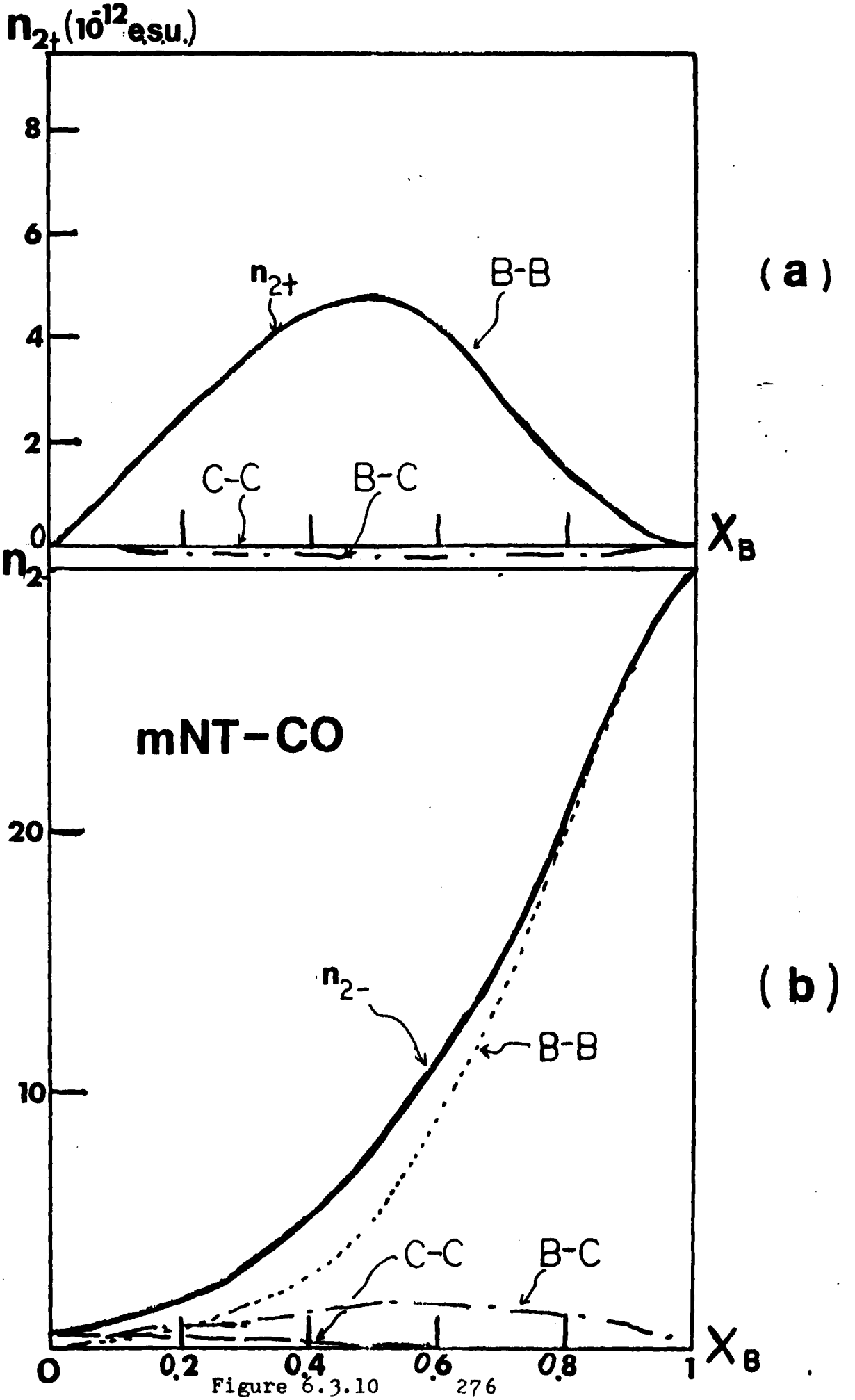
$n_{2+}(10^{12}$e.s.u.)
8
6
4
2
0
n_{2+}
B-B
(a)
C-C
B-C
X_B
n_2
mNT-CO
20
10
n_{2-}
B-B
(b)
C-C
B-C
0
0.2
0.4
0.6
0.8
1
X_B

Figure 6.3.10

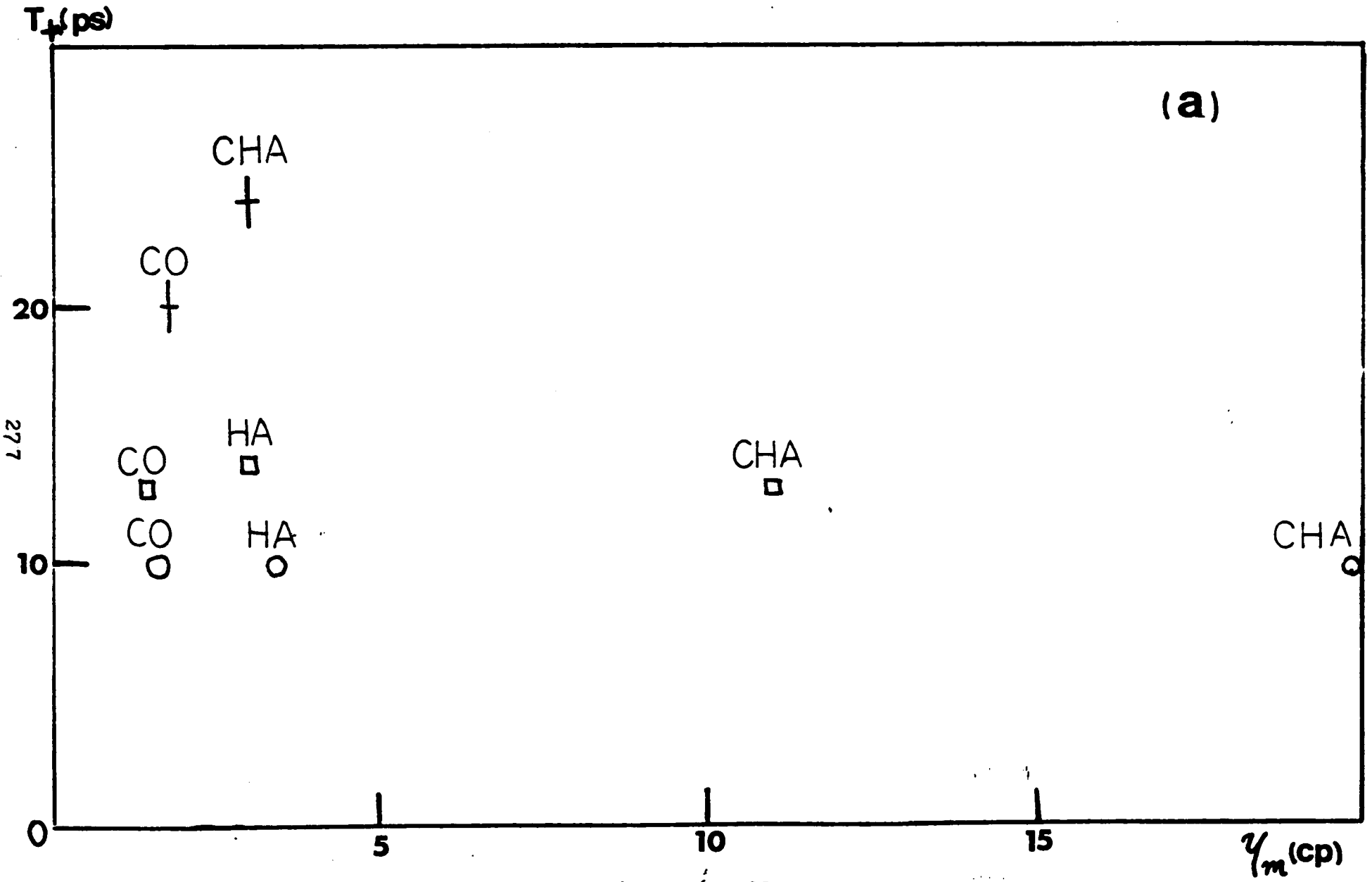

Figure 6.3.11a

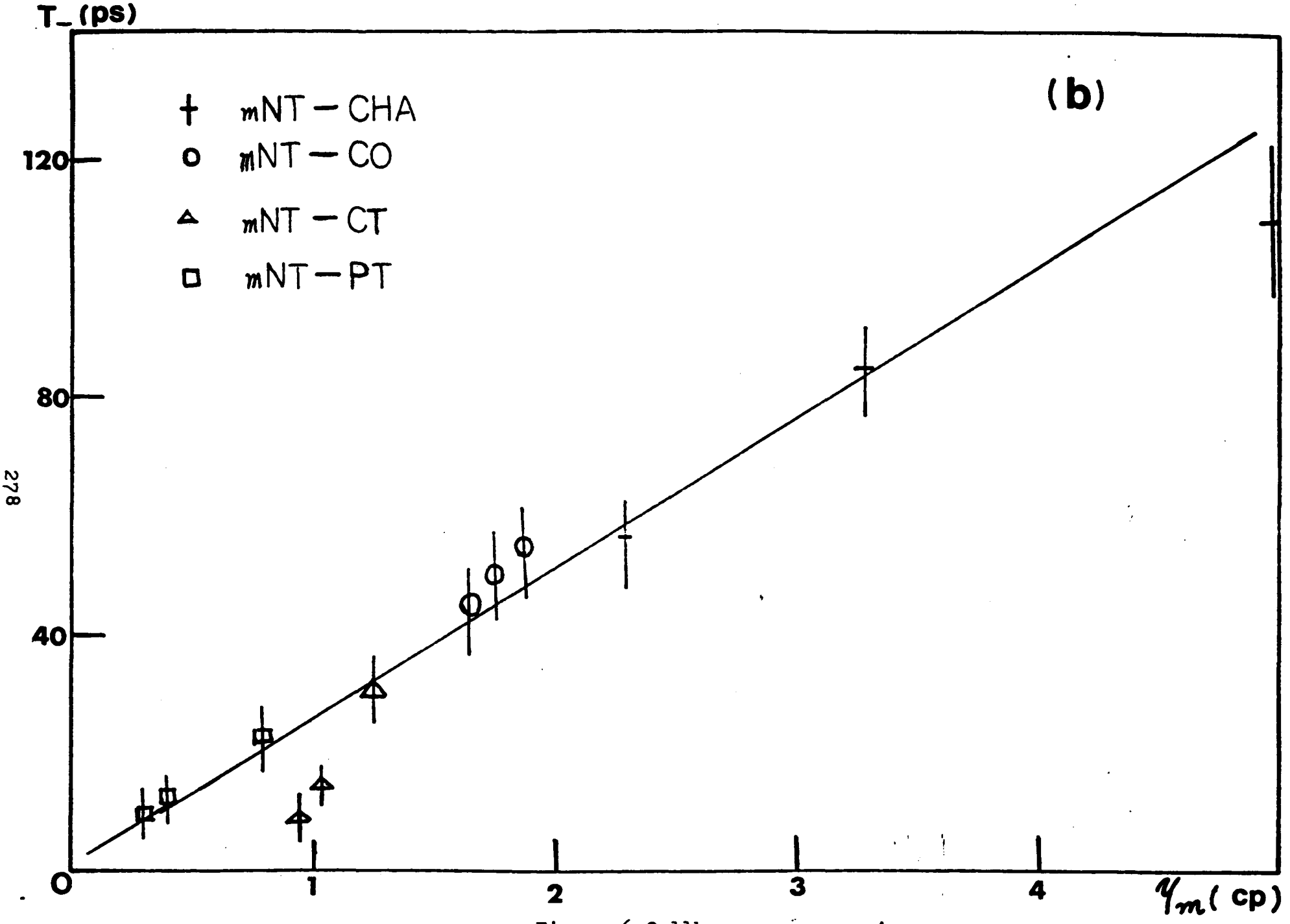

Figure 6.3.11b

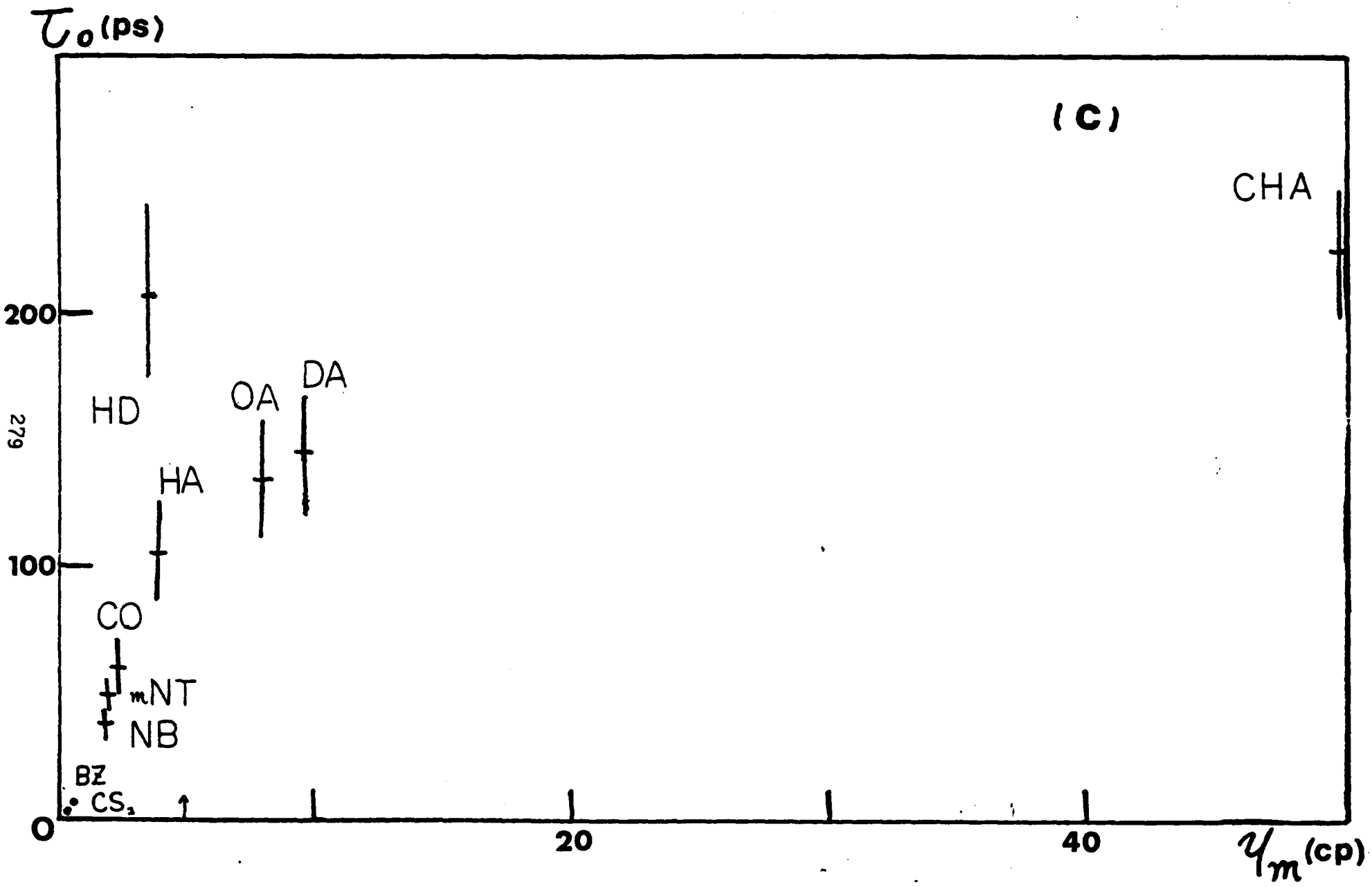

Figure 6.3.11c

6.4. Relaxation Kinetics of Salol In The Supercooled Liquid State Is Investigated With The Optical Kerr Effect

Knowledge of the kinetics of the nonlinear index of refraction of liquids can yield fundamental information on the molecular motion in the liquid state[1,2]. For anisotropic molecules, it is current believed that the dominant mechanisms responsible for the Kerr effect is the electronic cloud distortion and molecular reorientational motion of the molecules[3-5]. The electronic mechanism is temperature independent and is so fast that its time dependence cannot be resolved by picosecond laser techniques. The measurement of the temperature dependence of the Kerr relaxation can yield information on the kinetics of the molecular motion. By measuring the transient response of the optical Kerr effect as a function of temperature, we have separated a fast (electronic and molecular librational) and a slow molecular reorientational contributions to the nonlinear index of refraction of the supercooled[6] liquid - salol[7] (Phenyl Salicylate). The optical Kerr intensity versus time is found to decay with two distinct components. One component is fast and temperature independent and is mostly contributed to be of electronic origin. The second is relatively slow and is temperature dependent and is attributed to be of molecular orientational origin. This is the first direct kinetic measurement delineating the relative effects of ultrafast (electronic and molecular librational) and slow molecular reorientational contribution to the nonliner index of refraction. In the past, the relative contribution of the nonlinear index

were obtained from steady state temperature dependent[8,9], or calculated from a combination of careful measurements using different experimental techniques, such as electric field induced second harmonic generation[8], third harmonic generation[10], ellipse rotation[5], and the d.c.[8] and optical Kerr effect[11,12].

The experimental setup used to directly measure the relaxation kinetics of the optical Kerr effect has been described in chapter 5. The salol was the puriest grade available from the Eastman Kodak Company. The sample was placed in a one cm long optical cell and was situated in a glass dewar with strain free windows. A copper-constantan thermocouple was cleaned and immersed in the sample. The temperature was controlled by flowing cooled nitrogen gas into the dewar and by surrounding the sample cell holder with heating tape. The sample temperature was controlled to within $\pm$ 1°C and the temperature gradient across the sample was less than 1°C. Salol can be supercooled to a temperature well below its melting temperature of 42°C. A more detail preparation is discussed in section 5.4.

The Kerr intensity profile versus time for salol measured at different temperatures are shown in figure 6.4.1. The salient feature of these curves is the distinct two component decay. At temperature of 13°C, the decay profile is clearly composed of a slow and a fast exponential decay components. Within experimental error, the fast component is found to be temperature independent whereas the slow component is temperature

dependent. The decay of the slow component becomes faster as the sample temperature is increased, merging with the fast component forming a non-exponential decay, at the highest temperature (77°C) studied. The risetime of these curves are very fast ~ 5 ps. At a temperature of -10°C, the Kerr intensity profile versus time is essentially composed of only the fast component. The decay time of the fast component correspond to the convolution of laser pulse duration ~10 ps. The intensity of the slow component is extremely small because it can not respond significantly to the picosecond laser pulse excitation[4]. The decay time of the slow component estimated to be > 3 ns. Within a signal to noise ratio about 100 to 1, no other component is observed at -10°C.

The induced birefringence of the Kerr effect[4,11] can be described by the equation :

$$\delta n(t) = \delta n^e(t) + \delta n^o(t) \quad , \qquad (6.4.1)$$

where $\delta n^e(t)$ and $\delta n^o(t)$ denote the fast (electronic cloud distortion and molecular librations) and the slow molecular reorientational contributions, respectively. The fast (e) and slow (o) parts : $\delta n^i(t)$ are given by the equation :

$$\delta n^i(r,t) = n_2^i/\tau_i \int_{-\infty}^{t} \bar{E}_w^2(r,t) \exp(-(t-t')/\tau_i) dt' \quad , (6.4.2)$$

where i = o or e ; n_2^e is the change of nonlinear index of refraction through electronic cloud distortion and molecular librations; n_2^o is the change of nonlinear index of refraction from molecular reorientational motio; and τ_e, τ_o are the relaxation time of fast (electronic and molecular librational)

and slow molecular reorientational processes, respectively. Estimates of relaxation time of electronic process in most media lie in the range of 10^{-14} to 10^{-16} sec. and of the molecular libration is about 10^{-13} sec[16], and τ_o is longer than 10^{-12} second[4,12-15].

The transmitted light signal of the probe 0.53 um pulse through the Kerr gate is ;

$$I_t(\tau) \propto \int_{-\infty}^{\infty} I_{0.53um}(t-\tau) \sin^2 \tfrac{1}{2}\delta\phi(t) \quad dt , \qquad (6.4.3)$$

and $$\delta\phi(t) = 2\pi L/\lambda \, \delta n(t) , \qquad (6.4.4)$$

where L is the length of the sample , λ is the wavelength of the probe light, and $\delta\phi$ is the phase retardation in the sample. Using equation 6.4.2 to 6.4.4, the magnitude of n_2^e and n_2^o are computed from the experimental measurements of the transmission of the probe 0.53 um light pulse at different times, from the input power of the orienting 1.06 um pulse, and from the relaxation times : τ_e and τ_o. The table 6.4 lists the calculated values of n_2^e and n_2^o at different temperatures. The value of n_2 of carbon disulfide (2×10^{-11} e.s.u.)[5,12] is used as the standard to obtain the absolute values shown in the table. In the calculation, n_2^e is assumed to be independent of the temperature and the envelope of the laser pulse is assumed to be exponential. In accordance with

Table 6.4 Nonlinear Index Of Refraction For Salol

$n_2^e(10^{-12}$e.s.u.)	$n_2^o(T) \times 10^{-12}$e.s.u.						
	T(°C)	13	25	40	47	62	77
3	$n_2^o(T)$	58	46	37	32	25	19

the theories of Buckingham[8] and Keilich[3], the values of $n_2^o(T)$ measured at different temperatures follows a 1/T dependence.

In figure 6.4.2, the measured viscosity of η_m[17,18]; the relaxation time of the slow component (τ_o) of the optical Kerr effect; and the inverse of the depolarized Rayleigh wing linewidth[7,17] of salol are plotted versus 1/T. There is no discontinuity in the slope of the Kerr lifetimes as salol is supercooled through its melting temperature. The lifetime decreases approximately exponentially as 1/T. The Kerr relaxation times of the slow components from 7°C to 77°C follows the Arrhenius behavior[19-21]:

$$\tau(T) = A \exp(E/RT) \quad , \qquad (6.4.5)$$

where A is a proportionality constant $\sim 3.4 \times 10^{-15}$ sec from data fitting; and E is the potential barrier for molecules transiting from their original equilibrium positions to its new positions. The activation energy E of salol calculated from the Kerr effect measurements is 7.5 ± 0.5 kcal/mole closed to the activation energy = 5.6 kcal/mole calculated from viscosity measurements above the melting temperature. The Kerr relaxation times and the inverse of the depolarized Rayleigh wing linewidth measurements[7,17] are in good agreement with each other over this temperature range. The temperature data reasonably fits the viscosity data above the melting temperature; but below the melting temperature the measurments diverge rapidly. Therefore, Debye's equation[22] of molecular rotational relaxation time in liquids

$$\tau(T) = V \eta_m(T)/kT \quad , \qquad (6.4.6)$$

cannot be used to describe the temperature variation studied. It is apparent from figure 6.4.2 that the viscosity of salol does not follow a simple Arrhenius behavior below the melting temperature. This is a common characteristic of supercooled liquids which has been attributed to the progressive restriction of the different rotational degrees of freedom of the molecules with decreasing temperature[23]. These results suggest an ansatz that the Kerr relaxation data measures the rotational kinetics associated with a particular rotational degree of freedom of the salol molecules whose motion may only contribute partly to the overall measured viscosity of the supercooled liquid.

In summary, the Kerr relaxation kinetics of salol has been measured at different temperatures. The temperature variation of reorientational relaxation time τ_0 increases exponentially as 1/T following an Arrhenius behavior. No discontinuity is noticed at the melting point or in the supercooled region. Two distinct components of the Kerr decay profiles are observed. From the temperature dependence of these components, the mechanisms responsible for the fast and slow components are attributed to the electronic and molecular librational, and molecular reorientational parts of the nonlinear refractive index, respectively. This is the first clear observation delineating the fast (electronic and molecular librational) and molecular reorientational contributions to the nonlinear index of refraction in liquids.

Reference:

1. P.R. Jones and C.H. Wang, J.Chem. Phys. 65 1835 (1976).

2. C.W. Cho,N.D. Foltz, D.H. Rant and T.A. Wiggins, Phys.Rev.Lett.,18,107(1967).

3. S.Kielich, Acta Physica Polonica, 30,683, (1966).

4. K.Sala and M.C. Richardson, Phys.Rev. A12,1036 (1975).

5. R.W.Hellwarth,A.Owyoung, N.George,Phys.Rev. A4 ,2342 (1972).

6. G.Harrison, The dynamical properties of supercooled liquids,(Academic Press, New York, 1976.

7. L.M. Sabirou, V.S.Starunov and I.L.Fabelinskii, Soviet Phys.JETP 33,82(1971).

   V.S.Starunov and I.L. Fabelinskii, Soviet Phys. JETP, 39 , 854 (1974).

   S.M. Rytov, Soviet Phys. JETP 32 ,1153 (1971).

8. A.D. Buckingham and B.J.Orr, Trans.Faraday. Soc., 65,673 (1969).

   A.D. Buckingham and R.E. Raab, J.Chem.Soc., 2341 (1957).

9. J.F.Ward and I.J. Bigio, Phys. Rev. A11, 60 (1975).

10. P.D. Maker and R.W. Terhune, Phys.Rev., 137, A801 (1965).

11. G.L. Wong and Y.R. Shen, Phys. Rev. A10 ,1277 (1974).

12. M. Duguay and H.Hansen, Appl. Phys. Lett. 15 ,192 (1969).

    F. Shimizu and B.P. Stoicheff, IEEE QE-5 , 544 (1969).

13. P.P. Ho, Y.Yu and R.R.Alfano,Chem.Phys.Lett. 27, 91 (1976).

14. R.R. Alfano and S.L. Shapiro, Phys.Rev. Lett.24,592 (1970).

15. C.P.Smyth, Molecular relaxation processes (Academic Press, New York, 1966).

    R.G. Brewer and C.H. Lee, Phys. Rev. Lett. 29 ,592 (1970).

16. R. Polloni, C.A. Sacchi, and O.Svelto, Phys. Rev.,A2,955,(1968).

17. G.D. Enright, Ph.D thesis (Uni. of Toronto 1974).

18. Landolt-Bornstein Table Vol. 5 (Spring Verlag, Berlin 1969).

19. H. Erying, J. Chem. Phys. 3, 107 (1935).

20. P.Macedo and L. Litovitz, J. Chem. Phys. 42,245 (1965).

21. M.H. Cohen and J. Turnbull, J. Chem. Phys. 31, 1164 (1959).

22. P. Debye, Polar Molecules (Dover, New York 1946).

23. D.B. Davies and A.J. Matheson, J. Chem. Phys. 45, 1000 (1966).

Figure Captions

Figure 6.4.1 Decay profile of optical Kerr effect of salol at various temperature. The vertical axis is the intensity of the transmitted 0.53 um light pulse in arbitrary unit; and the horizontal axis is the time in picoseconds. The zero time is arbitrary. (a) 13°C, (b) 25°C, (c) 47°C, (d) 77°C.

Figure 6.4.2 The reorientational relaxation time and viscosity versus 1/T.

+ : optical Kerr effect, the lifetimes are doubled[12] from the decay profiles of figure 6.4.1,

● and x : inverse linewidth of the depolarized Rayleigh wing scattering from references 17 and 7, respectively,

o : measured viscosity from standard tables[17,18].

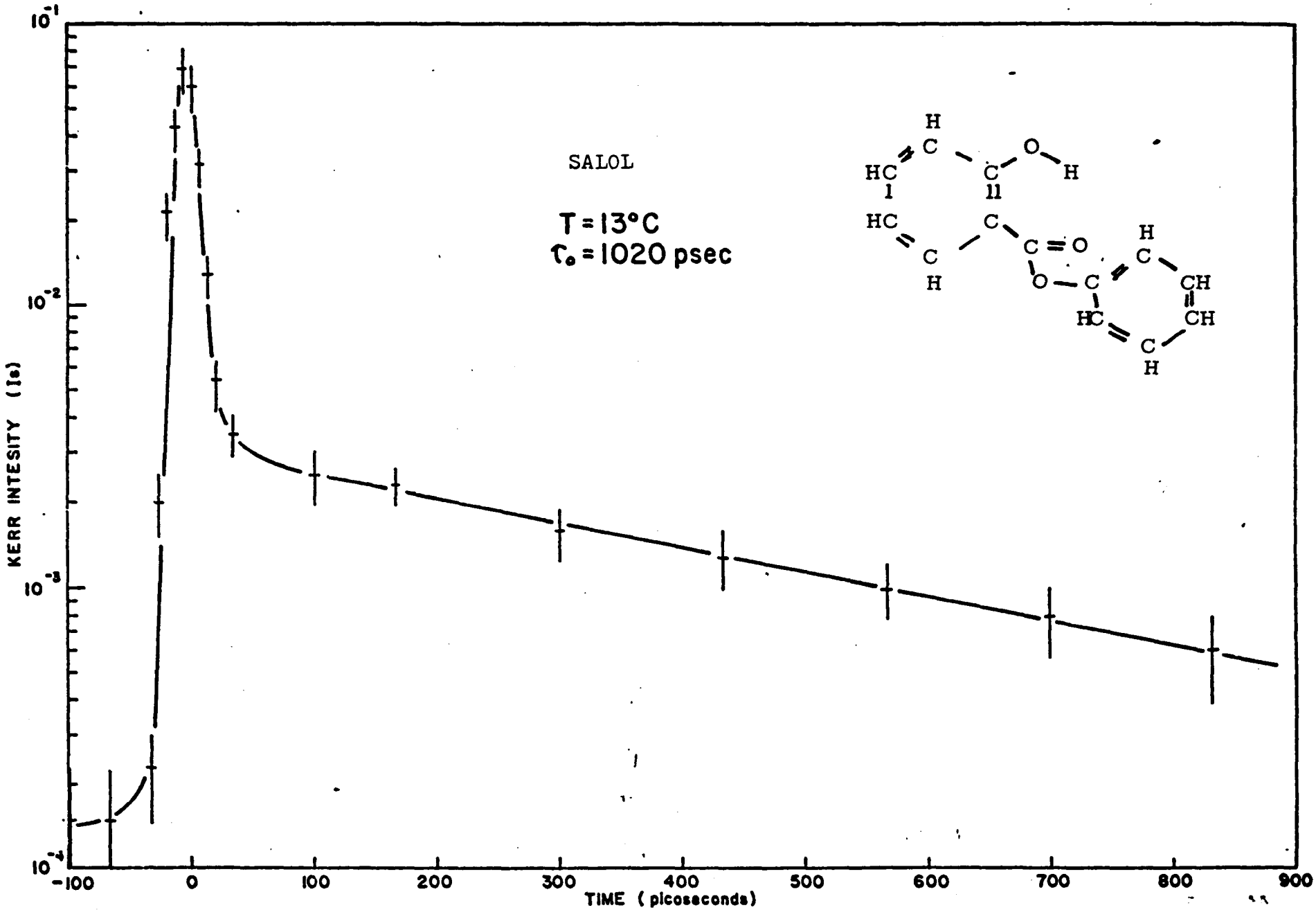
SALOL
T = 13°C
τ₀ = 1020 psec
KERR INTESITY (Is)
TIME (picoseconds)
10⁻¹
10⁻²
10⁻³
10⁻⁴
-100
0
100
200
300
400
500
600
700
800
900

Figure 6.4.1a

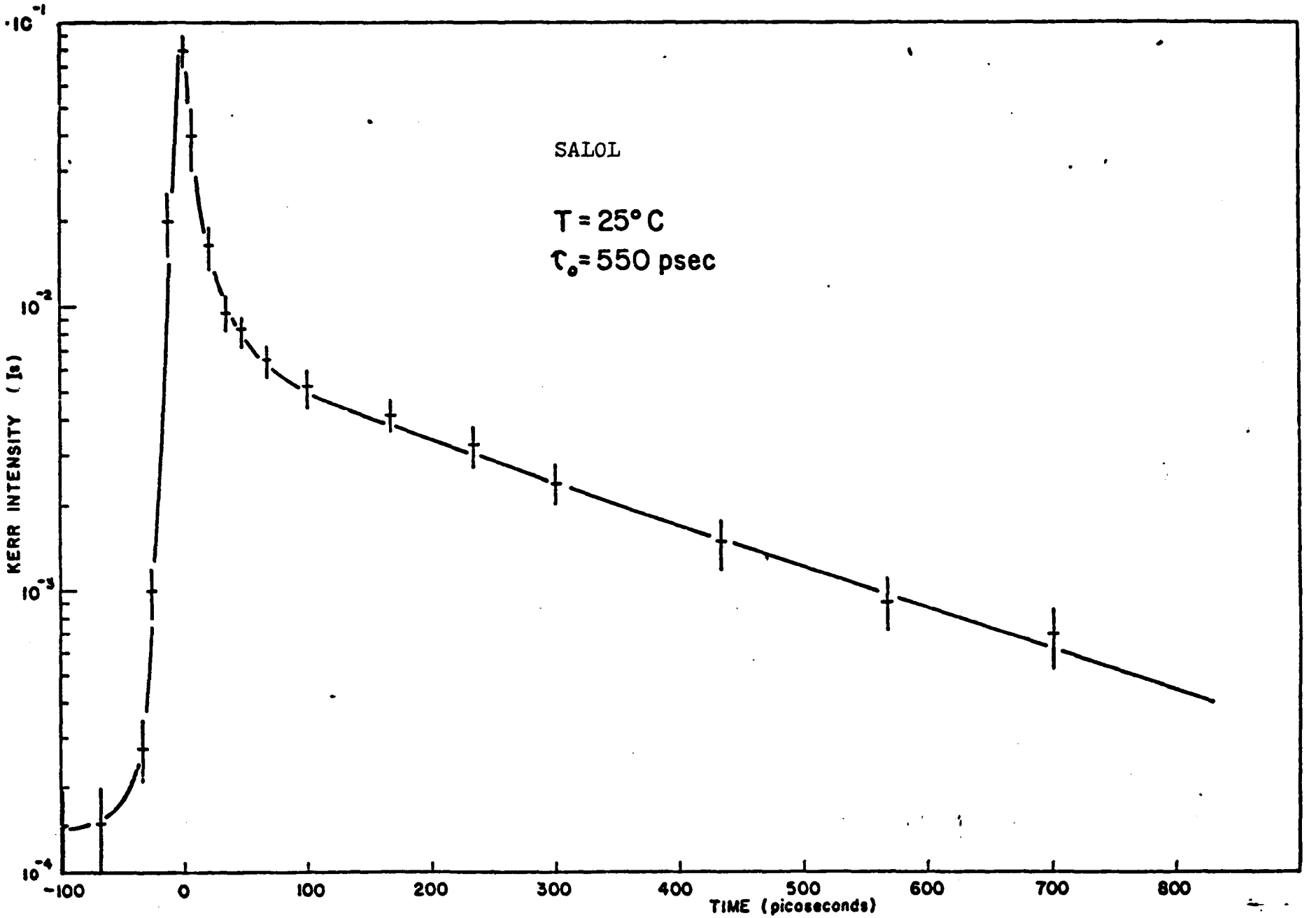
SALOL
T = 25° C
τ_o = 550 psec
KERR INTENSITY (Is)
10^{-1}
10^{-2}
10^{-3}
10^{-4}
-100
0
100
200
300
400
500
600
700
800
TIME (picoseconds)

Figure 6.4.1b

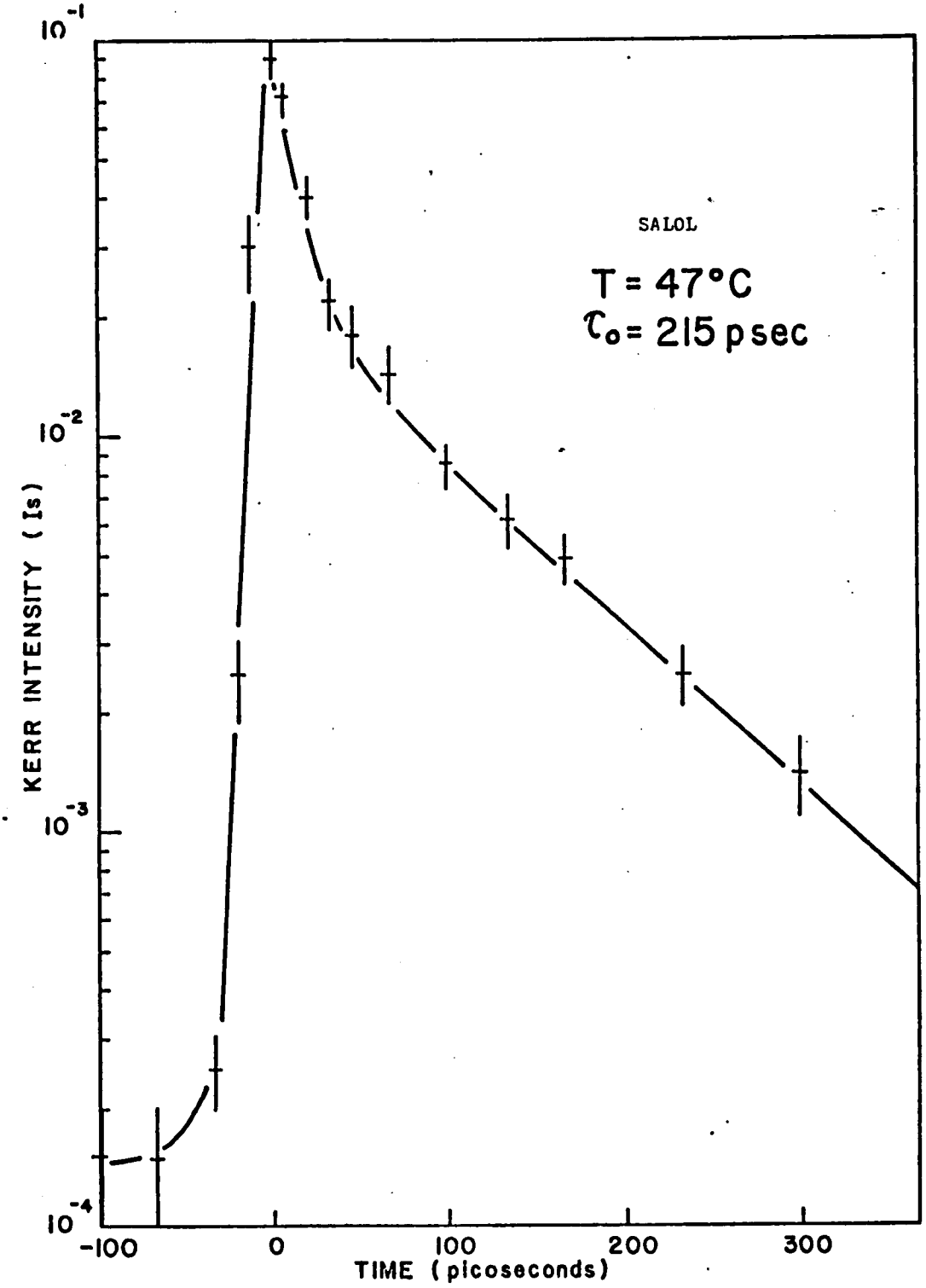
SALOL
T = 47°C
τo = 215 psec
KERR INTENSITY (Is)
10-1
10-2
10-3
10-4
-100
0
100
200
300
TIME (picoseconds)

Figure 6.4.1c

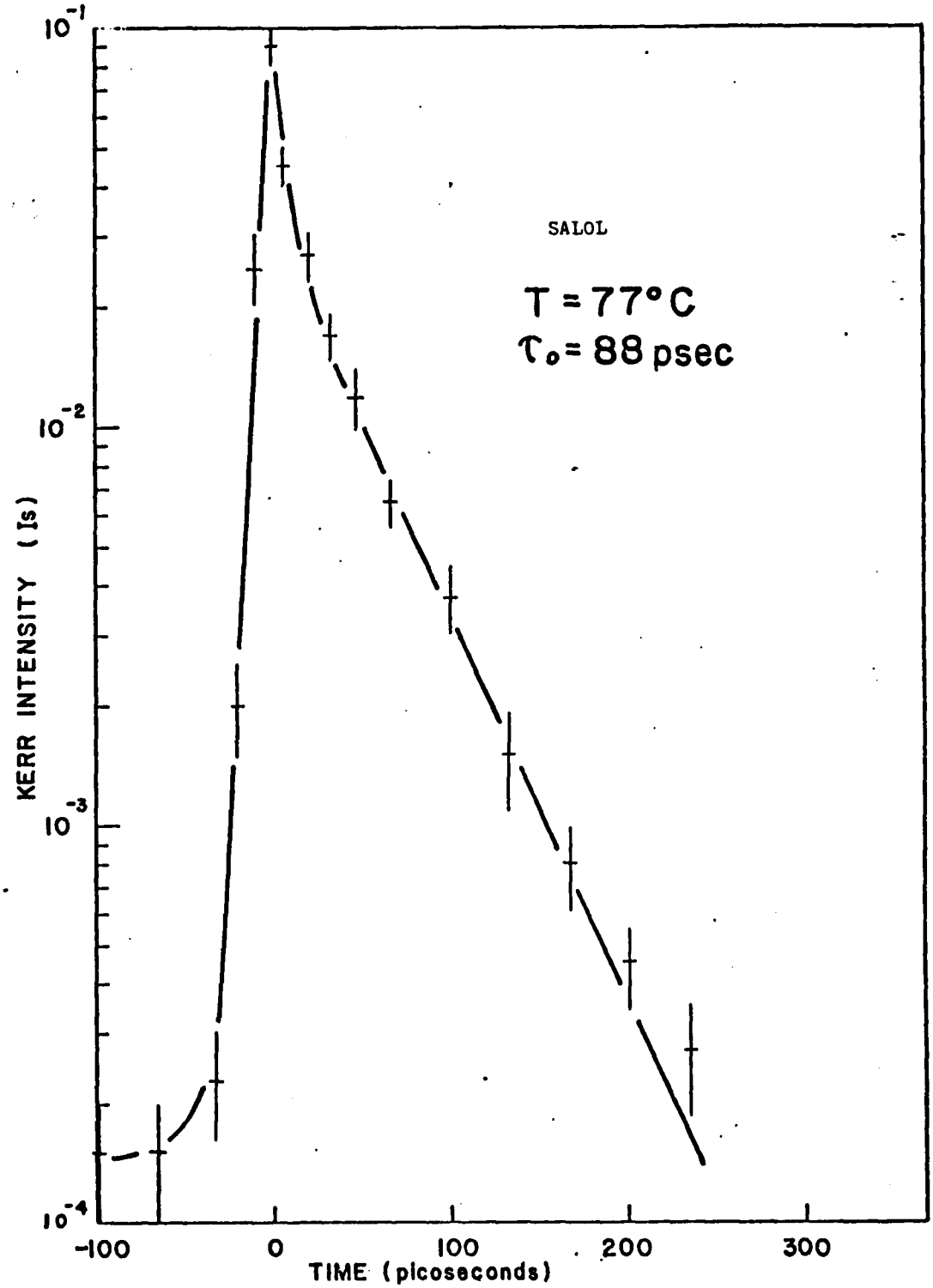
SALOL
T = 77°C
τ₀ = 88 psec
KERR INTENSITY (Is)
10⁻¹
10⁻²
10⁻³
10⁻⁴
-100
0
100
200
300
TIME (picoseconds)

Figure 6.4.1d

6.5 Relaxation Kinetics of The Plastic Crystal - Succinonitrile

The rotational motion of molecules is fundamental to the understanding of molecular interactions in liquids and solids[1]. The reorientational relaxation kinetics of the succinonitrile (SN) molecules in the plastic crystal phase has been studied by several techniques, such as dielectric relaxation[2], nuclear magnetic resonance[3], and depolarized Rayleigh scattering[4]. Recently, picosecond laser techniques have become available for directly measuring the subnanosecond time dependence of the optical Kerr effect in liquids[5,6]. This is a powerful technique for obtaining direct kinetic information about the motion of molecules in the condensed state[6]. In this section, we report the first direct measurement of the Kerr relaxation times of SN associated with its reorientational motion from the liquid to the plastic crystal phase by measuring the kinetics of the optical Kerr effect using picosecond laser pulse.

For anisotropic molecules in the liquid state, the dominant mechanisms responsible for the Kerr effect in the picosecond region are assoicated with electronic cloud distortion[7,8,9], molecular libration[10,11], molecular redistribution[12], and molecular reorientational motion[6,7,8]. In general, for glasses, polymers, and solids, due to the restrictive motion of the molecule and the available free volume[13], the Kerr constant associated with molecular reorientational motion is either too small to be observed or the relaxation time is too slow to respond to the picosecond laser pulse[6,8,14,15]. However, in

the plastic crystal phase, the molecule has a fast rotational degree of freedom due to its "globular"shape[16]. Though the SN molecule is globular in the Timmermans classification[16], the succinonitrile molecule is not truly spherical in shape. Its plastic phase is due to the gauche-trans isomerism[17,18]. The molecular reorientational motion in the plastic phase can be described as a series jump over barriers between potential energy minimum[15,16]. The magnitude of the nonlinear index of refraction change of the Kerr effect of SN in the isotropic liquid and the cubic plastic crystal phase is large and has been measured by Bischofberger and Courtens[19].

A schematic disgram of the experimental setup [5,6] used to directly measured the relaxation kinetics of the optical Kerr effect is shown in figure 5.1 of chapter 5. The relaxation time extracted from the Kerr intensity decay profile corresponds to an overall reorientational motion of the molecules. This relaxation time is a combination of the reorientation about the individual axis of the molecules, just like the relaxation time obtained from the depolarized Rayleigh wing linewidth[20]. The measured relaxation time is more strongly weighted by the reorientation about the axis which is associated with the largest polarizability change upon orientation. The activation energy deduced from the temperature dependence of the measured relaxation time is an overall weighted average. Picosecond laser single shot technique[21] was also applied to measure the relaxation time. The results were similar except the available dynamic range of the decay profile was reduced by an order of magnitude due to the dynamic range of the PAR optical multichannel analyzer I.

The SN was obtained from the Eastman Kodak Company. Single crystals of SN were grown by using the Bridgman-Stockbarger technique (see section 5.3). The trace of the x-ray diffraction pattern of the crystal showed a cubic crystal (a distinct sharp peak at the (001) plane diffraction) and a wide diffused band due to the large Debye-Waller factor[18]. The plastic crystal phase of SN is between -40°C to +57°C [2,3,15]. The SN crystal melts at about 56°C ± 1°C. Depending on the rate of cooling, the freezing temperature of the liquid SN occurs between 57°C to 50°C. A 1 cm long crystal was cut in the (1$\bar{1}$0) plane which was perpendicular to the propagation direction of the laser beam. The SN crystal was perpendicular to the propagation direction of the laser beam. The SN crystal was situated in a 1-cm long optical cell containing decane liquid for index matching. The geometry of the crystal related to the directions of the laser fields is shown in figure 6.5.1. The cell was placed in a glass dewar with strain free windows. The Kerr effect of the windows and decane was measured to be negligible. A copper-constantan thermocouple was cleaned and immersed in the cell. The temperature was changed by adjusting the flow rate of cooled nitrogen gas into the dewar and by applying to heater tape which surrounded the sample cell holder. The temperature was controlled to within one degree. The SN crystal occasionally damaged when the power density of 1.06 um laser beam exceeded 1 GW/cm^2. This limited the signal to noise ratio. In order to minimize the formation of defects in the crystal during a temperature depnedent experiments, the relaxation time measurements were performed in a series from low to high temperature.

The Kerr intensity decay profiles versus time of the SN measured at different temperatures are shown in figure 6.5.2. The prompt response curve of liquid CS_2 (the orientational relaxation time is about 1.8 ps[22]) is shown in figure 6.5.2a. After 20 ps away from the peak, the time slope for the decay profile is 2.5 ps. Therefore, the smallest reorientational relaxation time that can be reasonably extracted[23] from the data is $\gtrsim$ 8 ps. In figure 6.5.2a, the picosecond laser Kerr technique[5,23] can not resolve the contributions to the nonlinear index of refraction change due to the electronic cloud distortion, the molecular libration, the molecular redistribution, and the molecular reorientational motion[7,8]. It has been argued that the primary mechanisms for the Kerr effect in condensed matter arises from the electronic and reorientational motion of molecules. This point can be challenged in some cases.[7c] To obtain the molecular reorientational relaxation time (τ_o) of SN, the equation[5] $A \exp[-2(t-27)/\tau_o] + B$ which describes the time dependence of the Kerr intensity decay profile for $t \gtrsim 27$ ps is used to fit the data. The parameter A is a constant to fit the data at t = 27 ps, and the parameter B denotes the background light level originating from the leakage of the probe 0.53 um light through the polarizers. The Kerr intensity decay profile of liquid SN at 57°C is shown in figure 6.5.2b. The slope of this curve, 27 ps away from the peak is about twice as slow as that of the CS_2 prompt curve. The reorientational relaxation time for liquid SN is 11 ± 4 ps at 57°C.

The rotational relaxation time of the molecules for the different experimental methods in the diffusion and large jump limit can be expressed by[6,24] $\tau_\ell = \tau_o/\ell(\ell+1)$ and $\tau_\ell = \tau_o$, respectively, where τ_ℓ is the measured relaxation time for the particular experimental technique which measures the kinetics of the ℓ-th rank of susceptibility tensor, and τ_o is the time interval during which the molecules stay in the local equilibrium positions. In an analysis of the experimental data[6a] from the optical Kerr effect (ℓ=2), light scattering (ℓ=2), and dielectric relaxation (ℓ=1) for various liquids, the ration τ_1/τ_2 has been shown to lie between 1.1 to 1.5. This analysis suggests that the reorientational motion of small molecules is probably characterized by either jumps of intermediate size or more likely by a distribution of jump angles[6a]. Comparing the relaxation times of the liquid SN from the Kerr effect with the dielectric relaxation (τ_1 = 18 ps at 59°C and τ_1 = 14 ps at 74°C)[25], the ratio τ_1/τ_2 is in reasonable agreement with the above discussion.

The decay profiles of the transmitted Kerr signal of the SN plastic crystal at 45°C and 23°C are shown in figures 6.5.2c and 6.5.2d, respectively. The non-single exponential decay clearly indicates that different mechanisms are operative[7,8] - the fast component arises from the electronic cloud distortion and and molecular librational motion; and the slow component arises from the molecular reorientational motion. At 23°C, the ratio of the peak transmitted signal of the fast to slow component is estimated to be about 5 to 1. Within the experimental error, there is no noticeable temperature dependence to the fast component decay. Its shape is very close to that of the prompt

CS_2 curve. We have assumed the fast component is essentially temperature independent in this experiment. The relaxation time of the slow component tail at 23°C is 64 ± 20 ps which is in good agreement with the measurement from other techniques : [$\tau_{(\text{dielectric relaxation})}(23^{\circ}C)$ = 82 ps[2], or 64 ps[25], and $\tau_{(\text{depolarized Rayleigh scattering})}$ = 59 ps(25°C)[4c], 40 ps(19°C)[4a], 71 ps (23°C)[4b]]. The relaxation time at 45°C is 45 ± 15 ps. In figure 6.5.3, the relaxation times of slow component tail versus the inverse of temperature is compared with the relaxation times obtained by other techniques. The salient feature of these curves is the sudden jump of the relaxation time at the liquid to plastic crystal phase transition temperature. In this transition, the free energy decreases from liquid to solid state due to a change of entropy[25]. The activation energy estimated from the temperature dependence of the optical Kerr effect in the plastic phase is 2.6 ± 0.7 Kcal/mole. This value is in good agreement with the value obtained from the dielectric relaxation in the temperature range of this experiment (E_a = 2.5 Kcal/mole[2] and E_a = 2.1 Kcal/mole[25]) and is slightly lower than the activation energy obtained from the depolarized Rayleigh wing scattering (E_a = 3.8 Kcal/mole[4b]). The activation energy in the liquid is about 3 Kcal/mole[4b]. This suggests that the gauche-trans isomerization barrier of the SN molecules in the plastic crystal phases is similar to the overall barrier in the liquid state.

We also measured the relaxation times of SN at different crystal orientations by rotating the crystal around the [1$\bar{1}$0] [001] axes, respectively, at room temperature. Within the

experimental error, the measured relaxation times are roughly the same with respect to the different orientation axes of the crystal. We need to improve the accuracy in order to determine if the reorientation about the different axes may have different relaxation times. In this experiment, we are most likely measuring a weighted average relaxation time about the different axes. The reorientational nonlinear refractive index n_2^o of SN at 25°C is estimated to be about 2×10^{-12} e.s.u. by comparing the magnitude of the Kerr effect with that of CS_2 ($n_2(CS_2) = 2\times10^{-11}$ e.s.u.[5]). In this estimation, the response time of the transmitted Kerr signal of SN has been taken into account. In the plastic crystal phase of SN, the contribution to the nonlinear index of refraction (n_2) from the fast relaxation process(electronic cloud distortion and molecular libration) are estimated to be of the same order of magnitude as the orientational contribution. The total nonlinear index of refraction measured by the Kerr effect using a 30 ns pulse from a Q-switched Ruby laser is $\simeq 2.5\times10^{-12}$ e.s.u.[20b]

In conclusion, we have directly measured the Kerr relaxation time of SN molecules in the liquid and plastic crystal state at various temperatures. The relaxation kinetics is due to different mechanisms - a fast relaxation process (electronic cloud distortion and molecular libration) and a slow relaxation process (molecular reorientational motion). The activation energy for the slow decay in the plastic crystal state is 2.6 ± 0.7 Kcal/mole. The relaxation time in the plastic crystal state at room temperature about different axes are about the same within the experimental error. In the liquid

state of SN, the molecules are more freely to move in space. The net change of the susceptibility tensor can be attributed by the rotation or libration of molecules inside a potential minimum, and by the large jump of molecules between the potential energy minima or jump to the nearest available empty neighboring sites. In the plastic crystal phase, the molecule is restricted in certain crystal site. Only the small rotation or libration inside a potential barrier, or a large jump in the crystal site such as the gauche-trans isomerization is possible to contribute the molecular reorientational motion.

REFERENCE

1. R. G. Gordon, J. Chem. Phys., 44, 1830, (1966).
2. D. E. Williams and C. R. Smyth, J. Am. Chem. Soc., 84, 1808, (1962).
3. J. G. Powles, A. Begum, and M. D. Norris, Mol. Phys., 17, 489, (1969).
4. (a) D. A. Jackson, M. J. Bird, H.T.A. Pentecost, and J. G. Powles, Phys. Lett., 35A, 1, (1971).
   (b) M. J. Bird, D. A. Jackson, and H. J. Pentecost, Proc. of the 2nd International Conference of Light Scattering in Solids, P 493 (Flammanion, Paris, 1971)
   (c) I. Boyer, R. Vacher, I. Cecchi, M. Adam, and P. Berge, Phys. Rev. Lett., 26, 1435, (1971).
   (d) T. Bischofberger and E. Courtens, Phys. Rev. Lett., 35, 1451, (1975).
5. (a) M. Duguay and J. Hansen, Appl. Phys. Lett. 15, 192, (1969).
   (b) F. Shimizu and B. P. Stoicheff, IEEE QE-5, 544, (1969).
6. (a) P. P. Ho, W. Yu and R. R. Alfano, Chem. Phys. Lett., 37, 91, (1976), and reference therein.
   (b) P. P. Ho, R. R. Alfano, J. Chem. Phys., 67, 1004, (1977).
7. (a) S. Kielich, Acta Physica Polonica, 30, 683, (1966).
   (b) A. D. Buckingham, Proc. Phys. Soc. (London), B69, (1956).
   (c) R. W. Hellwarth, A Owyoung, and N. George, Phys. Rev., A4, 2342, (1972).
8. K. Sala and M. C. Richardson, Phys. Rev., A12, 1036, (1975).
9. R. G. Brewer and C. H. Lee, Phys. Rev. Lett., 21, 267, (1968).
10. A. C. Cheung, D. M. Rank, R. Y. Chiao, and C. H. Townes, Phys. Rev. Lett., 20, 786, (1968).
11. R. Polloni, C. A. Sacchi, and O. Svelto, Phys. Rev., A2, 955, (1970).

12. R. W. Hellwarth, J. Chem. Phys., 52, 2128, (1970).

13. M. H. Cohen and J. Turnbull, J. Chem. Phys., 31, 1164 ,(1959).

14. P. P. Ho, Unpublished data.

15. C. P. Smyth, J. Phys. Chem. and Solids, 18, 40, (1961).

16. J. Timmermans, J. Phys. Chem. Solids, 18, 1,(1961).

17. G. J. Janz and W. E. Fitzgerald, J. Chem. Phys., 23, 1973, (1955).

18. (a) H. Fontaine, W. Longueville, and F. Wallart, J. Chim. Phys. Phys.-Chim. Biol.,68, 1593.(1971).

(b) H. Fontaine and M. Bee, Bull. Soc. Fr. Mineral. Cristallogr., 95, 441, (1972).

19. (a) T. Bischofberger and E. Courtens, Phys. Rev. Lett., 32, 163, (1974).

(b) T. Bischofberger and E. Courtens, Phys. Rev., A14, 2278, (1976).

20. D. R. Bauer, G. R. Alms, J. J. Brauman, and R. Pecora, J. Chem. Phys., 61, 2255, (1974).

21. (a) M. A. Duguay and A. T. Mittick, Appl. Optics, 10, 2162, (1971).

(b) G. Mourou and M. M. Malley, Opt. Comm., 13, 412, (1975).

(c) P. P. Ho and R. R. Alfano, Chem. Phys. Lett., 50, 74, (1977).

22. E. P. Ippen and C. V. Shank, Appl. Phys. Lett., 26, 92, (1975).

23. R. R. Alfano, GTE Tech. Report TR-2301 (1972).

24. (a) E. N. Ivanov, Sov. Phys. JETP, 18, 1041. (1964).

(b) A. Ben-Reuven and E. Zamir, J. Chem. Phys., 55, 475, (1971).

25. C. Clement and M. Davis, J. Chem. Phys., 32, 316 ,(1960).

Figure Captions

Figure 6.5.1 Geometry of the SN crystal orientation for the optical Kerr effect. The dashed lines are the polarization directions of the electric field of the orienting and probing laser pulses. The dashed-dotted line is the propagation direction [$\bar{1}10$] of the orienting and probing beams.

Figure 6.5.2 The decay profile of the transmitted Kerr signal measured at various temperatures. I_s is the Kerr transmitted signal through the gate, and I_o is the signal through the gate with the polarizers' axes are set parallel. The horizontal axis is the decay time measured in picoseconds. The zero time is arbitrary. Each data point is the average of four to six laser shots. The solid lines are fitted to the following equations due to the molecular relaxation process. The intensity of the pumped 1.06 um laser beam was reduced by 10 times for the CS_2 prompt curve.

(a) Prompt CS_2 gate response curve;

(b) Liquid SN at 57°C, $\frac{I(t)}{I_o} = 2.2\times10^{-3} \exp[-2(t-27)/11] + 2\times10^{-4}$;

(c) Plastic crystal SN at 45°C, $\frac{I(t)}{I_o} = 9\times10^{-3}\exp[-2(t-27)/45] + 6\times10^{-}$

(d) Plastic crystal SN at 23°C, $\frac{I(t)}{I_o} = 8\times10^{-3}\exp[-2(t-27)/64] + 5\times10^{-}$

Figure 6.5.3 The reorientational relaxation time of SN versus the inverse of temperature.

+ : data from the optical Kerr effect;

dotted line : best fit curve from depolarized Rayleigh scattering (reference 4b);

dashed line : best fit curve from dielectric relaxation (reference 25); and

solid line : best fit curve from dielectric relaxation (reference 2).

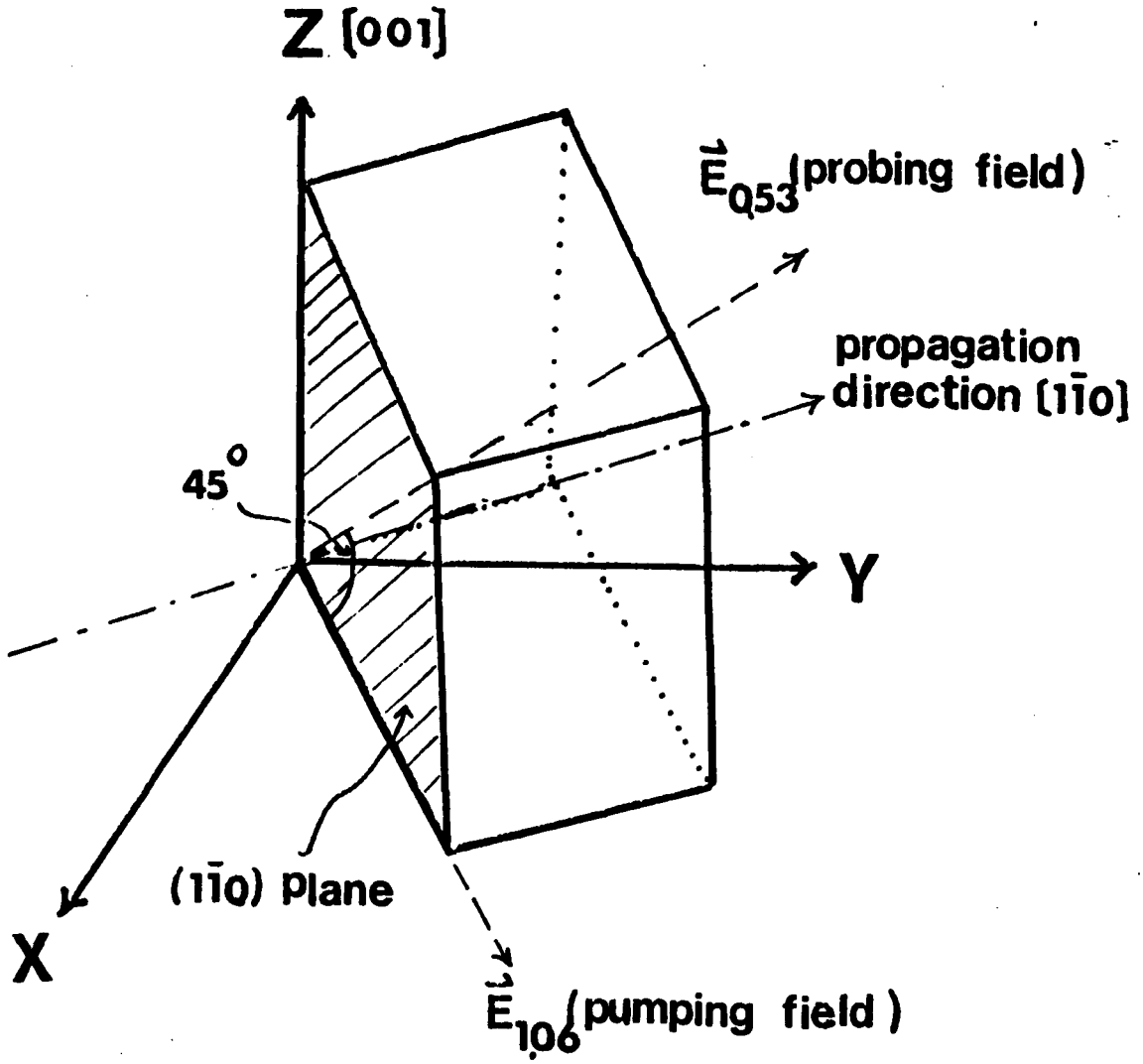
Z [001]
$\vec{E}_{Q53}$ (probing field)
propagation direction [1$\bar{1}$0]
45°
Y
X
(1$\bar{1}$0) Plane
$\vec{E}_{106}$ (pumping field)

Figure 1 (6.5)

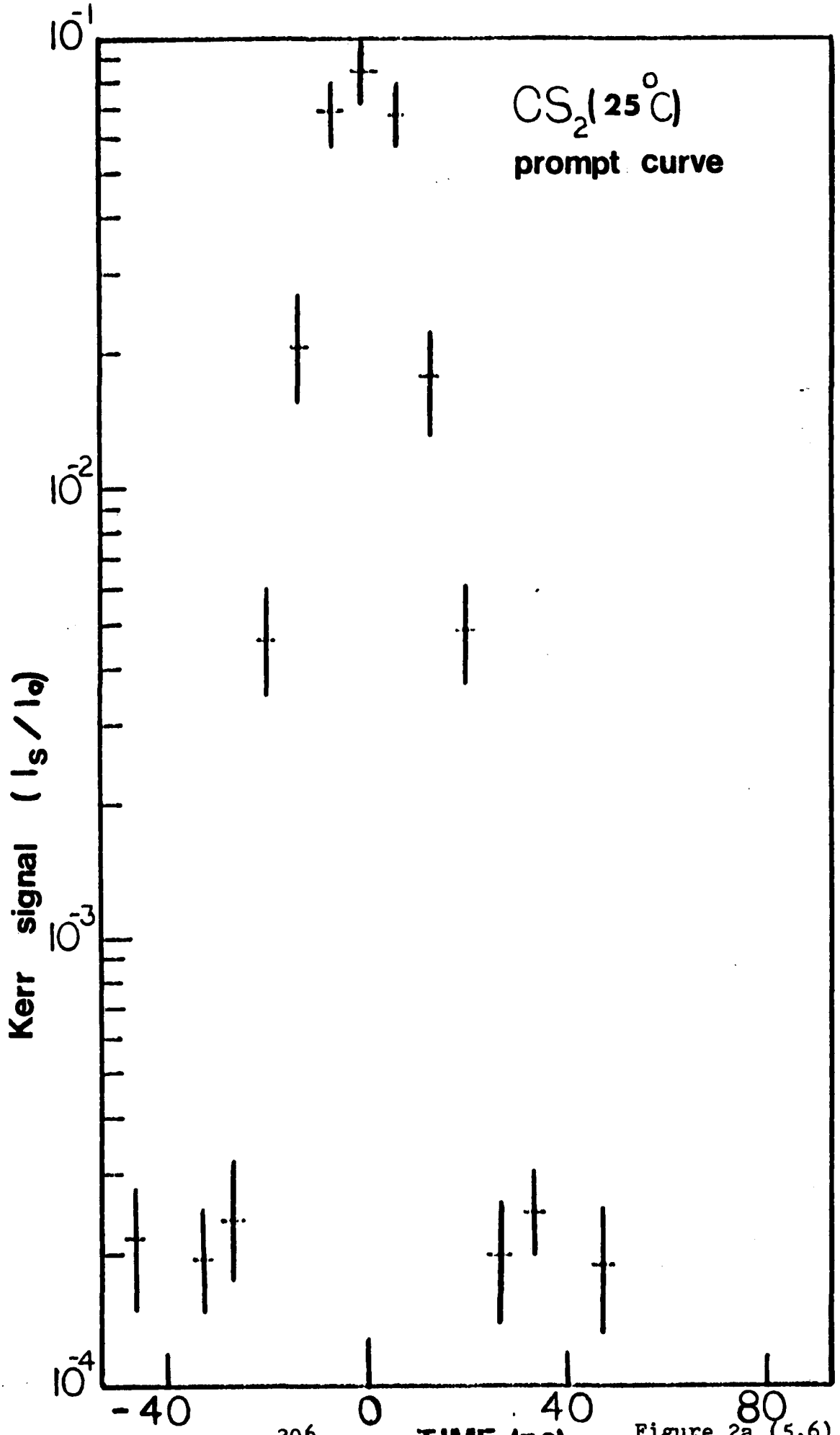
CS_2 (25°C)
prompt curve
Kerr signal (I_s / I_o)
10^{-1}
10^{-2}
10^{-3}
10^{-4}
-40
0
40
80
TIME (ns)

Figure 2a (5.6)

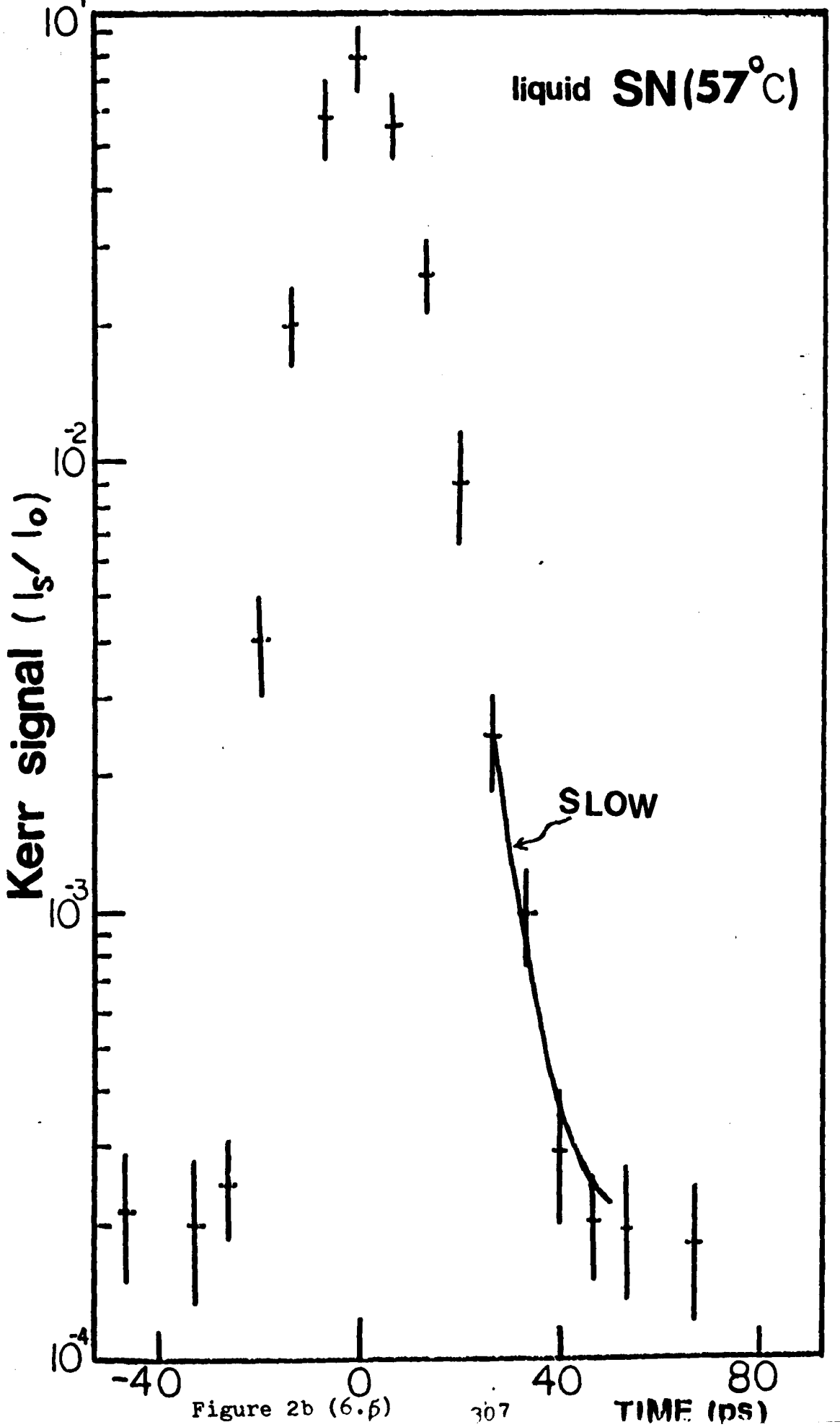
liquid SN(57°C)
SLOW
Kerr signal (Is / Io)
10-1
10-2
10-3
10-4
-40
0
40
80
TIME (ps)

Figure 2b (6.β)

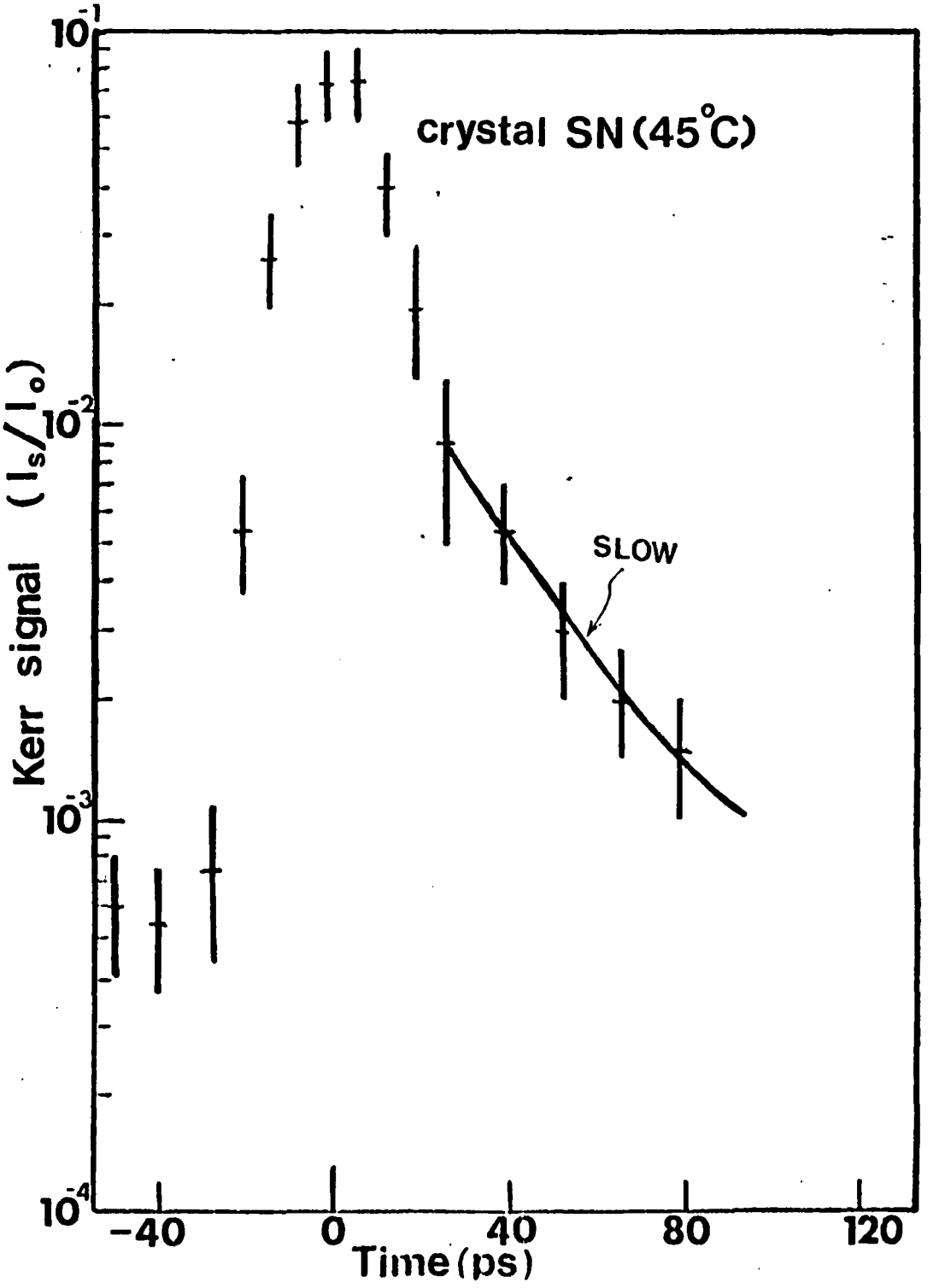
crystal SN (45°C)
SLOW
Kerr signal (I_s/I_o)
10^{-1}
10^{-2}
10^{-3}
10^{-4}
-40
0
40
80
120
Time (ps)

Figure 2c (6.5)

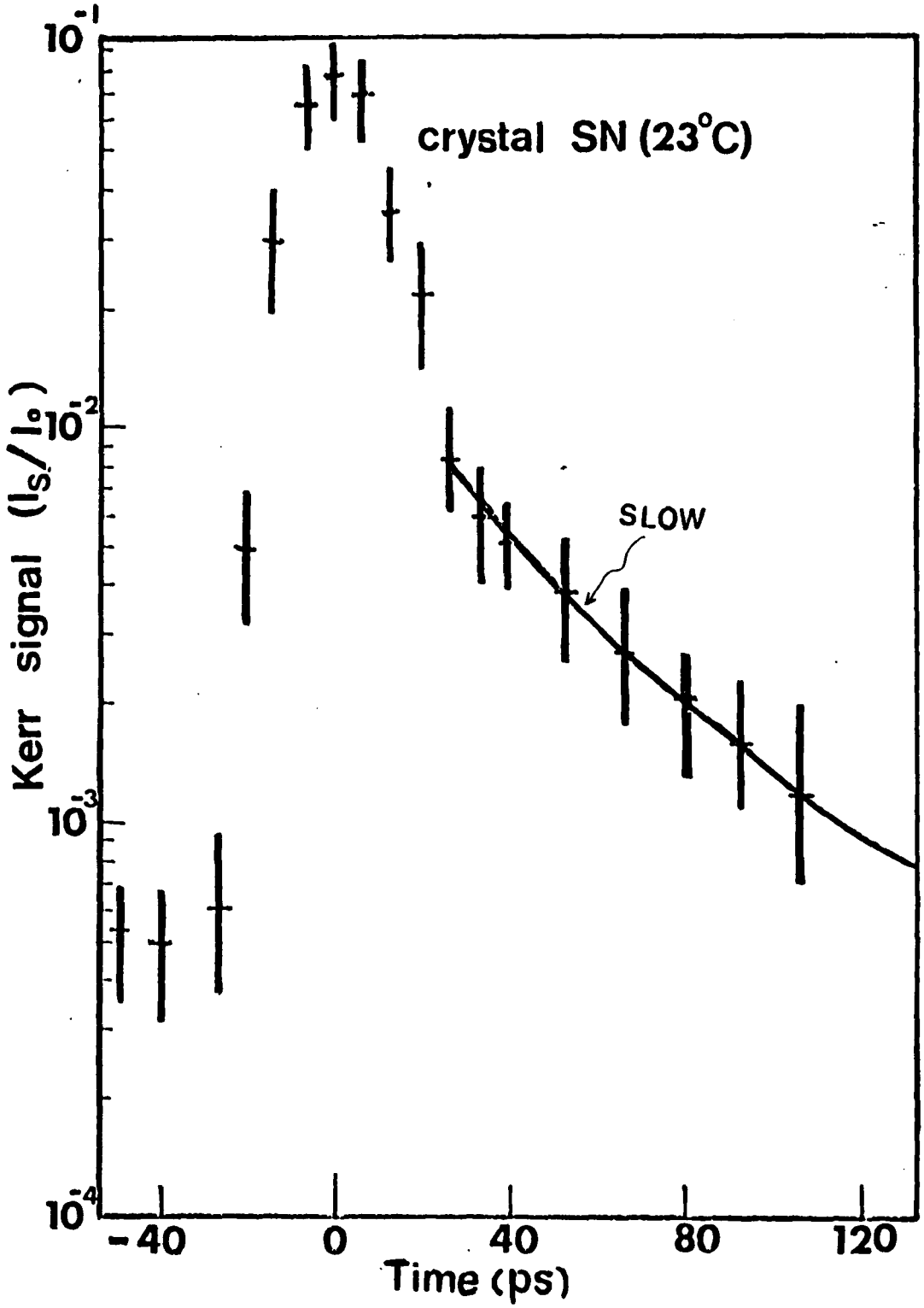
crystal SN (23°C)
SLOW
Kerr signal (I_S/I_o)
10^{-1}
10^{-2}
10^{-3}
10^{-4}
-40
0
40
80
120
Time (ps)

Figure 2d (6.5)

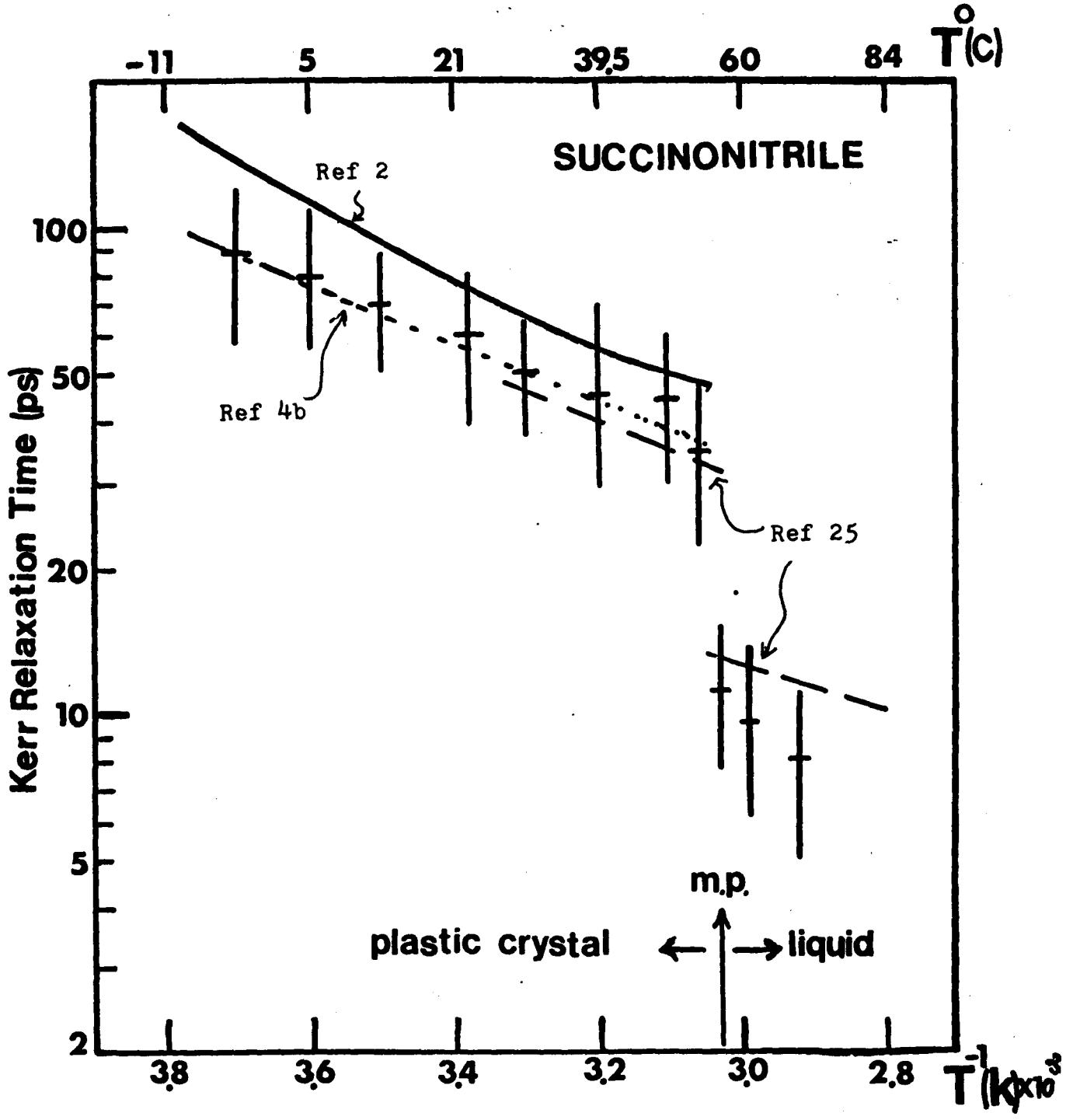
-11
5
21
39.5
60
84
T°(C)
SUCCINONITRILE
Ref 2
Ref 4b
Ref 25
Kerr Relaxation Time (ps)
100
50
20
10
5
2
m.p.
plastic crystal
liquid
3.8
3.6
3.4
3.2
3.0
2.8
T⁻¹(K)x10³

Figure 3(6.5)

6.6 Dynamical Optical Kerr Gate In Liquids

In this section, we report a detail analysis of the nonlinear index of refraction of the optical Kerr effect (OKE) by picosecond laser pulse. The peak transmitted signal of the OKE gate from various sample liquids are measured as a function of intensity of the orienting pulse, temperature, and concentrations of the Kerr solution. These measured values which correspond to the change of nonlinear index of refraction are interpretted by a calculation from the pulse shape in time and spatial distribution. There are also two major mechanisms operative in OKE of liquids[1-5] : a fast (electronic cloud distortion and molecular librations) and a slow (molecular reorientational motion) mechanisms. The optical Kerr constant of a liquid in the kinetic study from the mechanism of molecular reorientational motion is dependent on the inverse of temperature, its pair correlation factor, and function of relaxation time.

The experimental apparatus used in the optical Kerr gate is shown in figure 1 of chapter 5. The laser output train consists of about one hundred pulses were checked by a fast response photodiode and Tektronix 519 scope. Bad shots were eliminated from data. The output train is quite stable. Estimated fluctuation from shot to shot is within 10%.
The relaxation mechanism of the sample liquid used in the experiment is much faster than the round trip time of the laser cavity $\lesssim$ 7 ns (for simple liquids, it is generally true), then each laser shot roughly gives a measurement of statistical average from one hundred independent pulse experiments. For details of the experimental apparatus is given in section 5.1.

A dynamic range of the transmitted signal of about $5x10^3$ was obtained in this experiment. This range was determined by measuring the maximum value of the signal transmitted through the gate to the background noise signal. The noise is determined by blocking the intense orienting pulse or a lack of overalpping in time between the orienting and probe pulses.

By taking a photograph of the 0.53 um laser beam, the spatial distribution was found to be uniform with an approximate gaussian shape. Its full width at half maximum (FWHM) is about 1.5 cm. The 0.53 um which was not focused, travelled through a 2.5 mm aperture in front of the Kerr cell. The spatial distribution of 0.53 um laser with such an arrangement was nearly constant across the whole area of the aperture. The 1.06 um laser which was weakly focused into the Kerr gate. It has a beam diameter of about 5mm. For both beams, the condition $r_o \geq 2b$ (b=2.5mm) was achieved (see section 4.6A). In the calculation, the pulse profiles in time is described by either a gaussian or symmetrical exponential decay

The followingis adiscussion of the experimental results on the characteristics ofthe OKE;it is divided into subsections which parallel the subsections of the theory presented in section 4.6. In part A, the peak transmitted signal from CS_2 and NB gate were measured as a function of the intensity of the orienting 1.06 um laser pulse. The laser intensity was varied by inserting different neutral density filters (Hoya). In part B, the transmitted signal from a CS_2 gate at various length of sample Kerr cell were measured. In part C, the

wavelength of the probe laser pulse was varied in comparsion to the ratio of the transmitted signal. Self-phase modulation (SPM)[6] was used to generate different wavelengths. The continuum of few thousand wavenumbers (10 ps duration) was generated after sending the 0.53 um pulse through a ten centimeter long BK-7 glass. Stimulated Raman scattering[7] (SRS) of the 0.53 um laser pulse from ethanol or benzene liquid was also used. Appropriate filters and narrow band filters were placed in front of the detectors.

The concentration dependent experiment is discussed in part D. A Kerr non-active solvent (A), such as carbon tetrachloride (CT) (its transmitted signal through the gate is thousands time smaller than the Kerr active solute) is mixed with CS_2, nitrobenzene (NB), and m-nitrotoluene (mNT) at various concentrations. The total transmitted signal is proportional to the volume fraction of the solute or the total number of molecules in an unit volume. To avoid a complex calculation, the mixtures were chosen such that the mole fraction and volume fraction are approximately equal. Also the relaxation times were varied from different concentrations of the solute[8,9]. The peak transmitted signal at various relaxation times from NB and CT mixtures, and mNT and CT mixtures were measured at various concentrations.

In the temperature dependent part E, the sample was placed in a glass dewar with strain free windows. This has been described in section 5.3. All other experiments were performed at room temperature at 25 $\pm$ 2°C. In part F, the measured Kerr constant of twenty-nine neat liquids were measured and calibrated

with its power density of the orienting laser pulses. The phase retardation $\delta\phi(t)$ is less than one, so that the transmitted signal is quadratically proportional to the nonlinear index of refraction. These nonlinear index of refraction and separate bond strengths from a molecule are tabulated in tables 6.5 and 6.6, respectively.

6.6A Dependence On The Intensity Of The Orienting Laser Pulse For The Signal Transmitted Through The Kerr-Gate

The peak transmitted signal from the CS_2 and NB Kerr gate are plotted versus the power density of the orienting 1.06 um laser pulse, I_{2d}, in figures 6.6.1 and 6.6.2, respectively. Both the 1.06 um laser beam which is slightly focused into the sample gate and the probe 0.53 um laser beam have a constant spatial distribution within the 2.5 mm aperture.

In figure 6.6.1, the peak transmitted Kerr signal for the CS_2 gate varies quadratically with the mean power density of the 1.06 um laser pulse when I_{2d} is smaller than 0.1 GW/cm^2 ($\delta\phi \leq 0.45$). Above this pump intensity level, the transmitted signal increases slowly with the intensity of the orienting pulse. The signal reaches a maximum value of about 0.64 at I_{2d} = 0.48 GW/cm^2. When the intensity of the 1.06 um laser pulse raises above 0.48 GW/cm^2, the peak transmitted signal oscillates around the value of 0.5. The Kerr signal can be fitted by the equation 4.105 :

$$I_t(0) = \tfrac{1}{2} - \frac{\sin 2a}{4a} = \tfrac{1}{2} - \frac{\sin \delta\phi(0)}{2\,\delta\phi(0)} \quad , \qquad (6.6A\text{-}1)$$

where $a \equiv (\pi L/\lambda_1) n_2 I_{2d} \equiv \delta\phi(0)/2$. (6.6A-2)

The zero (0) in the above equations denotes the delay time of the Kerr gate is set at the peak transmitted signal (when $\tau_0 \ll \tau_\ell$). The power density of the orienting laser pulse I_{2d} is defined by,

$$I_{2d} \equiv E/(\sigma\tau \cdot A) \quad , \qquad (6.6A\text{-}3)$$

where E is the energy of a pulse (measured by an energy

meter), $\Delta\tau$ is the pulse duration (measured by TPF technique), and A is the effective area used in the Kerr gate (total area of aperture). Equation 6.6A-1 is obtained from equation 4.105 (at $\tau = 0$) with the assumptions of a constant spatial profiles ($r_o \geq 2b$) and a symmetrical exponential time profile of the laser pulses.

The solid line in figure 6.6.1a is a theoretical fit calculated from equation 6.6A-1, using the following parameters : $\lambda_1 = 0.53$ um, $\Delta\tau = 10$ ps, $A = (0.15\text{cm})^2\pi$, and $n_2(CS_2) = 2\text{x}10^{-11}$ e.s.u.. For example, at $I_{2d} \simeq 0.1$ GW/cm^2, equation 6.6A-1 can be approximated by :

$$I_t(0) = \tfrac{1}{2} - \tfrac{1}{2}\frac{1}{\delta\phi(0)}\left[\delta\phi(0) - \delta\phi^3(0)/3! + \cdots\right]$$

$$\simeq 1/3\ (\delta\phi(0)/2)^2 \quad . \qquad (6.6A\text{-}4)$$

The peak transmitted signal varies quadraitcally with $\delta\phi$ (0) or the intensity of the 1.06 um laser pulse. However, at $I_{2d} = 0.375$ GW/cm^2, we obtain $\delta\phi(0) = \pi$ (from equation 6.6A-2) and $I_t(0) = 0.5$ (from equation 6.6A-1); at $I_{2d} = 0.48$ GW/cm^2, we obtain $\delta\phi(0) = 1.25\pi$ and $I_t(0) = 0.61$ (the calculated maximum value of the transmitted signal from the CS_2 gate). The transmitted signal is no longer proportional to the intensity of the intense orienting pulse.

The transmitted signal $I_t(\tau)$ is the convolution of the time profile of the probe pulse and the reaction function of the gate $\sin^2\delta\phi(t)/2$ at a relative time τ (see equation 4.54). If $I_1(t)$ is a δ-function in time, then the transmitted signal will just behave as the function $\sin^2\delta\phi(t)/2$. For example, if $\delta\phi(\tau) = \pi$, then $I_t(\tau) = 1$; and if $\delta\phi(\tau) = 2\pi$, then the transmitted signal $I_t(\tau)$ is equal to zero. However, when

$I_1(t)$ has a duration comparable to the time variation of $\sin^2 \delta\phi(t)/2$, then the transmitted signal $I_t(\tau)$ will follow the convolution equation 4.105. The transmitted signal I_t can not be 1 or 0, as long as $\delta\phi \neq 0$. When $\delta\phi(0) \gg 1$, the peak transmitted signal oscillates around the value $\frac{1}{2}$ as preducted by equation 6.6A-1.

The phase $\delta\phi(t)$ is a time convolution of an intense orienting laser pulse and the molecular susceptibility tensor (equation 4.50). The time resolution of the Kerr gate can be affected by $\delta\phi$. At a very large value of $\delta\phi(0)$, the envelope of $I_t(\tau)$ is broadened. In the CS_2 gate, the relaxation time of the induced polarizability is much faster than the laser pulse duration, we can assume that $\delta\phi(t)$ follows the laser pulse shape - a function of the form $e^{-|t|/\tau_l}$ where τ_l is the pulse duration of the laser. When the power density of the orienting laser pulse increases, the condition $\delta\phi(0) \gg 1$ is reached. The maximum value of $\sin^2 \delta\phi(t)/2$ is 1, but the $\delta\phi(4\tau_l)$ is no longer negligible as it used to be (when $\delta\phi(0) \gg 1$). This cause a broadening in time response of the Kerr gate. An example of this phenomenon is shown in figure 6.6.1b. The FWHM of the CS_2 gate with $I_{2d} = 2 GW/cm^2$ is about twice as wide as the FWHM of the CS_2 gate with $I_{2d} = 0.08\ GW/cm^2$. The convolution function in equation 4.105 are graphically shown in figure 6.6.1c. The dotted line is the gate response function $\sin^2 \delta\phi(t)/2$ with the assumption $\delta\phi(0) = 6\pi$. The dashed line is the probing pulse function $e^{-|t-\tau|/\tau_l}$ at a delay time $\tau_l = 0$. The integrated area underneath the solid line is the measured

transmitted signal $I_t(0)$, which is a convolution of the above two functions. This area is measured to be about 0.5 and is the same as the calculated value from equation 6.6A-1. If the probe pulse $I_t(t-\tau)$ is translated from $\tau = 0$ to a relative time τ', then the convolution of $e^{-|t-\tau'|/\tau_l}$ with $\sin^2\delta\phi(t)/2$ gives the transmitted signal at τ' --$I_t(\tau')$.

One of the reason why the calculated curve (from equation 6.6A-1 does not perfectly fit the data of figure 6.6.1a is the use of a laser train. The measured value from one laser shot is the sum of about one hundred laser pulses. The pulses in the train have different pulse durations and energies. A difference in these two parameters will cause fluctuations from the average values for $\delta\phi$ (when $\delta\phi \gg 1$). The average result from about 100 pulses of a train will essentially gives the limitted value 0.5 ($\delta\phi \gg 1$).

For a pulse of gaussian shape in time is expressed by equation 4.96. If $\delta\phi < 1$ and $r_o \gg b$, equation 4.96 reduces to

$$I_t(t) \propto \delta\phi^2(t) \quad . \qquad (6.6A\text{-}5)$$

The transmitted signal still varies quadratically with the intensity of the orienting pulse. For $\delta\phi > 1$, there is no close form for equation 4.96 after the convolution integration. Numerically, at k = 1.87 ($\delta\phi(0) = 3.74$, $I_{2d} = 0.4$ GW/cm^2), the maximum value of the peak transmitted signal through the Kerr gate is 0.78. This value is larger than the actual measured value in this experiment (see figure 6.6.1a).

The peak transmitted signal of the NB Kerr gate versus the intensity of the orienting laser pulse is shown in figure 6.6.2a. The reorientational relaxation time of NB is 35 ps.

The induced index of refraction of NB is expressed as (from equation 4.50) :

$$\delta n(t) = n_2^e e^{-t/\tau_\ell} + n_2^o \left(\frac{2\tau_\ell \tau_o}{\tau_o^2 - \tau_\ell^2} e^{-t/\tau_o} + \frac{\tau_\ell}{\tau_\ell - \tau_o} e^{-t/\tau_\ell} \right), \quad \text{for } t \geq 0, \quad (6.6A\text{-}6)$$

There is no close form for the transmitted signal of the time convolution integration after inserting equation 6.6A-6, $\delta n(t)$, into equation 4.54 (see section 4.6A). Using the following parameters as $n_2^e = 3\times10^{-12}$e.s.u., $n_2^o = 25\times10^{-12}$e.s.u., and $\tau_o = 7\tau_\ell$; the peak transmitted signal at t_{max} is numerically calculated to be 0.75 at $I_{2d} = 2$ GW/cm^2. For $\delta\phi < 1$, the normal experimental case, the nonlinear index of refraction of NB gate has a fast rise time close to the laser pulse shape, τ_ℓ, and a decay time τ_o (after $t > 3\tau_\ell$). This is shown in figure 4.3 (page 130).

For $\delta\phi > 1$, the gate function $\sin^2\delta\phi(t)/2$ is shown in figure 6.6.2b (where $\delta\phi(0) = 6\pi$). It is a rather complex curve. Only after $t > 20\tau_\ell$, does the measured relaxation time correspond to the true reorientational time, τ_o. For $\delta\phi = 6\pi$, a strange mode pattern exists between the time of 0 to $15\tau_\ell$ which should be observable by using a fast probe pulse. This is pattern is more prominant when $\tau_o > \tau_\ell$ for intensity which is within the damage threshold of the window of the Kerr cell, e.g. NB. However, in order to reach $\delta\phi(0) = 6\pi$ in the NB gate, the intesnity of the laser pulse must exceed 8 GW/cm^2. This intensity is four times larger than we can obtain in the present setup.

6.6B Dependence of The Transmitted Signal To The Cell Length Of The Optical Kerr Effect

In figure 6.6.3, the optical Kerr effect for a 2 mm long CS_2 gate is displayed. Under our calculation, the Kerr signal profile is almost identical to the profile of the 1 cm long CS_2 gate (see figure 6.6.1a). This demonstrates the effect of dispersion is small in a 1 cm long cell. The CS_2 liquid has one of the largest index of refraction dispersion in the visible light region in comparison to the other organic liquids. The calculated time lag between 1.06 um and 0.53 um pulse through a 1 cm long CS_2 liquid is $\sim$ 4.6 ps[10]. This is smaller than the convolution of the laser pulse durations $\sim$ 10 ps. The dispersion effects between the two laser beams with different wavelengths were neglected at cell length L = 1cm, and within 1 ps error for L = 2cm. The FWHM of the Kerr gate is 16 ps at L = 2mm; 16 ps at L = 1cm; and 17 ps at L = 2cm. For cell length longer than 2 cm, the dispersion effects account for broadening of the gate profile[18]. To maintain the same phase retardation $\delta\phi < 1$ in the length dependent study, the laser intensity for the orienting pulse must be proportional reduced as the cell length is increased. When the cell length is increasing, the condition $\delta\phi \gg 1$ may be reached. The gate pattern is widened. This has been discussed in section 6.6A and displayed in figure 6.6.1c.

At the present intensity level of the orineting pulse, we can only observe a broaden peak region around the time of peak transmission with no noticeable mode pattern. We plan to investigate this mode in the near future with an amplified single pulse.

6.6C Dependence Of The Probe Wavelength Of The Transmitted Signal For The Optical Kerr Effect In Transparent Media

The measured wavelength dependence of the transmitted Kerr signal of the probe laser pulse for CS_2 gate is shown in figure 6.6.4. For $\delta\phi < 1$, $(I_t)^{\frac{1}{2}}$ is proportional to $\delta\phi$. The probe wavelength of 0.45 um and 0.63 um pulses were generated from stimulated Raman scattering from a 10 cm long ethanol liquid by the 0.53 um laser pulse. The other wavelengths were generated by the SPM or four waves mixing in glass. Filters were used to select the wavlength from the continuum. There is no absorption from electronic levels at any frequency used in this experiment. The transmitted signal is found to be inversely proportional to the square of the probe wavelength. Similar experiments have done by Shimizu[11] by using a continuous wave laser and a nanosecond laser pulse. The results are similar. Electronic and vibrational resonances effect can be investigated by the optical Kerr effect (see Raman induced Kerr effect)[12]. This can be used to investigate the kinetics of molecular vibrational motion.

6.6D Concentration and Relaxation Time Dependence Of The Nonlinear Index Of Refraction In Liquids

The nonlinear index of refraction of solutions of CS_2 in CT, NB in CT, and mNT in CT were measured and the results are displayed in figure 6.6.5. In these measurements, the phase retardation is smaller than one and the spatial profile of the laser beams are larger than the 2.5 mm diameter of the aperture.

In figure 6.6.5a, the square root of the peak transmitted signals of CS_2 in CT solvent gate are plotted versus the mole fraction of CS_2. Since the reorientational relaxation time is much faster than the laser pulse width (τ_o = 1.8 ps in neat liquid)[25], the molecules of CS_2 response to the laser pulse are immediately. The contribution to the transmitted signal from solvent CT is negligible for $0.1 \leq x_B$. In figure 6.6.5a, the square root of the peak (τ=0) transmitted signal, $I_t(0)$, follows a linear dependence :

$$(I_t(0))^{\frac{1}{2}} = C\, x_B\, n_{2B} \qquad \text{for } 0.1 \leq x_B \,, \quad (6.6D\text{-}1)$$

where C is a proportional constant, x_B is the mole fraction of CS_2, and n_{2B} is the nonlinear index of refraction of pure CS_2 liquid which is the sum of the electronic and molecular mechanisms.

In figure 6.6.5b, the peak transmitted signal from NB+CT, and mNT+CT Kerr gates are plotted versus the mole fraction of the solute molecules. The relaxation times of these mixtures decrease with respect to the concentration of the solute

molecules. The relaxation times of these mixtures decrease with respect to the concentration of the solute molecules. The nonlinear index of refraction in mixtures depend on both the electronic and molecular part. The square root of the peak transmitted signal is fitted by :

$$(I_t(0))^{\frac{1}{2}} = C' \cdot n_2^e + n_2^o/f(\tau_o) \cdot x_B \quad , \qquad (6.6D\text{-}2)$$

where C' is a proportional constant, x_B is the mole fraction of the solute, and n_2^e and n_2^o are the nonlinear index of refraction of the solute molecules arised from fast (electronic and molecular librational) and slow (molecular reorientational) mechanisms, respectively. The response function $f(\tau_o)$ depends on the inverse of the reorientational relaxation time[8](see figure 4.2). In the data fitting, n_2^e is assumed to be $0.12n_2^o$ in NB mixture and $n_2^e = 0.14n_2^o$ in mNT mixture. The solid lines in figure 6.6.5b are calculated from equation 6.6D-2. In this calculation, the profile of the laser pulses in time is assumed to be a symmetrical exponential decay. The contribution to the nonlinear index of refraction from the solvent CT is neglect.

The concentration dependence of the optical Kerr effect of CS_2, NB, and mNT shown in figures 6.6.5a and 6.6.5b, respectively, are in good agreement with the calculated values relating the mole fraction and measured relaxation time.

6.6E Temperature Dependence Of The Transmitted Signal On The Optical Kerr Effect In Neat Liquids

The square root of the peak transmitted signal from the Kerr gates of CS_2, NB, mNT, and C_2H_5I are plotted versus the temperature in figures 6.6.6a to 6.6.6d. As the temperature decreases, the transmitted signals for the CS_2 and C_2H_5I gates increase, while the transmitted signals for NB and mNT gates decrease. This data does not follow the simple equation 4.130 $\frac{1}{T f(\tau_o)}$. In figure 6.6.6b, the temperature dependence of the peak transmitted signal for NB in the optical Kerr effect is not identical to that of the steady state Kerr effect which monotonically increases as the temperature decreases. This is because the optical Kerr effect from equation 4.133 depends on $f(\tau_o(T))$ which governs the response of the peak amplitude of the transmitted signal to the relaxation time and the pulse duration. In the case of CS_2 and C_2H_5I, where $\tau_o \ll \tau_\ell$, then $I_t(0)$ increases when the temperature is lowered. However, because of the response function $f(\tau_o)$ for the NB and mNT gates where $\tau_o > \tau_\ell$, their behavior are reverse (see figure 6.6.6b).

Instead of assuming a temperature independent pair correlation factor which was assumed in the data reduction in section 6.2, a temperature dependent Arrhenius behavior for the pair correlation factor, J, is now required to fit the data. This was introduced by Kielich [14-16].

The data in figure 6.6.6 were fitted by equation 4.133 :

$$(I_t(0))^{\frac{1}{2}} = n_2^e + n_2^o \; [1 + J(T)][T\, f(\tau_o(T))]^{-1} \; , \quad (6.6E\text{-}3)$$

where $J(T) = A\, e^{E/RT}$. (6.6E-4)

The solid lines in figure 6.6.6 were calculated by choosing a suitable ratio of n_2^e to n_2^o, and parameters A and B in the temperature dependent pair correlation function of J(T). The fraction of the electronic mechanism in the total n_2 for CS_2 and C_2H_5I is about 10% and for NB and mNT is about 13%. These values are close to that obtained by other independent measurements[1,2]. The pair correlation factor J(T) at T = 25°C for NB is 1.62 and for mNT is 1.61. These values are in good agreement to the values deduced from the concentration dependent measurements (f_{NB} = 1.3[17] and f_{mNT}[18]). After introducing the temperature dependent pair correlation factor, the measured reorientational relaxation times of NB and mNT in the section 6.2 reasonably fits to the theoretical values within the experimental error. These measurements suggest a temperature dependent pair correlation factor J(T).

6.6F The Nonlinear Index Of Refraction Of Liquids Measured By Picosecond Laser Pulses

The nonlinear index of refraction for twenty-nine neat liquids measured at 25°C by the picosecond optical Kerr effect are listed in table 6.5. The absolute values are estimated from the n_2 of CS_2 ($=2\times10^{-11}$ e.s.u.). Using n_2 of CS_2 as the standard value, the values of n_2 for the other liquids were calculated from the following equation :

$$n_{2i} = \left\{ \left(\frac{I_p^{(i)}}{I_p^{(CS_2)}} \right)^{\frac{1}{2}} y_e + \left(\frac{I_p^{(i)}}{I_p^{(CS_2)}} \right)^{\frac{1}{2}} (1-y_e) \frac{f_i(\tau_o)}{f_{CS_2}(\tau_o)} \right\} \times n_2(CS_2) \frac{I_{1.06}^{(i)}}{I_{1.06}^{(CS_2)}} , \qquad (6.6F\text{-}1)$$

where i represent the i-th kind of liquid, $I_p^{(i)}$ is the peak transmitted signal of the Kerr gate with (i) liquid, y_e is the fraction of n_2 arising from the fast mechanisms, $I_{1.06}^{(i)}$ os the intensity of the orienting laser pulse used for the i-th kind of liquid in the experiment to induce the birefringence, and $f_i(\tau_o)$ is a response function of i-th liquid. For example, take the carbon tetrachloride gate, we use $y_e = 0.54$[1]. Moreover, if $\tau_e \gg \tau_o$, we can assume $f(\tau_o) = 1$ and there is no need to distinguish the response for the slow and fast mechanisms. Most of the liquids in table 6.5, y_e is not known. Therefore, these data are fitted by a simplified equation for the overall n_{2i} by :

$$n_{2i} = \left[\frac{I_p(i)}{I_p(CS_2)} \right]^{\frac{1}{2}} n_2(CS_2) \frac{I_{1.06}(i)}{I_{1.06}(CS_2)} . \qquad (6.6F\text{-}2)$$

These value are the peak amplitude value from a picosecond pulse excited Kerr gate. For those liquids in table 6.5 with a sign (*), we have observed an appreciate slow relaxation process. Extrapolating the slow decay curve to the zero time, we can obtain the ratio y_e. The overall n_{2i} is fitted by equation 6.6F-1.

The hyperpolarizability of bonds (γ) displayed in table 6.6 is deduced from those measured values of the nonlinear indices of refraction in table 6.5. It contains all the nonlinear contributions from electronic, librational, and reorientational motions. The strength of the Kerr constant depends on the molecular shape. The followings are some empirical rules. The induced birefringence is small for a spherical symmetric single covalent bond, such as C-H and O-H. If the two atoms are quite different in size, such as C-I or C-Br, its hyperpolarizability is larger than those bonds with two similar size of molecules such as C-O or C-H. There is a simple additive law to estimate the size of n_2 by adding each bond of a molecule in a vector sum[19-23]. If the whole molecule is spherical symmetrical such as CCl_4 or CH_4, then the total induced birefringence is small. The Kerr constant from double valence bond is larger than the singel bond. This is due to the asymmetry of each individual bond about a molecule.

The bond additivity rule[22,23] for unsubstituted alkanes (C_nH_{2n+2}) is written by

$$\gamma(C_nH_{2n+2}) = (n-1)\ \gamma(C\text{-}C) + (2n+2)\ \gamma(C\text{-}H)\ , \quad (6.6F\text{-}3)$$

where $\gamma = n_2/Nf$, N is the numer of molecules per unit volume, and f is a local field correction factor[24].

This equation can be generalized to most materials list in table 6.5. For CCl_4, the value of n_2 is much smaller than the simple addition of four C-Cl bond strengths. This is due to the symmetry of bonds of the CCl_4 molecules, such that the vector addition cancells out parts of the bond strength.

In conclusion, calculations are used in this section 6.6 to clairfy the experimental research of the optical Kerr effect. The time profile of the laser pulses is assumed a symmetric exponential decay in the data fitting. The spatial distribution of the laser beams is assumed to be gaussian. In this experiment, the spatial profile of the laser beams are uniform across the Kerr gate because of the use of an aperture with its diameter being much smaller than the waist of the laser beams. For $\delta\phi < 1$, the transmitted signal of the Kerr gate is proportional to the square of the orienting field. While for $\delta\phi \gg 1$, the transmitted signal follows a complex convolution function of the laser fields and the relaxation process. A complex structure is predicted. When the length of the Kerr cell is less than or equal to 1 cm, the group velocity dispersion effect is negligible. Without absorption of the liquid of the Kerr gate, the transmitted signal is measured to be inversely proportional to the square of the wavelength of the probe light. The peak transmitted siganl of the Kerr gate depends on the inverse of the relaxation time of the sample solution and the square of the concentration of the (Kerr-active) solute molecules. By measuring the Kerr constant at various temperature, the pair correlation factor of the liquid is deduced. This suggests a temperature dependent correlation function. The values agree reasonably well to that deduced from the concentration dependent experiments. The measured nonlinear index of refraction can be fitted by the sum of the molecular hyperpolarizability of each bond. We hope these calculations and measurements of the optical Kerr effect can yield more information in studying the molecular relaxation processes in liquids.

Table 6.5 Nonlinear Index Of Refraction In Liquids

* : with a noticeable slow decay component off the prompt gate

Liquid	Chemical Formula	n_2 (10^{-13} e.s.u.)
carbon disulfide	S = C = S	200
carbon tetrachloride	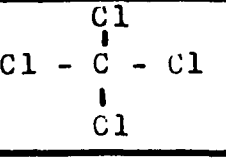	5.3
methanol	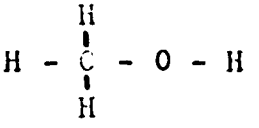	2.2
ethanol	CH_3CH_2OH	2.5
1-propanol	$CH_3(CH_2)\ CH_2OH$	2.7
1-octanol*	$CH_3(CH_2)_6CH_2OH$	4.1
1-decanol*	$CH_3(CH_2)_8CH_2OH$	3.9
cyclohexane	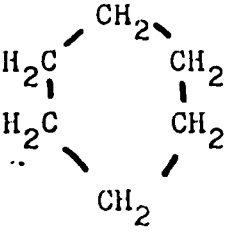	3.9
pentane	$CH_3(CH_2)_3CH_3$	4.2
octane	$CH_3(CH_2)_6CH_3$	5.5
decane*	$CH_3(CH_2)_8CH_3$	5.3
hexadecane*	$CH_3(CH_2)_{14}CH_3$	5.5
water	H - O - H	1.3
acetone	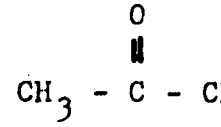	7.7
formic acid	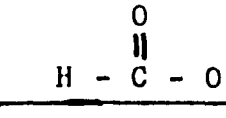	10

(continue)

(table6.5 continued)

glycerin	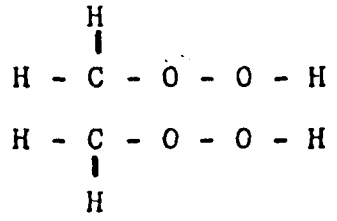	2.5
1,2-dichloroethane	$CH_3CH\ Cl_2$	12.5
chloroform	$HC\ Cl_3$	10.6
1,1,1-trichloroethane	CH_3CCl_3	8.2
trichloroethyene	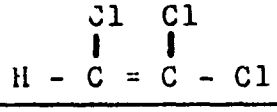	36.1
ethylene bromide	BrC_2H_4Br	34.3
ethyl iodide	CH_3CH_2I	22.6
benzene	(C_6H_6) 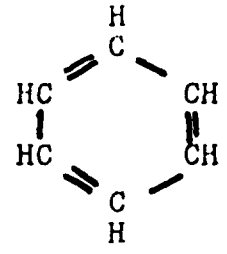	60
toluene	$C_6H_5CH_3$	60
nitrobenzene*	$C_6H_5NO_2$	280
m-nitrotoluene*	$C_6H_4NO_2CH_3$	300
salol*	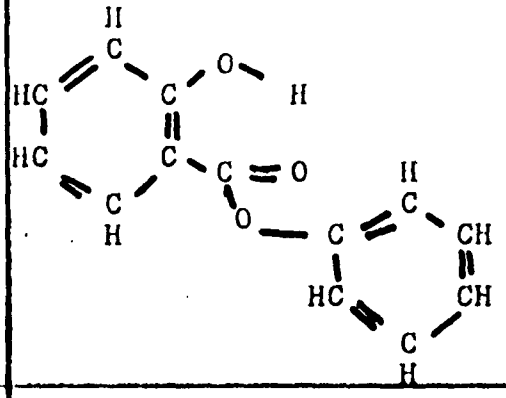	460
acetonnitrile	$CH_3C\equiv N$	9.5
succinonitrile*	$(CH_2CN)_2$	25

Table 6.6 Molecular hyperpolarizability of individual bond

bond	γ (arbitrary unit)
C - C	4
C - H	4
C - O	4
C - N	4
C - Cl	40
C - Br	160
C - I	220
O - H	2
C = C	240
C = O	145
C = S	700
N = O	950
C ≡ N	80

(γ is the sum of all possible mechanisms that contribute to the hyperpolarizability)

References

1. R.W. Hellwarth, A. Owyoung, and N. George, Phys. Rev., A4, 2343, (1971).
   A. Owyoung, IEEE J. Quantum Electronics, QE-9,1064,(1973).
   A. Owyoung, Ph.D. Thesis, (California Institute Technology,1972).
2. K. Sala and M. Richardson, Phys. Rev., A12, 1036, (1975).
3. M.A. Duguay and J. W. Hansen, Appl.Phys.Lett.,15,192,(1969).
4. P.M. Rentzepis, M.R. Topp, R.R. Jones, and J. Jortner, Phys. Rev. Lett., 25, 1742, (1970).
5. P.P. Ho and R.R. Alfano, J. Chem. Phys., 67, 1004, (1977).
6. R.R. Alfano and S.L. Shapiro, Phys: Rev.Lett.,24, 1219,(1970).
7. N. Bloemberger, Phys. Teachers, 35, 989, (1967).
8. P.P. Ho, W. Yu, and R.R. Alfano, Chem.Phys.Lett.,37,91,(1976).
9. P.P. Ho and R.R. Alfano, Chem. Phys. Lett., 50,74, (1977).
10. M.R. Topp and G.C. Orner, Opt. Comm., 13, 276, (1975).
11. F. Shimizu, J. Phys. Soc. (Japan), 22, 1070, (1967).
12. D. Heiman, R.W. Hellwarth, M.D. Levensen, and G. Martin, Phys. Rev. Lett., 36 ,189, (1976).
13. S.L. Shapiro and H.P. Broida, Phys. Rev.,154, 129,(1967).
14. G.K.L. Wang and Y.R. Shen, Phys. Rev., A10, 1277, (1974).
15. T.D. Glerke and W.H. Flygare, J. Chem.Phys., 61,2237,(1974).
16. S. Kielich, Acta. Phys. Polon., 30, 683, (1966).
    S. Kielich, J. Chem. Phys., 46, 4090, (1967).
17. P.P. Ho and R.R. Alfano, J. Chem. Phys., (to be published).
18. G.R. Alms, D.R. Bauer, J.I. Brauman, and R. Pecora, J. Chem. Phys., 59, 5310, (1973).

19. C.C. Wang, Phys. Rev., B2, 2045, (1970).

20. K.C. Denbigh, Trans. Faraday Soc., 36, 936, (1940).

21. A.P. Buckingham and B.J. Orr, Trans. Faraday Soc., 65, 673, (1969).

22. A.F. Levine and C.H. Betha, J. Chem. Phys., 63, 2666, (1975).

23. J.F. Ward and I.J. Bigio, Phys. Rev., A11, 60, (1975).

24. D. Kivelson and S.J. Tsay, Mol. Phys., 29, 29, (1975).

25. J.A. Giordmaine, P.M. Rentzepis, S.L. Shapiro, and K.W. Wecht, Appl. Phys. Lett., 11, 216, (1967).

26. Landolt-Bornstein Tables, (Spring Verlag, Berlin, V8, 1969).

Figure Captions

Figure 6.6.1a The measured peak transmitted signal (at $\tau = 0$) of the optical Kerr gate of liquid CS_2 is plotted versus the average orienting laser (1.06um) intensity. I_{2d} is estimated from the measured values of: the pulse energy E is measured by a calibrated joule meter, and the pulse duration time is measured by TPF[25]. The solid line is a theoretical fit from equation 6.6A-1.

$$I_t(0) = \tfrac{1}{2} - \frac{\sin 2a}{4a} ,$$

where $a \equiv (\pi L/\lambda_1)\, n_2\, I_{2d} \equiv \tfrac{1}{2}\,\delta\phi(0)$, and L = 1cm, λ_1 = 0.53 um, and $n_2 = 2\times10^{-11}$ e.s.u..

Figure 6.6.1b The transmitted signal $I_t(\tau)$ through the CS_2 gate of 1 cm length at various delay time τ for different orienting field intensities; + : I_{2d} = 2 GW/cm^2 ($\delta\phi = 6\pi$)
o : I_{2d} = 0.08 GW/cm^2 ($\delta\phi = 0.24\pi$).
The FWHM of the gate for I_{2d} = 2 GW/cm^2 is 34 ps, and for gate with I_{2d} = 0.08 GW/cm^2 is 16 ps. The rise time and decay time in both cases are about 3 ps.

Figure 6.6.1c A theoretical graphical convolution of the probe pulse ($e^{-|t|/\tau_p}$) and gate function ($\sin^2\delta\phi(t)/2$) at $\delta\phi(0) = 6\pi$ at delay time $\tau = 0$. The dashed line is the probe pulse. The dotted line is the gate function. The area under the solid line is the transmitted signal detected by a photo detection system at $\tau = 0$.

Figure 6.6.2a The measured peak transmitted signal for NB (at $\tau = 0$) is plotted versus the intensity of the 1.06 um laser. When $I_{2d} < 0.5$ GW/cm^2 ($\delta\phi < 1$), the transmitted signal is quadratically dependent on I_{2d}.

Figure 6.6.2b The gate response function $\sin^2\delta\phi(t)/2$ for NB is plotted versus the time in unit of τ_ℓ at the intensity of $I_{2d} = 8$ GW/cm^2 ($\delta\phi(0) = 6\pi$). The solid line is calculated from the equation :

$$\delta\phi(t) = \frac{\pi\delta n(t)}{\lambda_1} \qquad I_{2d} = \begin{cases} 29.5\, e^{-t/7\tau_\ell} - 17\, e^{-t/\tau_\ell} & \text{for } t \geq 0, \\ 12.5\, e^{t/\tau_\ell} & \text{for } t < 0. \end{cases}$$

Figure 6.6.3 The transmitted signal through a 2mm long CS_2 Kerr gate at various delay times ($I_{2d} = 0.2$ GW/cm^2). The FWHM of the gate is about 16 ps, and the rise time and fall time of the gate are about 3 ps. By assuming a gaussian time profile laser pulse, the solid line is a fit from equation 4.92 :

$$I_t(t) = (0.2)^2\, e^{-t^2/10^2} + 1.5\text{x}10^{-4} \quad .$$

Figure 6.6.4 The square root of the peak transmitted signal I_t through a 1 cm long CS_2 Kerr gate is plotted versus the wavelength of the probe laser pulses. Each data in the wavelength axis is about 200 cm^{-1} wide due to the bandwidth of the narrow band filters used in front of the detector.

Figure 6.6.5 The square root of the peak transmitted signal I_t from the mixed binary liquids are plotted versus the mole fraction of the solute (x_B). The contribution from the nonlinear index of refraction of the solvent CCl_4 is negligible for $x_B \geq 0.1$. The solid line is a calculated value for data fitting.

(a) CS_2 gate : $(I_t)^{\frac{1}{2}} = C\, x_B\, n_2 = 0.3\, x_B$.

(b) NB gate + : $(I_t)^{\frac{1}{2}} = 1.2\times10^{+10}\left[30\times10^{-13} + \frac{250\times10^{-13}}{f(\tau_o)}\right] x_B$.

mNT gate o : $(I_t)^{\frac{1}{2}} = 1.2\times10^{10}\left[30\times10^{-13} + \frac{210\times10^{-13}}{f(\tau)}\right] x_B$.

The response function $f(\tau_o)$ is shown in figure 4.2b.

Figure 6.6.6 The square root of the peak transmitted signal of various Kerr gates is plotted versus the temperature. The solid line is a data fitted curve of I_t from equation 6.6E-1. $f(\tau_o)$ is the response function displayed in figure 4.2b. The resonse function for C_2H_5I is assumed to be one in this fitting. The dashed line in (b) is measured by d.c. Kerr effect[26].

(a) CS_2 gate : $(I_t)^{\frac{1}{2}} = 16\,(1 + 0.3\, e^{400/T})/T\; f(\tau_o(T)) + 0.01$,

(b) NB gate : $(I_t)^{\frac{1}{2}} = 40\,(1 + 0.3\, e^{500/T})/T\; f(\tau_o(T)) + 0.03$,

(c) mNT gate : $(I_t)^{\frac{1}{2}} = 38\,(1 + 0.3\, e^{-500/T})/T\; f(\tau_o(T)) + 0.04$,

(d) C_2H_5I gate : $(I_t)^{\frac{1}{2}} = 12.5\,(1 + 0.3\, e^{400/T})/T \quad + 0.01$.

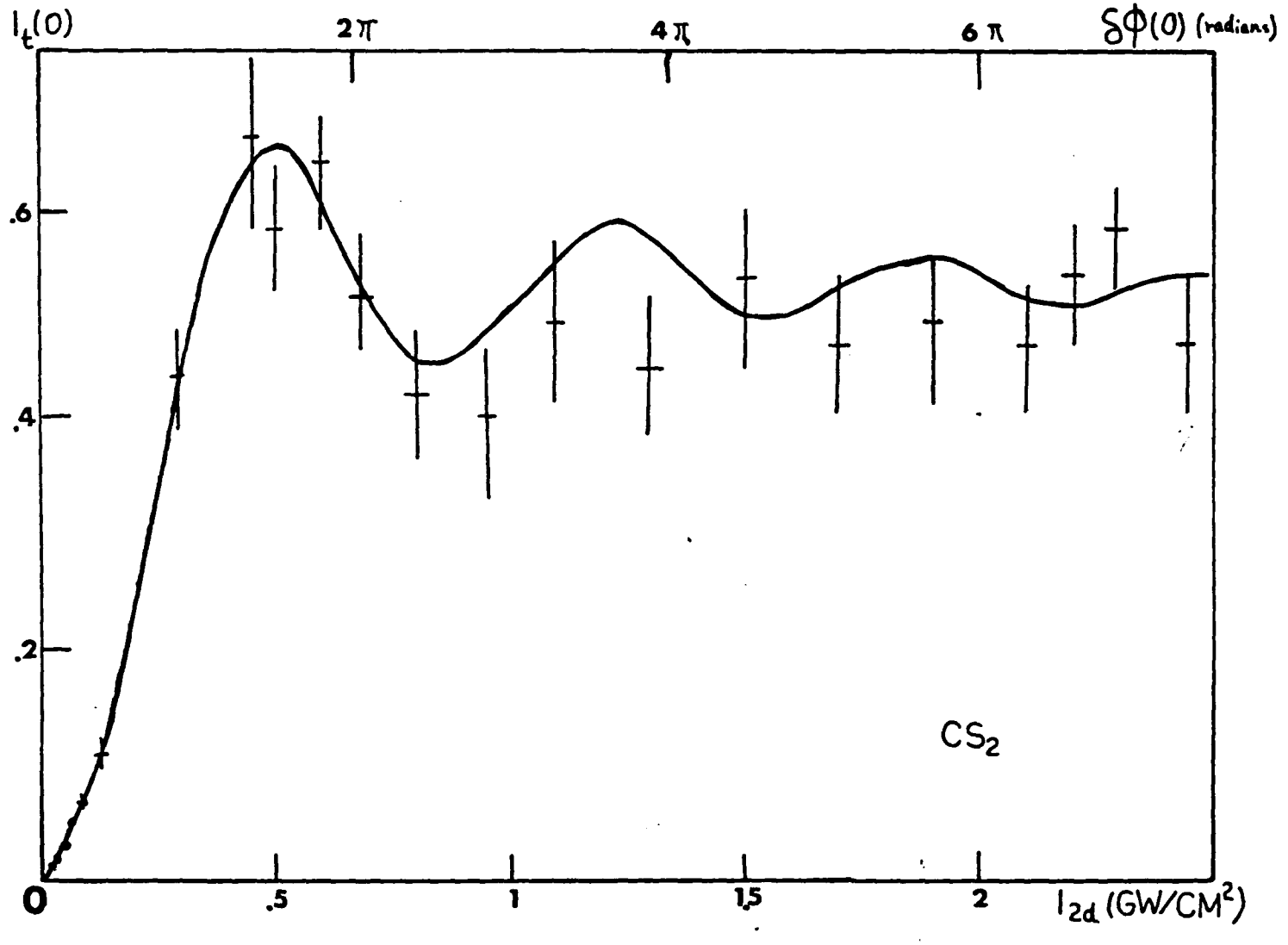

Figure 6.6.1a

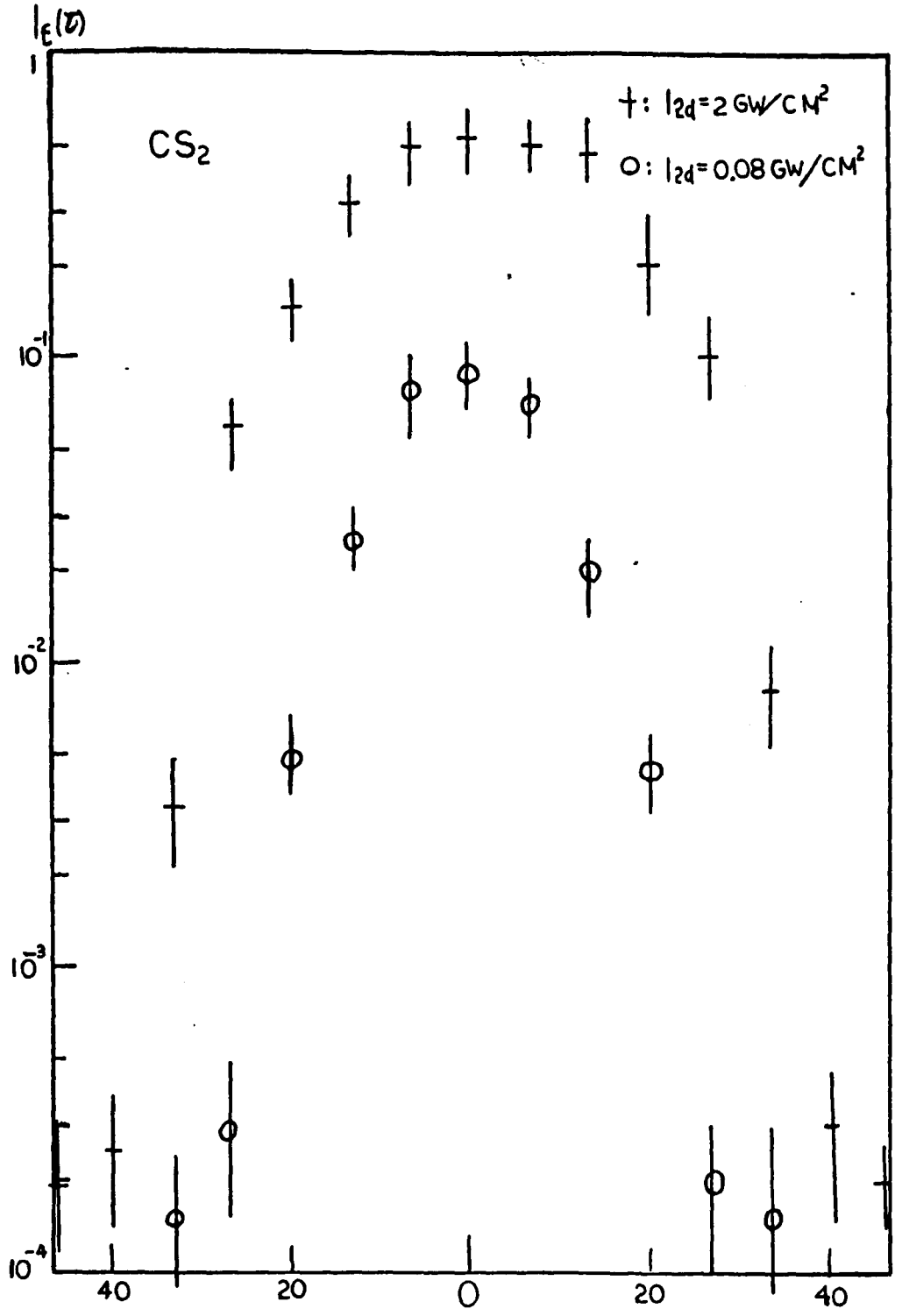
$I_E(\tau)$
1
10^{-1}
10^{-2}
10^{-3}
10^{-4}
CS_2
†: I_{2d}=2 GW/CM^2
O: I_{2d}=0.08 GW/CM^2
40
20
0
20
40

Figure 6.6.1b

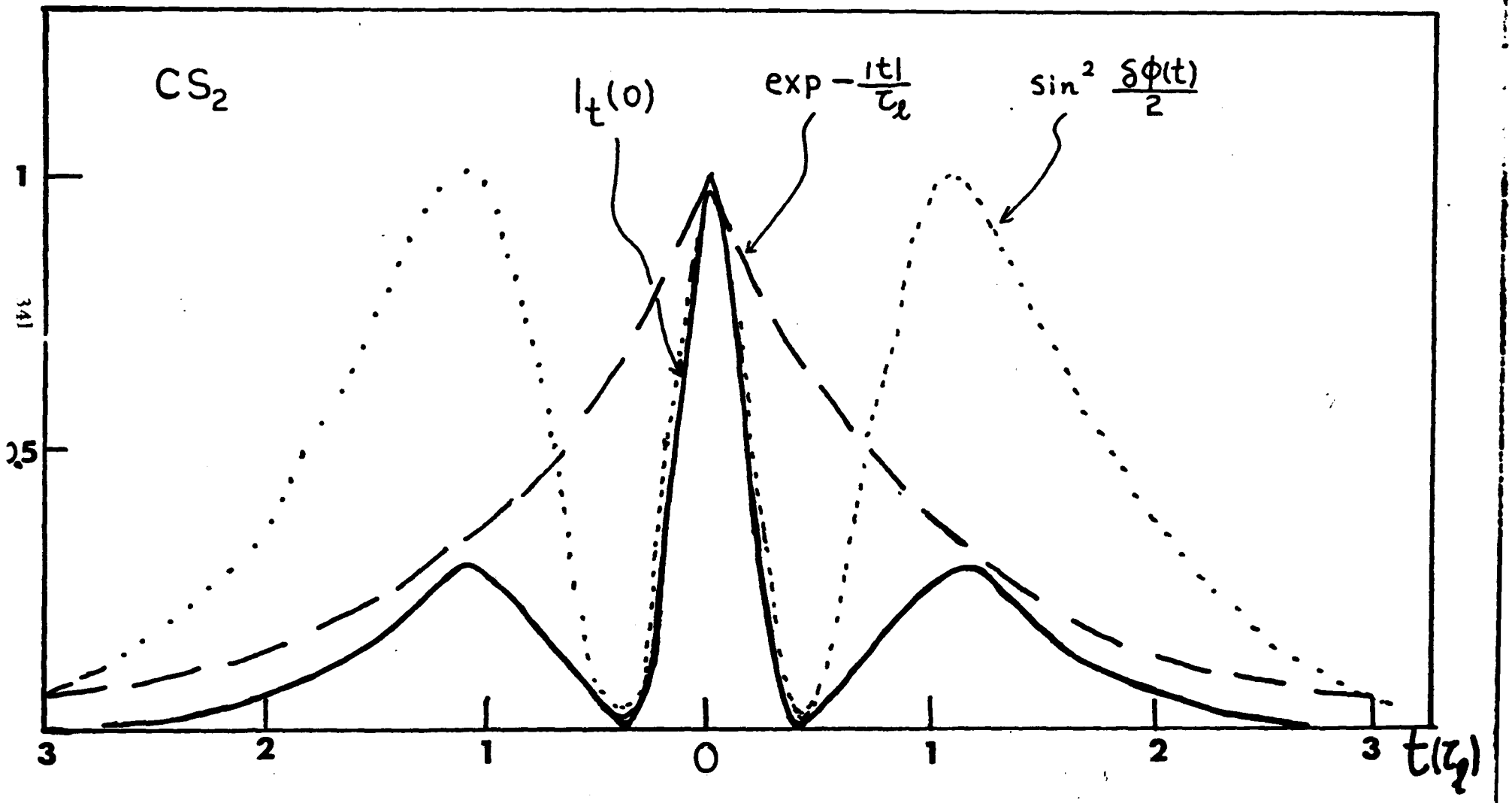
CS2
$I_t(0)$
$\exp -\frac{|t|}{\tau_l}$
$\sin^2 \frac{\delta\phi(t)}{2}$
1
.5
3
2
1
0
1
2
3
$t(\tau_l)$

Figure 6.6.1c

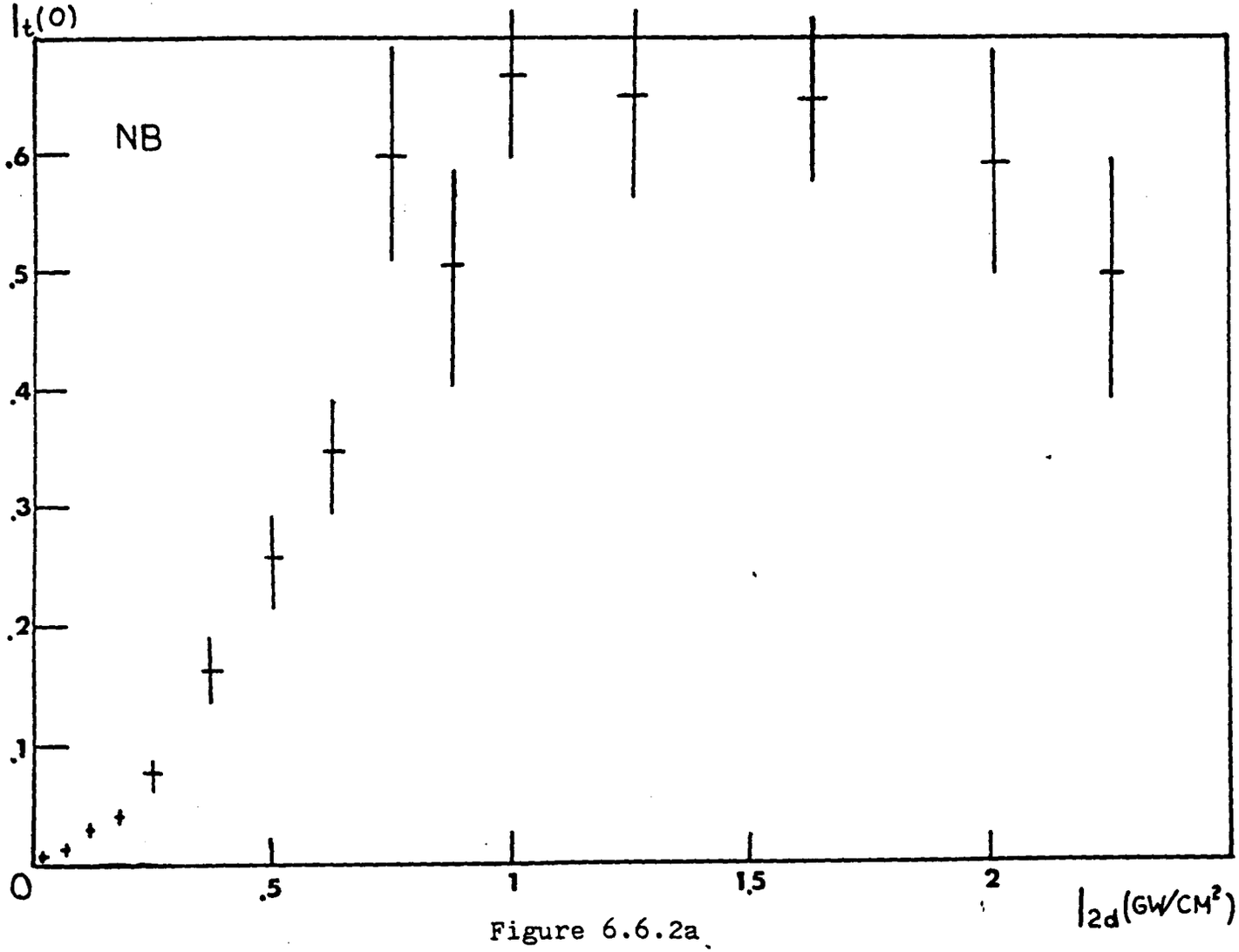

Figure 6.6.2a

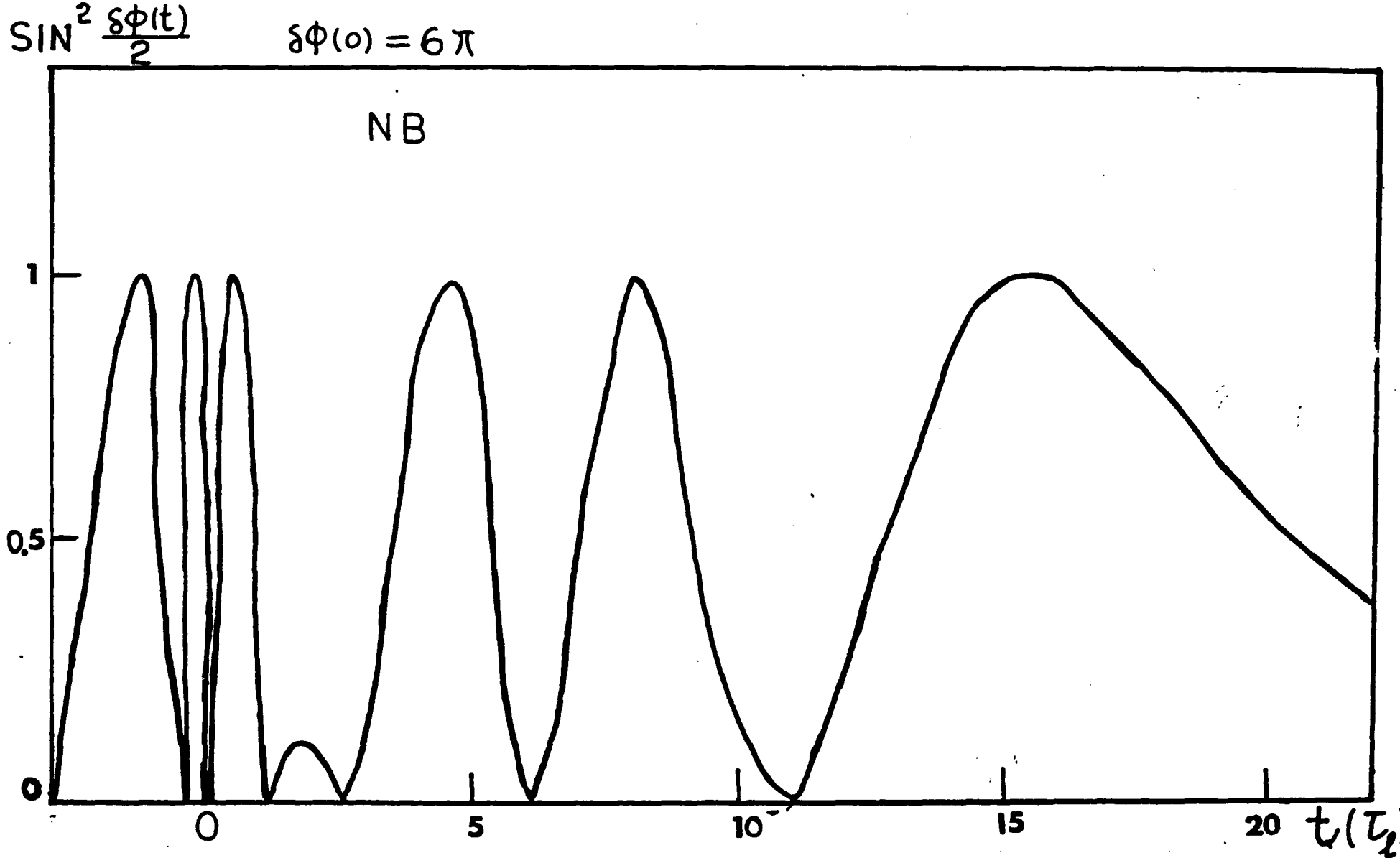

Figure 6.6.2b

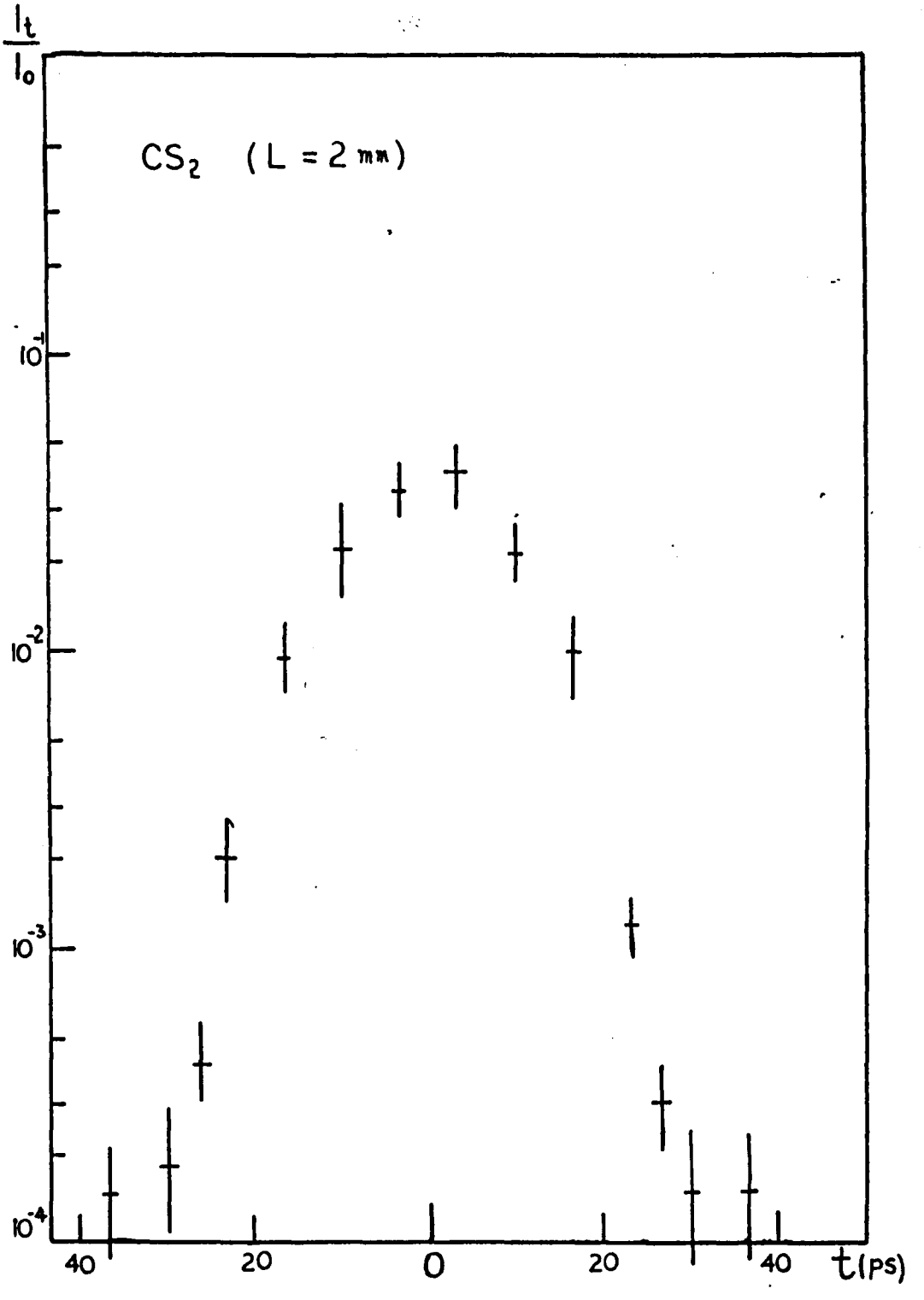

Figure 6.6.3

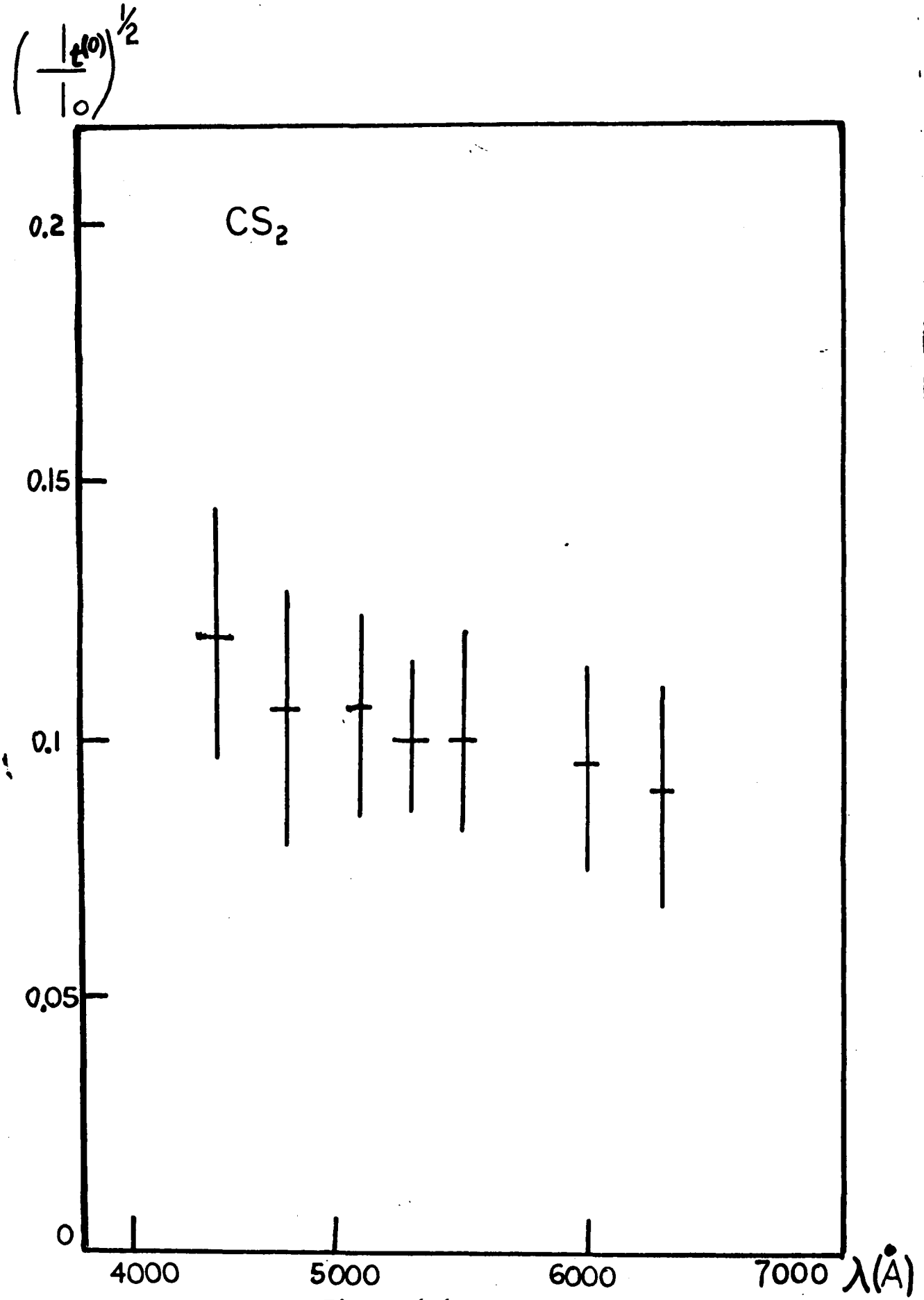
$\left(\frac{I_t(0)}{I_0}\right)^{1/2}$
CS_2
0.2
0.15
0.1
0.05
0
4000
5000
6000
7000
λ(Å)

Figure 6.6.4

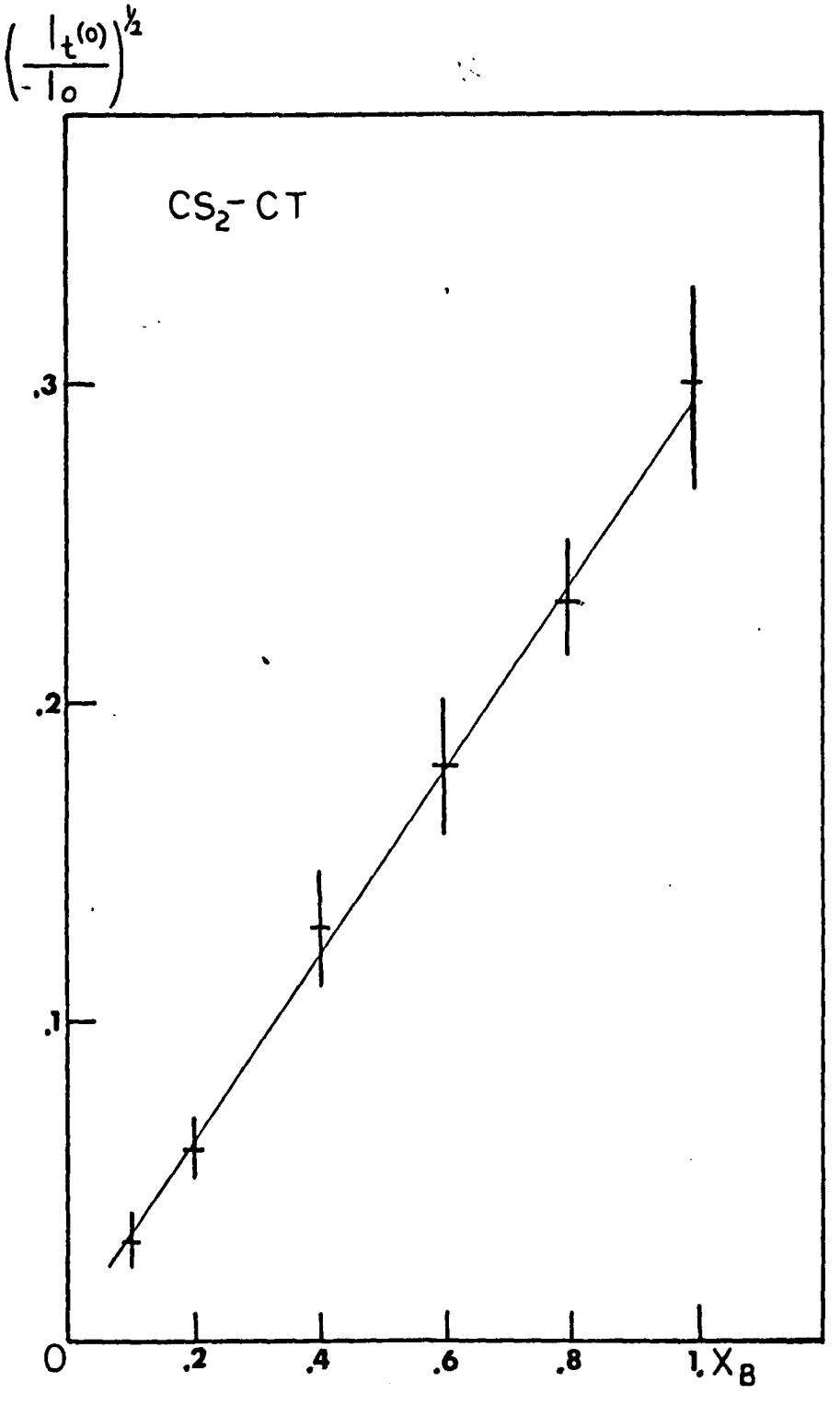

Figure 6.6.5a

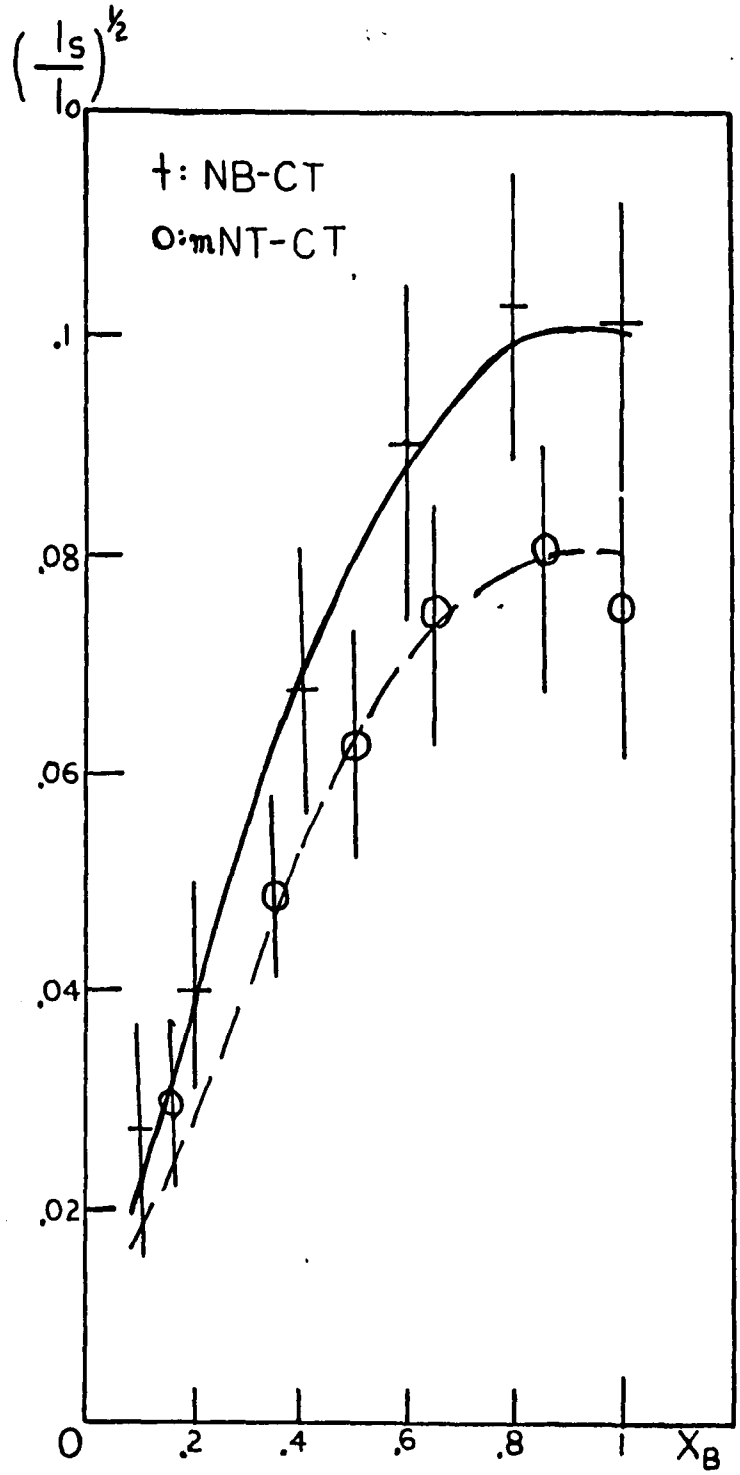

Figure 6.6.5b

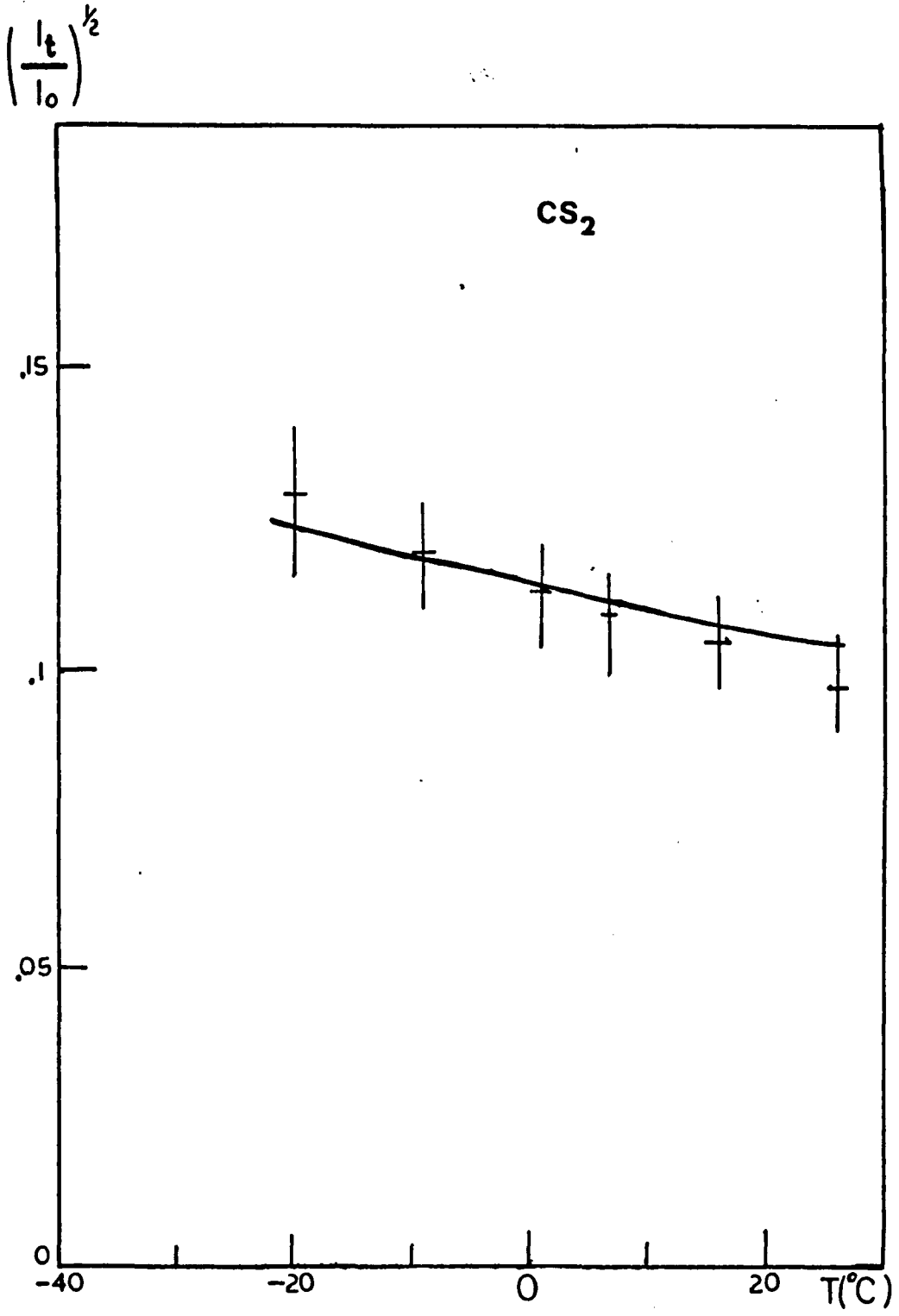

Figure 6.6.6a

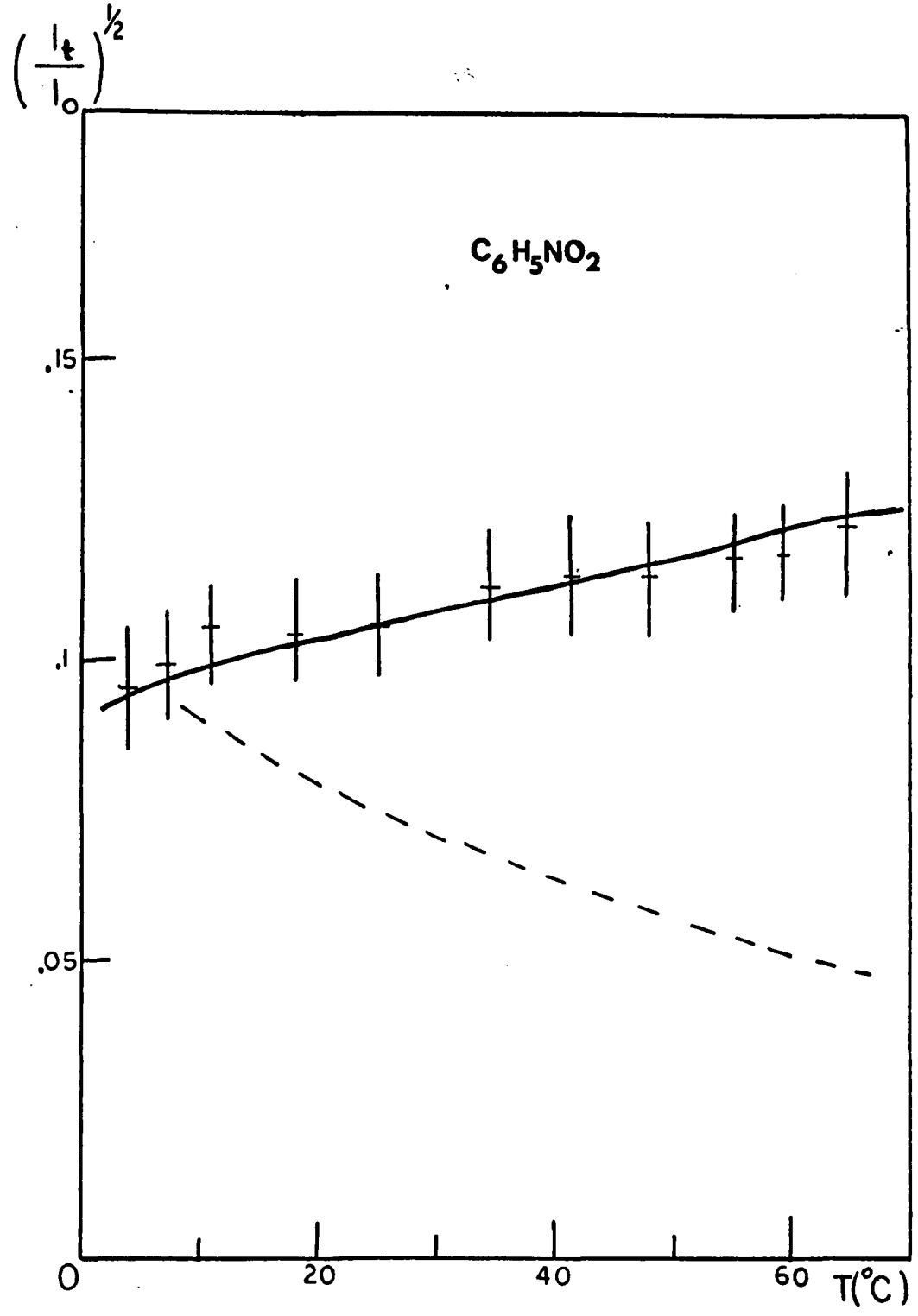

Figure 6.6.6b

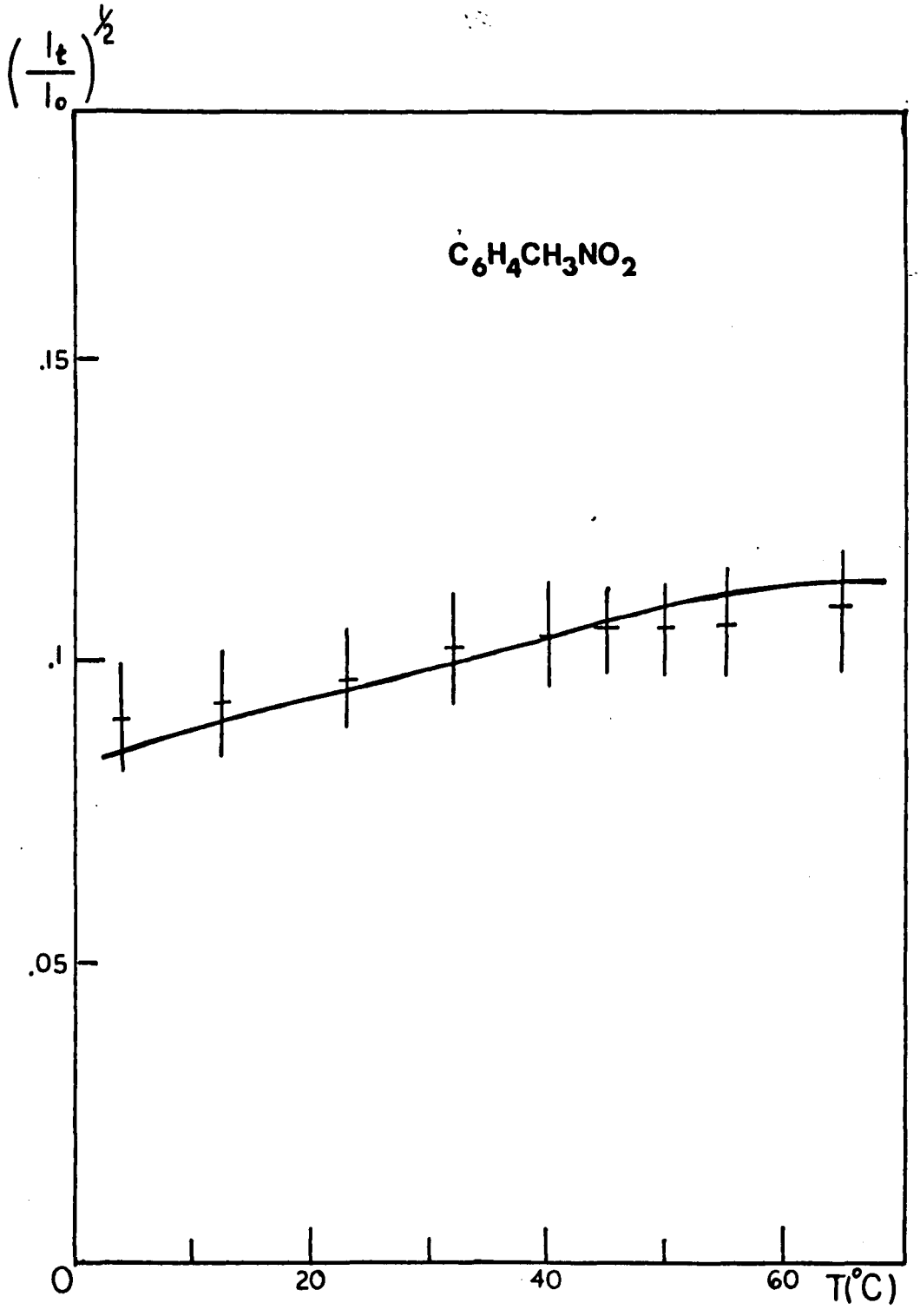

Figure 6.6.6c

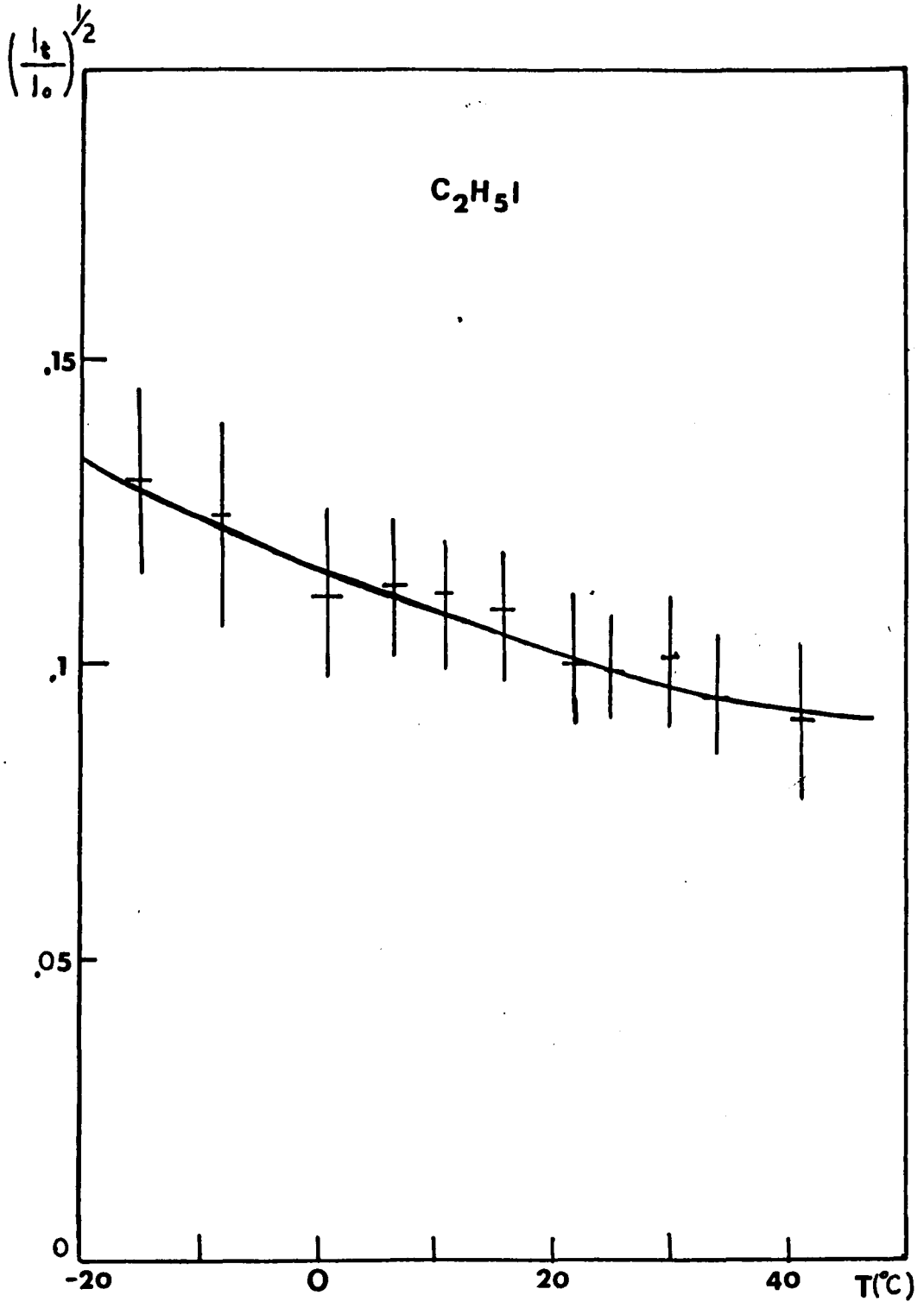

Figure 6.6.6d

CHAPTER 7

SUMMARY

In summary ., we have directly measured the relaxation kinetics of polyatomic molecules in different states of matter with the optical Kerr effect using picosecond laser pulses. The laser pulse is assumed to have either a Gaussian spatial profile and a Gaussian time profile or a Gaussian spatial profile and symmetrical exponential decay time profile. There is not too much difference between these two pulse shapes and both assumptions of pulse shapes can be used to fit our data properly. Most of the data were analyzed following the symmetrical exponential decay time profile which is easily deconvoluted.

The reorientational relaxation time in neat liquids such as nitrobenzene, m-nitrotoluene, salol, and succinonitrile, at moderate viscosity ($\eta_m \leq 5$cp) and above the melting temperature is linearly proportional to the measured viscosity.

In the supercooled liquid state of salol, where the temperature is far below the melting temperature, the reorientational relaxation time deviates from the viscosity. This can be accounted for by progressive restriction of molecular rotational motion. The internal frictional force which contributes to the measured viscosity is dominated by the translational motion of the molecules. The temperature dependence of the measured viscosity does not have the same characteristics as the molecular reorientational relaxation. There will be two different activation energies from these two different measurements. There are two distinct decaying

components from the Kerr gate of salol as the temperature falls below 50°C. The slow decay component is temperature dependent and has similar characteristics as the molecular reorientational motion. While the relaxation time of the fast decay component cannot be resolved with picosecond pulses and is assumed to arise from the relaxation processes of the electronic cloud distortion and molecular librations.

We have also studied the molecular reorientational relaxation in the solid state. Succinonitrile has two different crystal structures - cubic and monoclonic. Within the temperature region of the plastic crystal phase (cubic structure), the molecular reorientational motion is account for the molecular gauch-trans isomerization. The activation energy deduced from the temperature dependent relaxation time in the plastic crystal phase is similar to that from the liquid state. This suggests the reorientational motion in these two states ate similar. In the normal solid state (monoclinic structure), there is no evidence of rotational motion of molecules.

In mixed binary liquids possessing two components (B and C), the viscosity and the coupled molecular reorientational relaxation times are affected by three types of forces : the interactions between molecules of B-B, C-C, and B-C. In this research, B was chosen as a Kerr active solute (for example, carbon disulfide, nitrobenzene, and m-nitrotoluene), and C was chosen as a Kerr non-active solvent (for example, pentane, carbon tetrachloride, methanol, propanol, cyclohexanol,

cyclooctane, etc.). This coupled two-component relaxation theory which has been described by Mori, Keyes, Kivelson, and Tsay is successfully fitted to the experimental measured Kerr relaxation times. The magnitude of the relaxation processes in the optical Kerr effect are dependent on the nonlinear index of refraction of the original neat liquids, the relaxation times of neat liquids, the pair correlation factor, and the interspecies pair correlation factor, etc.. When the interspecies pair correlation is negligible small, the coupled mode disappears, the relaxation kinetics of the solute molecules can be approximated by a simplified Hill model.

In addition, we have characterized those parameters which affect the transmitted signal in the transient optical Kerr effect, and have measured the nonlinear index of refraction for twenty-nine different liquids. By assuming the shape of the laser pulse in time and space, I have precisely determined the prompt response curve of a Kerr gate [τ_0(molecular reorientational relaxation time) $>>$ τ_l(pulse duration)] and numerically deconvoluted all other relaxation times from the decay curves of the signal transmitted through the Kerr gate. The dispersion effects are neglected in this thesis because the length of the Kerr cell used in all studies is less than one centimeter. The signal transmitted through the Kerr gate is inversely proportional to the wavelength of the probe pulse when there is no absorption in these liquids. The signal transmitted through the Kerr gate of mixed binary liquids is found to be linearly dependent on the relaxation

time of the solution and the concentration of the Kerr-active molecules. The signal transmitted through the Kerr gate at various temperatures is also found to depend on the relaxation time of the liquid, the pair correlation factor of the molecule, and is inversely proportional to the temperature.

CHAPTER 8

FUTURE DIRECTIONS

Areas for future research are described below :.

1. The Raman induced Kerr effect from the optical Kerr effect is discussed in section 4.4. Due to the spectral width of laser pulses, the Raman induced Kerr effect may be washed out. If the bandwidth of the picosecond laser pulse can be reduced (such as by inserting a proper medium in the laser cavity as discussed in section 5.2) to the order of a few wavenumbers, then it may be possible to measure the kinetics of the relaxation mechanisms in the Raman induced Kerr effect.

2. In section 6.4, the relaxation kinetics in the supercooled liquid state of salol is studied. If the temperature is lowered down to the glass transition temperature, the orientational motion of molecules should be frozen out. However, in order to study the kinetics of this transition, a single picosecond laser pulse is needed for this study in the supercooled liquid state and glass state.

3. The orientational relaxation times in polymers[1] and liquid crystals[2] above the transition temperature have been measured on the order of a few nanoseconds. This is the rotational relaxation time of the whole molecule. However, there should be some fast relaxation mechanisms for these materials due to the shape of the molecules. These molecules consist of long rod-like chains which could have side chain orientational motion and backbone motion[1]. These mechanisms can be measured with the picosecond optical Kerr effect.

4. There is another parameter which can be varied to measure the pair correlation factor in liquids, namely the pressure. Changing the density of the liquid by pressure[3], the optical Kerr effect can support the results obtained from the concentration and temperature dependent optical Kerr effect.

5. As mentioned in sections 4.4 and 6.6, the pair correlation factor of the nonlinear index of refraction is not constant with temperature. This can also be measured more accurately from the depolarized Rayleigh scattering and by the steady state optical Kerr effect.

6. The dynamic pair correlation factor in mixed liquids is assumed to be zero for the data fitting. With a careful choice of mixtures, and more reliable results, one should be able to deduce reasonable values for g (though it is close to 0)[4].

7. In the viscosity measurement of mixed liquids, for example, $SnCl_4$ + $HCO_2C_2H_5$, at a certain temperature and concentration, the measured viscosity can increase by one hundred times over the original viscosities. This is a critical phenomena and is mentioned in section 3.1.[5] We have avoided this point during this research. It will be interesting to study the relaxation times at critical points by the OKE.

8. For more complex systems, such as mixing three or more different kinds of molecules. A more through study is needed in both theory and measurement.

Though there have been a lot of techniques to study the molecular reorientational motion in condensed media, this thesis on the direct measurement of the relaxation kinetics of the optical Kerr effect in liquids, mixed liquids, supercooled liquids, and plastic crystals has added both more information and questions as to the nature of the molecular rotational motion in the condensed states of matter. I hope this thesis will stimulate experimental and theoretical research, so that we can understand the motion of molecules in their microscopic world.

References

1. D.R. Jones and C.H. Wang, J. Chem. Phys., 66,1659,(1977).
ibid, 65, 1835, (1976).

2. G.K.L. Wang and Y.R. Shen, Phys. Rev., A10, 1277, (1974).
T.D. Glerke and W.H. Flygare, J. Chem. Phys.,61,2231,(1974).

3. S.J. Bertucci, A.K. Burnham, G.R. Alms, and W.H. Flygare, J. Chem. Phys., 66, 605, (1977).

4. G.R. Alms, D.R. Bauer, J.I. Brauman, and R. Pecora, J.Chem. Phys., 59, 5310, (1973).
E. Zamir, N.D. Gershon, and A. Ben-Reuven, J. Chem. Phys., 55, 3397, (1971).

5. G. D'Arrigo, L. Mistura, and P. Tartaglia, J. Chem. Phys., 66, 80, (1977).
N.S. Kurnalow, Zeit. Anorg. Chem., 135, 81, (1974).